Sedimentary environments and climate change: a case study (late Miocene, central Crete)

Dissertation
Zur Erlangung des Grades
Doktor der Naturwissenschaften

Am Fachbereich Geowissenschaften
Der Johannes Gutenberg-Universität Mainz

Karsten Friedrich Kröger
geb. am 29.12.1972 in Hamburg

Mainz 2004

Abstract

In this study, conditions of deposition and stratigraphical architecture of Neogene (Tortonian, 11-6,7Ma) sediments of southern central Crete were analysed. In order to improve resolution of paleoclimatic data, new methods were applied to quantify environmental parameters and to increase the chronostratigraphic resolution in shallow water sediments. A relationship between paleoenvironmental change observed on Crete and global processes was established and a depositional model was developed.

Based on a detailed analysis of the distribution of non geniculate coralline red algae, index values for water temperature and water depth were established and tested with the distribution patterns of benthic foraminifera and symbiont-bearing corals.

Calcite shelled bivalves were sampled from the Algarve coast (southern Portugal) and central Crete and then $^{87}Sr/^{86}Sr$ was measured. A high resolution chronostratigraphy was developed based on the correlation between fluctuations in Sr ratios in the measured sections and in a late Miocene global seawater Sr isotope reference curve. Applying this method, a time frame was established to compare paleoenvironmental data from southern central Crete with global information on climate change reflected in oxygen isotope data.

The comparison between paleotemperature data based on red algae and global oxygen isotope data showed that the employed index values reflect global change in temperature. Data indicate a warm interval during earliest Tortonian, a second short warm interval between 10 and 9,5Ma, a longer climatic optimum between 9 and 8Ma and an interval of increasing temperatures in the latest Tortonian. The distribution of coral reefs and carpets shows that during the warm intervals, the depositional environment became tropical while temperate climates prevailed during the cold interval.

Since relative tectonic movements after initial half-graben formation in the early Tortonian were low in southern central Crete, sedimentary successions strongly respond to global sea-level fluctuation. A characteristic sedimentary succession formed during a 3rd order sea-level cycle: It comprises mixed siliciclastic-limestone deposited during sea-level fall and lowstand, homogenous red algal deposits formed during sea-level rise and coral carpets formed during late rise and highstand. Individual beds in the succession reflect glacioeustatic fluctuations that are most prominent in the mixed siliciclastic-limestone interval.

These results confirm the fact that sedimentary successions deposited at the critical threshold between temperate and tropical environments develop characteristic changes in depositional systems and biotic associations that can be used to assemble paleoclimatic datasets.

Kurzfassung

Zur Voraussage der Auswirkungen der heutzutage beobachteten Klimaerwärmung ist es wichtig, genaue Klimadaten aus der geologischen Vergangenheit zu gewinnen, mit deren Hilfe Klimamodelle getestet werden können. Eine genaue Kenntnis der Auswirkungen globaler Klimaschwankungen auf marine Ablagerungsräume ist hierzu erforderlich. Ziel dieser Arbeit ist es, Methoden aufzuzeigen, um diese Zusammenhänge genauer zu erfassen und die Verbindung zu globalen Prozessen herzustellen. Zu diesem Zweck wurden Sedimente des jüngeren Tertiärs (Torton, 11-6,7Ma) untersucht, die im südlichen Zentralkreta exzellent aufgeschlossen sind.

Die Analyse der stratigraphischen Architektur und der Entwicklung der Geometrie des Ablagerungsraums ergab, dass die Sedimentation in einem tektonisch aktiven, E-W orientierten Halbgrabensystem begann. Im Laufe des Tortons kam es zu einer Änderung des Spannungsfeldes, woraus eine zunehmende Fragmentierung des Beckens unter anhaltend starker Absenkung resultierte. Im Zuge abnehmender tektonischer Aktivität verminderte sich auch der Eintrag von Siliziklastika und es bildete sich ein Rampensystem, in dem vor allem kalkige Sedimente abgelagert wurden.

Zur Untersuchung der Umweltbedingungen zur Zeit der Ablagerung der Kalksteine erwiesen sich nicht-geniculate coralline Rotalgen als wertvolle Indikatoren für Wassertemperatur und -tiefe. Durch detaillierte Bestimmung der im Torton auf Kreta vorkommenden Rotalgentaxa ließen sich Index-Werte zur Quantifizierung von Wassertiefe und -temperatur aufstellen und an der Verbreitung anderer Organismen wie benthischen Foraminiferen und Korallen testen.

Auf der Basis von an kalzitschaligen Muscheln aus Portugal (Algarve) und Zentralkreta gemessenen $^{87}Sr/^{86}Sr$-Daten wurde eine Methode der hochauflösenden Sr-Chronostratigraphie entwickelt. Diese Methode basiert auf der Korrelation von Fluktuationen in den Sr-Kurven gemessener Profile mit Fluktuationen in einer globalen Meerwasser-Referenzkurve aus dem späten Miozän. Auf diese Weise ließen sich die auf der Analyse von Umweltindikatoren beruhenden Klimadaten von Kreta in einen zeitlichen Rahmen setzen und mit globalen Klimasignalen vergleichen, wie sie sich in Sauerstoff - Isotopenverhältnissen widerspiegeln. Der Vergleich zwischen Paläotemperaturdaten auf der Basis von Rotalgen mit der globalen Sauerstoffisotopenkurve hat gezeigt, dass die verwendeten Index-Werte globale Temperaturschwankungen abbilden. Die Daten belegen eine Warmphase im frühesten Torton, eine weitere kurze Warmphase zwischen 10 und 9,5 Ma, ein längeres klimatisches Optimum

zwischen 9 und 8Ma, sowie eine Phase der Erwärmung im spätesten Torton. Diese Warmphasen sind auch durch das Auftreten von zum Teil Riff-bildenden Korallen mit Symbionten belegt. Dabei führte das längere klimatische Optimum zur flächendeckenden Verbreitung von Korallenteppichen. Lokal erhöhte Nährstoffkonzentrationen schränkten die Verbreitung von Korallenriffen und –teppichen im Untertorton ein. Dagegen konnten aufgrund der vorgefundenen Foraminiferenvergesellschaftungen insgesamt hohe Nährstoffkonzentrationen für das Obertorton ausgeschlossen werden.

Weit verbreitete sedimentäre Markerhorizonte spiegeln globale Meeresspiegelschwankungen wider. Solche eustatischen Einflüsse sind sowohl durch die Korrelation mit der Sr-Isotopenkurve als auch durch die auf Rotalgenvergesellschaftungen beruhende Wassertiefenkurve belegt. Durch den Einfluß langfristiger eustatischer Schwankungen auf die Topographie des Ablagerungsraumes entstand über eine Dauer von mehreren Millionen Jahren eine charakteristische Sedimentabfolge. Diese Abfolge entspricht der Dauer eines eustatischen Zyklus dritter Ordnung. Die vorgefundenen Merkmale eines solchen Zyklus sind gemischt siliziklastisch-karbonatische Sedimente, die während eines Meeresspiegelfalls und –tiefstands abgelagert werden, ungeschichtete Rotalgenkalke, die während eines ansteigenden Meeresspiegels entstehen und Korallenteppiche, die in der späten Phase des Anstiegs oder während des Meeresspiegelhochstands gebildet werden. Letzterer entspricht der wärmsten Phase des Zyklus, während der die polare Eisakkumulation am geringsten ist. Einzelne Schichten bilden wiederum kurzfristigere glazioeustatische Schwankungen ab. Diese treten am deutlichsten in den gemischt siliziklastisch-karbonatischen Ablagerungen hervor.

Die vorherrschende Topographie des Ablagerungsraumes, der eine dem Meer zugewandten Rampe darstellt, konnte nur dadurch erhalten bleiben, dass in dem Abschnitt der Rampe unterhalb der Sturmwellenbasis signifikante Sedimentmengen durch lichtabhängige Organismen gebildet wurden. Über geologische Zeiträume stabile Karbonatrampen sollten sich daher präferenziell in Nebenmeeren mit geringer Sturmwellenabrasionstiefe bilden.

Wie die Untersuchung von Rotalgenvergesellschaftungen gezeigt hat, bilden Karbonatrampen, die im kritischen Übergangsbereich zwischen gemäßigten und tropischen Klimaten entstanden sind, globale Klimaschwankungen besonders deutlich ab. Durch die Möglichkeit, diese Sedimente mit Hilfe der Sr-Isotopenchronostratigraphie in einen genauen, an der glazioeustatischen Meeresspiegelfluktuation orientierten zeitlichen Rahmen zu setzen, bietet sich ein Ansatzpunkt, genaue Klimadaten aus der geologischen Vergangenheit zu gewinnen.

1. Introduction

1.1. General introduction

The physiography of recent and fossil shorelines found around the world is characterized by considerable variation. Associated with them is a variety of submarine environments, where sediments transported from the continents into the oceans and produced on the ocean floor are deposited. The topography of nearshore sedimentary environments and the biota associated with them are controlled by a variety of factors. Many of these are related to the geographical position: Water temperature depends on latitude, oceanic circulation systems and climatic conditions. The morphology of depositional environments depends on hydraulic energy induced by currents and ocean swell that may be significantly increased during storm events. The continental hinterland behind the shoreline sheds variable amounts of siliciclastic particles in dependence of its relief and its climatic conditions. Sedimentary basins develop in dependence of regional tectonic settings. Associated with continental runoff, but also with oceanographic factors such as upwelling, nutrients are carried into the sedimentary environment and influence the kind of biota on the seafloor and in the water column. However, regardless of the geographical position, sedimentary environments respond to global climate change, be it through change in water temperature, eustatic sea-level change related to glaciation and deglaciation or through related change in precipitation and oceanic and atmospheric circulation patterns that influence nutrient budgets.

A better understanding of the effect of climate change and related processes on depositional systems and associated organisms is crucial for paleoclimatic studies. To understand ancient depositional environments, the analysis of recent systems and related biotic associations is fundamental. However, it has to be kept in mind that Quaternary climate with its high frequency change from glacial to interglacial periods and associated eustatic sea-level change in the order of 10m/1ka is fundamentally different from other geological periods including the Neogene. For this reason, Holocene depositional environments are in a state of disequilibrium and often consist only of thin veneers deposited on older rocks during the 130m sea-level rise since the last glacial maximum approximately 20ka ago (Walkden and Williams, 1998; Yokoyama et al., 2000). Consequently not all results of studies of recent environments may be readily applicable in ancient settings.

Neogene deposits have been a focus for paleoenvironmental studies since sediments are usually well preserved and biotic associations are very similar to modern associations. Not

only for these reasons the Neogene is important for the understanding of the climate of the earth: Interannual climate variability documented in coral aragonite from 10Ma old sediments on Central Crete indicates that North Atlantic Oscillation (NAO) patterns which affect the Mediterranean climate in the recent interglacial where already effective 10Ma ago (Brachert *et al. in prep.*). Global warming in consequence of emission of greenhouse gases therefore may lead to an environment very similar to Upper Miocene climate which was slightly warmer and lacked Pleistocene scale glaciations (Zachos et al., 2001).

For several reasons, Neogene deposits of the Mediterranean most effectively record climate change and variation of factors related to global climate: Miocene sediments that are widespread in the Mediterranean were deposited at the critical interface between the warm temperate and tropical biogeographic province (Brachert et al., 1996; Esteban, 1996; Braga and Aguirre, 2001). This province can be defined as the global area where water temperature allows the existence of hermatypic coral reefs (Brachert, 1996). In the following, sediments deposited in this area are called tropical regardless of geographical latitude. Sediments deposited in areas where shallow water temperature did not allow the formation of hermatypic coral reefs are addressed as non-tropical or temperate. An environment at the threshold between tropical and non-tropical conditions such as the Miocene Mediterranean thus will potentially record global climate change by a shift between deposition of temperate sediments and deposition of tropical sediments (Brachert et al., 1996). Biotic associations also respond to other factors such as water depth (Lees and Buller, 1972; Carannante et al., 1988) and nutrients (Hallock and Schlager, 1986; Halfar et al., 2004) that may be related to global climate change but may also be controlled by local parameters. Therefore, biotic associations that are typical for non-tropical environments may occur in environments where surface water temperatures are warm enough for tropical biota (James, 1997). Thus it is necessary to differentiate between influences of global climate and local factors. Moreover, for comparison with global climate change a high resolution time frame has to be established for the analyzed sediments. This prerequisite has been met in shallow marine deposits only in few cases, for example when a time frame was established based on intercalated volcanic rocks (Brachert et al., 1998). To carry out the present study, a new chronostratigraphic method based on correlation of high frequency fluctuations in the seawater $^{87}Sr/^{86}Sr$ record which responds to glaciation and deglaciation and related eustatic sealevel change has been developed. It was established in Middle Miocene mixed siliciclastic carbonate sediments of the southern

Algarve (Portugal) that well reflect eustatic sea-level change (Brachert et al., 2001). The method is discussed in detail in the original manuscript submitted for publication (chapter 4).
The Upper Miocene of central Crete is an area especially suitable to study the impact of climate change on sedimentary environments and biotic associations for several reasons: Sediments are easily accessible and most deposits are neither deformed nor significantly altered. Outcrop conditions allow the reconstruction of the extensional structural framework during deposition of Miocene sediments and therefore to recognize local influences on sedimentary basins. Shallow water sediments can be traced over an area of 50km^2 and correlated with Neogene deposits in other parts of central Crete. Sediments are rich in benthic foraminifera and in non-geniculate coralline red algae that are used in this study as indicators for water temperature, water depth and nutrient contents. Based on Sr isotope chronostratigraphy, a high resolution time frame was established that allows the correlation of local indicators with data on global climate change such as the $\delta^{18}O$ record assembled by Abreu and Anderson (1998). Facies associations and geometries of the identified depositional environments show marked responses to global climate change that are characteristic for environments in enclosed seas at the critical interface between the temperate and tropical province and that may be present in many ancient systems.

1.2. Geographic overview

Central Crete is subdivided into two basinal areas of the N-S oriented Iraclion Plain in the north and the E-W oriented Messara Plain in the south (Fig. 1.2.1.). The Iraclion Plain is inclined to the north towards the seaport of Iraclion and dissected by N-S trending valleys. The Iraclion Plain is separated from the Messara Plain by the E-W trending Central Iraclion Ridge that south of Agia Varvara steeply drops from 800m down to the Messara Plain at 200m. The basins are flanked by the steep mountain areas of the Ida Massif to the northwest and the Asteroussia Mountains between the Messara Plain and the southern coast of Crete. The Ida Massiv (Mount Psiloritis, Fig. 1.2.2.a) reaches a height of 2458m while the highest elevation of the Asteroussia Mountains reaches 1231m. Both mountain sites have pronounced escarpments to the south that reach more than 1000m in height. South of the city of Matala, the Asteroussia Mountains pass into a 5km wide tabelland dipping westward towards the Lybian Sea (Fig. 1.2.2.a). This tableland called West Asteroussia Tabellands (WAT) in the following is formed by inclined Neogene sediments that are dissected by deep and mostly dry

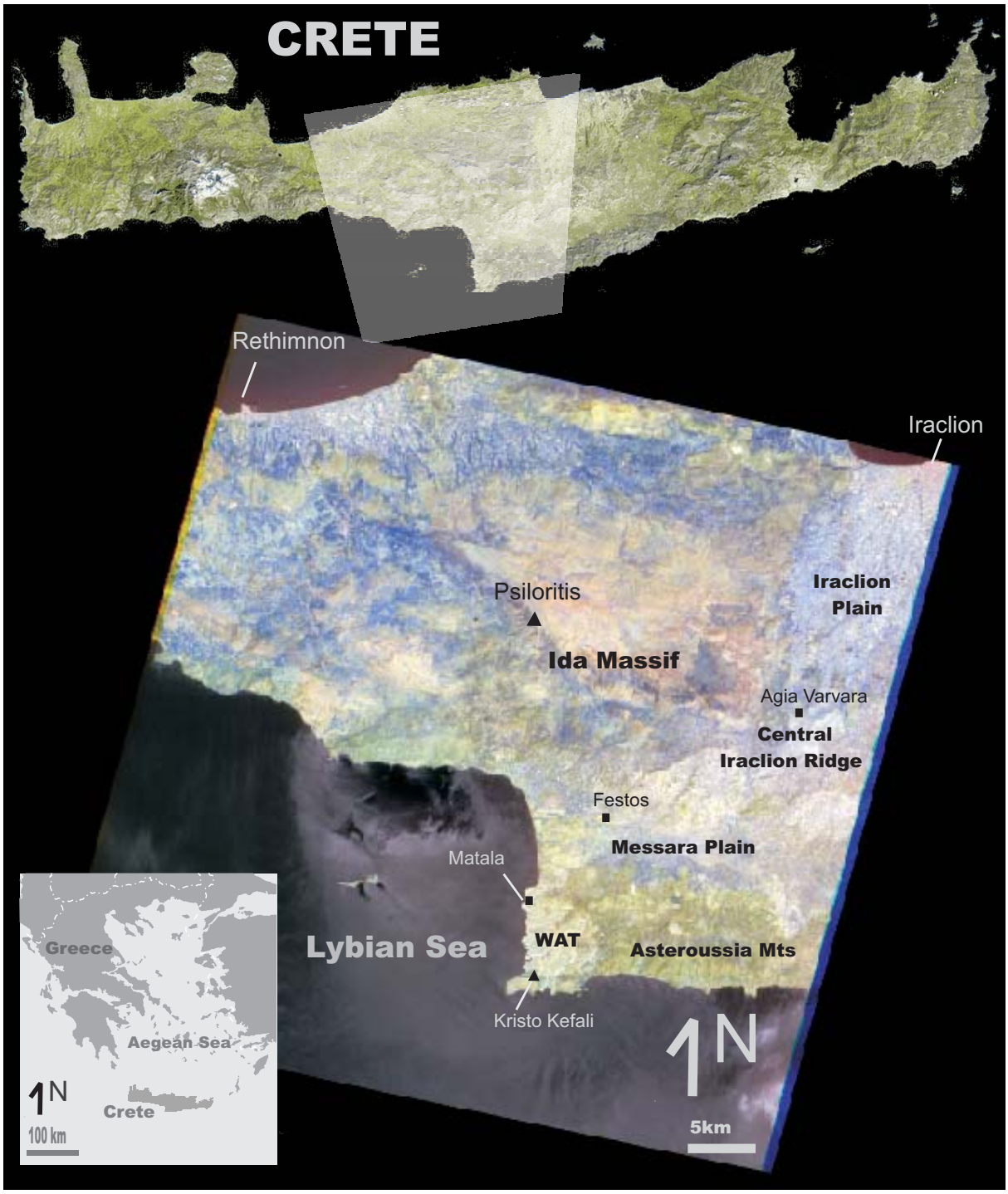

Fig. 1.2.1.: Geographic overview: Satellite image of central Crete rectified on UTM scale (centre of image) with satellite image of Crete (top) and location map (lower left)

valleys that may contain ephemeral or more rarely perennial creeks. These valleys are N-S oriented in the southeast of the WAT and E-W in the northwest. The escarpment in the south of the Asteroussia Mountains continues to the southwestern tip of the WAT formed by the 391m high Mount Kristo Kefali (Fig. 1.2.2.b). This steep ridge is dissected by the impressive and more than 100m deep Ayofarago Gorge (Fig. 1.2.2.c).

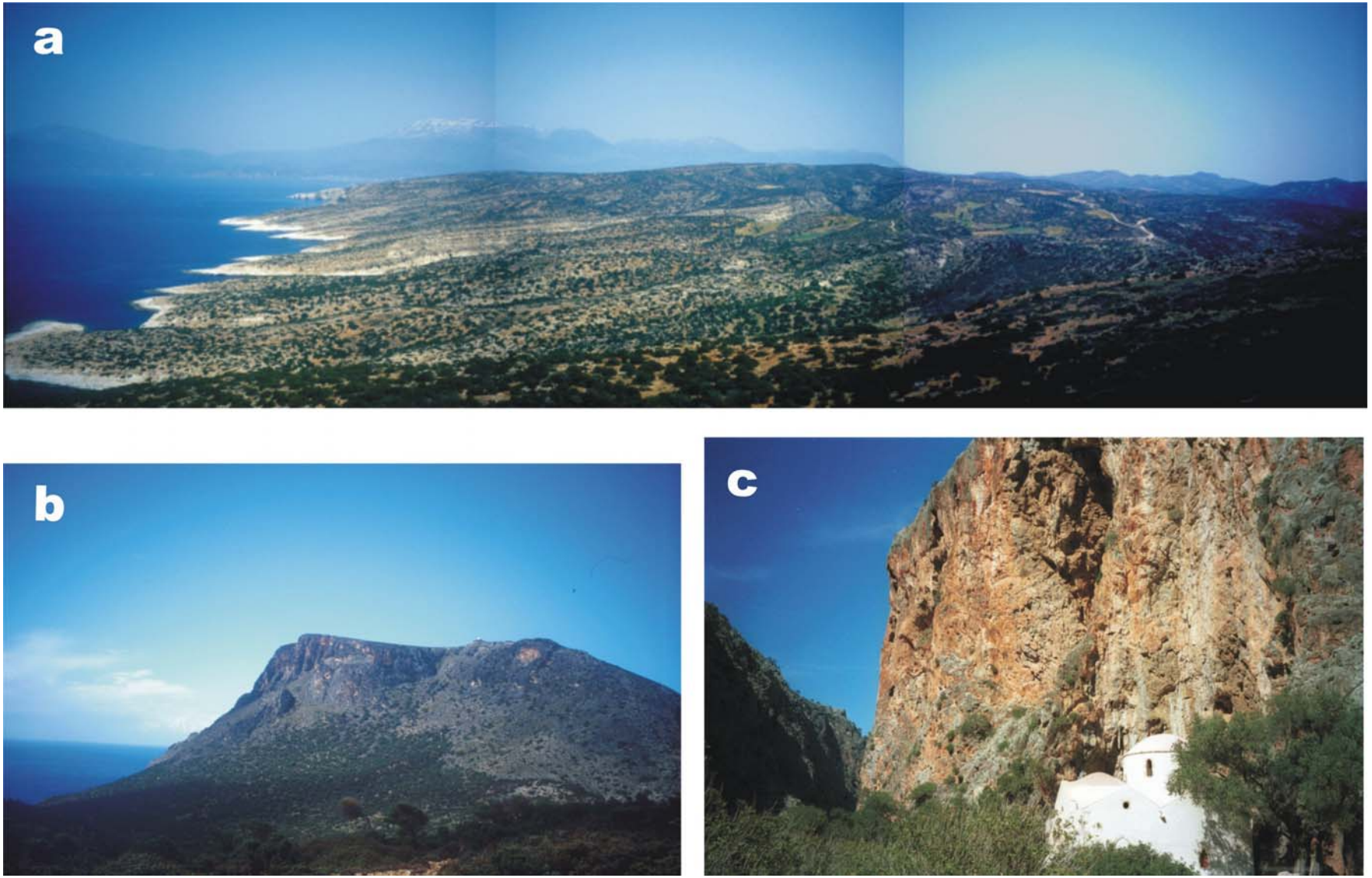

Fig. 1.2.2. **a:** View from Mount Kristo Kefali in northern direction across the Western Asteroussia Tabellands (WAT) with Mount Psiloritis in the background
b: Mount Kristo Kefali, view from the northeast

1.3. Geological setting

Crete is situated in an area of complex plate interactions between the African and Arabian plates and the Aegean and Anatolian microplates. The Neogene history of Crete has therefore been object of intensive research. Among the most often discussed mechanisms influencing the geological evolution of Crete are the extrusion of the Anatolian microplate as a consequence of the northward migration of Arabia (Le Pichon and Angelier, 1979; Kissel et al. 1988; Ten Veen und Postma, 1999a,b; Fassoulas, 2001) the rollback of the Hellenic subduction zone (Le Pichon and Angelier, 1979; Meulenkamp et al. 1988; Ten Veen und Postma, 1999 a,b; Fassoulas, 2001) and resulting extension and rotation of the Aegean microplate (Le Pichon and Angelier, 1979); Fig. 1.3.1. While recent GPS data (Le Pichon et al., 1995; Reilinger et al. 1997; Kahle et al. 1998; McClusky et al. 2000) support the existence of these patterns, the tectonic regimes in the past and the evolution and the controlling mechanisms of the tectonic framework observed in the recent are still being debated.

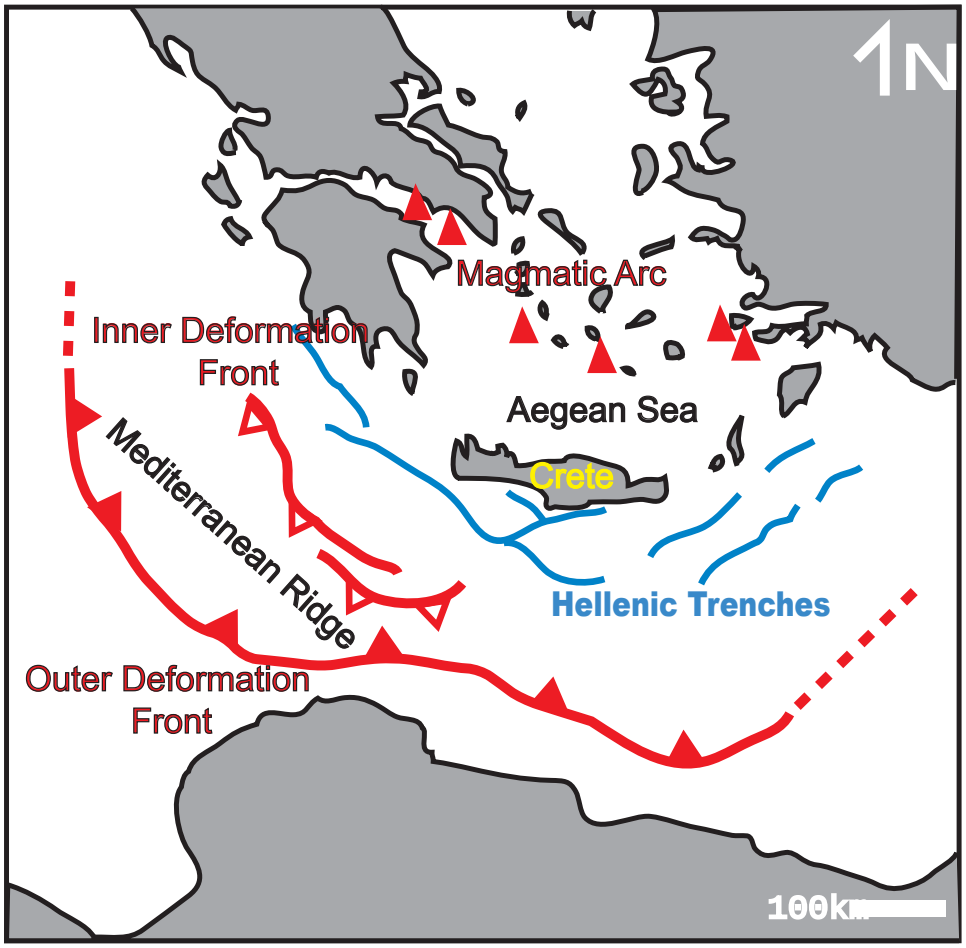

Fig. 1.3.1.: Overview of the Aegean region with recent position of deformation fronts associated with the Hellenic Subduction Zone, modified after Robertson et al. 1996

The evolution of the tectonic framework and the sedimentary history in the Neogene of Crete has been examined by many authors. This has led to a variety of interpretations of the changing stress fields and to structural models that relate to the different mechanisms mentioned above. Most models agree on the fact that in the Miocene, beginning with the exhumation of HP/LT rocks in the Lower Miocene (Fassoulas et al. 1994, Jolivet et al. 1996, Fassoulas 1999) the tectonic setting was largely extensional (Le Pichon and Angelier, 1979; Angelier et al. 1982; Fassoulas, 2001). Early, E-W oriented sedimentary basins formed in synclinals of the exhumed and now in N-S direction stretched Alpine nappe stack (Meulenkamp et al., 1988; Jolivet et al., 1996). Early sediments are siliciclastic fluviatile, brackish and marine deposits (Meulenkamp 1979, Meulenkamp et al. 1979, Fortuin und Peters 1983, Meulenkamp 1994, Ten Veen und Postma 1999a). Early marine sediments in the eastern Messara Basin of central Crete have been determined to be Upper Seravallian in age (Meulenkamp et al., 1979). Accompanied by increasing fragmentation of the basins by normal faulting, a transition from siliclastic to carbonate sedimentation is observed (Meulenkamp 1979, Meulenkamp et al. 1979, Angelier et al. 1982, Postma et al. 1993, Ten Veen und Postma 1999a). Around the Miocene-Pliocene boundary, a compressional event has been described (Fassoulas, 1999). Meulenkamp et al. (1994) interpret the uplift of parts of central Crete to modern elevations of approximately 2500m to be a consequence of this event.

1.4. Methodology

To determine the controlling factors on depositional environments of Neogene deposits in southern central Crete, a combination of fieldwork, thin section analysis and geochemical analysis was undertaken.

During fieldwork, mappable lithofacies associations, consisting of various lithofacies units characterized by their field aspects, textures and biofacies where identified. Lithofacies associations in the Western Asteroussia Tabellands (WAT) were mapped in detail (1:10000). To analyse vertical successions, 24 sections were measured in the WAT, at the southern margin and the centre (Festos Horst) of the Messara Plain (Fig. 1.4.1.).

Using thin sections of samples taken along several sections, sediments were analyzed in detail. Samples were picked randomly from each bed and in intervals of 50cm at section MO1 and no more than 200cm in 6 other sections. Three types of thin section analyses were undertaken: 1) petrolographical and microfacies analysis as well as semiquantitative biofacies

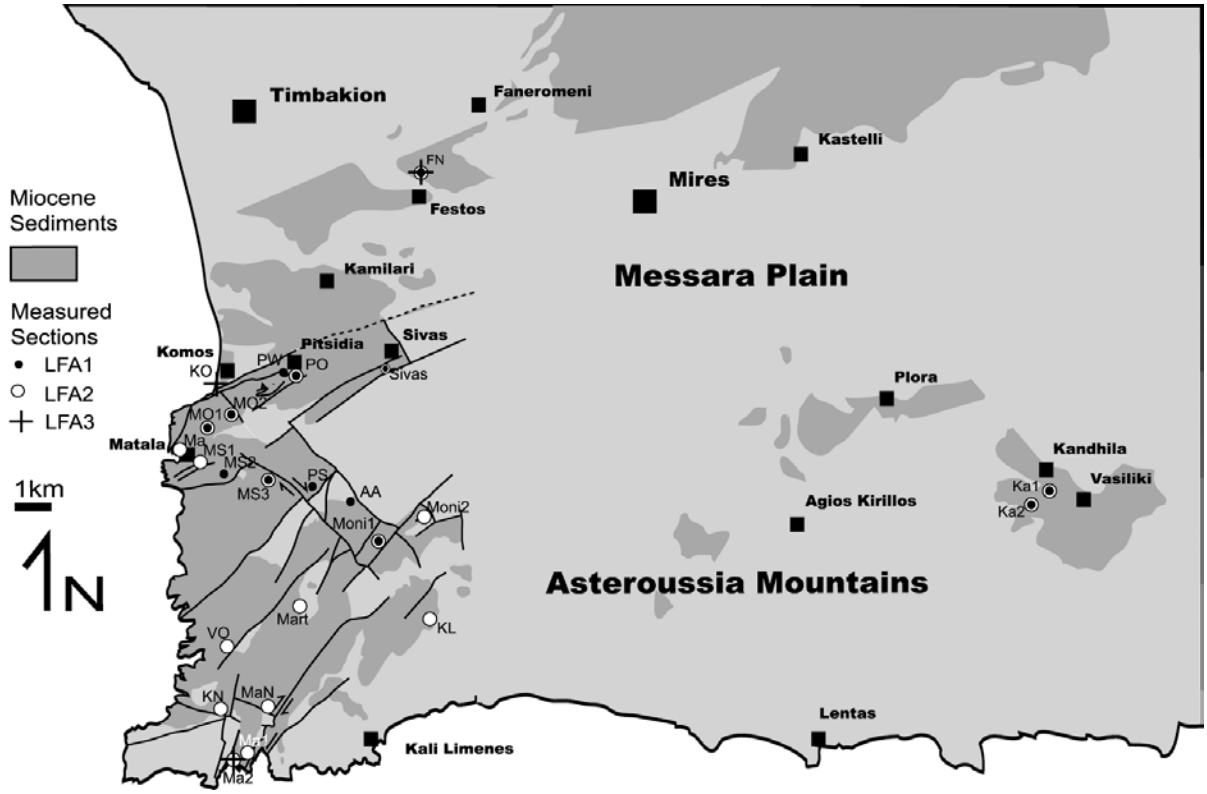

Fig. 1.4.1.: Geographical map of the Western Asteroussia Tabellands (WAT) and the western Messara Plain with all measured sections. Symbols indicate lithofacies associations sampled by the sections. Outcrops of Miocene sediments modified after I.G.M.E. sheets Timbakion and Andiskarion. See table A1 for position of sections and sample information

analysis (chapter 2); 2) semiquantitative analysis of foraminifera and 3) taxonomic and semiquantitative analysis of non-geniculate coralline red algae (chapter 3).

Petrographical and microfacies analysis of thin sections was qualitative. Semiquantitative analysis was applied for siliciclastic contents, using reference images of Flügel (1978).

Semiquantitative biofacies analysis was carried out using classes of relative abundance. The employed classes were common (3/6; 50%), uncommon (2/6; 33,3%) and rare (1/6; 16,7%). For the quantification of skeletal elements in many sections classes were modified due to the dominance of one type of components to dominant (3/4; 75%), rare (1/6; 16,7%) and very rare (1/12; 8,3%). All identifiable fragments of skeletal elements in thin sections were included in quantification. Semiquantitative analysis has been chosen since the variation between samples of the same bed is assumed to be higher than the error between quantitative and semiquantitative analysis. Quantification of foraminifera and coralline red algae was carried out similarly using abundance classes of 50%, 33,3% and 16,7%. All results are equivalent to volume percent of volume total of skeletal components.

Independent from lithofacies units, datasets on climate change reflected by water temperature and water depth were developed based on semiquantitative analysis of distribution of foraminifera and coralline red algae.

To establish a high resolution time frame of Neogene carbonate deposits, Sr isotope analysis on bivalve shells (*Pecten, Chlamys*) was carried out. Using additional data from central Crete and southern Portugal, a method to correlate these datasets with high frequency fluctuation of the global seawater Sr isotope record was developed. The applied methods are discussed in detail in chapter 4. Water depth and water temperature indices resulting from the analysis of coralline red algae were calibrated by Sr chronostratigraphy and compared with published data on global climate change and eustatic sea-level variation. Finally, facies associations are interpreted in the context of the depositional environments and their relationship to global climate.

2. The Neogene of the western Messara Basin and the Western Asteroussia Tabellands

2.1. Basement

Neogene deposits in the Western Asteroussia Tabellands (WAT) overlie Mesozoic to Paleogene basement. The basement is composed of either limestone (Fig. 1.2.1.; Jurassic to Eocene) or Flysch (sandstone with subordinate claystone; Upper Eocene) of the Tripolitza Unit (Creutzburg, 1975; Bonneau, 1984; Hall et al., 1984; Jakobshagen, 1986). Limestone of the Tripolitza Unit forms the mountain chain along the southern coast west of Kali Limenes (Fig. 1.2.1.). Sandy Flysch deposits which form the top of the Tripolitza Unit underlie Neogene deposits in the WAT north of Kristo Kefali.

2.2. Subdivision of Neogene deposits

Neogene sediments in the Messara- and Iraclion Basins have been described by Meulenkamp (1979), Meulenkamp et al. (1979) and ten Veen and Postma (1999). Upper Miocene siliciclastic deposits with intermittent brackish and marine influence and marls have been named Ambelouzos formation, while Upper Miocene marls and carbonates have been named Varvara formation by the authors. Mixed siliciclastic deposits with large foraminifera, echinoids and rhodoliths have been described as Pirgos Member. Of these sediments, only marl deposits in the central Messara Basin at Kastelli have been dated. The resulting age is late Tortonian to Messinian (Zachariasse, 1975; Langereis et al., 1984; Hilgen et al., 1995; Krijgsman et al., 1995). The lithological subdivision of these stratigraphic units in the field is problematic and the relationship between the units is not well established. Therefore, an informal division is used here based on lithological aspects, which are easily identified in the field and have a genetic connotation. Three mappable lithostratigraphic units (LFA1-3) are identified (Fig. 2.2.1): A basal unit that consists of siliclastic deposits (LFA1), a second unit that is formed by limestone (LFA2), and a third unit that is characterized by marl with

Fig. 2.2.1. (next page): Geological Map of the Western Asteroussia Tabellands (WAT) with two cross-sections. Quaternary cover is not shown. Neogene deposits are subdivided into siliciclastic deposits of LFA1, carbonates with minor siliciclastics (LFA2) and open marine marl (LFA3). LFA2 is subdivided into three mappable units a-c, of which a is characterized by increased contents in siliciclastics, b by massive rhodolith rudstone to floatstone and c by coral framestone or single coral colonies at the base.

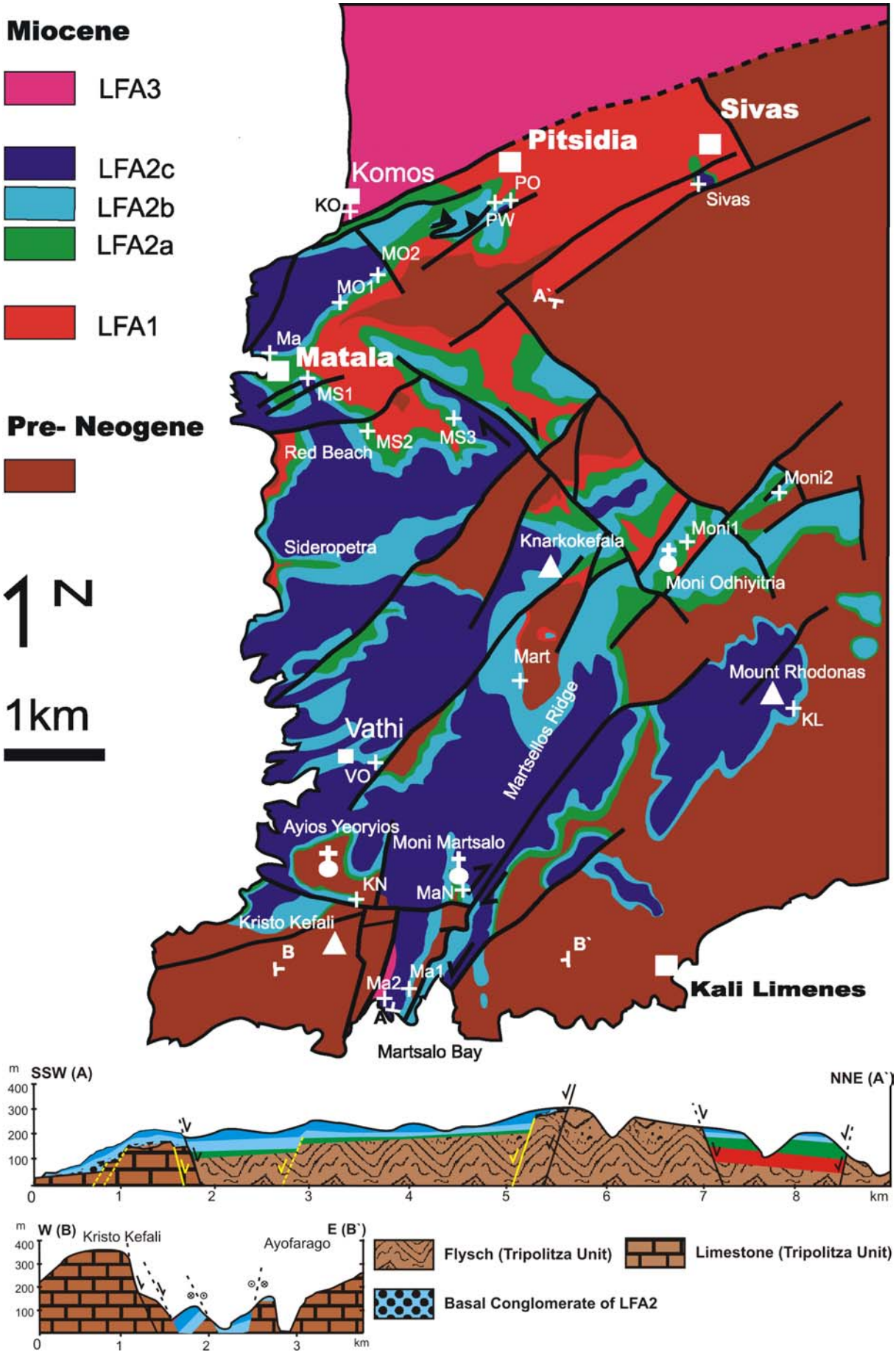
Miocene
LFA3
LFA2c
LFA2b
LFA2a
LFA1
Pre- Neogene
1 N
1km
Sivas
Pitsidia
Komos
KO
PO
PW
Sivas
MO2
MO1
A`
Ma
Matala
MS1
MS2
MS3
Red Beach
Moni2
Moni1
Sideropetra
Knarkokefala
Moni Odhiyitria
Mart
Mount Rhodonas
KL
Vathi
VO
Martsellos Ridge
Ayios Yeoryios
Moni Martsalo
KN
MaN
Kristo Kefali
B
B`
Ma2
Ma1
A
Kali Limenes
Martsalo Bay
m
SSW (A)
NNE (A`)
400
300
200
100
0
1
2
3
4
5
6
7
8
km
m
W (B)
Kristo Kefali
Ayofarago
E (B`)
400
300
200
100
0
1
2
3
km
Flysch (Tripolitza Unit)
Limestone (Tripolitza Unit)
Basal Conglomerate of LFA2

abundant planktonic foraminifera (LFA3). The siliciclastic unit comprises a variety of lithologies that are described in detail below. Moreover, LFA2 can be subdivided into three subunits (LFA2a-LFA2c) that each consist of several different lithologies most of which are below mapping resolution. The subdivision into the three subunits is based on lithological marker horizons and characteristics that are easily recognized in the WAT and widely traceable: LFA2a consists of limestone that is rich in siliciclastics with intercalated calcareous sandstone and underlies a rudstone bed with quartz pebbles. In areas where several stacked beds of the rudstone occur, the uppermost and most extensive bed defines the upper limit of the subunit. It is overlain by massive (*sensu* Ingram, 1954) rhodolith rudstone to floatstone and bioclastic packstone (LFA2b). This subunit includes basal conglomerate with a limestone matrix and directly overlies basement, where LFA2a is not present. The subunit is overlain by rhodolith rudstone and floatstone with subordinate bioclastic packstone and with coral framestone horizons or single zooxanthellate coral colonies at the base (LFA2c). Over the largest part of the WAT the base of the LFA2c unit is formed by one or two laterally extensive coral framestone horizons that form up to 5m high steps in the field.

Applying the lithostratigraphic units, the WAT was mapped in detail (Fig. 2.2.1.). The variation in thickness of the four units is shown in profiles along two lines in Fig. 2.2.1. and in schematic transects shown in Fig. 2.2.3 – 2.2.6. Both, synsedimentary and postsedimentary faults occur (see chapter 5).

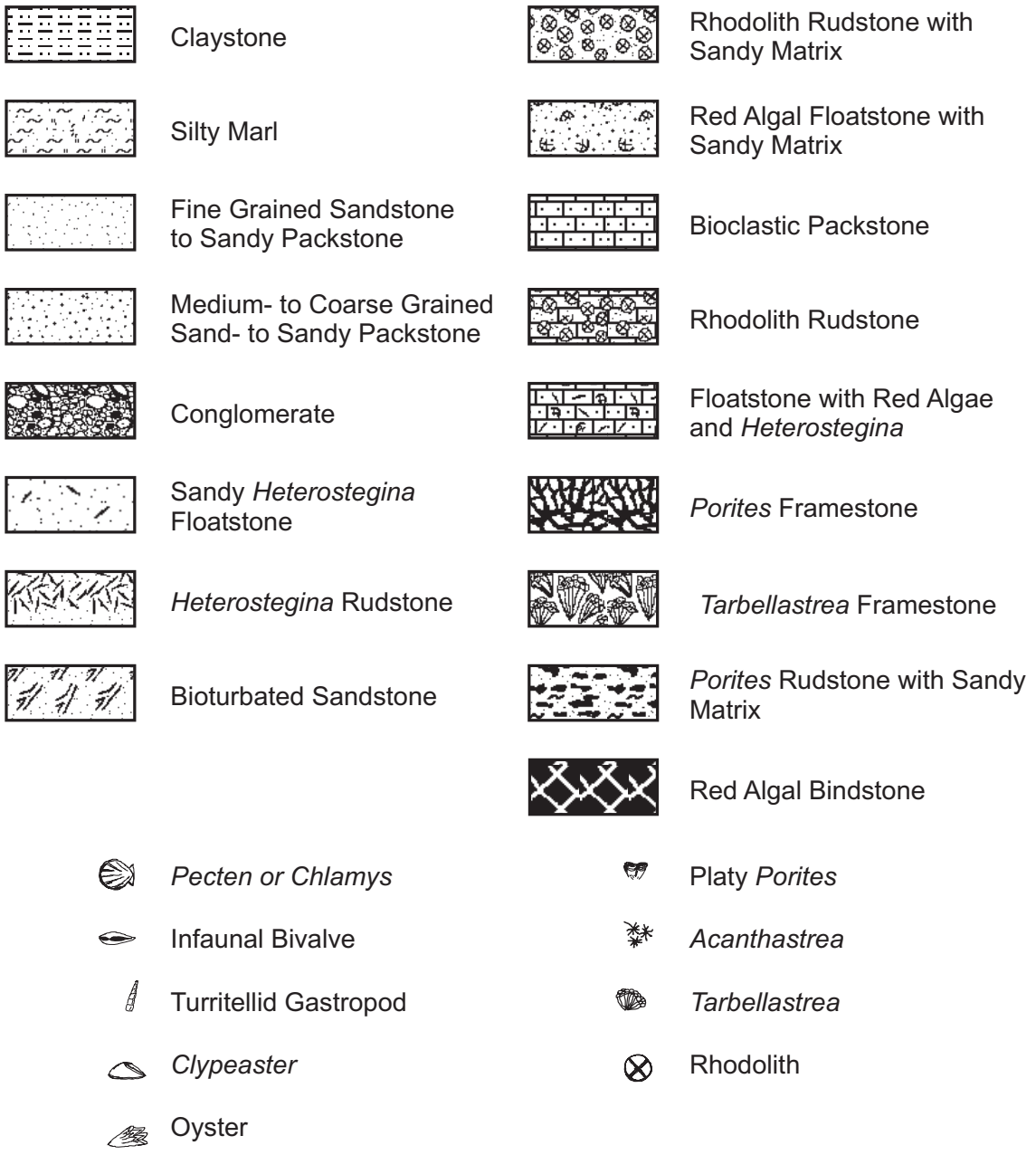

Fig. 2.2.2.: Legend of lithologies; biotic and textural elements are used for all sections in this study if not indicated otherwise

Fig. 2.2.3. (page 14): Schematic N-S transect of the WAT showing selected measured sections. See Fig. 2.2.2 for lithological legend. Yellow lines indicate position of synsedimentary faults

Fig. 2.2.4. (page 15): Schematic SW-NE transect of the WAT showing selected measured sections. See Fig. 2.2.2 for lithological legend. Yellow lines indicate position of synsedimentary faults

Fig. 2.2.5. (page 16): Schematic NW-SE transect of the WAT showing selected measured sections. See Fig. 2.2.2 for lithological legend. Yellow lines indicate position of synsedimentary faults

Fig. 2.2.6. (page 17): Schematic SW-NE transect of the WAT showing selected measured sections. See Fig. 2.2.2 for lithological legend. Yellow lines indicate position of synsedimentary faults

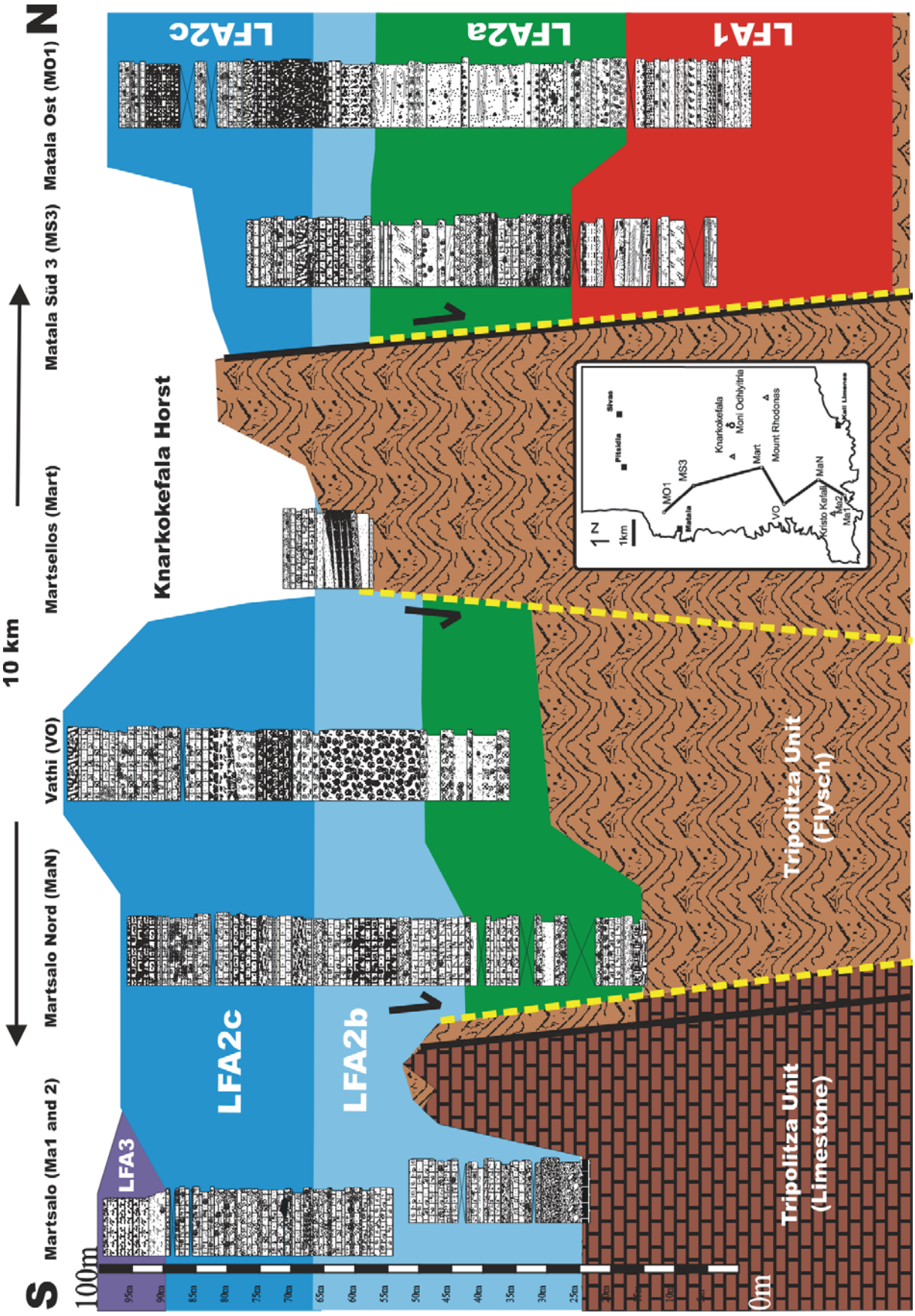
S
Martsalo (Ma1 and 2)
Martsalo Nord (MaN)
Vathi (VO)
Martsellos (Mart)
Matala Süd 3 (MS3)
Matala Ost (MO1)
N
10 km
LFA1
LFA2a
LFA2c
LFA2c
LFA2b
LFA3
Knarkokefala Horst
Tripolitza Unit (Flysch)
Tripolitza Unit (Limestone)
100m
0m
Sivas
Pitsidia
Matala
MO1
MS3
Knarkokefala
Moni Odhiyitria
Mart
Mount Rhodonas
VO
Kristo Kefali
MaN
Ma2
Ma1
Kato Limenas
N
1km

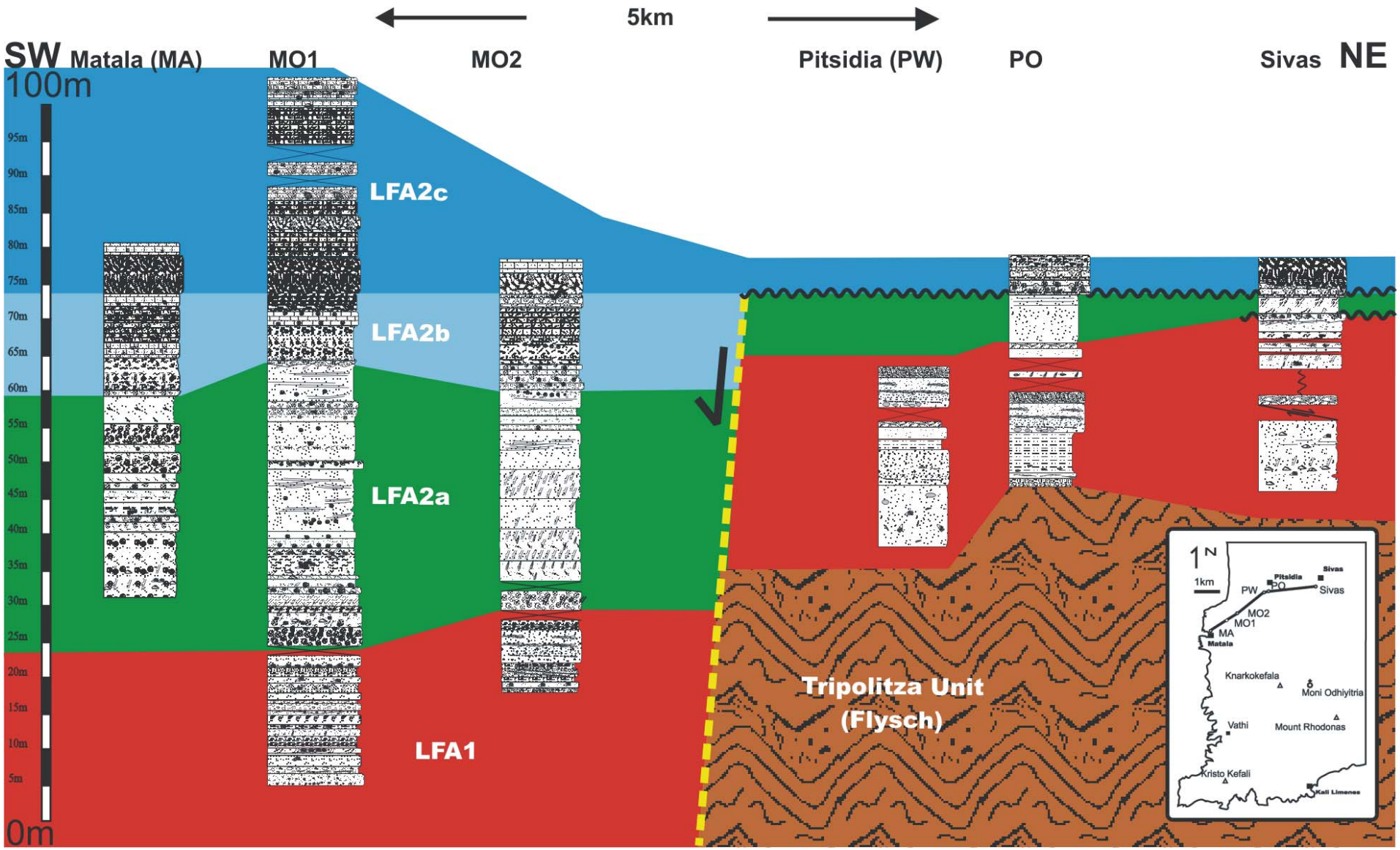
SW
Matala (MA)
MO1
5km
MO2
Pitsidia (PW)
PO
Sivas
NE
100m
95m
90m
85m
80m
75m
70m
65m
60m
55m
50m
45m
40m
35m
30m
25m
20m
15m
10m
5m
0m
LFA2c
LFA2b
LFA2a
LFA1
Tripolitza Unit
(Flysch)
N
1km
Pitsidia
Sivas
PW
PO
Sivas
MO2
MO1
MA
Matala
Knarkokefala
Moni Odhiyitria
Vathi
Mount Rhodonas
Kristo Kefali
Kali Limenes

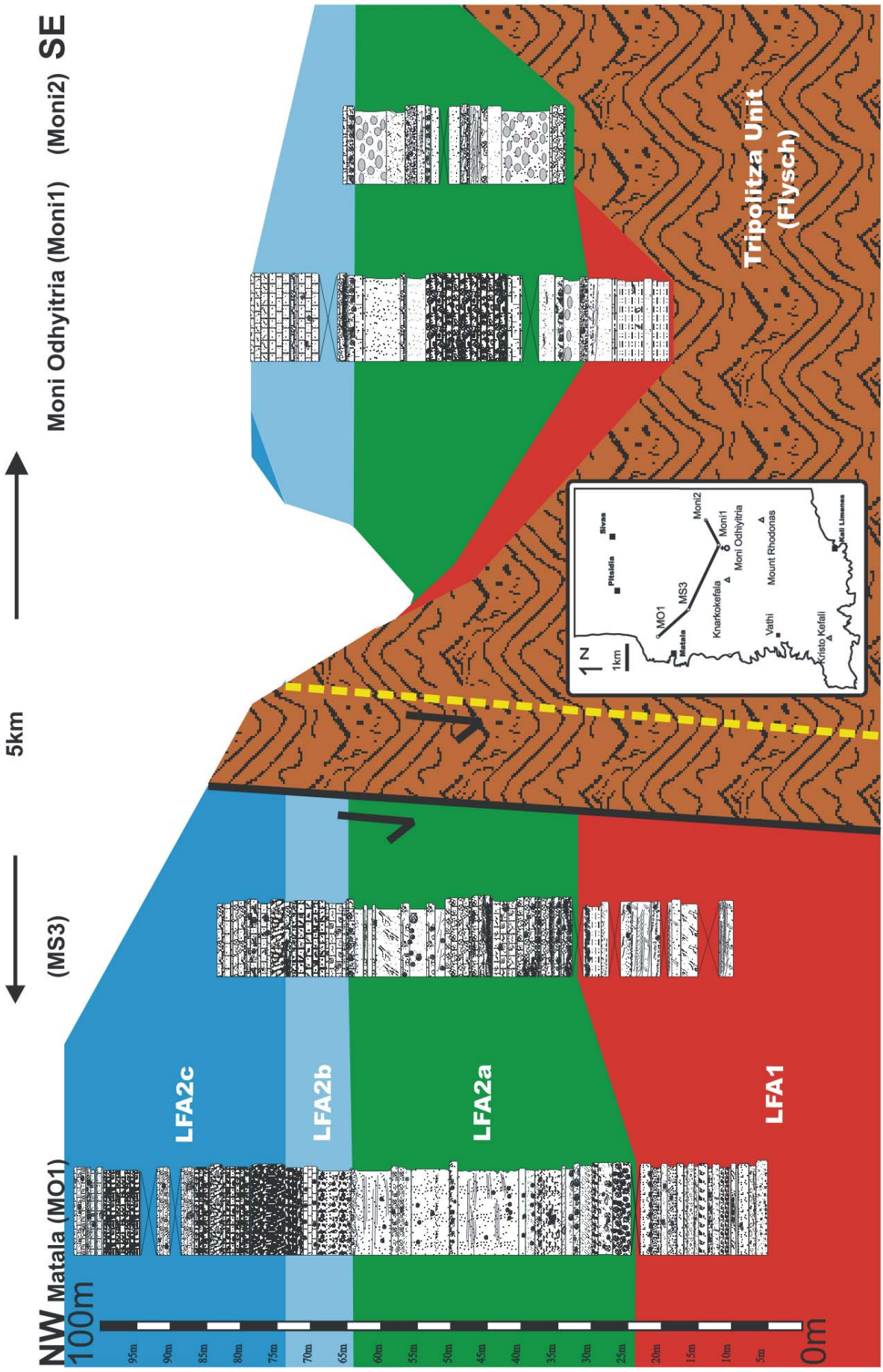
NW
Matala (MO1)
(MS3)
5km
Moni Odhyitria (Moni1)
(Moni2)
SE
100m
0m
LFA2c
LFA2b
LFA2a
LFA1
Tripolitza Unit
(Flysch)
Sivas
Pitsidia
Matala
MO1
MS3
Moni2
Moni1
Moni Odhyitria
Knarkokefala
Mount Rhodonas
Vathi
Kristo Kefali
Kefi Limenas
N
1km

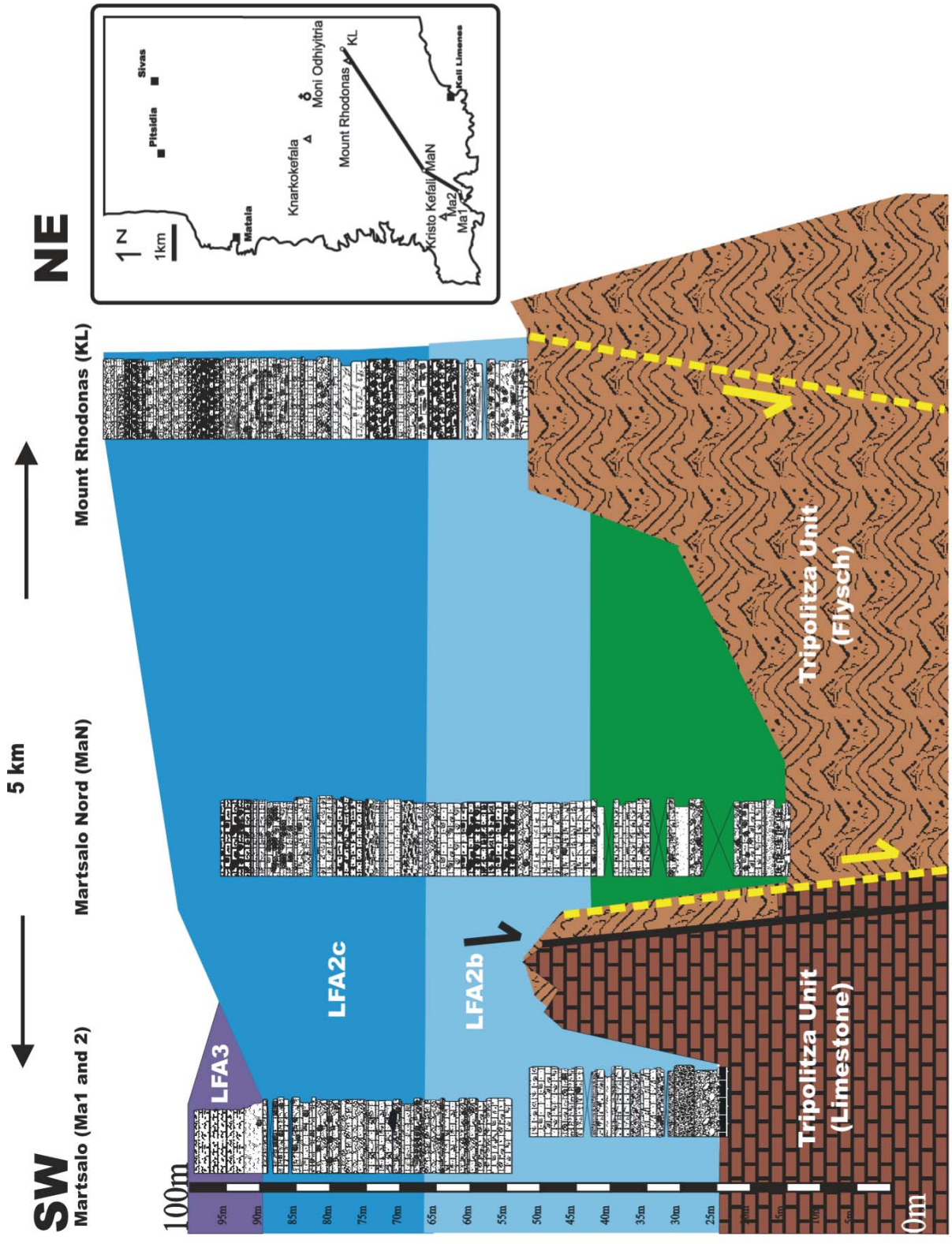
SW
Martsalo (Ma1 and 2)
Martsalo Nord (MaN)
Mount Rhodonas (KL)
NE
5 km
100m
0m
LFA3
LFA2c
LFA2b
Tripolitza Unit
(Limestone)
Tripolitza Unit
(Flysch)
N
1km
Matala
Pitsidia
Sivas
Knarkokefala
Moni Odhiyitria
Mount Rhodonas
KL
Kalí Limenes
Kristo Kefali
MaN
Ma2
Ma1

2.3. Siliciclastic deposits (LFA1)

Introduction

In the WAT, north of an east-west oriented line between the western coast and mount Rhodonas (Fig. 2.2.1.) the basal Neogene sediments are claystone, sandstone and conglomerate. The unconformity at the base of the Neogene is often characterized by conspicuous reddish colouring of the sediments overlying dark brown Flysch deposits (thin to medium bedded sandstone with clay-rich interbeds; Fig. 2.3.1.a). This colouring gave rise to names like Red Beach or Sidheropetra (iron stone). The base of the Neogene is usually formed by blue-greenish to greyish, poorly lithified clay with basal layers of breccia. Between Pitsidia and Sivas, these clays are widespread in the olive orchards. Two kilometres east of Matala clay deposits reach a thickness of 16m (section MS2; Fig. 2.3.1.b, Fig. 2.3.2.). Thickness is variable and is lowest in the southernmost outcrops of LFA1. South of Matala, Pitsidia and Sivas, a horizon of laminated marly limestone and black lignite overlies or is intercalated into basal clay (Fig. 2.3.1.c). Basal clay interfingers with and is overlain by sandstone and conglomerate some of which contains marine fossils (Fig. 2.3.1.d). Clay and silt horizons with an up to 1m thick bed of densely packed *Crassostrea* shells (Fig. 2.3.1.e) are commonly intercalated in the succession. At four locations in the WAT, reef bodies or reef debris occur (Fig. 2.3.1.f).

A maximum thickness of 20-30m of the dominantly siliciclastic succession is reached southeast of Matala and between Pitsidia and Sivas (sections MS3, PS and Sivas; Fig. 2.3.2.). Thickness decreases to the south along the western coastline of the WAT. Wedging out of the unit to the south is also observed in a series of outcrops 1km west of Moni Odhyitria. The unit is characterized by rapid lateral facies change and typically overlain by rhodolith floatstone and –rudstone. Small synsedimentary faults are present at several outcrops. (Fig. 2.3.1.g)

LFA1 deposits are also found along the southern margin of the Messara Plain between Sivas

Fig. 2.3.1. (next page): Sediments of LFA1 (see Fig. 2.3.2. for locations)
a: Intensely coloured base of LFA1 with conglomerate overlying Flysch basement (1,5km southwest of Pitsidia)
b: Basal clay at section MS2 southeast of Matala
c: Laminated marly limestone overlying basal clay at section MS2 with 30cm thick dark layer of coal at the base
d: Sandstone with quartz pebbles typical for LFA1 at section PO 0,5 km southeast of Pitsidia
e: 30cm thick bed formed mainly by the oyster *Crassostrea* intercalated into a succession of clay, sandstone and conglomerate at section MO2 northeast of Matala
f: *Porites* reef 0,5km southeast of Kandhila with columnar to branching corals in a marly matrix. Reef corresponds to the second reef horizon at section Ka1 (Fig. 2.3.4., A1)
g: Synsedimentary fault within clay, silt and coarse sandstone with pebble deposits 2km northeast of Matala at the road to Pitsidia with an offset of approximately 1m

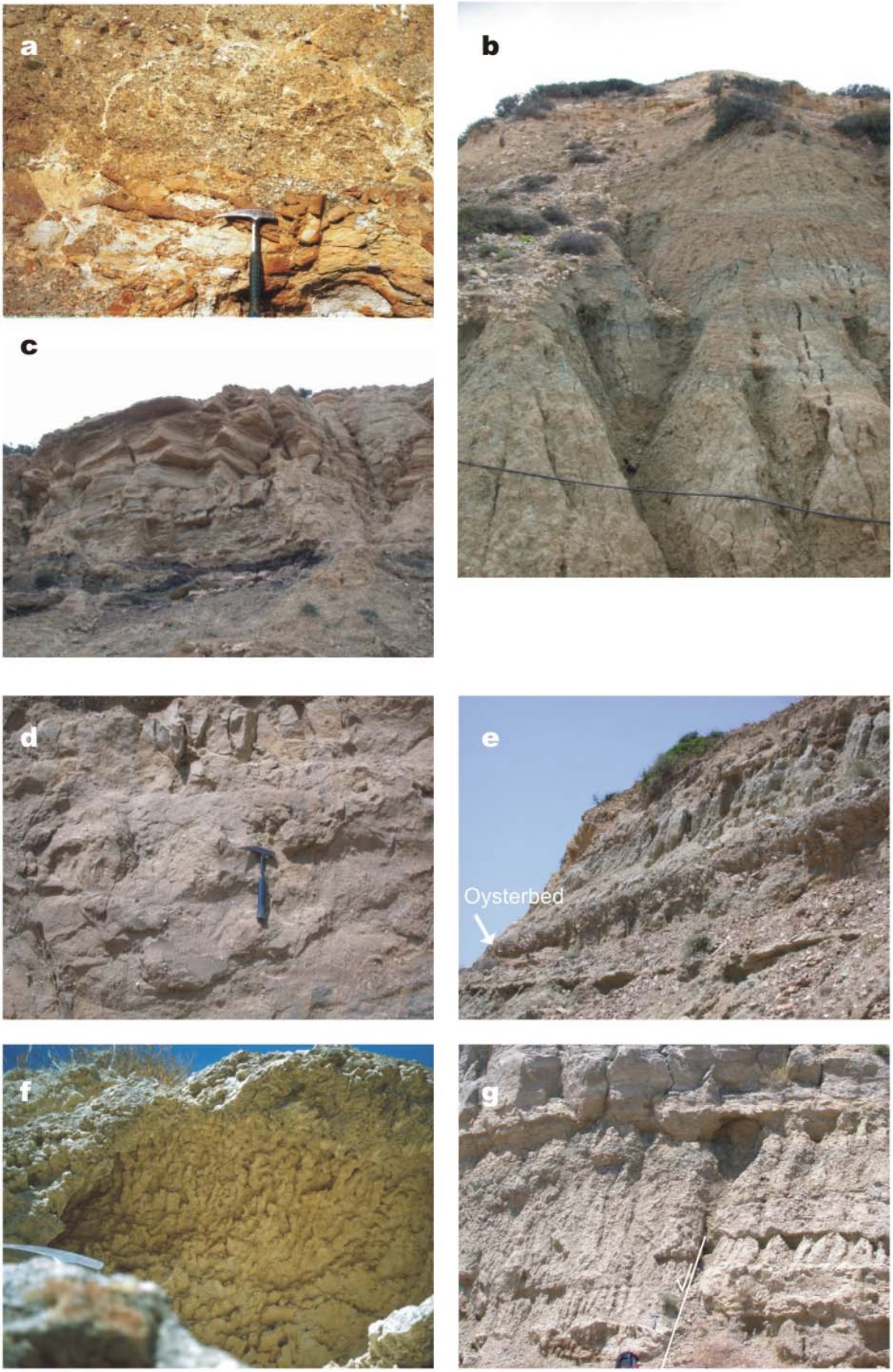
a
b
c
d
e
Oysterbed
f
g

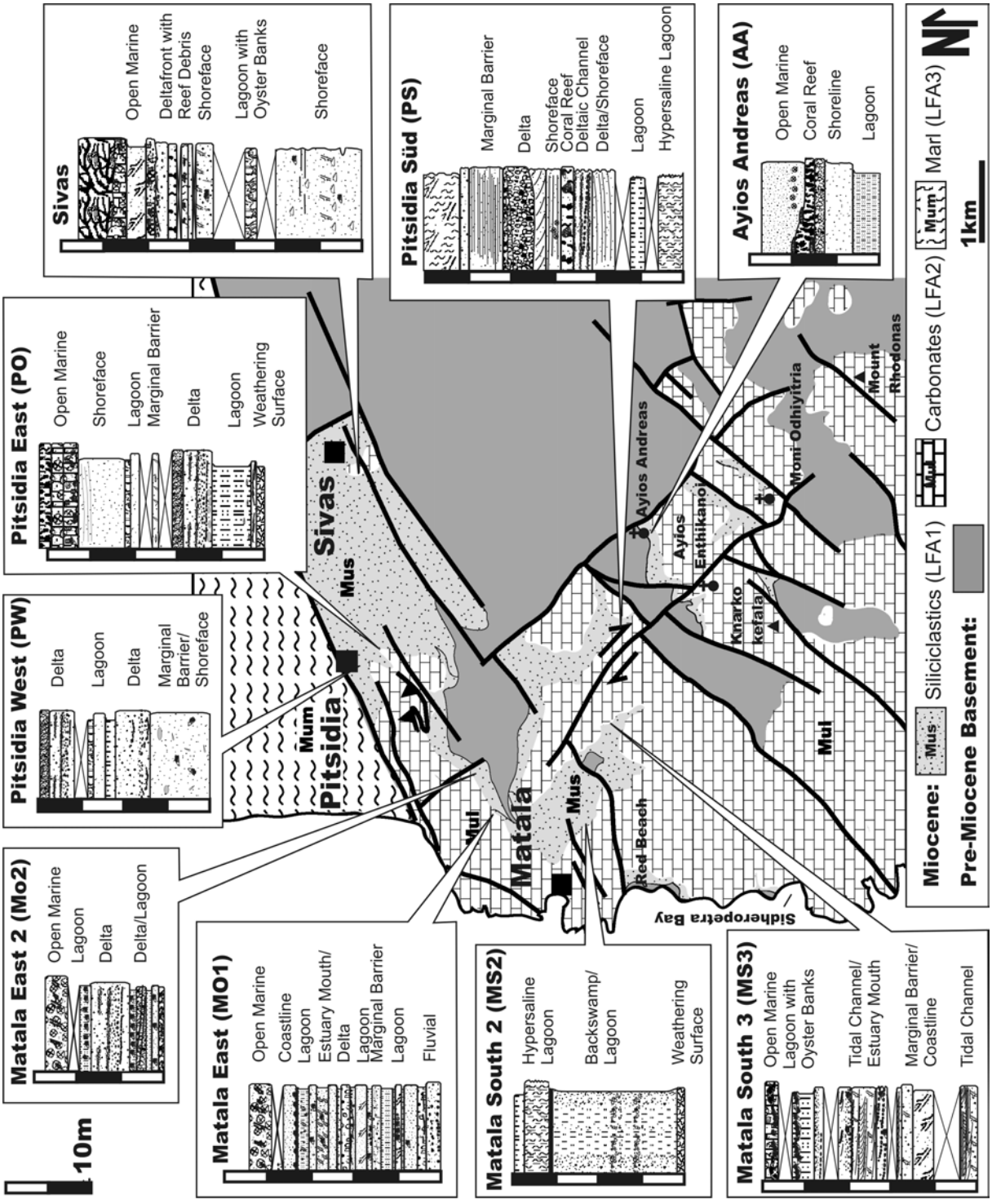

Fig. 2.3.2.: Geological map of the northern part of the WAT with sections of LFA1 and interpretation of sedimentary environments. Note rapid lateral and vertical facies change between sections. See Fig. 2.2.2. for lithological legend

and Vasiliki (Fig. 1.4.1.) and reach a thickness of 22m 0,5 km south of Kandhila (section Ka1, Fig. 2.3.3.; Fig. A1). Like in northern part of the WAT, the unit is characterized by interfingering of clayey and sandy lithologies with conglomerate and horizons with coral framestone and coral debris. In the transect south of Kandhila (Fig. 2.3.3.) and at the road to Lentas, directly south of Vasiliki (Fig. 1.4.1.), the unit is observed to wedge out to the south.
In the central Messara Plain in a section 1km north of Festos (Fig. A2), clay with *Crassostrea,* sandstone and conglomerate of LFA1 are overlain by LFA2 and 3.

Lithologies

Clay and silt with plant remains

Description: The blue-greenish to greyisch, poorly lithified clay is either horizontally bedded and contains silty to sandy interbeds (Fig. 2.3.4.a) or lacks pronounced sedimentary structures (Fig. 2.3.1.b). The clay may contain angular gravel and commonly overlies a basal layer of breccia. Two kilometres southwest of Pitsidia it contains plant remains of *Carpinus betulus, Salix sp., Pinus sp.,* and *Taxodium sp.* as well as specimens of the family of the Leguminosae and Lauraceae (Sachse, pers. comm.; Fig. 2.3.4.b-d). No marine fossils have been found in these sediments. The lithology is found southeast of Matala (section MS2, Fig. 2.3.2.), north of Moni Odhiyitria (section Moni1) and south of Pitsidia (section PS, Fig. 2.3.2.; 2.3.5.a).
Facies analysis and interpretation: The described lithology is interpreted to represent overbank and backswamp deposits with soil horizons and sediments of fresh water dominated lagoons. Plant remains reflect the proximity of forests with a flora typical for humid, temperate to subtropical climatic conditions (Sachse, 1997).

Fig. 2.3.3. (next page): Transect south of Kandhila. See Fig. 1.4.1. for location and Fig. A1 for enlarged sections. Note that section Ka 2 has been measured on the opposite side of the valley, approx. 100m to the southeast.

Fig. 2.3.4. (page 23): Lagoon and Estuary deposits of LFA1 (see Fig. 2.3.2. for locations)
a: Clay and silt with plant remains facies at the base of section PO
b: Inflorescence of *Carpinus betulus*, 1km southwest of Pitsidia, scale is 2cm
c: Leaves of 1: Lauraceae indet and 2: *Salix* sp., 1km southwest of Pitsidia, scale is 2cm
d: Fragmented leave of *Taxodium* sp., 1km southwest of Pitsidia, scale is 2cm
e: Laminated marly limestone facies with basal lignite, section MS2
f: Oysterbed with abundant *Crassostrea* (Clay- and siltstone with *Crassostrea*-beds facies) 300m northeast of red beach (see Fig. 2.2.1. for location)
g: Siltstone of the Clay- and siltstone with *Crassostrea*-beds and intervals bioturbated by *Thalassinoides*; 15m above the base of section MO1

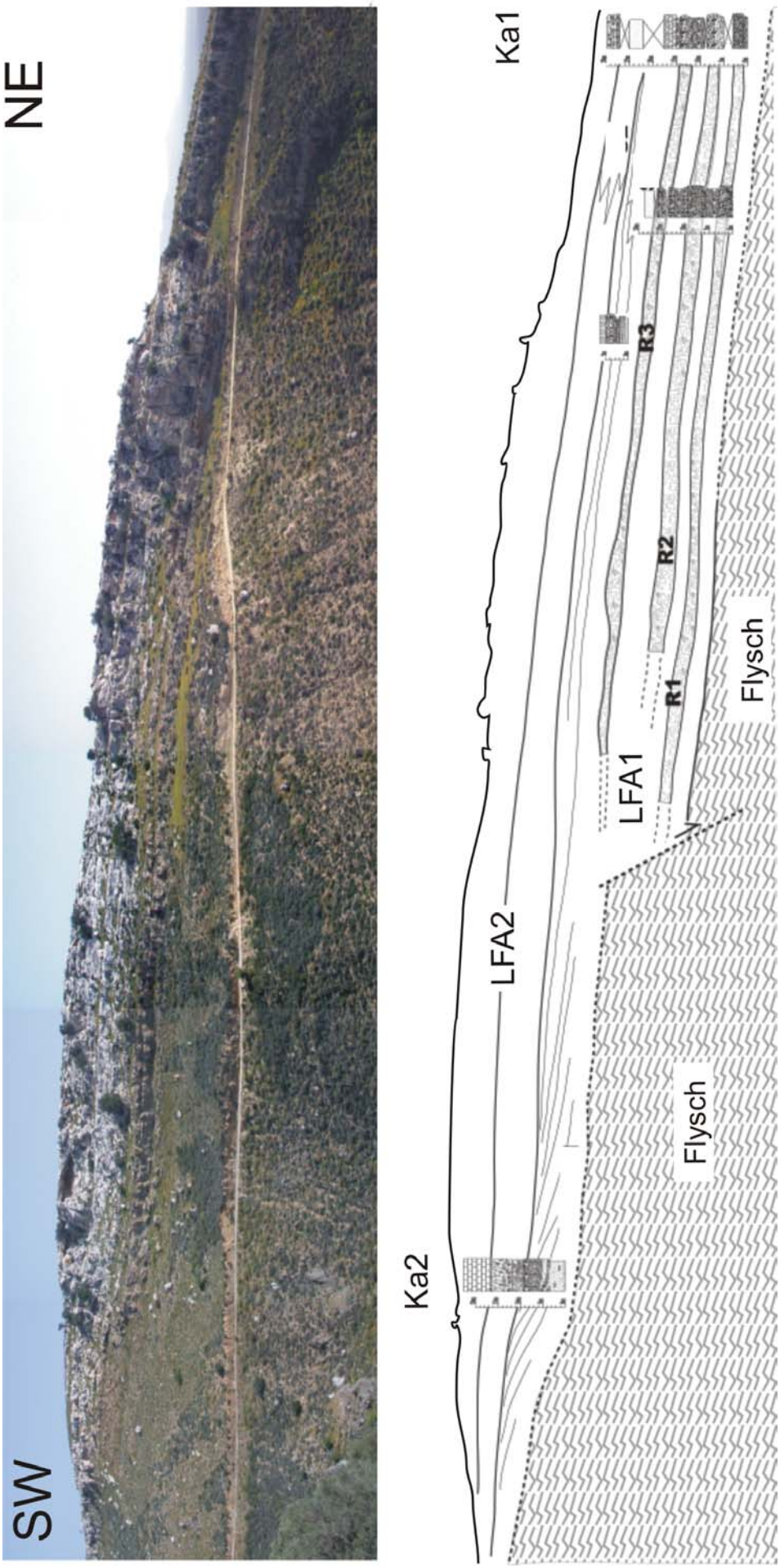
NE
SW
Ka1
Ka2
LFA2
LFA1
R3
R2
R1
Flysch
Flysch


a


b


c
②
①


d


e


f
100μm


h

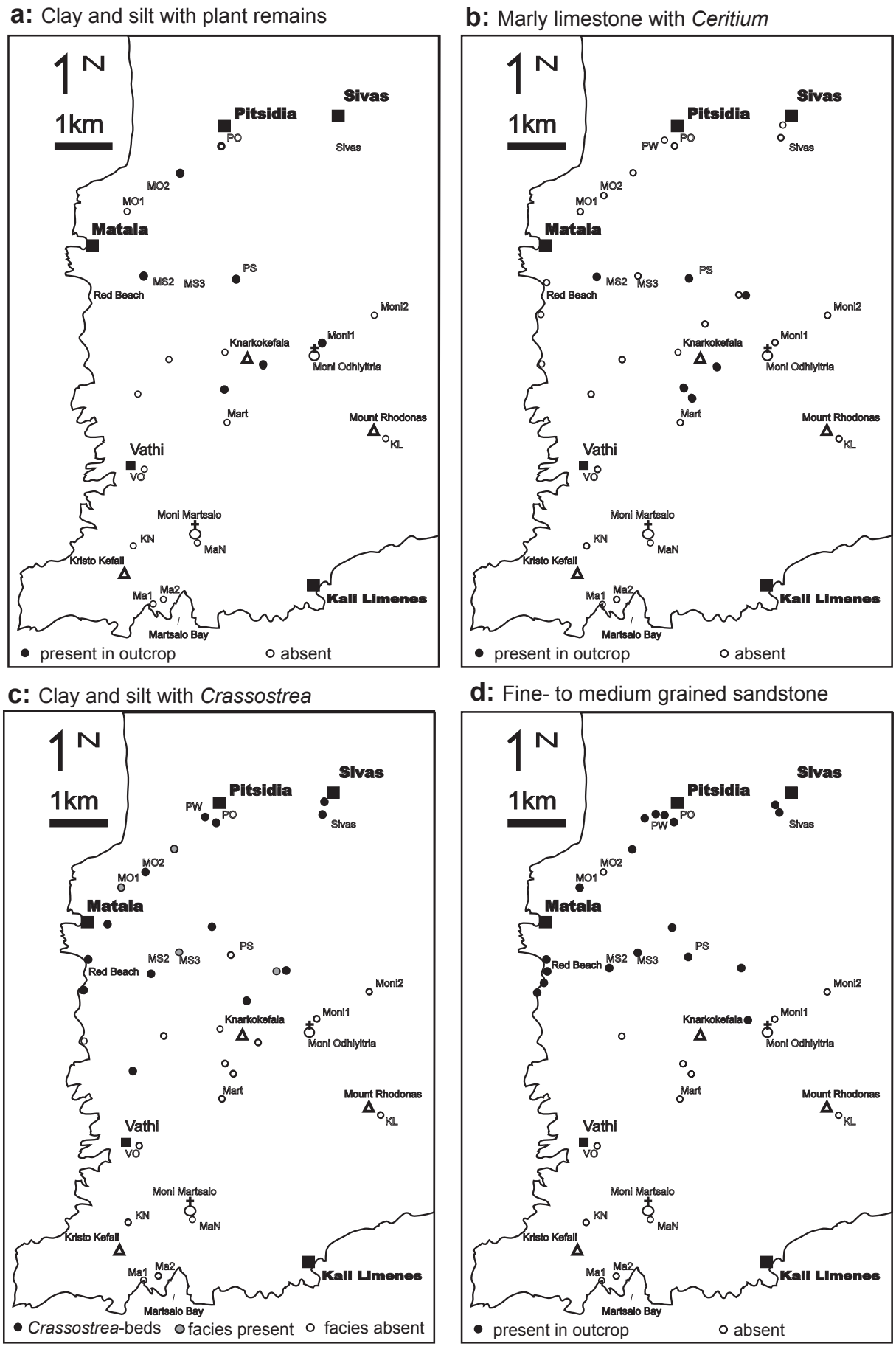

Fig. 2.3.5.: Outcrops of lagoon and coastal sand deposits of LFA1 in the WAT

Marly limestone with Ceritium

Description: The lithology is characterized by thin-bedded, whitish, marly limestone (Fig. 2.3.4.e). Beds are internally laminated or homogenous and contain gastropods (e.g. *Theodoxus sp., Ceritium sp.*), bivalves, ostracods (*Cyprideis sp.*) and charophytes. Small gypsum crystals or pseudomorphs after gypsum crystals occur also. The unit overlies or is intercalated into basal clay and at the base up to 50 cm thick coal beds are found. Marly limestone reaches a thickness of 3m (sections MS2, PS; Fig. 2.3.2.). The lithology is common southeast of Matala (Fig. 2.3.5.b) and it forms the southernmost outcrops of LFA1 one kilometre south of Knarkokefala.

Facies analysis and interpretation: Horizontal lamination in fine-grained sediments reflects low energy hydraulic conditions and the absence of endobenthos due to hostile bottom conditions. Faunal elements found in the laminated marly limestone tolerate variable salinity: Species of the genus *Cyprideis* are found in fresh water to hypersaline environments (Athersuch et al., 1989). Gypsum crystals or pseudomorphs after gypsum document hypersaline conditions. The occurrence of charophytes on the other hand evidences temporal or seasonal fresh water input. This implies an environment, which is subject to seasonal salinity changes such marginal marine lagoons that have limited access to ocean waters. Temporal hypersaline conditions require high rates of evaporation and indicate arid climatic conditions.

Lignite underlying the limestone is interpreted to have been formed in coastal marshes and swamps bordering the lagoon

Clay- and siltstone with Crassostrea

Description: The blue-grey to brownish clay and silt is characterized by the occurrence of *Crassostrea* shells and up to 1m thick beds with densely packed *Crassostrea* (Fig. 2.3.4.f). Specimens reach a length of 20cm and besides *Crassostrea* various specimens of *Ostrea* and infaunal bivalves occur. The sediment is poorly classified and contains coarse sand and pebbles. It is also poorly lithified and bedding is rarely preserved. Silty intervals are bioturbated by *Thalassinoides* (Fig. 2.3.4.g).

Up to 3m thick units of clay- and siltstone with *Crassostrea* beds are intercalated into the sandy lithologies east and south of Matala (Fig. 2.3.5.c; Fig. 2.3.2.; sections MS3, MO1 and 2;), at Pitsidia (sections PW and PE) and south of Sivas (section Sivas). The southernmost occurrence of an oyster bed is 1,5km southeast of Sidheropetra Bay. Two kilometres southeast of Matala, two levels with densely packed *Crassostrea* occur. At section MO2 *Terebralia* sp. occurs together with *Crassostrea*. At section MO1 (7,5m above the base) sandy layers are interbedded with wavy clay layers that are up to 1cm in thickness.

At the road to Lentas, 0,5km south of Vasiliki, a 30cm thick bed with *Crassostrea* encrusted by *Porites* is intercalated in a 10m thick unit of marl and blue and yellow silt at the base of the succession. It is overlain by 6m of blue and yellow clay and silt with infaunal bivalves, *Conus* sp. and *Strombus* sp. One kilometre north of Festos, clays with *Crassostrea* are found in olive orchards.

Facies analysis and interpretation: Species of *Crassostrea* are commonly found in marine settings with slightly reduced salinity and in brackish environments. They are thus typically found in lagoons with perennial fresh water input and near river mouths (Pastorino and Guineri, 2000). *Crassostrea* banks are also commonly associated with magroves in tropical estuaries, for example in Chesapeake Bay in the southeastern United States (Cowardin et al., 1979). An association with mangroves has also been reported for several modern species of *Terebralia* (Ellison et al., 1999). Deposition of the clay and silt deposits with *Crassostrea* in an estuarine environment as described by Reinson (1992) is also suggested by sedimentary structures and composition: Dominance of fine-grained sediments indicates deposition in a low energy environment. Poorly classified sediments are deposited on the landward side of estuaries as a consequence of rapid loss in current energy at river mouths. Wavy clay drapes on sand layers that probably represent wave ripples found at section MO are interpreted as tidal deposits (Dalrymple, 1992) that reflect marine influence. Bioturbation by *Thalassinoides* is also common in estuarine environments (Howard and Frey, 1973).

Fine- to medium grained sandstone with molluscs and echinoids

Description: Sandstone of this lithology is beige to brown in colour, poorly lithified with low amounts of carbonate cement and relatively immature. Grain size ranges from silt to coarse sand but is dominantly fine to medium sand. Apart from quartz, the sandstone contains varying amounts of feldspar, mica and lithic minerals. In most cases the sandstone it is either

without preserved sedimentary structures or shows horizontal bedding to low angle planar- and trough crossbedding (Fig. 2.3.6.a). In some cases, bioturbation by *Thalassinoides* is observed. Marine fossils, such as bivalves (mostly *Ostrea*), gastropods (*Turitella* s.l.), irregular echinoids (*Schizaster* sp.) and foraminifera (*Amphistegina* sp., *Elphidium* sp., *Ammonia* sp., *Triloculina* sp. and various miliolids; Fig. 2.3.6.b) are common. At Sivas, where sandstone under- and overlies coral debris, *Borelis* sp. is also common.

Up to 10m thick (section Sivas, Fig. 2.3.2.) units of the sandstone are intercalated in LFA1 in the WAT north of Moni Odhiyitria and Sidheropetra Bay (Fig. 2.3.5.d) and interfinger with the clay and silt with *Crassostrea* facies and with conglomerate. At the southwestern margin of the village of Pitsidia (section PW) the base of the section is formed by 7 m of massive, brown, fine grained sandstone with turritellid gastropod casts and small oyster shells. It replaces the blue-greyish clay and silt with infaunal bivalves found east of Pitsidia (section PE). Concretions formed around pieces of fossil wood or molluscs are also common southwest of Pitsidia.

At section MS3, decimetre scale to metrescale trough crossbeds cut into horizontally laminated sandstone and sandstone with wave ripple crosslamination and centimetre scale sigmoidal crossbeds (Fig. 2.3.6.c-e). Carbonate content in the horizontally laminated limestone is higher than in other sediments of this lithology. Grains are moderately rounded and a large proportion consists of quartz sand. Thin section analysis of a laminated bed reveals that alternating 1-5mm thick laminae have very distinct petrographical and biotic compositions (Fig. 2.3.6.f): Well cemented limestone laminae with few siliciclastic components rich in miliolid foraminifera and geniculate coralline red algal fragments (Fig. 2.3.6.g) alternate with sandstone that has similar components as in other sections (Fig. 2.3.6.b).

Fig. 2.3.6. (next page): Coastal sands of LFA1 (see Fig. 2.3.2. for locations)
a: Low angle planar and trough crossbedding in sandstone at the road from Pitsidia to Matala 0,5km west of Pitsidia. West is to the right
b: Thin section photograph of sandstone at 18m above the base of section Sivas (sample S1). Benthic foraminifera are 1: *Elphidium* sp., 2.*Amphistegina* sp. and 3. *Borelis* sp. and various miliolids
c: Sandstone with sigmoidal crossbeds, base of section MS3. View to the east
d: Sandstone displaying horizontal bedding cut by trough cross-bedding, base of section MS3. View to the northeast
e: Wave ripple crosslamination in sandstone at the base of section MS3, 2km southeast of Matala. View to the east
f: Thin section photograph of horizontally laminated sandstone (sample MD1) at the base of section MS3. Note that laminae that are a few mm in thickness have conspicuously different components characteristic of a restricted marine environment in the upper half of image and characteristic for open marine sediments in the lower part of the image similar to Fig. 2.3.6.b
g: Thin section photograph of horizontally laminated sandstone at the base of section MS3 showing a layer with biotic elements indicative of restricted environments such as miliolid foraminifera (1) and geniculate coralline red algae (2), MD1

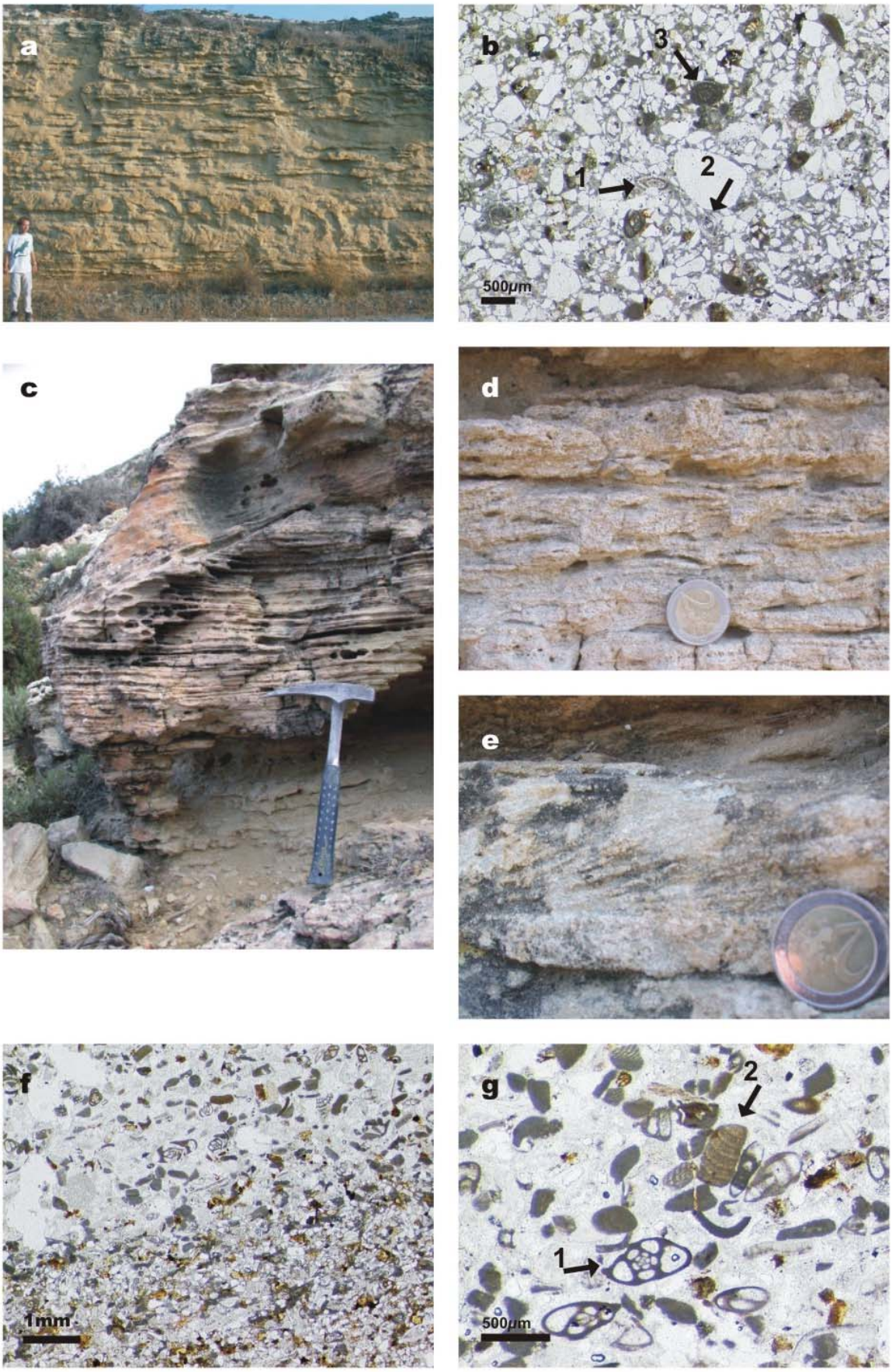
a
b
3
1
2
500µm
c
d
e
f
1mm
g
2
1
500µm

Fine- to medium grained sandstone is also found in outcrops of LFA1 at the southern margin of the Messara Plain: South of Kandhila (section Ka1, Fig. A1) and 500m south of Vasiliki at the road to Lentas (Fig. 1.4.1.) it is intercalated between conglomerate and coral horizons. It is also found at the top of the 20m thick succession of LFA1 deposits. West of the road from Plora to Ayios Kirillos, 1km south of Plora similar sandstone occurs interbedded with *Porites* debris. At the top of the succession sandstone contains angular cobbles and blocks up to 30cm in diameter. Sandstone rich in Heterostegina overlies the succession.

Facies analysis and interpretation: In many cases original sedimentary structures appear to have been destroyed by bioturbation. *Thallassinoides* burrows are typical for sandy sediments in a variety of marine environments from shallow subtidal to outer shelf (Bromley, 1999). The combination of trough- and planar crossbedding of the fossiliferous sandstone, however, indicates that it was deposited in a coastal environment. While trough crossbeds indicate deposition in a shoreface environment, planar crossbeds are interpreted to be associated with barrier systems such as washover deposits on the landward side and barrier beaches on the oceanward side. Wave ripple crosslamination at section MS3 indicates an intertidal origin that is also documented by the bimodal composition of laminae: Limestone laminae are rich in geniculate corallines that are often found in subtidal channels and intertidal flats of temperate environments (Burne and Colwell, 1982) and miliolid foraminifera that are common in restricted environments with increased salinities (Hallock and Glenn, 1986). Sandstone laminae are deposited during incoming tide while limestone laminae are deposited during outgoing tide, when lagoon sediments are transported seaward. Tidal environments are described in detail in Dalrymple et al. (1992) and Reinson (1992). Accordingly, trough crossbedded units cutting into horizontally laminated sediments and sandstone with wave ripples are interpreted to represent scour channel sediments that cut into tidal ridge and shallow channel sediments situated between the open sea and the landward lagoon. The interfingering of sediments of this lithology with lagoon sediments argues for a deposition in a coastal environment including shoreface and shore parallel sand bar systems.

Pebble conglomerate with siliciclastic matrix and coarse grained sandstone with pebbles

Description: Trough crossbedded conglomerate and coarse grained sandstone forms up to 6m thick beds and laterally limited bodies in erosional contact with underlying sediments. More rarely up to 1m thick beds of conglomerate with sigmoidal bedding occur. Conglomerate beds

and -bodies consist of sub- to well rounded, poorly sorted pebbles < 3 cm in diameter. Conglomerate is either component supported or becomes matrix supported to the top and grades into coarse grained sandstone. The matrix is composed of silt to coarse grained immature sand (poorly classified, angular grains, rich in feldspar, lithic components and mica). Coarse grained immature sandstone bodies have layers of pebbles at the base. Fossils are rare fragments of bivalves and oysters or non-geniculate coralline red algae (Fig. 2.3.7.a).

Bodies and beds of trough bedded coarse grained sandstone with pebbles are intercalated into fine grained sand and clay deposits in a well defined area in the northern part of the WAT between Matala and Sivas and up to 2km to the southeast of Matala (Fig. 2.3.8.a). A component supported conglomerate body with a calcareous sand matrix is found 2km south of Pitsidia (section PS, Fig. 2.3.2.). At this location, the cross-cutting relationship of trough bedded sand- and conglomerate bodies with surrounding fine grained sandstone is well documented (Fig. 2.3.9.). The thickest (6m) body of trough bedded conglomerate is found 0,5km southwest of Sivas, north of the measured section. South of Pitsida (sections PW, PE; Fig. 2.3.2.), a 1m thick bed of sigmoidally crossbedded conglomerate (Fig. 2.3.7.b) with foresets dipping in a southwesterly direction overlies sandstone with gravel.

A succession of sandstone is also found at the base of section FN (Fig. A2) situated 1km north of the archaeological site of Festos. It consists of 5m of poorly lithified, non-fossiliferous fine- to middle grained, well-rounded quartz sand. The sandstone is overlain by non-fossiliferous decimetrescale planar crossbedded fine to coarse grained sandstone with pebbles (Fig. 2.3.7.c). In one bed decimetrescale sigmoidal crossbedding is visible (Fig. 2.3.7.d). The succession overlies blue to brown clay and silt with *Crassostrea* that is poorly represented in outcrop and underlies 3m of LFA2 equivalent deposits.

Facies analysis and interpretation: Grain composition and sedimentary structures of the described sandstone and conglomerate is typical for alluvial channel fills or bar and bedform deposits described by Miall (1992). Sigmoidal foresets in finegrained conglomerate indicate

Fig. 2.3.7. Delta deposits of LFA1 (see Fig. 2.3.2. for locations)
a: Sandstone with pebbles and rare oyster fragments (arrow) 1km southwest of Sivas
b: Sigmoidally crossbedded conglomerate at section PO. View is to the northwest
c: Planar bedded sandstone and conglomerate north of Festos (basal part of section FN)
d: 10cm thick bed with sigmoidal crossbedding 8m above the base of section FN
e: Massive conglomerate in the basal 5m of LFA1 at the road from Vasiliki to Lentas. Arrow points to sea cow rib
f: Sigmoidally crossbedded conglomerate in the southern part of the transect south of Kandhila (Fig. 2.3.4.). View is to the northwest
g: Cobble conglomerate at the top of LFA1 south of Kandhila. Matrix is sandy limestone. Note high proportion of green to brown serpentinized ultramafic rocks
h: Boulder of reworked reef limestone (arrow) in conglomerate at the top of LFA1 south of Kandhila


a
b
c
d
e
f
g
h

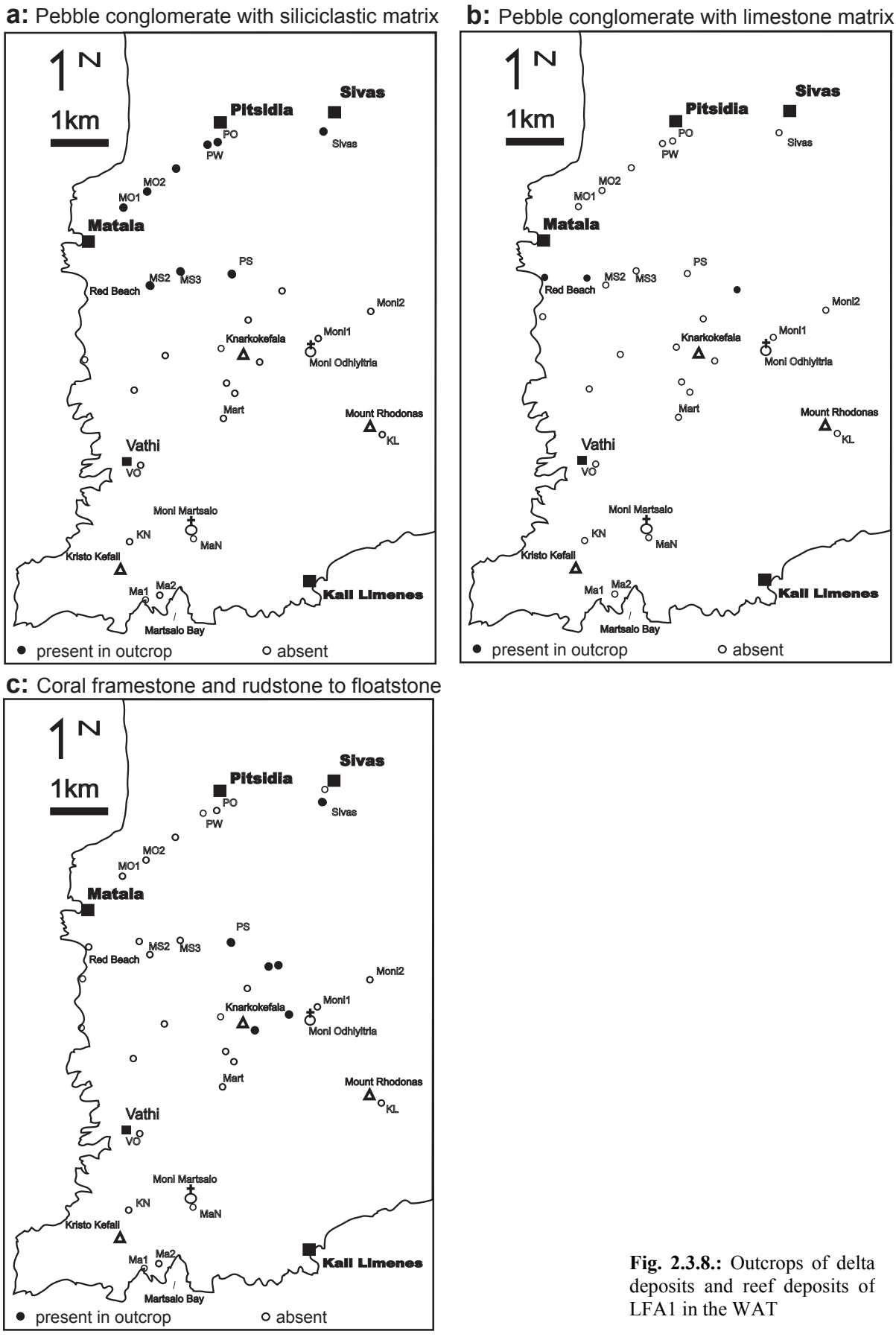

Fig. 2.3.8.: Outcrops of delta deposits and reef deposits of LFA1 in the WAT

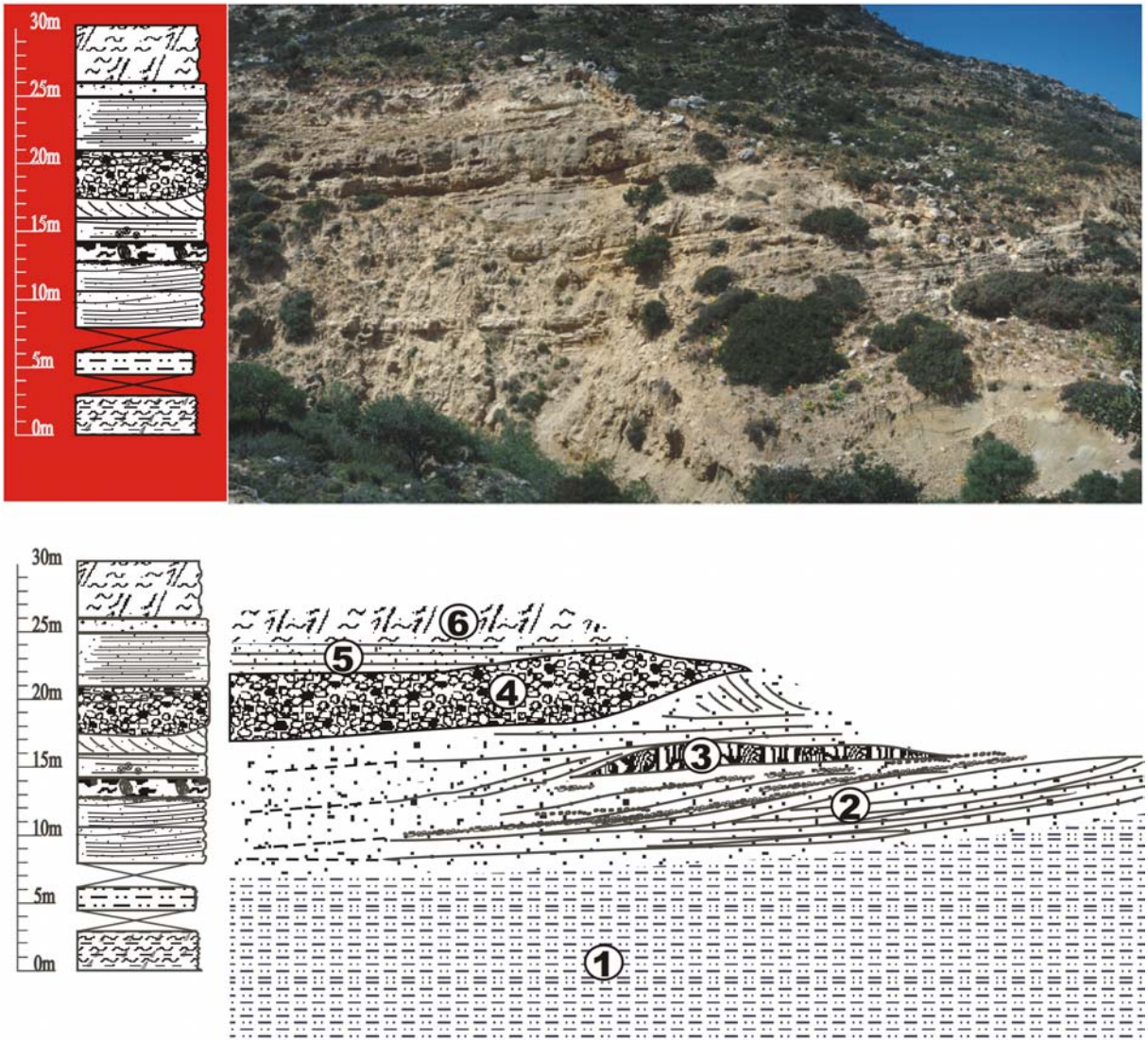

Fig. 2.3.9.: Outcrop situation of LFA1 south of Pitsidia (section PS, Fig. 2.3.2). The lower part of the figure shows a sketch of spatial extent of lithologies in the picture above. Note rapid vertical and lateral facies change: 1: brackish lagoon deposits; 2: planar to trough crossbedded coastal and deltaic sandstone; 3: coral reef; 4: deltaic trough crossbedded sandstone and conglomerate; 5: hoizontal to low angle crossbedded coastal sandstone; 5: marl deposited in a protected marine environment

propagation into relatively low energy water bodies. The association of the described, mostly non-fossiliferous lithology with brackish clays and coastal sands suggests deposition on a delta plain of a braid delta *sensu* McPherson et al. (1987) by delta distributaries in a marginal marine environment.

Pebble conglomerate with limestone matrix

Description: Instead of a sandstone matrix, conglomerates are also observed to have a well cemented micritic limestone matrix with fine grained siliclastic sand. These conglomerates

are grain or matrix supported and poorly sorted with well classified pebbles 0,5-1cm in diameter. Rare larger pebbles are up to 3cm in diameter. Pebbles are moderately to well rounded.

Outcrops of this lithology are found north of Red Beach, where it overlies a 6m thick succession of sandstone with a silty *Crassostrea* bed at the base and at Ayios Andreas, overlying 4m of fine sandstone and underlying a coral reef. At red beach, the conglomerate contains bivalve shells. At Ayios Andreas, horizontal to low angle planar crossbedding is preserved. Conglomerate with limestone matrix occurs east and west of locations where trough crossbedded conglomerate bodies are found (Fig. 2.3.8.b). Both types of conglomerate are not found together in the same area.

Facies analysis and interpretation: Conglomerate that is matrix supported and consists of two grain size classes of material, gravel sized clasts and a sand and/or mud matrix is typical for gravely shorefaces and beaches (Hart and Plint, 1995). The presence of bivalves also indicates marine influence and planar crossbedding at Ayios Andreas is indicative of a beach environment. The distribution of conglomerate with limestone matrix relative to trough bedded conglomerate bodies suggests that they represent delta deposits reworked along the shoreline.

Pebble - cobble conglomerate

Description: Conglomerates of this lithology are characterized by cobble sized components including blocks up to 30cm in diameter.

Conglomerates with cobble-sized components within LFA1 were not found in the WAT but only along the southern margin of the Messara Plain.

At the road to Lentas, 0,5km south of Vasiliki (Fig. 1.4.1.), 2m of crossbedded coarse sand with conglomerate and 1m of massive conglomerate with coarse gravel up to 25cm in diameter overlies basal clay and silt with *Crassostrea*. Conglomerate contains rare sea cow ribs (Fig. 2.3.7.e). It is overlain by a 2m thick bed of limestone with *Porites* debris and gravel that wedges out to the north.

At the southern limit of the village of Kandhila (Fig. 1.4.1.; section Ka1, Fig A1), three beds of conglomerate, interbedded with coral framestone and coral debris occur. The lowermost bed consists of coarse, poorly rounded and sorted, grain supported conglomerate with a clay-silt to sand matrix as in Fig. 2.3.7.e. Components in the second conglomerate horizon are well

rounded, up to 20cm in diameter, poorly sorted and the matrix is marly. The third horizon overlying the uppermost coral reef unit has a poorly cemented siliciclastic limestone matrix and is normally graded. Internal sedimentary structures are not observed. To the southwest, in the transect south of Kandhila (Fig. 2.3.3.), this succession is in tectonic contact with Flysch basement. Eastward, towards the road to Lentas, conglomerates wedge out and become interbedded with marly and sandy deposits. The succession is overlain by fine to coarse grained sandstone.

Southwest of Kandhila (Fig. 2.3.3., section Ka2 – Fig. A1), the uppermost conglomerate that overlies Flysch basement and sandstone in the southern part of the transect and the succession described above in the northern part, shows metre-scale sigmoidal crossbedding (Fig. 2.3.7.f). Foresets are formed by conglomerate with coarse grained sandstone matrix that passes into sandstone. Foresets dip in a northeasterly direction. To the top of the unit and towards the village of Kandhila, the proportion of limestone in the matrix increases and the conglomerate becomes matrix supported (Fig. 2.3.7.g). The top of the conglomerate shows subhorizontal planar bedding. Components are up to 25cm in diameter and contain a large fraction of green, serpentinized mafic basement (Fig. 2.3.7.g, h) and red chert. The conglomerate also contains a block of *Porites* framestone 30cm in diameter that is lithologically similar to underlying coral framestone units (Fig. 2.3.7.h). Northward, the conglomerate with limestone matrix passes into bioturbated, fine to middle grained calcareous sandstone that overlies the interbedded conglomerate and coral horizons in the north of the transect, near the village of Kandhila. Conglomerate is overlain by a rudstone with *Clypeaster*, *Pecten, Heterostegina* and balanids of LFA2.

Facies analysis and interpretation: The large size of components suggests high relief and the predominance of certain types of components indicates a local origin. Conglomerates form extensive sheets without internal sedimentary structures that indicate deposition in a fan delta described by Massari and Colella (1988) rather than on an extensive delta plains. The high amount of well rounded components and the grain supported character of the sediments rules against deposition as mass flow deposits. According to the description of Massari and Colella (1988), conglomerate south of Kandhila that is interbedded with coral debris or coral framestone is interpreted to represent the inner to middle fan deposits that pass into subtidal outer fan deposits towards the east.

Conglomerate with sigmoidal crossbeds in the transect southwest of Kandhila shows foresets similar to a Gilbert type delta. Crossbeds are according to the original concept of Gilbert the result of the delta front prograding into a standing body of water (Postma and Roep, 1985). In

the case of the conglomerate south of Kandhila it reflects progradation in a lagoon or low energy marine water body. At a wave influenced shoreline, however, delta front deposits, may partially be reworked (Colella, 1988; Massari and Parea, 1990). Reworking is observed at the top of the sigmoidally bedded conglomerate bed south of Kandhila: The top is formed by subhorizontally bedded wave-worked topset beds and the northward transition of the conglomerate into sandstone is interpreted to represent the transition into deeper water.

Coral framestone and rudstone

Coral framestone forms up to 8m wide and 4m thick bodies that are build up mostly by *Porites* (Fig. 2.3.10.a) and to a lesser degree by *Tarbellastrea,* rare *Acanthastrea* (Fig. 2.3.10.b) and *Siderastrea*. *Porites* colonies show columnar to coniform-branched, nodular and platy morphologies. Branches of colonies are between 1 and 5cm in diameter. *Tarbellastrea* forms massive, tabular to globular colonies up to 40cm in diameter. Framestone bodies laterally pass into up to 2,5m thick beds mainly consisting of horizontally oriented columnar *Porites* (Fig. 2.3.10.c, d) and, more rarely, of fragments of *Tarbellastrea* or *Acanthastrea*. Matrix ranges from marly silt to coarse grained sandstone. Diameter of erect *Porites* colonies is observed to increase with grain size of the matrix.

In the WAT, occurrences of coral framestone and beds with coral debris within LFA1 are concentrated in the Ayios Andreas – Moni Odhiyitria area (Fig. 2.3.8.c; sections AA, PS; Fig. 2.3.2.). Beds are intercalated into fine grained sandstone or trough bedded coarse grained sandstone. At Ayios Andreas, an up to 4m thick framestone body with *Tarbellastrea* colonies up to 40cm in diameter in the upper central part of the body and *Porites* at the base overlies a 2m thick bed of conglomerate with limestone matrix.

In the Kandhila – Vasiliki area, up to three distinct coral units are intercalated into conglomerate and fine grained sandstone described above (Fig. 2.3.3.; A1). They have a lateral extent of at least 100m and wedge out to the east. Frameworks have extents of up to 8m and laterally pass into coral debris. In the lower two units, up to 3m thick frameworks are formed by in situ bunches of columnar to branched *Porites* (Fig. 2.3.10.a) that laterally pass into intervals with horizontally layers of broken branches. In the lowermost unit, *Porites* together with vermetids is observed to encrust the underlying gravel. Corals are extensively bored by *Lithophaga*. Oysters and rare *Siderastrea* also occur. The most diverse framework regarding not only the number of taxa but also the observed growth forms is found in the

uppermost coral horizon (Fig. 2.3.3.). It is up to 3m high and 6m wide and passes laterally into reef debris. While the basal one metre consists of *Porites* only, the upper 2m contain in the centre *Tarbellastrea, Acanthastrea* and *Siderastrea* colonies up to 20cm in diameter.
West of the road to Ayios Kirillos, 1km south of Plora, two up to 2m thick horizons of *Porites* debris are intercalated in a succession of fine to medium grained sandstone overlain by coarse conglomerate and limestone at the top.

Facies analysis and interpretation: Coral framestone forms distinct build-ups that display an internal zonation and succession of framework forming coral taxa. They are therefore classified as reefs, which formed low topographic elements on the sea floor and had extensive belts of reef debris surrounding them. Coral diversity is low. This has been found to be characteristic for many coral reefs in recent and late Miocene siliciclastic environments (Hayward, 1982; Dabrio and Polo, 1988; Santisteban and Taberner, 1988; Braga et al., 1990).

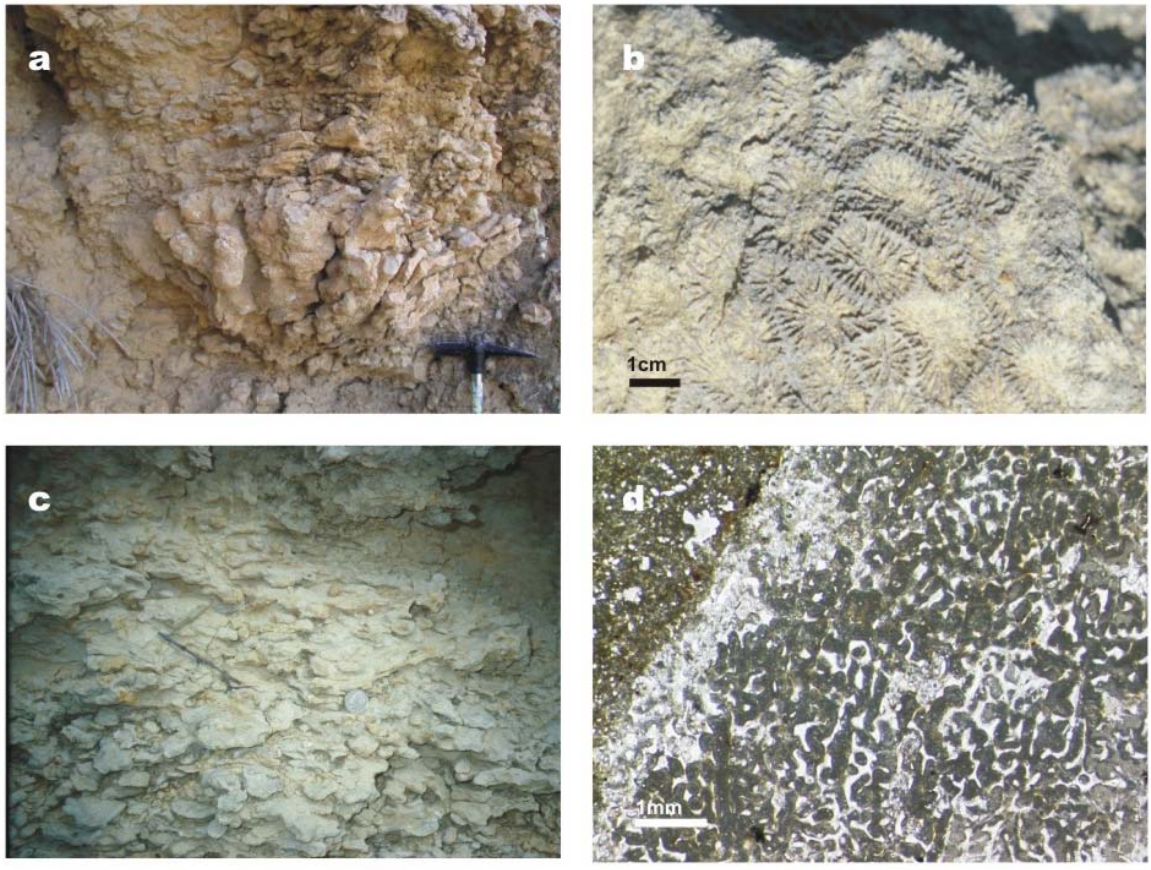

Fig. 2.3.10. Corals in LFA1
a: Massive branching *Porites* colony, lowermost reef horizon south of Kandhila, section Ka1
b: Colony of *Acanthastrea* sp. (location: Larani, southeastern Iraclion Plain)
c: Bed of broken and horizontally oriented *Porites* branches in a silty matrix, section Sivas. Note coin for scale
d: Thin section photograph of *Porites* sp. in a silty matrix, section Sivas, S3

The dominance of *Porites* in clastic environments is explained by its ability to remove sediment on its surface (Hubbard and Pocock, 1972).

In the WAT and at the southern margin of the Messara plain, coral reefs overlie a variety of facies ranging from coastal sand and -conglomerate to delta deposits, showing that coral reefs were able to colonize a variety of near-shore environments and substrates: Coral reefs developed on mid- to outer fan deposits in the Kandhila area. In the WAT, coral debris overlies coastal sands and braid delta deposits. The reef at Ayios Andreas overlies coastal conglomerate. These settings are very similar to those described from Upper Miocene deposits in Spain (Dabrio and Polo, 1988; Santisteban and Taberner, 1988; Martin et al., 1989; Braga et al., 1990). Braga et al. (1990) describe a typical succession with dominant *Porites* at the base of reefs, being early colonizers and increasing proportion of *Tarbellastrea* to the top. This is observed in the uppermost reef unit south of Kandhila and at Ayios Andreas. It mainly depends on the time span of unperturbed reef growth whether a complete *Porites*-*Tarbellastrea* cycle develops and therefore on the length of time intervals between destructive channel propagations (Braga et al., 1990). It is thus concluded that reefs in LFA1 that lack this succession in coral taxa grew in relatively short time intervals. Nevertheless, inactivity of delta lobes lasting long enough to allow colonization by corals indicates semi-arid climatic conditions (Braga et al., 1990).

Grain size of the substratum does not appear to be a prerequisite for coral settlement in the LFA1 deposits on Crete: *Porites* colonies in low energy environments are characterized by lower diameter of branches than in coarse grained high energy environments. Coral reefs on fine grained substrates intercalated in conglomerates may thus reflect lowering of water energy in consequence of marine transgression and landward migration of the unstable shoreline. In siliciclastic rich settings, intervals of coral reef growth thus appear to be not only limited by destructive deltaic channel migration but also to be favoured by relative sea level rise.

Paleogeography

The described lithologies and facies successions reflect a transition from terrestric and marginal marine environments to open marine conditions. Therefore they represent an overall transgressive succession. Stratigraphical architecture is characterized by interfingering of lithologies and lateral facies variation as shown in Fig. 2.3.9. Both, lateral facies variation and

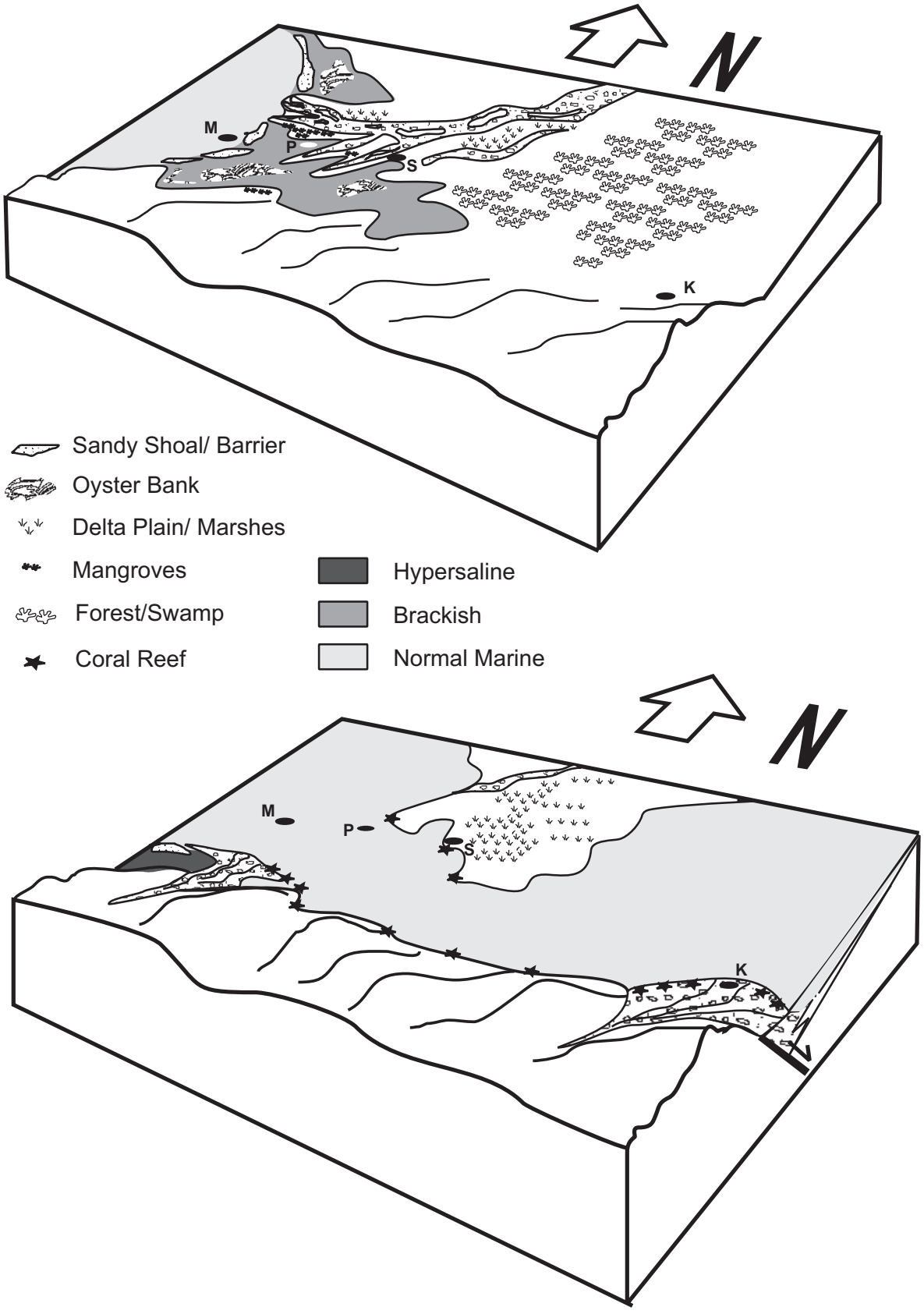

Fig. 2.3.11. Paleogeographic reconstructions of the WAT and southern Messara Plain during deposition of LFA1 (M=Matala, P=Pitsidia, S=Sivas, K=Kandhila)
a: Estuarine environment where interfingering lagoonal, deltaic, and coastal deposits were deposited in a warm humid environment
b: Flooding of the LFA1 depositional environment and relief intensification at the southern basin margin by synsedimentary faulting. Deposition of fan delta deposits at the basin margin and colonization by coral reef in a (semi)arid climate. Braid delta remains active in the northern part of the basin (Festos area)

the transgressive character are typical for estuarine environments (Woodroffe et al., 1989; Dalrymple et al., 1992; Reinson, 1992; Borrego et al., 1995). Estuaries can be classified as tide dominated or wave dominated estuaries (Reinson, 1992). If a closed sea such as the modern Mediterranean, where the tidal range is low (microtidal, <2m), is taken as an analogue, a Miocene estuary on central Crete was most likely wave dominated. These conditions favour the formation of barrier systems if the amount of sand transported along the shoreline is high enough. Tidal deposits on the other hand play only a minor role in microtidal environments (Reinson, 1992). This is not in contradiction with the local occurrence of decimetre to metre scale tidal channel scours found southeast of Matala since the depth of tidal channels does not depend on the tidal range but on the volume of back-bar lagoons and the number of tidal outlets (Dalrymple, 1992).

The occurrence of LFA1 lithologies is limited to the northern part of the WAT (Fig. 2.3.5.; 2.3.8.). LFA1 wedges out southward of Moni Odhiyitria and Sidheropetra Bay. Thus an east-west orientation of the basin margin is indicated (Fig. 2.3.11.a,b). Similarly, the area of maximum deposition is also east west oriented between Red Beach and Ayios Andreas in the south and Pitsidia and Sivas to the north. A synsedimentary fault in the Kandhila area, where a reef block was eroded and redeposited in the sediments overlying the fault (Fig. 2.3.3.; 2.3.7.h) suggests that the east-west oriented basin margin was fault controlled (Fig. 2.3.11.b). Angular blocks and pebbles in coastal sandstone south of Plora also indicate synsedimentary fault activity. Structural control on Neogene basin formation will be discussed in detail in chapter 5.

Facies expected in an estuarine environment are well represented by sediments of the WAT and the southern margin of the Messara Plain, including shoreface, barrier, estuarine lagoon and river mouth (delta) deposits (Fig. 2.3.11a). In the WAT, lagoonal deposits extend the furthest to the south (Fig. 2.3.5.a-c), whereas coastal sands do not occur south of Moni Odhiyitria (Fig. 2.3.5.c). This reflects an early paleogeography characterised by lagoons forming behind sandy barrier systems. Trough crossbedded conglomerate and coarse grained sandstone bodies between Matala and Sivas (Fig. 2.3.8.a) are interpreted to be the consequence of deltas formed by river discharge into the lagoons. The resulting brackish estuarine environment is characterized by widespread oysterbanks and mangrove swamps (Fig. 2.3.11.a). Lateral facies variation observed in all sections is a consequence of delta channel and sand bar migration and swift transgression and regression of the shallow depositional system in response to relative sea level change. Progressive transgression is evidenced by the deposition of shallow open marine sands that are found at the top of LFA1

(Fig. 2.3.2.). Synsedimentary faulting resulted in relief intensification at the southern basin margin and formation of fan deltas (Fig. 2.3.11.b). Distribution of lithofacies south of Pitsidia indicates that fan delta deposits were reworked and deposited as limestone rich coastal conglomerates (Fig. 2.3.8.b,c). Increased limestone contents in coastal sediments and the colonization of fan deltas by coral reefs indicate continuing warm and increasingly arid climatic conditions. Progressive transgression results in the deposition of limestone of LFA2 with basal rhodolith rudstone.

2.4. Carbonate deposits (LFA2)

Introduction

Siliclastic deposits (LFA1) described in chapter 2.3. are overlain by a unit dominated by carbonate sediments (LFA2) which represent the most widespread Neogene deposits in the Western Asteroussia Tabellands (WAT). An interfingering of LFA1 with LFA2 or lateral transition of facies is not observed in outcrop. The LFA1-LFA2 transition is not well exposed in the Matala area (Fig. 2.3.2.) but is conformable southeast of Matala (section MS3). It is unconformable, on the other hand, in the area between Pitsidia and Sivas (Fig. 2.2.3.). The LFA2 succession reaches a thickness of 80m at the western coast between Matala and Vathi and in the south at Martsalo (Fig. 2.2.1.; 2.2.3.; 2.4.1.). The fossil content documents fully marine character of the sediments. In contrast to the underlying siliciclastic deposits, lateral facies change is gradual and vertical variation in lithology is more pronounced than lateral variation. Similarly, sedimentary architecture of LFA2 is characterized by flat lying laterally continuous beds and the absence of pronounced three-dimensional geometries (Fig. 2.4.1.). Where the unit overlies siliciclastic deposits of LFA1, the base is defined by a basal bed of rhodolith rudstone (sections MO1, MO2, MS1, MS3, Moni1, 2; Figs. 2.2.3. – 2.2.5.). LFA2 is observed to wedge out from Sidheropetra Bay to the east towards a fault bounded outcrop of Flysch and olistolithic limestone (Fig. 2.4.2.a) that is situated 1km west of Ayios Enthikianoi and 0,5km west of Knarkokefala (Fig. 2.2.1.). An onlap towards the north can be seen in an outcrop 1,5km south of Knarkokefala west of Martsellos ridge (Fig. 2.2.1.), where the unit is reduced to 15m (section Mart, Fig. 2.2.3.). Here, the base is formed by a 6m thick bed of conglomerate with well rounded quartz pebbles in a limestone matrix, overlying Flysch basement. It has meterscale planar crossbeds dipping to the south (Fig. 2.4.2.b). A section where thickness of LFA2 is also reduced to 15m with conglomerate at the base is also found

Fig. 2.4.1.: LFA2 succession at Vathi with section VO measured on the opposite side of the gorge to the left. See Fig. 2.2.2. for lithologic signatures. View is to the north, approximately parallel to the orientation of the Miocene shoreline to the east. Note horizontal architecture of the succession with little lateral facies variation

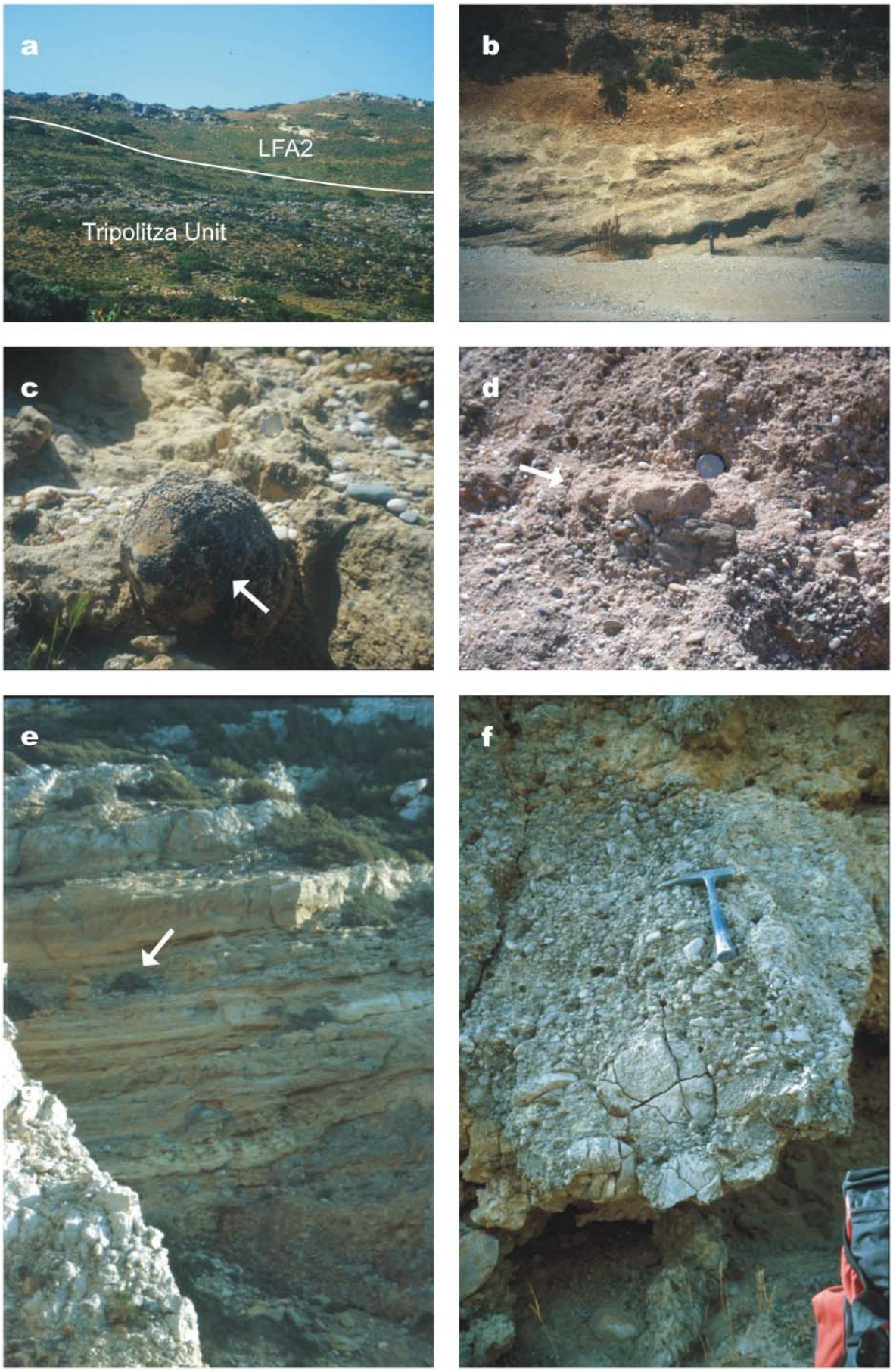
a
LFA2
Tripolitza Unit
b
c
d
e
f

Fig. 2.4.2. (previous page): Basal sediments of LFA2 (see Fig. 2.2.1. for locations)
a: Onlap of LFA2 limestone on basement (olitstolithic Tripolitza Limestone) east of Sidheropetra Bay to the east on Knarkokefala Horst. View is to the south
b: Planar crossbedded conglomerate at Martsellos (section Mart). Dip of crossbeds is to the south, view is to the west
c: Conglomerate north of Kristo Kefali (section KN) with well rounded Tripolitza Limestone cobbles (arrow)
d: Conglomerate intercalated into sandy sediments (LFA2) east of Moni Odhiyitria (section Moni2). Note reworked angular sandstone clasts (arrow)
e: Succession of sandy limestone and conglomerate north of Kristo Kefali. Note boulders of Tripolitza Limestone that reach up to 2m in diameter (arrow)
f: Basal conglomerate of the LFA2 succession west of Martsalo Bay

where the unit wedges out to the south at the northern flank of Kristo Kefali (Fig. A5). At Sivas and Pitsidia, carbonate sediments are restricted to the upper 5m of sections. LFA2 can be subdivided into three parts: The lowest part (LFA2a) consists of limestone rich in siliclastics and intercalated calcareous sandstone while the upper two part (LFA2b and c) are mainly formed by pure limestone (packstone, floatstone, rudstone and framestone). LFA2a can be subdivided into four distinct lithofacies types: fine to medium grained bioturbated packstone with sand (PS), fine to coarse grained calcareous sandstone with cross stratification (CS), rhodolith rudstone (RFR1 to 3) and rudstone with quartz pebbles at the base (RP). The uppermost RP horizon defines the upper limit of LFA2a. This boundary can be traced over the largest part of the WAT. It is, however, absent at the southern coast (section Ma1) and at Mount Rhodonas (section KL, Fig 2.2.6.; 2.2.1.) and less defined east and southeast of Moni Odhiyitria where the largest part of the successions is rich in siliciclastics (sections Moni1, Moni2; Fig. 2.2.5.). LFA2b consists of massive (*sensu* Ingram, 1954) rhodolith floatstone to rudstone bed without visible internal sedimentary structures (MRB, RFR2 facies) and bioclastic packstone (BP). The base of LFA2c is marked by the occurrence of laterally continuous horizons of coral framestone (CF) or single coral colonies within rhodolith rudstone (RFR3). Additionally, bioclastic packstone of the BP facies occurs. At the top, rudstone with *Terebratula* (RT) occurs northeast of Matala (section MO1) and west of Martsalo Bay where it is overlain by marl of LFA3. The thickness LFA2a decreases from 39,5 m (section MO1) in the north of the area to 12,5 m (section VO) and 16,5 m (section MaN, Fig. 2.2.3.) in the south. LFA2b reaches a thickness between 17m at Vathi and 23m at Martsalo (section MaN) in the south of the WAT and decreases in thickness to the north (10m at sections MO1, MO2 and Moni1). Thickness is further reduced where the unit onlaps basement highs. LFA2c reaches a thickness between 5m at Sivas and 30m northeast of Matala (section MO1) in the north and more than 40m at Vathi to the south and at Mount Rhodonas in the southeast.

Lithification of the carbonates is poor and neither early marine, later diagenetic nor meteoric cements are well developed. Especially in coral horizons, however, caliche crusts are abundant. Dolomitization is subordinate except in the Kristo Kefali area where limestone in section Ma1 and the lower 20m of section Ma2 is strongly affected by fabric destructive dolomitization.
Lithologies are described in detail below and appear in the sequence of their first appearance in the measured sections.

Conglomerate

Description: Conglomerate occurs at the base of LFA2 where it overlies basement. Grain sizes range from pebbles to blocks up to 2m in diameter. The matrix consists of marl, sandstone or limestone. Both planar- and trough crossbedding are common.
Outcrops of up to 6m thick units of LFA2 conglomerate 1,5km south of Knarkokefala (section Mart, Fig. A5, 2.2.1. and 2.4.2.b), in the Moni Odhiyitria area at section Moni2 (Fig. 2.2.5.) and north of Kristo Kefali (section KN, Fig. A5; 2.2.1.) are similar in several aspects: Conglomerate is poorly sorted, grain supported and has a marly to sandy matrix. Components are usually between 0,5 and 3cm but may be as large as 10cm and poorly to well rounded. In intervals, components are disc shaped and imbricated. At section Mart, the basal 1,5m have steeply dipping (30°) tabular crossbeds. Disc shaped components are oriented parallel to the orientation of crossbedding. Upsection the angle of crossbedding decreases and decimetrescale crossbedded sandstone wedges occur. Dip is to the south and bedding disappears to the top. At section Moni2, the base of the conglomerate shows low angle trough crossbedding and subhorizontally oriented clasts in the upper part. Apart from rounded pebbles, the conglomerate contains shell fragments, rare oysters and rhodoliths as well as angular clasts of the underlying sandstone (Fig.2.4.2.d). At section KN, poorly sorted conglomerate is interbetted with calcareous sandstone with pebbles. Components are also disc shaped in intervals but no sedimentary structures are observed. At the base of the section, well rounded cobbles of black Tripolitza Limestone up to 25cm in diameter occur (Fig. 2.4.2.c). At the top, large *Clypeaster* is present. To the west, at the coastline north of Kristo Kefali, abundant cobbles and boulders of Tripolitza limestone up to 2m in diameter occur in an approximately 20m high coastal cliff (Fig. 2.4.2.e).

A succession of conglomerate with intercalated beds of bioturbated bioclastic limestone, marl and clay at western Martsalo Bay (section Ma1, Fig. 2.2.3.) at the base of LFA2 reaches a thickness of 18,5m. Angular clasts of Tripolitza Limestone are abundant throughout the succession. It overlies limestone of the Tripolitza Unit. The basal 4m consist of a coarse, poorly sorted breccia and conglomerate with components up to 30cm in diameter in a limestone matrix (Fig. 2.4.2.f). It is covered by 3,5m of well sorted and classified black conglomerate in a well cemented limestone matrix. Components are Tripolitza limestone. On top of this bed is a matrix supported conglomerate that vertically grades into packstone. It contains poorly classified pebbles and red algae. Moulds of regular echinoids and bivalves are common. Pebbles of Tripolitza limestone are perforated by sponges. Matrix of this bed is intensely red and it is overlain by 2m of orange to red coloured bioclastic, dolomitized limestone. On top of it are 1,5m of well classified and well rounded, poorly sorted and in intervals matrix supported conglomerate with a marly limestone matrix. Components are horizontally oriented. Upsection, 5m of bioclastic floatstone to rudstone, crossbedded bioclastic limestone and red, marly limestone or dolomite follow. Rudstone contains abundant poorly sorted pebbles up to 5cm in diameter, red algal fragments, moulds of bivalves and echinoids. Red algal rudstone (RFR facies, see below) containing angular to subrounded Tripolitza Limestone clasts that range in size from silt to blocks up to 2,5m in diameter overlies the described succession. West and northwest of Martsalo Bay, Flysch (Sandstone) and the underlying Tripolitza Limestone form a level paleosurface overlain by Neogene conglomerate. Thickness of the basal Tripolitza conglomerate is approximately constant along the eastern flank of Kristo Kefali. East of Martsalo Bay, thin, up to 10m thick bodies of conglomerate and limestone (rhodolith rudstone) overlie Flysch. Clasts at the base reach a diameter of 5cm. Conglomerate is poorly sorted and contains sandstone clasts instead of clasts of Tripolitza Limestone.

At Moni Martsalo (section MaN, Fig. 2.2.3.; 2.2.1.), thickness of immature conglomerate overlying Flysch is reduced to 2m.

Fazies analysis and interpretation: Conglomerate at the base of LFA2 is lithologically similar to conglomerate found in LFA1. However, no sediments typical for LFA1 like lagoon or delta deposits are associated with this lithology, and limestone in the matrix is more abundant than in LFA1 conglomerates.

Conglomerate at Martsellos Ridge is interpreted to represent a typical gravel beach succession with a lower beach facies characterized by steeply inclined tabular crossbeds and an upper beach facies with low angle crossbedding, sand layers and imbrication of oblate clasts (Hart

and Plint, 1995; Reading and Collinson, 1996). This facies apparently formed the southern shoreline of a basement high in the Knarkokefala area. Conglomerate at section Moni2 is interpreted to represent a similar but less well developed facies that also includes trough crossbedded shoreface deposits at the base. The latter deposits are interpreted to represent coastal sediments of the eastern shoreline of the LFA2 marine basin. The conglomerate unit at the base of section Ma1 and the overlying carbonate succession differs from other outcrops in that lithoclasts of Tripolitza Limestone are present. The angular shape of clasts indicates a local source. The presence of cobbles and boulders in the rhodolith floatstone and rudstone facies that is interpreted to be a low energy deposit (see below) indicate rockfall related to a paleocliff formed by Tripolitza Limestone. High paleorelief is also indicated by Tripolitza boulders in deposits north of Kristo Kefali. The presence of oblate pebbles and marine fossils in section KN are interpreted to represent associated shoreline deposits.

Rhodolith floatstone to rudstone (RFR)

This lithology can be subdivided into three subunits (RFR1 - 3), which are distinct in terms of siliciclastic content, texture and bedding thickness and characterized by the presence or absence of zooxanthellate corals and are therefore identifiable in the field. RFR is the dominant lithology of LFA2 in the WAT and the southern margin of the Messara Plain (top of sections Ka1 and 2; Fig. A1). RFR1 is common in LFA2a while RFR2 is typical for LFA2b and RFR3 is most common in LFA2c.

RFR1

Description: This lithofacies unit comprises rhodolith floatstone to rudstone that is characterized by a matrix consisting of 10-50% of fine to medium grained siliciclastic (mainly quartz) sand. Dominant components >2cm are rhodoliths and less common unattached branches and foliose red algae (Fig. 2.4.3.a). Rhodoliths are commonly ellipsoidal in shape and laminar to open branched or columnar and not spherical (see Bosence (1983) for classification of rhodoliths; Fig. 2.4.3.b). Size ranges from nodules smaller than 1cm to rhodoliths up to 8cm in diameter. Densely branched to concentric rhodoliths occur in the basal part of the rhodolith rudstone bed at the base of LFA2. Unattached branches are mostly

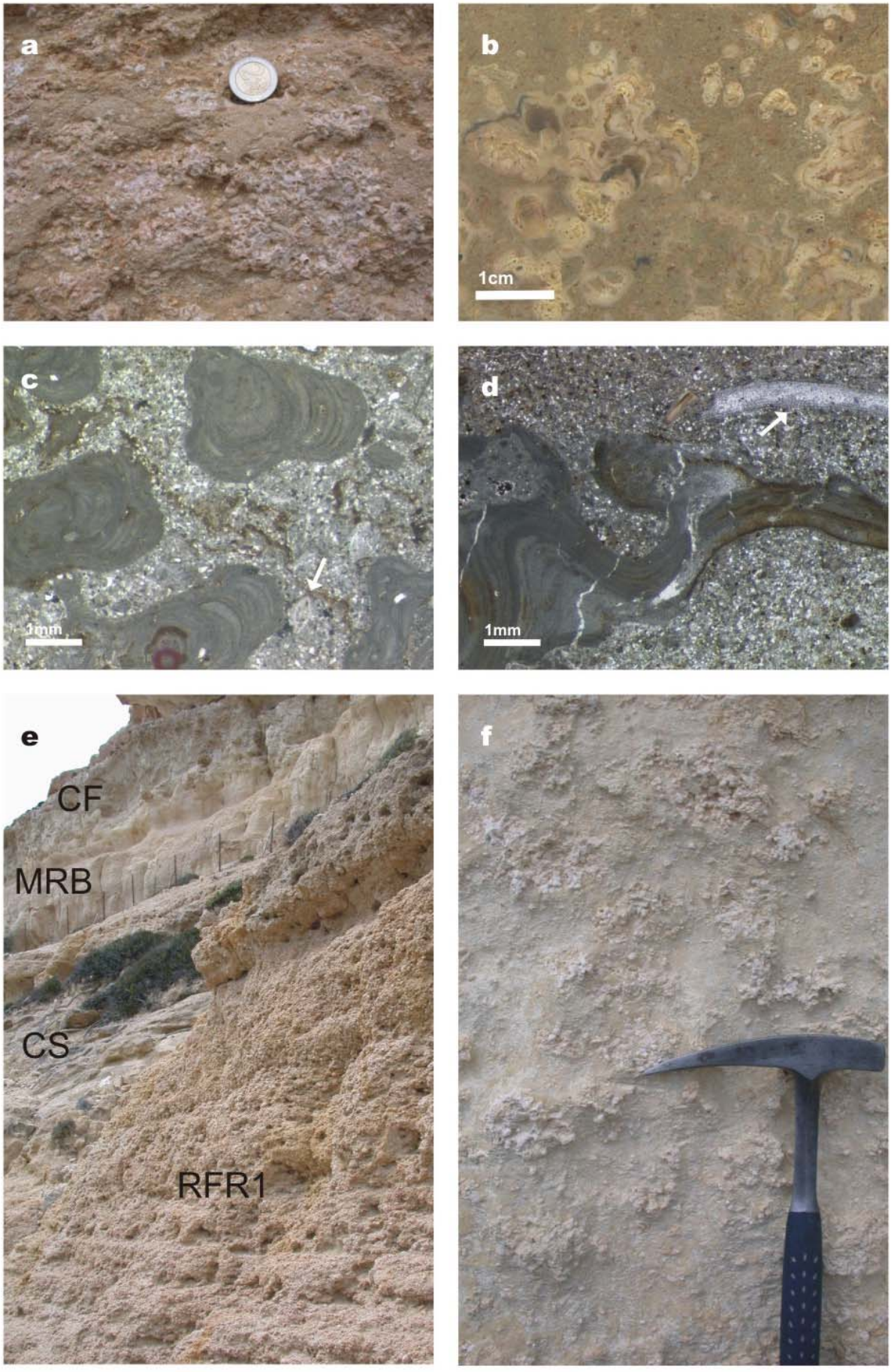
a
b
1cm
c
1mm
d
1mm
e
CF
MRB
CS
RFR1
f

Fig. 2.4.3. (previous page): Rhodolith floatstone to rudstone (RFR1 and2), see Fig. 2.2.1. for locations
a: Rhodolith rudstone of RFR1**,** section MO1
b: Polished rock section of rhodolith rudstone of RFR1, base of section MO1, with open branched rhodoliths, sample MO1
c: Thin section photograph of rhodolith rudstone of RFR1 with red algal branches and rare benthic foraminifera (arrow) in an argillaceous matrix rich in fine grained siliciclastics, base of section VO (sample VO1)
d: Thin section photograph of rhodolith rudstone of RFR1 with foliose to branching red algal thallus and echinoid fragment (arrow) in an argillaceous matrix rich in fine grained siliciclastics, section MO1 (sample MO3)
e: Outcrop situation at the archaeological site west of Matala (section MA): Rhodolith rudstone in the foreground is overlain by sandstone of the CS facies. Above the fence the massive rhodolith rudstone bed (MRB) of the RFR2 facies crops out, overlain by coral framestone (CF)
f: Massive rhodolith rudstone of RFR2 northeast of Matala

between 1,5 and 4mm in thickness. The matrix consists of mud rich packstone with fine grained (<0,15mm) siliciclastics being the most abundant constituent and minor contributions of foraminifera, bryozoans or echinoids (Fig. 2.4.3.c,d). Macrofossils in addition to red algae are *Pecten, Ostrea* and celleporiform bryozoans. At section MS1 (Fig. A3), a fragment of *Acanthastrea* has been found. Shells and rhodoliths are mostly intact, fragmented bioclasts play only a minor role. The degree of fragmentation, however, is higher in the basal rhodolith rudstone bed of LFA2 and in RFR1 beds in the south (section Vathi, Fig. 2.2.3.) and southeast (Mount Rhodonas, section KL, Fig. 2.2.6.) of the WAT. RFR1 beds are overlain by bioturbated packstone with sand (PS), which contains few macrofossils and has a higher mud and silt content. Rhodolith rudstone is also intercalated in the overlying calcareous sandstone with crossbedding (CS; sections MA, MS1, Fig. 2.2.4) and wedges out towards the east (Fig. 2.4.4.). Beds of RFR1 have no visible internal sedimentary structures and reach a thickness of up to 4m at Matala (Fig. 2.4.3.e).

RFR2

Description: Rhodolith floatstone to rudstone of RFR2 (Fig. 2.4.3.f) consists of openly branched or approximately elliptical and laminar rhodoliths up to 7cm in diameter (Fig. 2.4.5.a) and minor amounts unattached branches. The matrix consists of marly limestone (wackestone or packstone, Fig. 2.4.5.b) with low (<5%) and upward decreasing content of siliciclastic silt and fine sand. It also contains unsorted unidentifiable carbonate grains, bioclasts and intact skeletons (Fig. 2.4.5.c). The unit usually lacks internal structures and bedding planes. Other macrofossils apart from red algae are rare *Pecten, Clypeaster* and bryozoans. Preferential orientation of grains is not observed. The amount of bioclasts in the

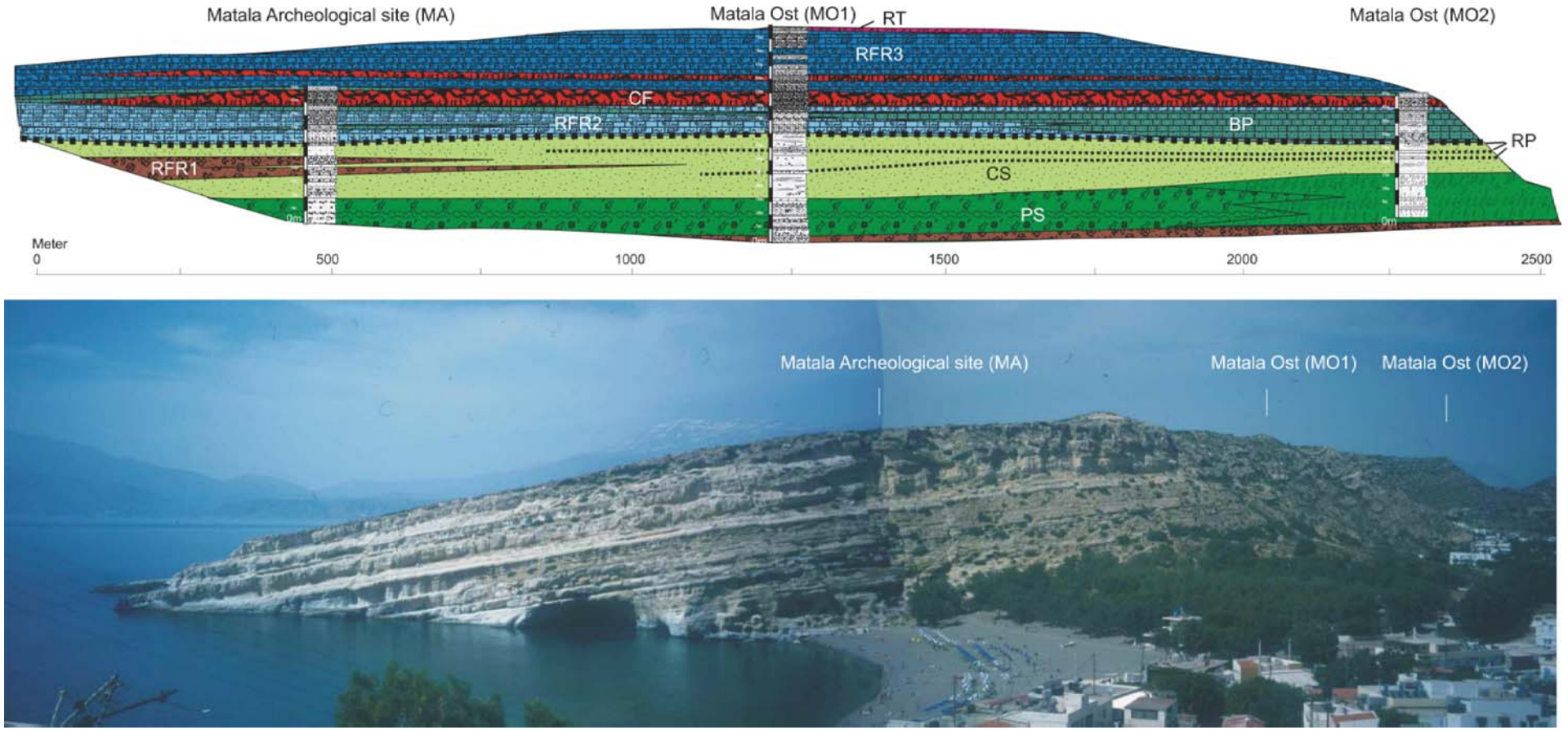

Fig. 2.4.4: Transect at Matala along sections MA, MO1 and MO2 showing facies distribution within LFA2. Note low-angle prograding clinoforms of CS-RP couplets. View of the photograph is to the northeast, orientation of the transect is E-W near section MA and SW-NE between sections MO1 and 2

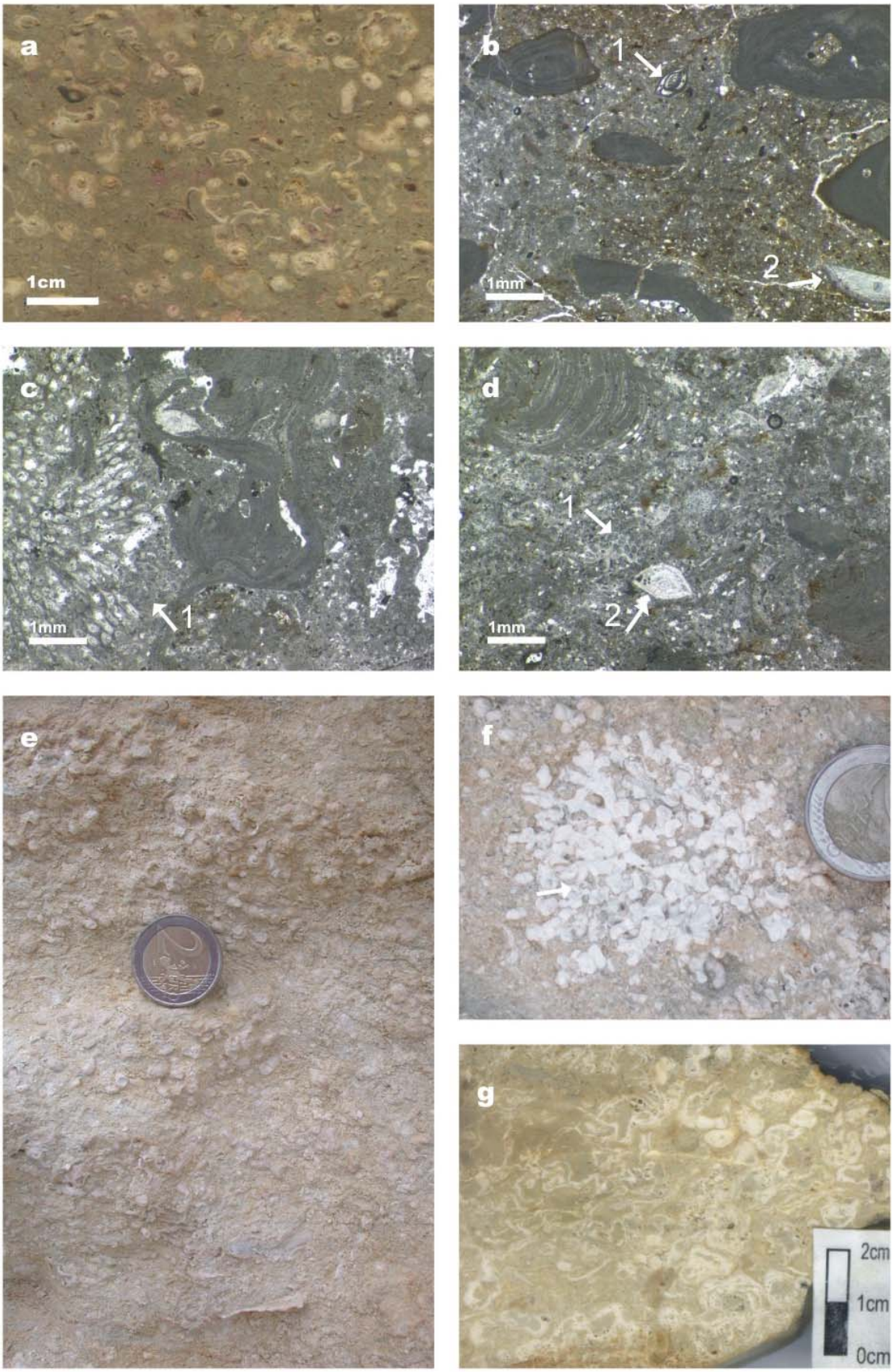
a
1cm
b
1
2
1mm
c
1
1mm
d
1
2
1mm
e
f
g
2cm
1cm
0cm

Fig. 2.4.5. (previous page): Rhodolith floatstone to rudstone (RFR2 and 3), see Fig. 2.2.1. for locations
a: Polished rock section of rhodolith rudstone of RFR2, MRB, section VO (VO8b)
b: Thin section photograph of rhodolith rudstone of RFR2 with red algal branches and rare benthic foraminifera (1: miliolid form) and bivalve shells (2) in marly matrix, MRB, MO16c
c: Thin section photograph of rhodolith rudstone of RFR2 with abundant coralline red algae and celleporiform bryozoa (arrow); MRB, section VO (VO8d)
d: Thin section photograph of rhodolith rudstone of RFR2 with bioclastic matrix (1: bryozoan fragment, 2: *Amphistegina* sp.); top of MRB, section VO (VO8c)
e: Rhodolith rudstone of RFR3, section MO1
f: Open branched rhodolith of *Spongites albanensis*, RFR3, section MO1
g: Polished rock section of rhodolith rudstone of RFR3 (boxwork rhodolith, VO20b)

argillaceous matrix and the degree of fragmentation of skeletal components, however, increases upward in the MRB (Fig. 2.4.5.d).

RFR2 is widespread in the interval between the upper rudstone with quartz pebbles horizon (RP) and the lowermost coral framestone horizon (CF). The massive rhodolith floatstone to rudstone bed (MRB) that is found in the largest part of the WAT overlying the RP horizon forms the largest part of the RFR2. It reaches a thickness of 5m in the area of Matala (sections MA, MO1, MS1 (Fig 2.2.3.; 2.2.4.; 2.4.4; A3). Along the western coast to the south it increases to 16m (section VO). Some of the increase in thickness appears to occur over a short distance north of Vathi (Fig. 2.2.3.). The maximum thickness is reached at Martsalo (25m at section MaN). From Matala to the east (Fig. 2.4.4.), the MRB, however, is reduced in thickness to 1,5m at section MO2 where it also loses its massive character. The MRB is also not developed at Mount Rhodonas (section KL, Fig. 2.2.6.) and west of Martsalo Bay. It is also not present in the Knarkokefala area and directly north of Kristo Kefali. The RFR2 lithology is absent in the Sivas-, Pitsidia- and Moni Odhiyitria.

RFR3

Description: The dominant constituents of RFR3 (Fig. 2.4.5.e) are openly branched rhodoliths like in the RFR1 and 2 lithologies that are up to 10cm in diameter (Fig. 2.4.5.f). However, foliose red algae are more common and large boxwork rhodoliths (Bosence, 1983) up to 10cm in diameter are abundant in intervals (Fig. 2.4.5.g). Matrix varies between mud- to wackestone and packstone. Packstone matrix is poorly to well classified with medium grain sizes around 0,5-1mm. It has a mottled appearance due to partially decomposed and disintegrated grains (Fig. 2.4.6.a). Rudstone with packstone matrix is interbedded with rudstone and floatstone with a mudstone or wackestone matrix that contain pockets of

packstone. Cavities of boxwork rhodoliths are often filled with a more finegrained sediment than the surrounding matrix (Fig. 2.4.6.b).

Macrofossils in addition to red algae are *Clypeaster,* celleporiform and robust branching bryozoans and rare *Pecten.* Single tabular colonies of *Tarbellastrea* occur at several locations in the RFR3 facies, for example in section VO below the lower coral framestone horizon (Fig. 2.4.1), in section KL (Fig. 2.2.6.) and section Ma (Fig. 2.2.3.). Large isolated *Tarbellastrea* colonies occur at several locations within RFR3 at sections VO (Fig. 2.4.6.c), MO and KL, as well as at the bay west of Ayios Yeoryios and west of Martsalo Bay (Fig. 2.2.1.). They reach a maximum diameter of 260cm at section KL, 42m above the base of the section. Skeletal elements in many cases show evidence of reworking. Ripped-off foliose thalli of red algae, fragments of echinoids and fragmented *Heterostegina* are common (Fig. 2.4.6.d). Horizontally continuous beds are usually between 1m and 5m in thickness and show no visible internal sedimentary structures. However, horizontal orientation of components (Fig. 2.4.6.e) or internal layering can be observed in thin section of some samples: Packstone layers are between few millimetres and few centimetres in thickness and are covered by micritic limestone mineralised by (iron?) oxides or encrusted by red algae (*Titanoderma* pustulatum; Fig. 2.6.4.f). At section VO (33,5m above the base), a 5cm thick, well cemented hardground occurs that is overlain by a 6m thick bioclastic rhodolith rudstone containing celleporiform bryozoans with a central void.

Fig. 2.4.6. (next page): Biota and components in rhodolith rudstone (RFR3), see Fig. 2.2.1. for locations
a: Thin section photograph of rhodolith rudstone of RFR3. Foliose red algae encrust serpulid worm tube (arrow). Packstone matrix has a mottled appearance due to partially decomposed and disintegrated grains, section KL (K20)
b: Thin section photograph of rhodolith rudstone of RFR3. Boxwork rhodolith with pockets of mudstone and surrounding bioclastic packstone, upper part of section VO (VO21b)
c: Large colony of *Tarbellastrea*, RFR3 (LFA2c), section Vathi
d: Thin section photograph of rhodolith rudstone of RFR3 with abundant red algal fragments, *Amphistegina sp.* (1) and fragments of *Heterostegina* (2), section MO1 (MO23b)
e: Thin section photograph of rhodolith rudstone of RFR3 with horizontally oriented components (1: ripped off foliose red algal thallus, 2: *Heterostegina* sp.), top of section MO1 (MO28a)
f : Thin section photograph of RFR3 with hardground consisting of wackestone with iron(?) oxide crusts, overlain by bioclastic packstone, section VO below coral framestone horizon encrusted by *Titanoderma pustulatum* (arrow), VO11
g: Base of LFA2a at section MS3 southeast of Matala with conspicuous black oyster colonies overlain by red algal rudstone of RFR3
h: Boulder of Tripolitza Limestone that is extensively bored by *Lithophaga* in rhodolith floatstone of RFR3 in section Ma, west of Martsalo Bay

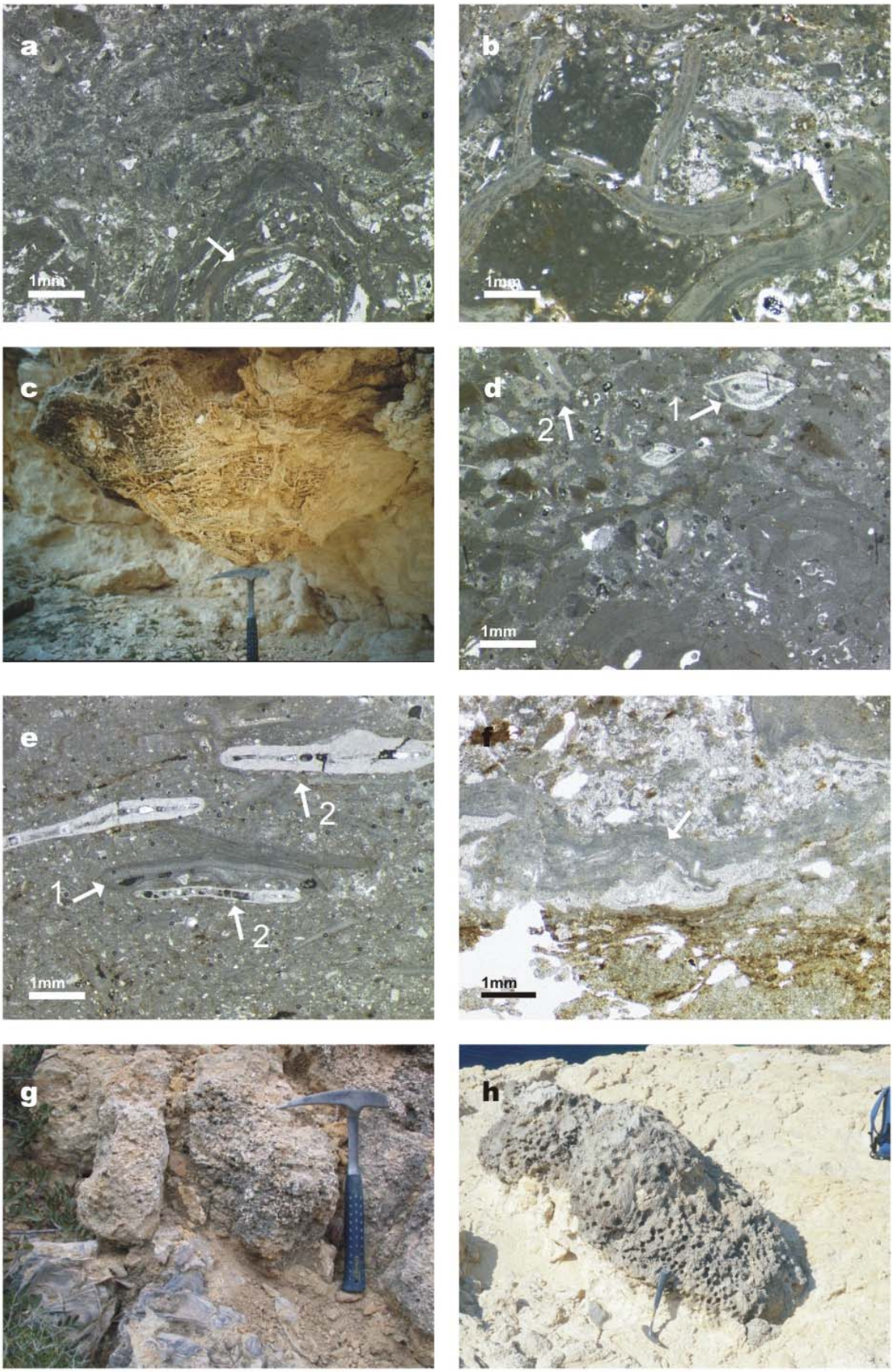
a
1mm
b
1mm
c
d
2
1
1mm
e
2
1
2
1mm
f
1mm
g
h

Rhodolith rudstone and floatstone of RFR3 dominates in LFA2c but is also intercalated in LFA2a. The RFR3 lithology dominates in the upper part of the carbonate succession (LFA2c). Red algal rudstone and floatstone overlying the uppermost coral horizon (see below) reach a thickness of 15m in the Matala area (section MO, Fig. 2.4.4.) and more than 20m at Vathi (Fig. 2.4.1.) and Moni Martsalo (Fig. 2.2.5.).

Thickness of basal rhodolith rudstone to floatstone that overlies LFA1 is increasing significantly to the southeast of Matala: It reaches a maximum of 28m at section MS3. At the base colonies of large (10cm) black oysters occur (Fig. 2.4.6.g). They are overgrown by 50cm of red algal bindstone (RB lithology, see below). Twelve meters upsection, red algal bindstone is overgrown by 1 – 2cm thick tabular colonies of *Tarbellastrea* and *Acanthastrea*, solitary corals and pyrgomatid cirripeds. Broken parts of *Porites* and *Tarbellastrea* occur in the bed overlying this horizon. In contrast to rhodolith rudstone underlying the RP facies elsewhere in the WAT, a more foliose character of red algae and the occurrence of red algal bindstone characterize the rhodolith rudstone southeast of Matala. Rhodolith diameter may reach 10cm in the upper part of the 28m thick unit. The 15m thick succession of red algal rudstone in LFA2a in the Moni Odiyitria area (section Moni1, Fig. 2.2.5) is very similar and also contains red algal bindstone but no corals. The matrix is mainly composed of inhomogeneous wackestone with pockets or intervals of poorly sorted bioclastic packstone. Siliciclastic content is predominantly silt to fine sand and is usually below 10%. Individual beds are up to 5m in thickness but are internally layered in intervals. Other faunal components are *Pecten* and in a 50cm thick layer at 31m above the base of the section *Heterostegina* is also present. This layer is overlain by 2,5m of marly rhodolith floatstone with abundant infaunal bivalves.

Red algal floatstone to rudstone that occurs west of Martsalo Bay (sections Ma1, Ma2) is very similar to RFR3 but is characterized by the content of clasts of Tripolitza Limestone. They are angular and their size ranges from silt to pebble size. Four metres above the base of section Ma2, rhodolith rudstone contains abundant subrounded to rounded Tripolitza clasts with a diameter of up to 10cm and at 17m above the base, several blocks up to 250cm in diameter occur that are extensively bored by *Lithophaga* (Fig. 2.4.6.h). Towards the top of the section (29 - 35m above the base), content in red algae decreases and *Heterostegina* becomes abundant.

At Mount Rhodonas, the basal rhodolith rudstone with intercalated beds of sandstone has a variable siliciclastic content of up to 10% that disappears upsection from 32m above the base. Since siliciclastic contents in rhodolith rudstone in the basal 15m of the section are commonly >5%, it has been classified as RFR1 while rhodolith rudstone in the upper 45m of the section has low siliciclastic contents and is similar to RFR3.

The upper 5m (section MO) to 10m (section MaN) of the carbonate succession become increasingly marly and red algal content decreases. This is the also the case in the Mount Rhodonas area and west of Martsalo. Single tabular colonies of *Tarbellastrea* or *Porites* may occur. In the area north and northeast (section MO) of Matala and between Martsalo Bay and Kristo Kefali (section Ma2), marly limestone is overlain by a bed with abundant *Pecten* and *Terebratula* (see below).

Quantitative biofacies analysis: Results of semiquantitative thin section analysis (see chapter 1.4. for description of applied methods) show very similar compositions of skeletal components in all RFR lithologies (Fig. 2.4.7.). Red algae are dominant (50 – 70% of total fossil content) while foraminifera (10-30%) and, to a lesser degree, echinoids, bryozoans and bivalves are also common. Serpulids are restricted to the RFR1 and 3 lithologies whereas corals are abundant in the RFR3 lithology at section KL (Fig. A4). Generally, biofacies of RFR lithologies does not differ significantly between sections except that in the RFR1 lithology at section VO bryozoans are absent and at section MS bivalve shells are very rare. According to the original definition of Lees and Buller (1972), the RFR1 and 2 lithologies are classified as foramol ("temperate") due to the presence of bryozoans and to the absence of calcareous green algae and zooxanthellate corals that define the chlorozoan "warm water" association. Carannante et al. (1988) introduced a type of sediment termed rhodalgal that is intermediate between molechfor-foramol and chloralgal-chlorozoan and thus defines a warm temperate sediment type. This association, characterized by the occurrence of abundant red algae together with bryozoans and benthic foraminifera such as *Heterostegina* and by the absence of framework-forming zooxanthellate corals, is found in RFR1 and 2. Halfar et al. (2000) introduced an additional subdivision called rhodozoan that applies on the RFR3 facies with non-framework forming zooxanthellate corals.

Facies analysis and interpretation: While RFR1 and 2 differ only in siliciclastic content and thickness of individual beds, RFR3 is different in several aspects: In intervals it contains

zooxanthellate coral colonies. Moreover a foliose red algal habit and the formation of boxwork structures is common and the sediment shows a higher degree of reworking.

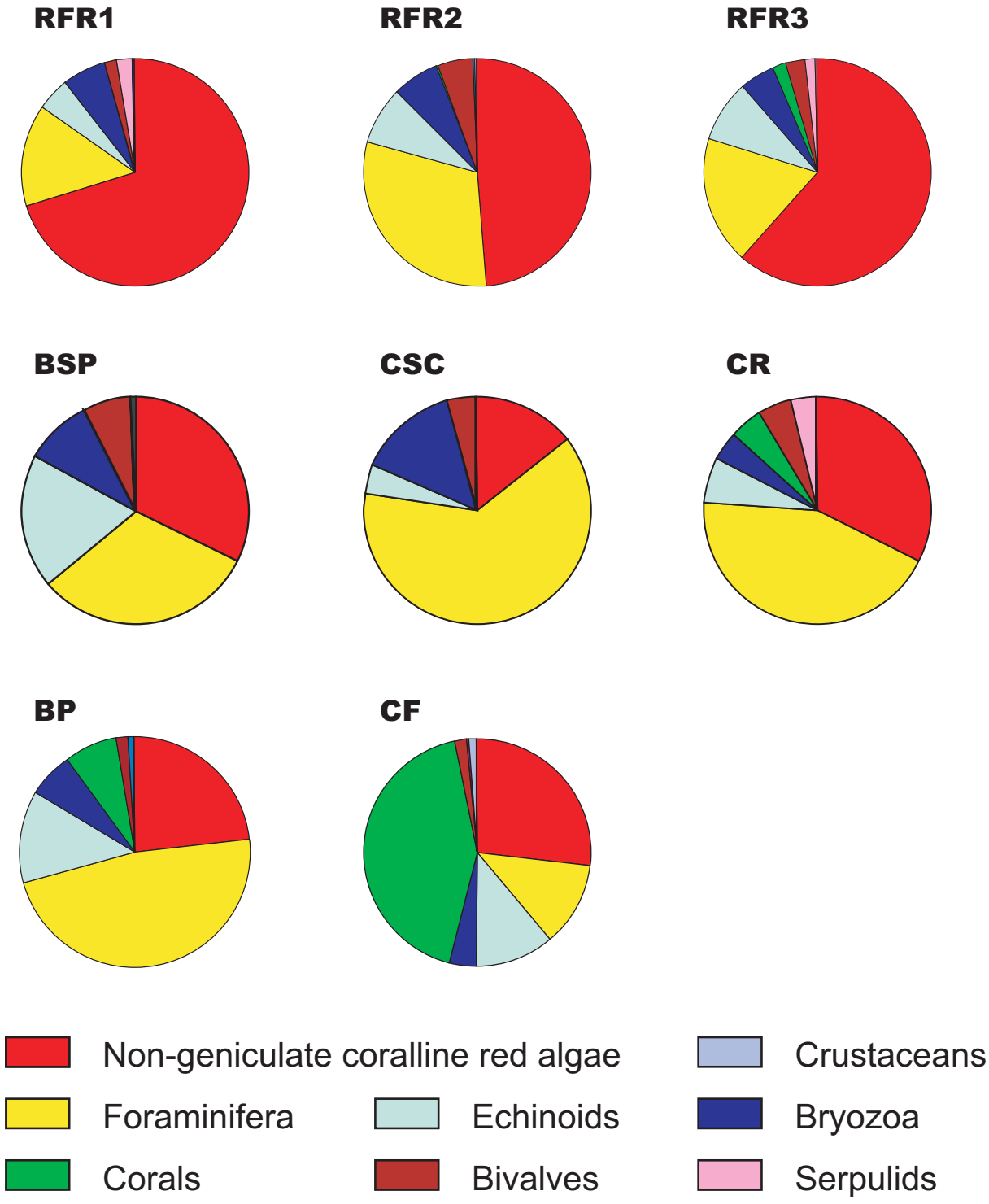

Fig. 2.4.7.: Results of semiquantitative biofacies analysis of sections MO1, MS1, VO and KL shown as volume percent of identifiable skeletal component total. See table A3 for data

In RFR1 and 2, grain size of siliciclastic content reflects the maximum grain size of components that are reworked from shoreward located higher hydraulic energy environments. The small grain size (silt to fine sand) of siliciclastic components in most RFR1 and 2 deposits therefore suggests low hydraulic energy conditions. An upward decrease in grain size of siliciclastics in RFR1 in the Matala area suggests a deepening upward trend while an increasing amount of fragmented bioclasts upsection in RFR2 indicates shallowing upward. Similarly, a high degree of fragmentation and orientation of skeletal components in RFR3 reflects increased hydraulic energy. On the other hand, carbonate mud content is also high in intervals and robust branching bryozoans which are most susceptible to mechanical abrasion (Smith and Nelson, 1996) are well preserved. This indicates prevalent low energy conditions but also reflects the capability of sediments rich in red algae to trap fines during times of high hydraulic energy (Pedley, 1998). Additionally, microbes, algae or other sessile and encrusting organisms may have stabilized sedimentary surfaces. Stabilization through colonization by sea grass as described by Fornos and Ahr (1997) from the recent Balearics and postulated by Pomar (2001) for the Tortonian Belearics is possible but hard to identify in fossil material. The rarity of marine cements shows that stabilization by early lithification is not common. Mineralized sediment layers encrusted by red algae, however, indicate local hardground formation.

The type and shape of rhodoliths also gives information about the hydraulic regime: Open branched, non-spherical rhodoliths reflect low energy conditions and infrequent turning (Bosence, 1976; Bosence, 1991). In low energy environments, rhodoliths are mostly turned by animals such as sea urchins or fishes (Bosence and Pedley, 1982; James, 2000). A different mode of transport and turning is by rafting wherein phylloids function as a sail that results in positive buoyancy even in low energy currents (Freiwald and Taviani, in prep.). Boxwork rhodoliths have also been interpreted to reflect relatively low energy conditions (Basso, 1998; Rasser and Piller, 2004). Basso (1998) suggest, that low sedimentation rates as a result of winnowing out of sediment in high energy environments may favour the formation of spherical rhodoliths ("prâlines"). It follows, that high sedimentation rates and intermittent partial burial of rhodoliths may favour the development of a boxwork structure: If rhodoliths become partially buried in the sediment, higher energy is necessary to turn them over. To cope with increased sedimentation rate the thallus becomes thinner and more foliose to be able to propagate upward more quickly. Thereby red algae may act as bafflers and binders and stabilize the substrate. During periods of low sedimentation and agitation, the thallus

propagates parallel to the sedimentary surface and forms inclusions of more fine grained sediment.

All three floatstone to rudstone units are found to have been deposited under prevalent low energy conditions. Laterally continuous horizontal beds indicate deposition on a vast submarine plain where, during deposition of RFR1 and 2, only the finest sedimentary particles were transported from environments closer to the shoreline. For RFR3, intermittently elevated water energy that resulted in a higher degree of reworking and fragmentation of skeletal components is indicated. Along with increased hydraulic energy, higher sediment transport from environments closer to the shore occurred and increased sedimentation rate. Hydraulic energy, however, rarely was high enough to turn partially buried boxwork rhodoliths.

Burchette and Wright (1992) subdivide ramps in inner ramp, middle ramp and outer ramp. The middle ramp is defined as the part of the ramp below fair weather wave base and above storm wave base. Accordingly, RFR deposits are interpreted to have formed in a mid- to outer ramp setting although stabilization by plants may indicate lower than the effective hydraulic energy conditions. Nevertheless, RFR1 and 2, which show little evidence of reworking by waves, are interpreted to represent outer ramp deposits whereas some of the RFR3 facies shows evidence of intermittent reworking and is therefore interpreted to have been deposited in a mid ramp setting.

Analogues, modern and ancient: One of the best known modern red algal facies is the maerl facies that was originally defined by Lemoine (1910) as a sediment formed predominantly by two distinct species at the Breton coast (*Phymatolithon calcareum* and *Lithothamnion coralloides*). These species commonly form thin, brittle branches <1,5mm in diameter (Irvine and Chamberlain, 1994) that break off easily, for example from algal build-ups and are carried away to continue to grow as unattached branches or rhodoliths (Henrich et al., 1995). The formation of Maerl implies high hydraulic energy conditions and therefore is found predominantly in shallow water in a depth of up to 30m, for example along the coast of Britanny or Norway (Henrich et al., 1995). In the Mediterranean, the maerl facies is reported down to 60m (Jacquotte, 1962) or 75m water depth (Freiwald and Taviani, in prep.). Maerl forms a part of the “biocoenose des fonds detritiques” of Pérès and Picard (1964). Pérès and Picard (1964) state that in depths where hydraulic energy is low, organisms such as sponges, annelids and pelecypods are responsible for the high degree of fragmentation in this environment. Biodegradation thus could also provide detritus with solid surfaces (mostly red algal fragments) necessary for the germination of red algae in low energy environments. The

RFR facies are different from the typical maerl facies in two aspects: 1) the common maerl species have not been identified in the material from Crete (see chapter 6.2.) and branches with a diameter smaller than 1,5mm are uncommon; 2) even if biodegradation plays a role, in contrast to most of the RFR facies, maerl is commonly associated with high energy deposits.

Pérès and Picard (1964) differentiate between maerl and the "faciès des prâlines". The latter has been found on isolated plateaus with especially low turbidity and is characterized by irregularly shaped laminar nodules, much more like the RFR facies than the maerl facies. Pavements with "prâlines" have been described to form facies belts in deeper water adjacent to the maerl facies on structural highs in the Strait of Sicily, in water depth between 50m and 120m (Freiwald and Taviani, in prep.). Within the "faciès à prâlines" the abundance of boxwork rhodoliths was observed to increase with depth. Thus, if the modern Mediterranean is taken as an analogue, for the RFR3 facies an increased water depth compared to the RFR1 and 2 would have to be assumed. At the same time, however, analysis of the RFR3 facies indicates an increase in hydraulic energy, reworking and sedimentation rate.

While living coralline red algae are found down to 134m water depth (Freiwald, pers. comm.), many of the deep rhodolith accumulations and bioclastic sediments (détritique du large) found in the Mediterranean represent relic facies (Caulet, 1972; Freiwald and Taviani, in prep.). This is a consequence of the Holocene sea level rise to approximately 130m above the past glacial lowstand. Another consequence is that in many areas the subtidal shoreline is formed by rocky substrates with little sediment cover that favour encrusting communities (Pérès and Picard, 1964; Fornos and Ahr, 1997). For these reasons, the modern Mediterranean, which has often been used as an analogue for the past, may not be such a good analogue for the Neogene of Crete.

On the other hand outer to middle ramp rhodolith deposits are abundant in Miocene carbonates in the Mediterranean. They have been described from the Lower-Middle Miocene in the central Apennines of Italy and have been compared to the modern faciès à prâlines (Carannante and Simone, 1996; Brandano and Corda, 2002). Mid ramp rhodolith rudstone with red algal build-ups very similar to RFR3 facies with associated RB facies (see below) are also described from the Oligo-Miocene of Sicily (Pedley, 1998). Outer ramp rhodolith rudstone deposits are described from the Upper Miocene of Menorca but have been interpreted to have been deposited under the influence of strong currents (Pomar et al., 2002).

Red algal bindstone (RB)

Description: Coralline red algal bindstone is restricted to the occurrences of RFR3 in LFA2a (sections MS3 and Moni1; Fig. 2.2.5.; 2.4.8.a). The extent of three-dimensional networks of red algae is hard to identify in outcrop. The thickness of bindstone intervals is <1m. It consists of branching and foliose red algae (*Mesophyllum sancti dionysii, Mesophyllum* sp.2 and *Lithophyllum incrustans*; see chapter 3.3.) and a marly matrix with few benthic foraminifera and bioclasts (Fig. 2.4.8.b). It overlies beds with abundant rhodoliths or oysters.

Facies analysis and interpretation: The formation of red algal bindstone is usually restricted to relative low sedimentation rates and high substrate stability under moderate hydraulic energy conditions (Rasser and Piller, 2004). The marly matrix reflects the ability of the structure to trap fine sediment particles. Red algal bindstone found in the RFR3 facies in LFA2a may be comparable to the coralligène de plateau found in the recent Mediterranean (Pérès and Picard, 1964; Bosence, 1985) that is also constructed by *Mesophyllum sancti dionysii* (as *M. lichenoides* in Bosence, 1985) among others.

Packstone with sand (PS)

Description: Components are mainly sand sized micritized carbonate grains and 10% to 40% silt to medium sand sized siliciclastic grains. The poorly rounded siliciclastic grains are dominantly quartz and moderately classified. Matrix is rich in clay, sedimentary structures are

Fig. 2.4.8. (next page): Red algal bindstone (RB), packstone with sand (PS) and calcareous sandstone facies (CS) of LFA2
(see Fig. 2.2.1. for locations)
a: Red algal bindstone interval in LFA2 of section MS3
b: Thin section photograph red algal bindstone in section MS3. *Lithophyllum incrustans* (lower right) is overgrown by *Mesophyllum sancti dionysii* (arrow), *Mesophyllum* sp. and *Titanoderma pustulatum*, MD14
c: Field aspect of packstone with sand (PS) northeast of Matala (section MO1)
d: Thin section photograph of *Heterostegina* floatstone in sandy packstone matrix of the BSP facies, section MS1 (MS6)
e: Pocket of *Heterostegina* rudstone in sandy packstone of the PS facies, section MO1
f: Fine grained calcareous sandstone of the CS facies, section VO (VO6)
g: Meterscale low-angle crossbedding in calcareous sandstone of the CS facies northeast of Matala


a

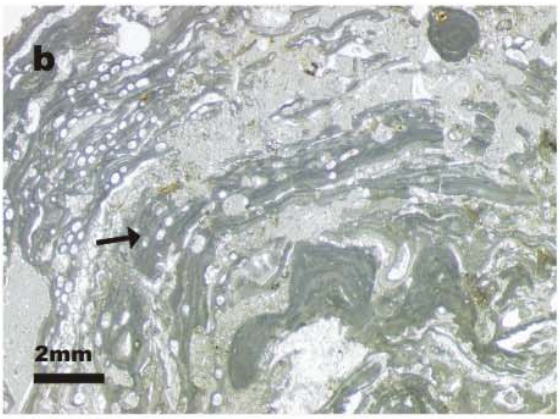
b
2mm


c

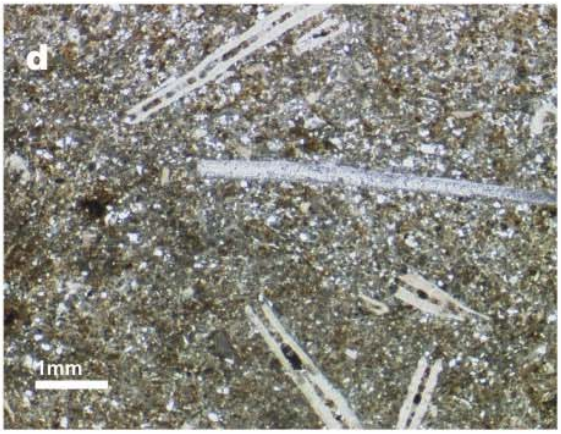
d
1mm


e

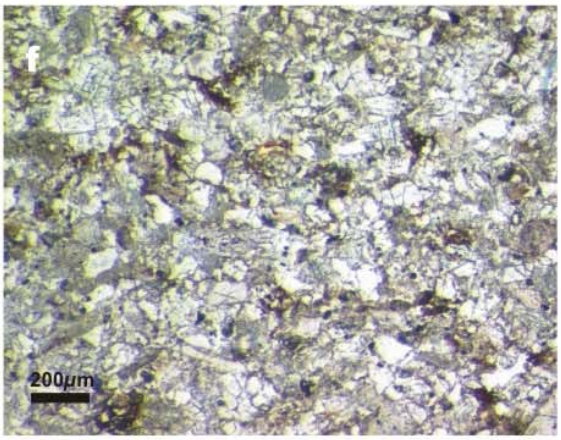
f
200μm


g

not visible but bioturbation by *Thalassinoides* is common. In the Matala area between sections MO1 and MO2, the content and grain size of siliciclastics increases towards the east. Marked bedding planes are absent in the unit (Fig. 2.4.8.c). Packstone contains intervals of rhodolith- or *Heterostegina* floatstone (Fig. 2.4.8.d). Other macrofossils are infaunal echinoids (*Schizaster* sp.), various bivalves (*Pecten* spp., *Chlamys* spp., *Ostrea* sp., *Cardium* sp., *Panopea* sp.), Gastropods (*Turritella* sp., *Conus* sp., *Strombus* sp.). More rarely, celleporiform bryozoans occur. *Turritella* sp. is especially abundant in the lower part of section MO2. Calcite shells are little fragmented whereas aragonite shelled molluscs are only preserved as casts. In the Matala area, intervals with pockets of *Heterostegina* rudstone resulting from bioturbation occur (Fig. 2.4.8.e).

The packstone with sand lithology is found in the basal part of the carbonate succession LFA2a) around Matala (sections MS1, MA, MO1, MO2, Fig. 2.2.3.; 2.4.4.) and along the western coast (section VO, Fig. 2.4.1.). It overlies a basal bed of rhodolith rudstone (RFR1; sections MO, MO2, VO) and reaches a thickness of 15m in the area of Matala (Fig. 2.4.8.c) and 4m at Vathi.

Quantitative biofacies analysis: Thin section analysis shows that coralline red algae and foraminifera each account for one third of total faunal elements. The remaining 30% are echinoids, bryozoans and bivalves (Fig. 2.4.7.). To the south (section VO), the proportion of red algae and red algal fragments increases to more than 70% (Fig. A4). The amount of casts of aragonite shelled molluscs found in this lithology, however, suggests that the proportion of molluscs was considerably higher in the living faunal assemblage than indicated by thin section analysis. Bryozoans are dominantly delicate branching forms. The proportion of red algae is variable and depends on whether rhodoliths are sampled by the analyzed thin sections. According to the definitions of Lees and Buller (1972) and Carannante et al. (1988), the sediment is classified as foramol or rhodalgal, respectively.

Facies analysis and interpretation: While sedimentary structures have been destroyed by bioturbation, low grain size and high clay content indicate deposition in a low energy environment. Preservation of casts of infaunal bivalves shows that the sediment was not significantly reworked. Therefore an environment comparable to RFR1 and 2 is assumed. However, the substrate was muddier and softer compared to the RFR facies and scarcity of solid substrates for germination of red algae explains their limited occurrence. High siliciclastic input may also have hampered coralline growth and limited carbonate production.

A shoreward transition into sandstone found in the Pitsidia, Sivas and Moni Odhiyitria area (CS facies) is assumed but poorly represented by outcrops.

Calcareous sandstone (CS)

Description: The sandstone consists of well classified fine to medium grained sand. Proportions of siliciclastic grains are 40-70%. Grains are angular and siliciclastic grains are predominantly quartz (Fig. 2.4.8.f). Sandstone is poorly cemented and matrix content is low. It is usually not bioturbated but shows decimeterscale to meterscale low angle (usually <10°) trough crossbedding (Fig. 2.4.8.g). Macrofossils are rare rhodoliths that mostly occur in pockets and locally *Heterostegina* as well as rare large (up to 15 cm) specimens of *Pecten* or *Chlamys*.

The calcareous sandstone always underlies the rudstone with pebbles facies (RP; Fig. 2.4.3.e) that is traceable over the largest part of the WAT. The sandstone is also intercalated into rhodolith floatstone at section KL (Fig 2.2.6.). East of Matala (section MO1), it reaches a maximum thickness of 24m, including intercalated rudstone beds, and decreases in thickness to the east and west (Fig. 2.4.4.). Southward it decreases to 11,5m at section MS3 and 6,5m at section VO (Fig. 2.2.3.). At Moni Martsalo (section MaN), the bed underlying the RP horizon is 2m thick and at Mount Rhodonas the maximum thickness of intercalated sandstone is 1,5m (Fig. A6). Comparable sandstone is found at Pitsidia and Sivas (sections PE, Sivas, Fig. 2.2.4.) where it is unconformably overlain by coral framestone with a basal layer of rhodolith rudstone with quartz pebbles. At Sivas, the fine grained sandstone is intensely bioturbated. Between 31m and 35m above the base of section Moni1 (Fig. 2.2.5.), a comparable sandstone bed is found underlying limestone with quartz pebbles. The number of sandstone intervals underlying RP beds increases to three at section Moni2 of which the thickest interval that overlies basal rhodolith rudstone reaches a thickness of 9m. It has concretions up to 30cm in diameter in the lower 5,5m, has no visible sedimentary structures in the middle part and is trough crossbedded in the upper 1,5m. It contains a 30cm thick layer with oval, densely branched, concentric rhodoliths. Grain size is fine sand but increases to coarse sand in beds underlying the RP facies

Quantitative biofacies analysis: The proportion of faunal elements recognizable in thin section among components is usually <10%. Foraminifera, mostly miliolids, contribute the largest part (40 - 70%; Fig. 2.4.7.; A4). Additionally, delicate branching bryozoans and bivalve shells occur together with rare echinoid fragments and red algal debris. In certain intervals (section MO), incrusting bryozoans with a central void are common.

Facies analysis and interpretation: The described lithology is characterized by the relatively uniform size of components and the low matrix content. Large scale crossbedding indicates formation of submarine dunes by swell or by currents. The size of components indicates moderate hydraulic energy: Only components smaller than fine to medium sand and most of the matrix were winnowed out from the sandstone. Intercalated rudstone of the RP facies within the sandstone wedges out towards the west at the Matala transsect (Fig. 2.4.4.) and grain size of allochtonous components (siliziclastic pebbles) within RP beds increases to the east (see below). Compared to the RP facies, the well sorted CS facies reflects lower hydraulic energy conditions. Similar to the RP facies, increasing grain sizes to the east of the WAT (Moni Odhiyitria area) in the CS reflects an increase of hydraulic energy. The fine grained CS facies in the Pitsidia-Sivas area on the other hand is interpreted to represent a nearshore equivalent of the PS facies.

The common association of the CS facies with the RP facies suggests a genetic relationship: The accumulation of sandstone is interpreted to be the result of winnowing out of this material from the high energy rudstone facies that formed a facies belt shoreward of the CS facies (see below). A sandstone-rudstone couplet is thus the result of progradation of facies belts. The scarcity of large faunal components in the sandstone suggests high sediment instability, preventing either colonization by or preservation of macro-organisms. On the other hand, local occurrence of bryozoans with a central void most likely reflects a not preserved plant host such as kelp (Spjeldnaes and Moisette, 1997) and therefore indicates intermittent colonization of the sandy ocean floor by plants that provided a habitat for benthic foraminifera. Constant or episodic detritus input from the rudstone facies and substrate unstability, however, inhibited colonization by slow growing organisms such as red algae. The more short living and vagile foraminifera, however, may have lived in this environment. Foraminifera tests, due to their relatively low specific weight, which was possibly further reduced by gas accumulation in the chambers as a consequence of decay (Racey, 2001), may also have originated from the rudstone facies situated landward of the CS facies.

Crossbedded marine sands are usually interpreted to represent inner ramp shoal deposits (Burchette and Wright, 1992). The deposition seaward of the condensed rudstone facies that was deposited under intermittent high energy conditions, however suggests a mid ramp setting. Mid- and outer ramp cross-bedded sandstone has been described by Pomar et al. (2002) from the Upper Miocene of Menorca.

Rudstone with pebbles (RP)

Description: The rudstone with pebbles facies (Fig. 2.4.9.a) is characterized by the occurrence of well rounded quartz pebbles that are especially abundant at the base and up to 4cm in diameter (Fig. 2.4.9.b). Diameter is increasing towards the east between Matala and Pitsidia (Fig 2.4.9.c). Grain size composition is bimodal with a matrix of calcareous sandstone (Fig. 2.4.9.d). The rudstone beds are 0,5 – 2m in thickness and commonly bioturbated. This results in an uneven, undulating base and the formation of pockets of pebbles at the top of the underlying sandstone. Macrofossils are rhodoliths, celleporiform bryozoans, *Pecten*, *Ostrea*, *Clypeaster* and *Heterostegina*. Rhodoliths are densely to open branched except in a 50cm thick bed at section Moni2, where oval, concentric and horizontally oriented rhodoliths of uniform size (4cm) occur. Many bivalve shells are bored by sponges. To the south (section VO) the occurrence of *Heterostegina* in the section may be limited to the uppermost of the rudstone horizons whereas the lowermost rudstone bed is colonized by *Tarbellastrea* and *Acanthastrea*.

At section MS1, the rudstone horizon shows a distinct vertical organisation: It is characterized by a 120cm thick basal rudstone with quartz pebbles and abundant *Heterostegina* (Fig. 2.4.9.b) overlain by a 50cm thick rudstone bed with quartz pebbles, abundant rhodoliths, celleporiform bryozoans, *Pecten*, *Ostrea* and *Clypeaster* and *Heterostegina*. Shells are usually intact but extensively bored by sponges. Some tests of *Heterostegina* are broken. The top of this bed is plastered by *Pecten*, *Ostrea* and *Clypeaster* in upright position. In the basal part of the overlying massive rhodolith bed the content of these components decreases upward. Rudstone grades into carbonate mud and clay rich rhodolith floatstone (RFR2) and the siliciclastic content decreases considerably.

Up to four rudstone horizons are found intercalated into and overlying calcareous sandstone of the CS facies (Fig. 2.4.9.a). The uppermost horizon separates LFA2a with limestone rich in siliciclastics from LFA2b with mostly pure limestone. It can be traced in the area of Matala (Sections, MA, MO1, MO2, MS1, MS3; Fig. 2.2.3; 2.4.4., A4), along the western coast (section VO, Fig. 2.4.1.) and eastward into the Moni Odhiyitria area (sections Moni1 and 2, Fig. 2.2.5.). It can also be traced north of Ayofarago Gorge to Moni Martsalo (section MaN). It is, however, absent in the southernmost outcrops (western Martsalo Bay, sections MA1, MA2, Fig. 2.2.3.) and the outcrops situated the furthest to the southeast (Mount Rhodonas, section KL, Fig. 2.2.6.). It is also absent north of Kristo Kefali (section KN) and at Martsellos

Fig. 2.4.9.: Rudstone with pebble beds (RP facies) and bioclastic packstone facies (BP) (see Fig. 2.2.1. for locations)
a: Upper rudstone with pebbles horizon (RP facies) at section MO2 overlying calcareous sandstone
b: Base of the uppermost rudstone with pebbles horizon at section MS
c: Upper rudstone with pebbles horizon (RP facies) close to the waste dump west of Pitsidia, outcrop has been destroyed
d: Thin section of RP facies at section MO1, top of upper condensed horizon. 1: Melobesoid coralline red alga, 2: bivalve shell, 3: *Heterostegina* with thick tests. Matrix consists of calcareous sandstone similar to CS facies, MO16a
e: Bioclastic packstone (BP facies) east of Matala with *Clypeaster*
f: Thin section of BP facies (section MS) with abundant *Amphistegina* (1) and delicate branching bryozoa (2), MS16

Ridge (section Mart) where thickness of LFA2 is reduced. In the north, at Pitsidia and Sivas, a 1,6m thick rudstone bed underlies the coral rudstone at Pitsidia (section PE) and coral framestone at Sivas (section Sivas).

Additional rudstone horizons that are intercalated in the crossbedded sandstone below have a more limited spatial extent. In the Matala area these horizons wedge out to the west of section MO1 and become richer in pebbles to the east towards section MO2 (Fig. 2.4.4.). At section Moni2, the second horizon of a total of four is characterized by decimetre scale trough crossbedding and a well rounded sand fraction.

A second rudstone bed with pebbles underlying bioturbated sandstone at Sivas differs from the described lithology in that pebbles are poorly sorted and rounded. *Ostrea* is more abundant and *Porites*- and *Acanthastrea* fragments occur also. This horizon unconformably overlies sandstone of LFA1 (Fig. 2.2.3.).

Quantitative biofacies analysis: Average content in red algae is below 50% in all sections and thus significantly lower than in the RFR facies (Fig. 2.4.7.; A4). The results of thin section analysis, however, vary considerably due to the size of components but also reflect a pronounced heterogeneity of the rudstone horizons: The content in foraminifera (mainly *Heterostegina*) in the Vathi section is significantly lower than in both sections at Matala (MO1, MS, Fig. A4). The colonization of the lower condensed bed in the Vathi section by framework builders is reflected by an increased content in corals and serpulids. The condensed rudstone below the bioturbated rudstone at Sivas is characterized by the absence of bryozoan and echinoid particles.

Facies analysis and interpretation: The RP facies shows evidence for high energy conditions as well as low to moderate energy conditions: High hydraulic energy is indicated by quartz pebbles that are up to 4cm in diameter and well rounded. Large biota, on the other hand may as well be autochthonous and therefore not indicative of high hydraulic energy. However, proportions of *Pecten* and *Ostrea* that have the ability to attach themselves to a hard substrate, are higher in this sediment than in other lithologies. They occur together with *Clypeaster* that is found in high numbers along omission surfaces (Forst, 2003). *Heterostegina depressa* is also preferentially found on hard bottom substrates in the modern Red Sea (Gulf of Aqaba; Reiss and Hottinger, 1984) and Bay of Safaga (Piller, 1994) and on coarse skeletal debris (Hottinger, 1977). Extensive boring of shell surfaces indicates long times of exposure on the sea floor that may have resulted in a taphonomic bias by preferential preservation of faunal elements that are more resistant to (bio-)degradational processes.

Intervals of moderate water energy are indicated by the bimodal grain composition with a fine to medium sand matrix between coarse skeletal elements. However, the finer grain fraction may have been stabilized through fleshy algae or baffling by plant roots (Gómez-Pérez et al., 1998). A similar association of *Heterostegina* with stabilizing small green algae has been observed by Hottinger (1977) in the Gulf of Elat. Pedley (1998) describe the ability of red algal pavements to protect some of the fine grain fraction from being winnowed out. Stabilization by cementation, on the other hand, is not observed. Nevertheless the relatively low degree of fractionation of shells precludes permanent reworking. Moreover, celleporiform bryozoans that are sensitive to abrasion (Smith and Nelson, 1996) and therefore not likely to have been preserved under lasting high energy conditions are abundant. The open branched character of many rhodoliths that rules against frequent turning by waves (Bosence, 1976) also precludes constant reworking of the sediment.

The described horizons lack the characteristics of tempestites *sensu* Ager (1974), Aigner (1982) formed during one storm event such as graded bedding, imbrication and high proportions of disarticulated shell material. Instead, an amalgamation of several storm events and successive quiet periods is indicated by the composition of components. An event condensation process that leads to the amalgamation of two communities, one associated with periods of hard substratum after storm events and the other associated with soft substratum conditions during quiet intervals has been described by Seilacher (1984). A similar condensation process of components indicative of high energy conditions such as quartz pebbles, *Pecten* and *Clypeaster* and biota associated with low energy conditions such as open branched rhodoliths and celleporiform bryozoans explains the composition of the RP facies. Seilacher (1984) have shown that condensation down to one initial event deposit can operate in geologic time scales and that, depending on the frequency of storm events, the degree of fragmentation and abrasion of biota is not necessarily high. Additional to sediment of the amalgamated storm lags, the facies consists of fine sediment deposited during quiet intervals. Protection from being winnowed out by possible plant cover or pavements of coarse skeletal elements explains the preservation of fines. However, it is likely that most of the fines relate to the latest stage of the formation of the condensed horizon whereas the earlier deposited fines were winnowed out to form the CS facies. Bioturbation resulted in homogenization of the sediment and in mixing of older and younger elements of the horizon. The similarity of the matrix of the RP facies to the CS facies suggests, that during quiet phases, the ocean floor was quite similar in both facies types with the difference, that in the RP facies, the soft sediment cover was stripped off and redeposited seaward during storm events.

A multi-stage process for the deposition of the RP facies is best reflected at section MS1, where in successive amalgamated horizons a change of biotic associations is observed. The transition into the overlying RFR2 facies with a more marly matrix suggests deepening and decrease in storm wave influence. The top of the RP horizon thus has characteristics of a lag deposit.

Conditions to form the RP deposits are met in a mid-ramp setting below fair weather wave base but above storm wave base. High energy concentric rhodoliths and a matrix of well rounded sand east of Moni Odhiyitria, on the other hand, reflect more constant high energy conditions and thus frequent storm influence or even reworking by fair weather waves.

An erosional character of the base of rudstone beds is precluded by the relatively constant thickness of the underlying calcareous sandstone. A higher stratigraphic position of the uppermost RP horizon underlying coral framestone in the Pitsidia-Sivas area and the presence of a hiatus at the base of the condensed bed, however, is indicated by the absence of the transgressive RFR2 facies or its nearshore equivalents.

Bioclastic packstone (BP)

Description: The packstone consists of bioclasts and skeletal fragments that are mainly fine to medium sand sized (0,1-0,3mm in diameter) and some intact tests that are mostly <1mm in size. Components are oriented horizontally. The matrix has a mottled texture that results from partially decomposed bioclasts and silt sized peloids. Mud content is variable and mud-rich wackestone intervals occur. The packstone is usually rich in *Heterostegina* (Fig. 2.4.9.f) contains *Clypeaster* (Fig. 2.4.9.e) and in the uppermost BP beds in section MS also coral fragments up to 4cm in diameter. Large red algal components are rare.

The BP lithology is intercalated into rhodolith floatstone and rudstone (RFR2) above the uppermost RP horizon and below the framestone horizons (CF) of LFA2c. Eastward of Matala, the bioclastic packstone (Fig. 2.4.9.e) increases in thickness while the MRB above the condensed horizon becomes thinner or wedges out (Fig. 2.4.4.). The unit reaches a thickness of 10m at section MO2, 5m at section MS3 and 4m at section MS1 (Fig. 2.2.5.; A4). The lithology can be traced as far east as Moni Odhyitria, where it reaches a thickness of 7m (section Moni1). In this area, where no coral horizons are present, the lithology usually is found at the top of the Neogene deposits. At sections MA and MO, this lithology is reduced to a thickness of <2m. Bioclastic packstone also directly overlies the RP horizon at section MaN.

It is, however, absent below the coral horizons at section VO. At Mount Rhodonas (section KL, Fig. 2.2.6.), a 3m thick bed of bioclastic packstone is intercalated at 30m above the base of the section that contains abundant siliciclastic components. Upsection it occurs associated with small, 50-100cm high coral build-ups. West of Martsalo Bay (section Ma2), bioclastic packstone occurs only as thin (<50cm thick) layers.

Quantitative biofacies analysis: Quantitative analysis shows, that proportions of biotic groups vary considerably from section to section (Fig. A4). Most samples are, however, dominated by foraminifera (Fig. 2.4.7.). Similar as in the CS facies, the proportion of miliolids is very high. In contrast to CS, however, *Heterostegina* and *Borelis* are also abundant (see chapter 3.2.). Red algae, on the other hand are only present as fragments. Bryozoans are mostly delicate branching (Fig. 2.4.9.f). Bioclastic packstone intercalated in the KL section, however, is different, in that it contains not only abundant red algae and coral fragments as in section MS1 but also bivalves and serpulids.

Facies analysis and interpretation: The grain size classified character of the sediment and orientation of components suggests a moderate energy environment in a setting comparable to the CS facies. The similarity is also reflected by high proportions of miliolid foraminifera. Horizontal orientation of components indicates reworking. Crossbedding is not preserved in the bioclastic packstone lithology but the abundance of thick shelled *Clypeaster* also indicates elevated hydraulic energy conditions. The abundance of *Heterostegina* indicates open marine conditions rather than a restricted environment (Hottinger, 1977; Hallock and Glenn, 1986; Hohenegger, 1995). *Heteostegina* is found commonly in sand and gravel on the seaward side of coral reefs (Hottinger, 1977). In the Cretan sections, this facies, however is mainly found underlying laterally continuous biostromes (Fig. 2.4.4.) and in areas where no reefs occur. Interfingering with a reef facies has not been observed. The occurrence of coral debris in the packstones, however suggests that small reefs existed landward of the BP facies that are not preserved. In spite of the differences in lithology and biotic associations, the BP facies is interpreted to have formed analogous to the CS facies by winnowing out of sand sized material from a higher energy facies and/or shore parallel transport. As in the CS, the facies is characterized by unstable substrate that did not permit large and long living organisms such as red algae to thrive.

Coral framestone and –rudstone to floatstone

Description: Coral frameworks form laterally extensive sheets with gradual changes in thickness. In situ framework laterally passes into intervals with massive coral debris (coral rudstone) or debris floating in a fine grained and locally marly wackestone to packstone matrix (coral floatstone, Fig. 2.4.10a). Framework builders are *Porites* and *Tarbellastrea* with rare *Acanthastrea.* Common growth forms of *Porites* are 1 - 4cm thick branches or columns that are up to 1m high and may be stabilized by lateral bridges (Fig. 2.4.10.b). It also forms massive encrustations (Fig. 2.4.10.c). *Tarbellastrea* (Fig. 2.4.10.d) forms tabular to globular colonies that are usually 5 - 10cm in diameter. While either massive or columnar growth forms dominate frameworks and the relative abundance of *Tarbellastrea* varies, lateral or vertical zonation is not observed. Preservation, however, is poor and framework density therefore can only be roughly estimated to reach 50-70% (Fig. 2.4.10.c). Intraframework sediments are mudstone or packstone (Fig. 2.4.10.e) but space filled by rudstone also occurs.
Laterally continuous coral framework and coral debris horizons are present at the base of LFA2c across the largest part of the WAT (Fig. 2.2.3. – 2.2.5.; 2.4.11.). In the northwestern part and along the western coast down to Vathi, two continuously present coral horizons form a conspicuous cliff, often with caliche-covered overhangs (Fig. 2.4.10f). The thickness of each horizon is between 1 and 5m. Coral horizons occur 8 - 12m above the RP horizon (top of LFA2a) in the Matala area (sections MO, MS, PW; Fig. 2.2.3.; 2.4.4.; 2.4.11.) but thickness of sediment between the RP horizon and the lower coral horizon increases to 25m in the south of the WAT (section MaN). Coral horizons wedge out towards the west as can be seen at the westernmost tips of the coastline (Fig. 2.4.4.). Along the southern rim of the Messara basin, at

Fig. 2.4.10 (next page): Coral framestone (CF facies) and associated lithologies of LFA2c and rudstone with *Terebratula* facies (RT)
(see Fig. 2.2.1. for locations)
a: Coral floatstone to rudstone with coral debris in the lower coral horizon at section VO
b: Columnar *Porites* at the base of the lower coral horizon south of Matala
c: Massive *Porites* (red) and *Tarbellastrea* (green) in the lower coral horizon at section MO1
d: Thin section of *Tarbellastrea* framestone, lower framestone horizon, section MO1. Of the coral, only micritic infillings are preserved, MO19c
e: Intraframework wackestone with abundant echinoid fragments and crustacean carapace (arrow), lower coral horizon, section MO1 (MO19g)
f: Bay of Matala, view from the south. Note conspicuous cliffs formed by the two coral framestone horizons (arrows). Mount Psiloritis is visible in the background
g: Red algal boundstone on top of the lower coral framestone horizon, section MO1. Encrusters are 1: foraminifera, 2: melobesoid red algae, 3: serpulids. MO20a
h: Rudstone with *Terebratula* (arrow), RT facies, top of section MO1

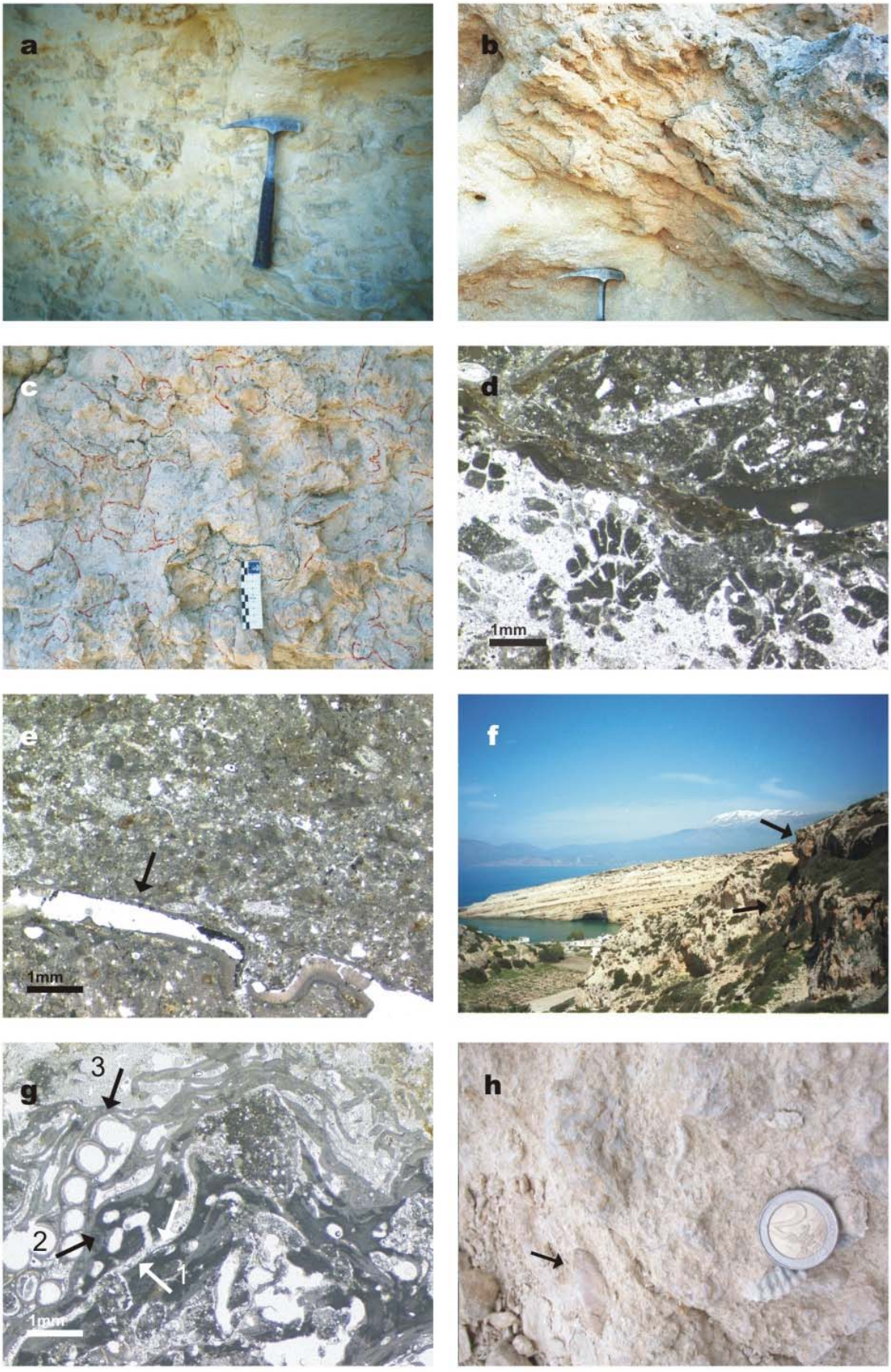
a
b
c
d
1mm
e
1mm
f
g
3
2
1
1mm
h

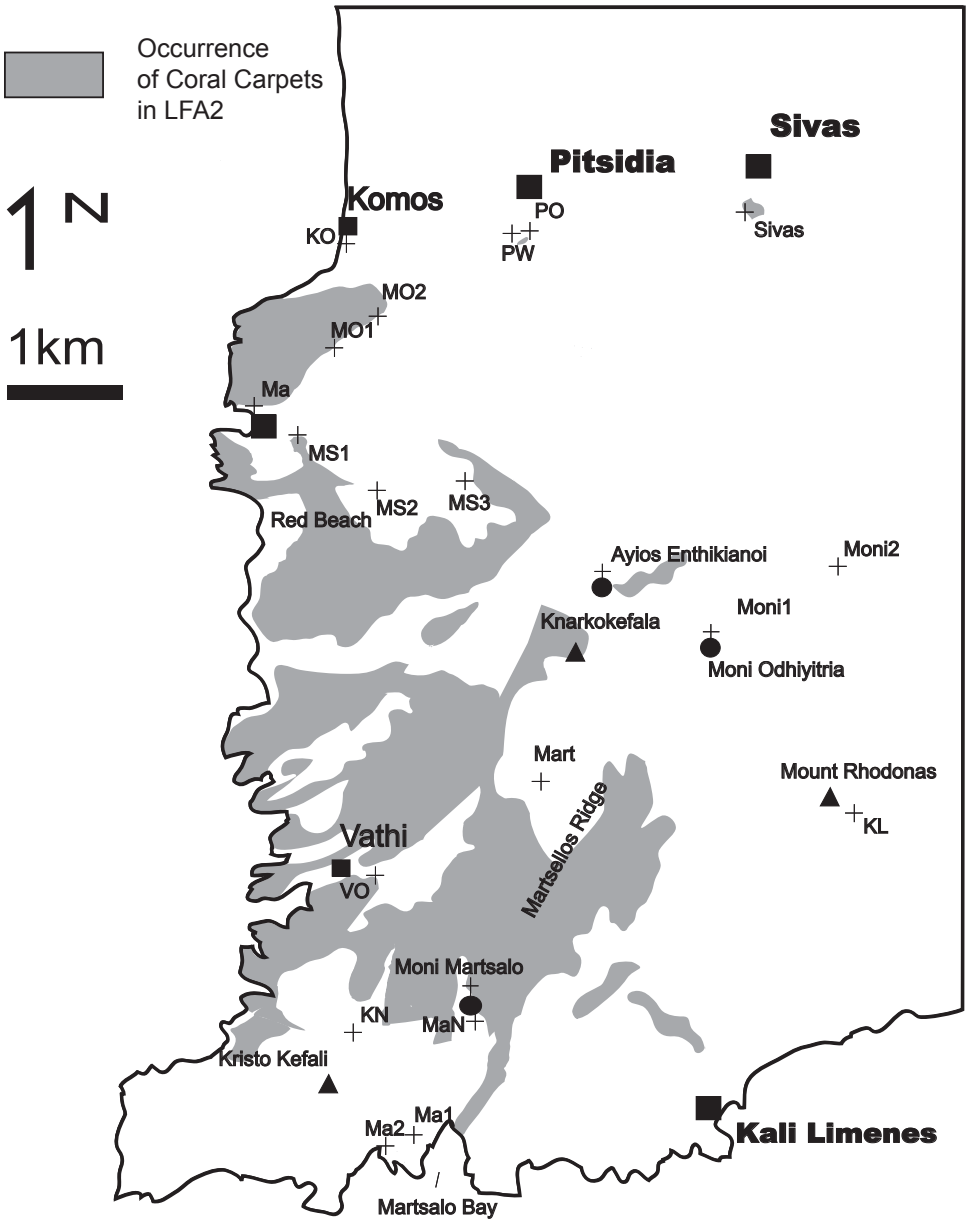

Fig. 2.4.11: Distribution of coral carpets in LFA2c in the WAT

Pitsidia and Sivas (Sections PO and Sivas), only one 1 - 3m thick coral horizon occurs that almost directly overlies rudstone with pebbles. West of Martsalo Bay, laterally extensive coral units are absent. Around Moni Odhiyitria, no corals are present in LFA2. At Mount Rhodonas, only patches of framework forming corals occur.

At section MO1, the lower coral horizon is covered by 1m of red algal bindstone with abundant serpulids (Fig. 2.4.10.g). Thin, a few mm thick incrustation by encrusting foraminifera or red algae (*Mesophyllum sancti dionysii*) of corals is also observed within the framework.

Quantitative biofacies analysis: Results of quantitative thin section analysis indicate that coral skeletons contribute an average proportion of 50% of skeletal elements total (Fig. 2.4.7.). The low number compared to estimated framework density results from the

incorporation of the coral floatstone and rudstone lithology as well as the encrusting coralline red algal lithology covering biostromes. It also explains the relatively high red algal content that reaches 50% in samples of the intraframework sediments. Proportions of other skeletal elements are similar to other lithologies except that crustacean carapaces occur in several samples (Fig. 2.4.10.e; A4).

Facies analysis and interpretation: The coral horizons are best described as biostromes (autobiostromes or autoparabiostrome) *sensu* Kershaw (1994) or coral carpets (Riegl and Piller, 1997; Riegl and Piller, 1999). Coral carpets have been studied in detail in the modern Red Sea by Riegl and Piller (1997)and Riegl and Piller (1999): Coral carpets occur in areas with no pronounced seafloor relief and/or low hydraulic gradients. These frameworks do not produce an accentuated three dimensional relief of their own but roughly follow the underlying topography. Since the hydraulic gradient and the gradient in light intensity are low, they possess only weak internal zonations. Instead they are observed to thin out and become patchy towards their periphery. Their lateral extent, however, may be vast, depending on the area suitable for colonization. They reach a thickness of at least 8m and cover an area of 16,6km^2 in the Bay of Safaga. Coral carpets formed chiefly by *Porites* as framework constructor occur in water depths between 5 and 25m. They occur in areas with low turbidity and sedimentation. Like in the coral facies on Crete, *Porites* with laterally fusing columnar growth forms dominate. The framework is strengthened further by massive and encrusting corals. In the case of the Crete carpets, these are *Tarbellastrea* and platy forms of *Porites*. The columnar framework is effective to trap sediments of variable grain sizes. Of the *Porites* columns, only the tips are alive and growing upward (Riegl and Piller, 1997; Riegl and Piller, 1999).

In Miocene *Porites* carpets on Crete, it appears that *Porites* has the ability to regenerate from fragments partially buried in sediment and to thereby establish new frameworks (Reuter *in prep*.).

Porites carpets that are the only form of coral framework in LFA2c cover large areas of the WAT (Fig. 2.4.11). Since sedimentary structures such as prograding clinoforms are absent, and the coral horizon forms a laterally continuous unit, an aggradational mode of growth of the *Porites* carpets similar as in their modern equivalents is inferred. Growth rates of coral carpets are assumed to be as high as 1-2m/k.y. (Riegl and Piller, 1999). Carpets are therefore interpreted to have covered a large level shelf area in a short time. Due to the lack of pronounced three dimensional seafloor topography and the low export of detritus, characteristic forereef and backreef facies do not occur.

Riegl and Piller (1999) stress the systematic difference between coral reefs and coral carpets. Coral carpets dominantly formed by *Porites* with additional *Tarbellastrea* have also been described from the Middle Miocene Leitha limestone of Austria (Riegl and Piller, 2000). In the Mediterranean, the Upper Miocene coral carpets found on Crete appear to be unique: While low diversity *Porites-Tarbellastrea* dominated frameworks are observed to be abundant in the upper Miocene of the Mediterranean during Late Tortonian and Messinian sea-level highstands, they commonly show a clear zonation (Esteban, 1996). In most cases however, they are related to high, often tectonically controlled relief that favours the formation of zoned fringing or barrier reef complexes.

Rudstone with Terebratula (RT)

Description: A rudstone bed with abundant *Terebratula, Pecten, Clypeaster, Heterostegina*, celleporiform bryozoans and laminar rhodoliths is found at the top of the carbonate succession in the area northeast of Matala (section MO1; Fig. 2.4.10.h) and at an outcrop between Kristo Kefali and Martsalo Bay (section Ma2) where it underlies marl of LFA3. The matrix consists of yellowish, marly mudstone with bioclasts of bryozoans and echinoids.

Facies analysis and interpretation: Since the *Terebratula* bed forms the top of LFA2c and is overlain by basinal marl of LFA3 (see below) the bed is interpreted to represent a lag deposit that formed in response to sea-level rise and resulted in sediment starvation on the outer ramp. Large biota are autochtonous and accumulated on the omission surface. A very similar *Terebratula* bed has been described by Pedley (1976) from the Miocene of Malta. There it has also been interpreted to reflect low energy conditions and the association with glauconitic sand also indicates sediment starvation. The widespread occurrence of this lag in the Matala area indicates that LFA3 may originally have been deposited over vast areas of the WAT but is preserved only in the Kristo Kefali area, where uplift occurred most recently.

2.5. Marl (LFA3)

This lithology consists of brown to grey, clay rich marl to marly limestone and siliciclastic rich intercalations. Sediments are rich in *Globigerina* and *Orbulina.*

Marl is the prevalent lithology in the Messara Plain. Outcrops are at Komos, east and southeast of Agia Triada and 1km north of Festos and at Kastelli, 2km northeast of Mires (Fig. 2.5.1.a). At most locations a transition from brown to blue-grey, thickly bedded, predominantly clay rich marl without sedimentary structures to more thinly bedded marl and marly limestone and rudstone at the top is observed.

At Komos, a 28m thick succession of alternating beds of clay rich marl and marly limestone (mudstone to wackestone) occurs (section Ko, Fig. A5). Marl beds are 0,5-2m in thickness and 20-70cm thick sandy packstone layers are intercalated. Beds are without internal structures or more rarely horizontally laminated. Bioturbation occurs also. Packstone layers often show centimetre scale wavy crossbedding or convolute bedding and in some cases graded bedding. Fossils are almost exclusively planktonic foraminifera (Fig. 2.5.1.b), only in the basal part of the succession, small gastropods occur in sandy interbeds. The top of the succession is formed by two well lithified limestone beds. The lower, 2m thick bed consists of graded rudstone with a micritic matrix. Components are *Halimeda* plates, bryozoans, mollusc and echinoid fragments, gastropods, red algae, planktonic foraminifera and *Heterostegina*. It also contains abundant lithoclasts of limestone similar to the RFR3 lithology found in the WAT (Fig. 2.5.1.c). The overlying 1,5m thick grainstone to packstone largely consists of planktonic foraminifera and bioclasts and shows wavy horizontal lamination. The top of both beds is bioturbated.

Fig. 2.5.1. (next page): Sediments of LFA3 (see Fig. 1.4.1. for locations)
a: Laminated marl of LFA3 at section FN with beds of wavily laminated limestone beds (top)
b: Thin section photograph of marl of LFA3 rich in planktonic foraminifera, top of section Ma2 (MB24)
c: Thin section photograph of rudstone at the top of LFA3, section KO, that consists of lithoclasts of LFA2 with *Heterostegina*, rounded basement gravel, red algae and *Halimeda* plates in a marly matrix with planctonic foraminifera (KO21)
d: Rudstone bed at the top of LFA3 (section FN)
e: Slumped succession of marl and coarse gravel 2km southwest of Timbaki, hammer for scale
f: Bioclastic rudstone with gravel at the base at the top of LFA3 1km north of Faneromeni, hammer for scale
g: Laminated marl of LFA3 between Kristo Kefali and Martsalo Bay overlying condensed bed (RT facies)

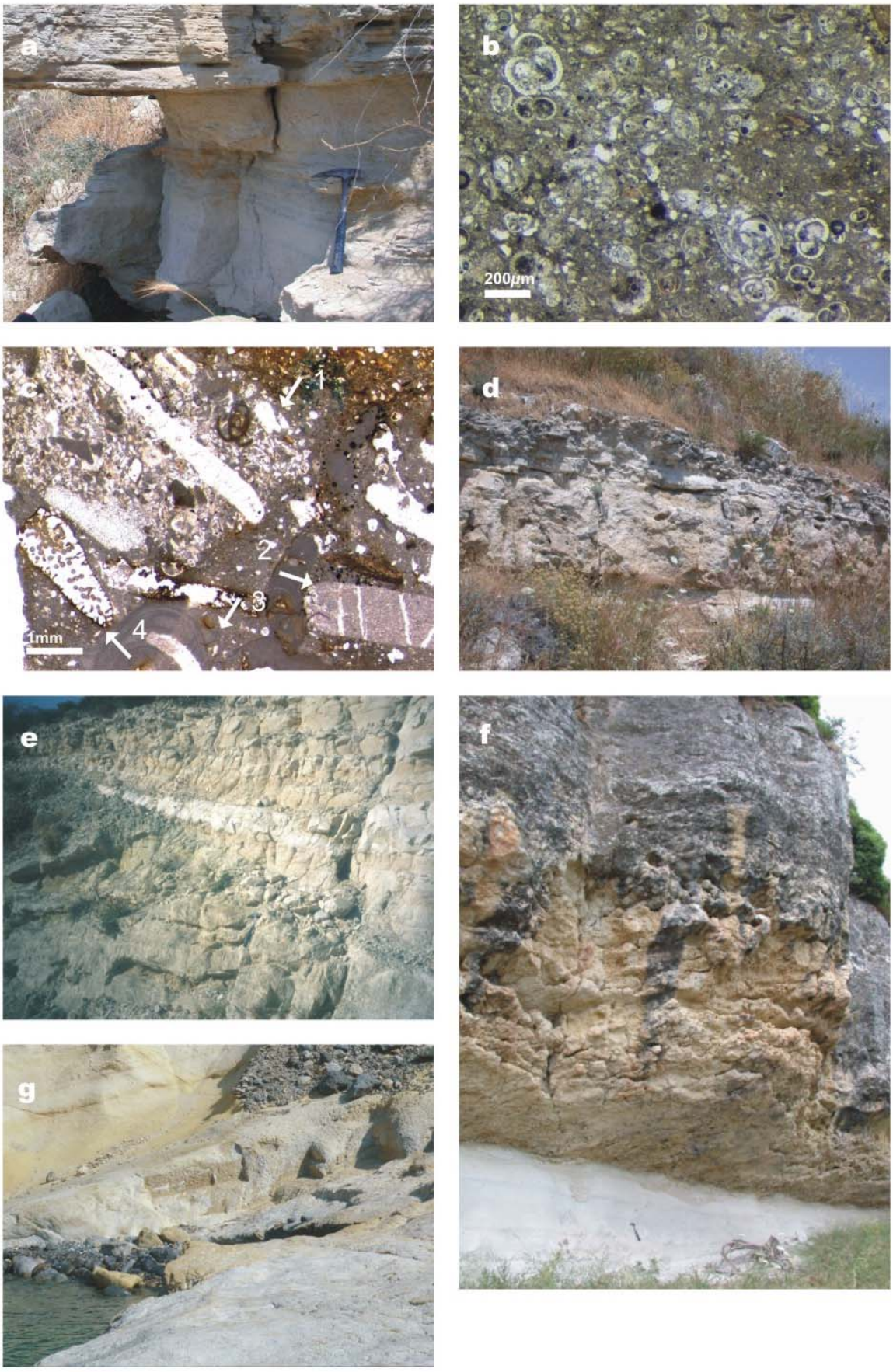
a
b
200μm
c
1
2
3
4
1mm
d
e
f
g

North of Festos (section FN) is the only location in the Messara Plain, where the base of the marl is exposed: It overlies basal sandstone of LFA1 (chapter 2.3.) and 4m of bioclastic rudstone (LFA2; chapter 2.4.). The rudstone consists of a basal bed of silty marl with abundant gastropods, small oysters and bivalves, overlain by *Heterostegina* rudstone and red algal framestone and rudstone with coral fragments up to 10cm in diameter. This succession is overlain by 38m of clay rich, blue-grey marl. The top of the section is formed by thin-bedded horizontally laminated marl and bioclastic packstone, occasionally with small pebbles at the base and bioturbation at the top. The uppermost 1,5m thick bed consists of graded bioclastic grainstone to packstone with pebbles and rip-off clasts at the base and vermetid and echinoid fragments together with *Halimeda* (Fig. 2.5.1.d).

The section near Kastelli dated by (Zachariasse, 1975; Langereis et al., 1984; Hilgen et al., 1995) has a thickness of 60m. It is described to consist mainly of blue-grey homogenous marl overlain by an alternating laminated-homogenous marl succession (Meulenkamp *et al.*,1979).

East of Agia Triada, at the road to Festos, an up to 2m thick bed of graded bioclastic rudstone to packstone that overlies alternating marl and limestone beds contains *Porites* fragments up to 1cm in diameter.

In the west of the Messara Plain, 2km south of Timbaki, coarse (up to 15cm in diameter) gravel is intercalated into thinly bedded marl. Gravel is poorly sorted and gravel-sized lithoclasts of *Porites-Tarbellastrea* framestone and Neogene sandstone is found among it. The succession shows evidence of large scale synsedimentary slumps (Fig. 2.5.1.e).

North of the village of Faneromeni, at the northern margin of the Messara Plain, 3km north of Festos, a succession of 50m of whitish, thin bedded marl to marly limestone and blue-grey, clay-rich marl is overlain by an up to 8m thick bed of bioclastic rudstone with abundant pebbles, *Pecten* and *Ostrea* at the base that grades into bioclastic packstone with benthic foraminifera (Fig. 2.5.1.f). The thickness of this bed is highly variable and it is overlain by a succession of boulder conglomerates that is tens to hundreds of metres thick.

In the WAT, marl occurs in a small outcrop between Martsalo Bay and Kristo Kefali (section Ma2, Fig. 2.2.3.; Fig. 2.5.1.g). It overlies a condensed bed with abundant *Pecten, Clypeaster* and *Terebratula* (RT facies) that forms the top of LFA2. Fossils in the marl are almost entirely planktonic foraminifera.

Facies analysis and interpretation: While limestone underlying LFA3 north of Festos is very similar in its faunal content to middle to outer ramp limestone found in the WAT, the dominance of planktonic foraminifera and small grain size in LFA3 sediments suggests an off shore depositional environment. Intercalated beds of sandy packstone with graded or

convolute bedding are interpreted to represent volumetrically small or distal turbidites. Therefore an outer ramp to basinal setting is assumed. The intercalation of laminated beds in the upper part of sections indicates fast sedimentation related to turbidite events and/or the absence of infauna due to hostile bottom conditions.

The succession of nearshore siliciclastics, middle to outer ramp limestone and outer ramp to basinal marl at section FN suggests progressive deepening. While a lateral facies transition between LFA2 and LFA3 is not observed in outcrop, LFA3 likely represents the basinal equivalent of LFA2.

Graded rudstone to packstone beds that are found to be widespread at the top of the marl succession on the other hand reflect more proximal or more extensive turbidites compared to turbidites in the underlying succession. These turbidites contain reworked components typical for a near-shore environment: Lithoclasts of carbonate sediments similar to those found in the Matala area suggest that these uppermost turbidites were deposited after deposition, lithification and following exposure of the carbonates of the WAT. Coral fragments, coarse gravel and slumps in the sediments south of Timbaki suggest relief intensification and reworking of shallow water carbonates not preserved in outcrop. Relief intensification is also indicated at Faneromeni where a thick succession of course siliciclastic conglomerate overlies laminated marl and possibly turbiditic rudstone.

3. Paleoecology

3.1. Microfacies and paleoenvironment

The interpretation of skeletal components based on fieldwork and thin section analysis is an important tool for the classification of carbonate sediments (Wilson, 1975; Flügel, 1978). The recognition of non-tropical carbonates is also largely based on analysis of skeletal components (Lees and Buller, 1972; Carannante et al., 1988; Nelson, 1988). Results of biofacies analysis of sedimentary facies types found in the WAT (Fig. 2.4.7.) place all facies types except the CF facies into the rhodalgal facies of (Carannante et al., 1988) that was defined to be characteristic for the warm-temperate faunal province due to its high content in larger benthic foraminifera. The CF facies that contains abundant framework forming zooxanthellate corals is defined to belong to the tropical faunal province in spite of the absence of skeletal and non-skeletal grains (ooids, *Halimeda*) otherwise typical for the tropical realm. The abundance of coralline red algae and symbiont-bearing foraminifera in all lithofacies units of LFA2 documents deposition within the photic zone. Compared to microfacies analysis from various fossil and modern temperate sediments (Brachert et al., 1998; James et al., 2001; Forst, 2003), bryozoans and molluscs are little represented in the sediments from Crete. This might be explained by a twofold taphonomic bias: 1) skeletal components susceptible to abrasion are preferentially reduced in number and become unidentifiable through fragmentation in the process of reworking, 2) due to the low degree of cementation in non-tropical carbonates and high dissolution potential of aragonite during early diagenesis, aragonite skeletons are preferentially removed from the rock record (Brachert et al., 1998). Preferential dissolution of aragonite shells may have played an important role in the reduction of mollusc shells in the poorly lithified sediments where they were not preserved: This is evident in the PS facies where abundant bivalves occur as casts that are identified as macrofossils in the field but not represented as shells, shell fragments or molds in thin sections. Preservation by micrite envelopes is not observed. In the better lithified CF facies, however, some mollusc molds are preserved by early lithification and aragonite corals are preserved by micritic infillings. Preferential removal of aragonite skeletons in non-tropical environments is also a consequence of microboring leading to destruction and dissolution of skeletons since borings are not filled by cements (Nelson *et al.,* 1988, James 1997). Similarly the absence of *Halimeda* in LFA1 and 2 is explained by its low preservation potential (Purser, 1983). Reduction of certain components by reworking and

abrasion, however, appears to play a minor role in the sediments of the WAT since most sediments are low to moderate energy mid- to outer ramp deposits. Mechanical abrasion may be an important factor in facies types that are the result of winnowing out of sand sized particles (CS and, to some degree, BP facies) or episodic reworking during storm events (RP facies). The significance of reworking and redeposition has been discussed in chapter 2.4. and can be expected to be low for most facies types.

In their original papers, Lees and Buller (1972), Lees (1975), Carannante et al. (1988) and Hallock and Schlager (1986) have concluded, that factors other than temperature such as water depth and salinity influence biotic associations. Therefore it is to be expected that biotic associations reflect a combination of ecological factors. Consequently, a certain biotic association may be indicative of environments very different from each other. For example, while the abundance of bryozoans in most studies is observed to increase with depth (James et al., 2001; Brachert et al., 2003; Forst, 2003) and foraminifera and red algae dominate in shallower waters (Piller, 1994; Halfar et al., 2000), bryozoans may also be the dominant skeletal element in sediments shallower 25m water depth in enclosed bays (Upper Miocene of southern Spain, Brachert et al., 1998). The expression of the interplay of different ecological factors in skeletal associations has lead to a variety of additional names to describe them and to further subdivisions to adapt the names to a multitude of intermediate states. This has inspired James (1997) to introduce a simplistic terminology that divides faunal associations into warm water and light depending photozoans and heterozoans that may also dwell in other environments. Consequentially, to analyse factors that control carbonate sedimentary environments, which are in turn strongly influenced by the biota inhabiting them and producing the sediment, it is necessary to find and to study groups of fossils that have a simple response to a limited number of ecological factors. In the following chapters the groups of fossils that are most common in LFA2, foraminifera and non-geniculate coralline red algae are studied in detail to asses their response to environmental influences and their potential as indicators for environmental and climatic change.

3.2. Foraminifera

Systematic palaeontology

Classification of foraminifera found in Neogene sediments of southern central Crete follows Hottinger *et al.* (1993) and Loeblich and Tappan (1987). Identification is based on thin section analysis and allowed identification on genus level only. Taxa that are abundant in samples of LFA2 are listed in the order used by Hottinger *et al.* (1993). Examples of taxa uncommon in the analysed material are listed without detailed diagnosis. The spatial distribution of foraminifera in sections of LFA2 is discussed in the chapter following the taxonomic description.

Order **Foraminifera** (Eichwald. 1830)
Suborder **Textulariina** (Delage and Hérouard, 1896)
Family **Textulariidae** (Ehrenberg, 1839)

Genus ***Textularia*** Defrance, 1824
See Loeblich and Tappan (1988) for synonyms
Diagnosis: Test biserial or may have an adventitious third chamber against the first pair of chambers in the microspheric generation. Wall agglutinated, traversed by canaliculi that may be open as perforations or be closed externally by a thin agglutinated layer and typically are closed internally by the organic lining of the test. Aperture a low arch or slit at the base of the apertural face (Loeblich and Tappan, 1988).

Remarks: Based on the test shape and test structure, most agglutinating foraminifera in thin sections from Crete are classified as *Textularia* (Fig. 3.2.1.a).

Fig. 3.2.1. (next page): Textulariid, milioliid and globigerinid foraminifera
a: Biserial agglutinated foraminifer, most likely *Textularia* sp., K28
b: Transverse section of ?quinqueloculine foraminifer , K13
c,d: Axial sections of quinqueloculine foraminifer c: VO15; d: VO20c
e: Axial section of triloculine foraminifer , K13
f: Subaxial section of *Borelis* sp. , VO15
g: Axial section of *Pyrgo* sp. , K28
h: Oblique section of a globigerinid foraminifer, KO8

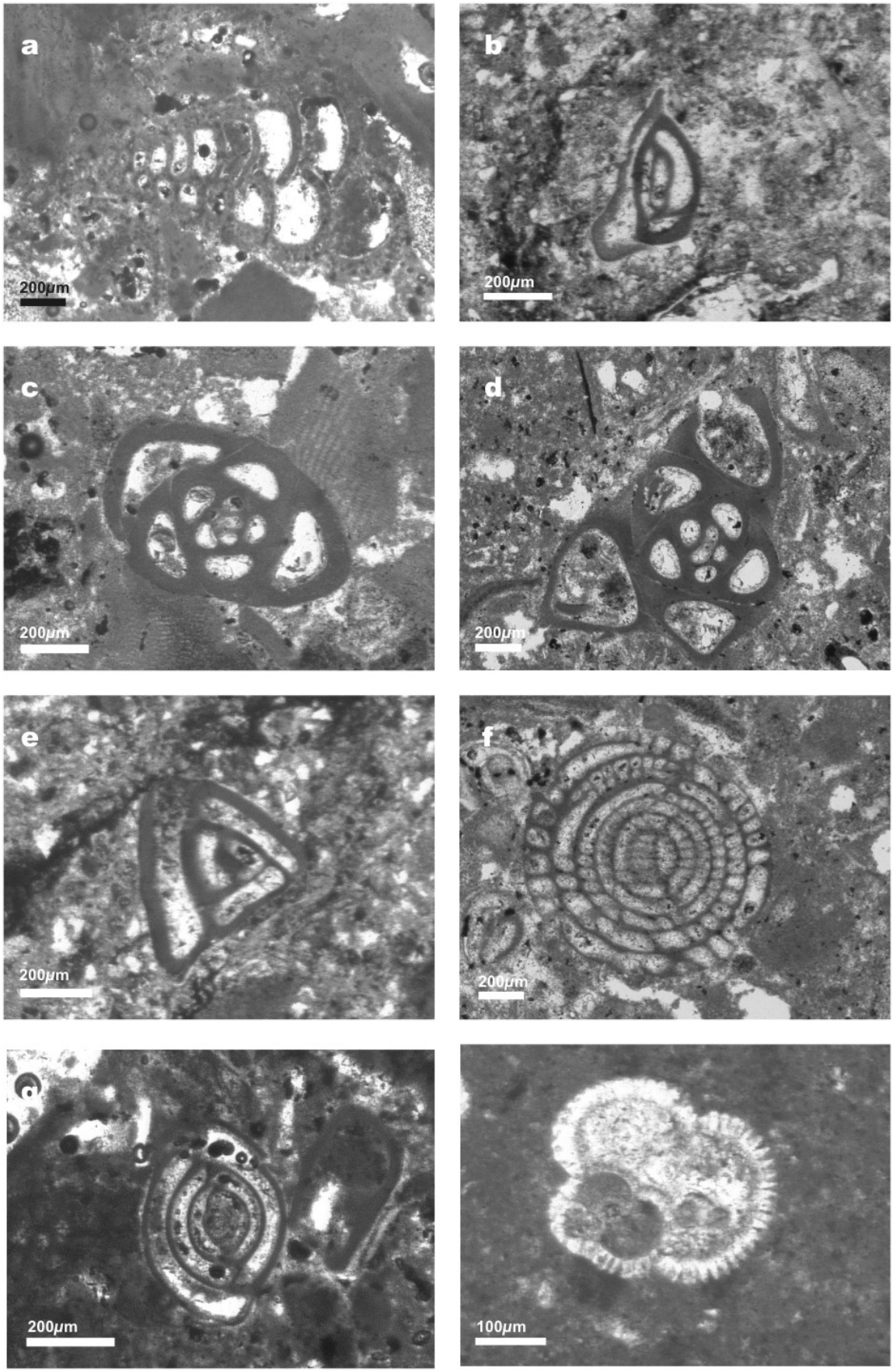
a
200μm
b
200μm
c
200μm
d
200μm
e
200μm
f
200μm
g
200μm
100μm

Suborder **Milioliina** (Delage and Hérouard, 1896)

Family **Hauerinidae** (Schwager, 1876)

Genus ***Quinqueloculina*** D´Orbigny, 1826

See Loeblich and Tappan (1988) for synonyms

Diagnosis: Test porcelaneous, ovate in outline, early chambers quinqueloculine. Aperture ovate, flush with the surface, provided with a bifid tooth (Loeblich and Tappan, 1988).

Remarks: In thin sections from Crete a variety of miliolid foraminifera with ovate outline and a characteristic 144° angle between successive chambers were counted as *Quinqueloculina* (Fig. 3.2.1.b-d).

Genus ***Triloculina*** D´Orbigny, 1826

See Loeblich and Tappan (1988) for synonyms

Diagnosis: Test porcelaneous, ovate in outline, equilaterally triangular or subtriangular. Aperture rounded, at the end of the final chamber, with a short bifid tooth (Loeblich and Tappan, 1988).

Remarks: In sections from Crete, *Triloculina* is locally common in sandy deposits (Fig. 3.2.1.e). Most forms have peripheral wall with carinated shoulders and may therefore belong to *Triloculina tricarinata* D´Orbigny.

Family **Alveolinidae** (Ehrenberg, 1839)

Genus ***Borelis*** De Montfort, 1808

See Loeblich and Tappan (1988) for synonyms

Diagnosis: Test porcelaneous, planspiral involute, spherical to fusiform. Adult chambers subdivided into subsidiary chamberlets by septula perpendicular to the chamber wall. Apertures in a single row (Loeblich and Tappan, 1988).

Remarks: Forms of *Borelis* from the Miocene of Crete are strictly spherical (Fig. 3.2.1.f). Another miliolid form found in the material from Crete is *Pyrgo* Defrance (Fig. 3.2.1.g).

Suborder **Lagenina** (Delage and Hérouard, 1896)

Familiy **Vaginulinidae** (Reuss, 1860)

The suborder Lagenina is represented by rare *Lenticulina* Lamarck, 1804 (Fig. 3.2.2.a) at the base of LFA3.

Suborder **Globigerinina** (Delage and Hérouard, 1896)

Family **Globigerinidae (**Carpenter, Parker and Jones, 1862)

Genus **Globigerina** d´Orbigny, 1826

Test globose, trochospirally enrolled, chambers spherical to ovate but not radially elongate, enlarging rapidly as added, commonly only three to five in the final whorl, sutures distinct, depressed, wall calcareous, perforate.

Remarks: Globigerinid foraminifera with additional *Orbulina* are the main constituent in LFA3. They were counted as *Globigerina* but no further subdivision has been made.

Suborder **Rotaliina** (Delage and Hérouard, 1896)

Family **Cibicididae** (Cushman, 1927)

Genus ***Cibicides*** De Montfort, 1808

See Loeblich and Tappan (1988) for synonyms

Diagnosis: Test lamellar, found often attached on spiral side, plano-convex to concavo-convex, evolute. Sutures thickened and may be elevated. Test coarsely perforated on spiral

Fig. 3.2.2. (next page): Milioliid and rotaliid foraminifera
a: Axial section of *Lenticulina* sp., MB23a
b: Axial section of *Cibicides* sp., K25
c: Equatorial section of *Cibicides* sp., VO15
d: Victoriellid foraminifer on coralline red alga, K19
e: *Sphaerogypsina* sp., K24
f: *Homotrema* sp., VO8b
g: Axial section of *Amphistegina lessonii*. Note thick laminar shell with thick ventral umbo and concave ventral bulge especially of older whorls. Large outer chambers (1) are subdivided by umbilical plates that are strongly bent backward, forming a stellar chamberlet (2). Near the aperture, a broad area of the test is covered with pustules (3). Inner chamber walls are covered with egg-holder structures (4), K26
h: Subaxial section of *Amphistegina lobifera* with thick subglobular test. Knobby and pustular dorsal hemiseptae give rise to heavy calcification of chambers, MS1

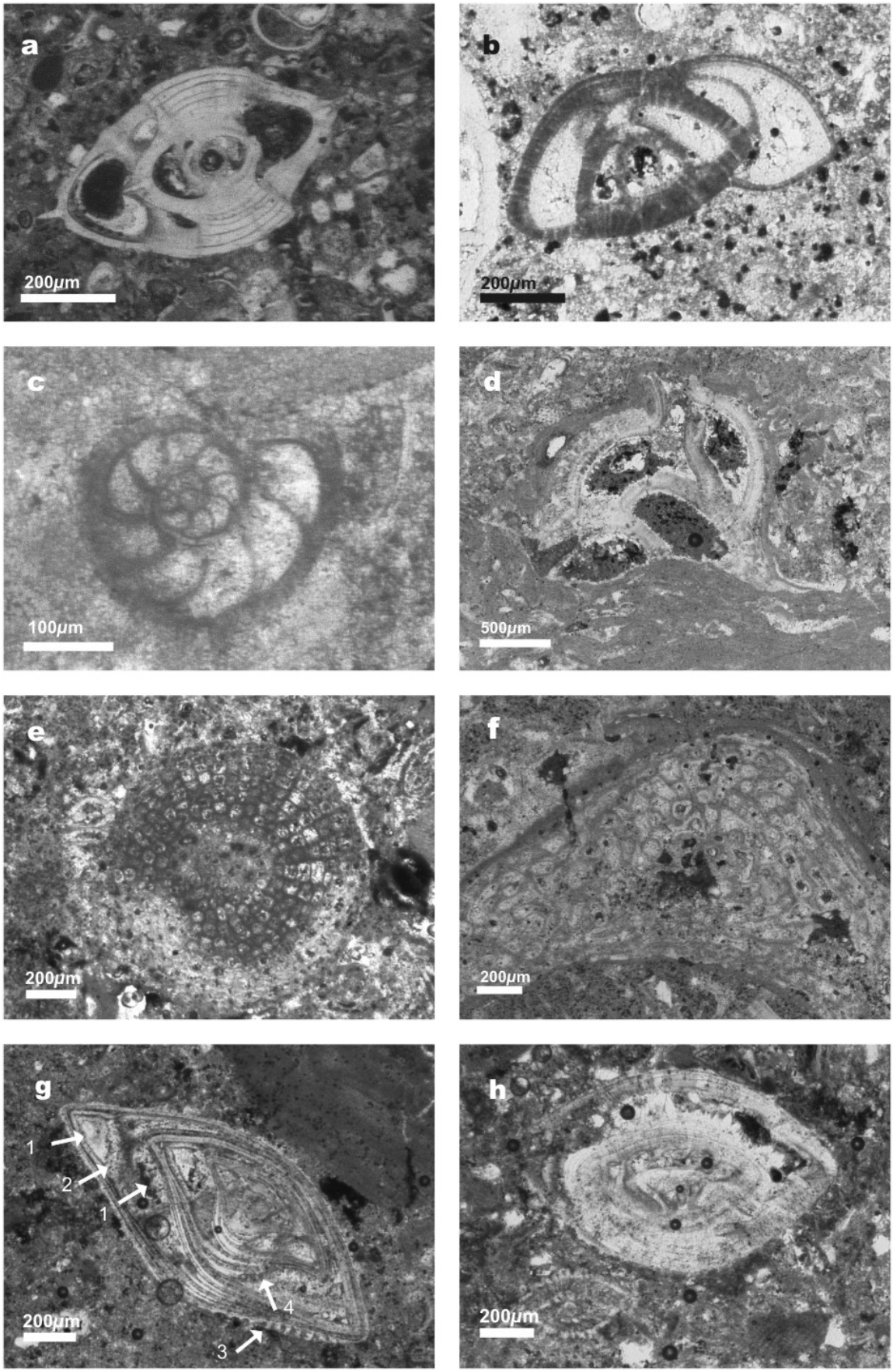
a
200μm
b
200μm
c
100μm
d
500μm
e
200μm
f
200μm
g
1
2
1
4
3
200μm
h
200μm

side. Wall calcareous, optically radial, pores being filled in earlier chambers by lamellar thickening of the wall. Aperture interiomarginal (Loeblich and Tappan, 1988).

Remarks: In thin sections of Neogene LFA2 deposits on central Crete, *Cibicides* may occur either attached and overgrown by coralline red algae or free. Free specimens are abundant in sandy packstone of the PS facies. It is recognized by the characteristic test shape and in many cases brownish-coloured tests with thickened walls and radial whitish pores (Fig. 3.2.2.b,c).

Family **Victoriellidae** (Chapman and Crespin, 1930)

Genus ***Victoriella*** Chapman and Crespin, 1930

See Loeblich and Tappan (1988) for synonyms

Diagnosis: Test lamellar, conical, becoming temporarily or permanently attached in the adult stage, attached by the apex with a sharp reverse in coiling direction and then high spired around an axial hollow, chambers inflated, three to four per whorl. Walls thick and coarsely perforate, except for the imperforate region around the aperture. Apperture umbilical, bordered by a thick lip (Loeblich and Tappan, 1988).

.

Remarks: In thin sections of Neogene LFA2 deposits on Crete a variety of sessile foraminifera with a limited number of large, inflated chambers and thick coarsely perforate walls (Fig. 3.2.2.d) occurs that were counted as *Victoriella*, which is also described from the modern gulf of Aqaba (Reiss and Hottinger, 1984) but that may also include other genera from the family Victoriellidae such as *Rupertina* and *Carpenteria.*

Family **Acervulinidae** (Schultze, 1854)

Acervulinid foraminifera are represented by *Sphaerogypsina* Galloway (Fig. 3.2.2.e), that occurs in many samples, especially in LFA3 but in very low numbers. *Acervulina* has not been identified without doubt in the analysed material.

Family **Homotrematidae** (Cushman, 1927)

Genus ***Homotrema*** Hickson, 1911

See Loeblich and Tappan (1988) for synonyms

Diagnosis: Test lamellar, encrusting, reaching considerable size (up to 8mm) with conical, dome or club-shaped projections or arborescent. Chambers arranged in numerous layers incompletely subdivided by a polygonal network of beams. Walls may be partially resorbed as layers are added. Upper chamber walls coarsely perforate. Perforated areas are resorbed when covered by the next chamber (Hottinger *et al.;*1993, Loeblich and Tappan 1988).

Remarks: *Homotrema* is found in samples from Crete mainly on or intergrown with red algae. In thin section, however, the separation from *Miniacina* is difficult and some specimens identified as *Homotrema* may belong to this genus.

Family **Amphisteginidae** (Cushman, 1927)

Genus *Amphistegina* D´Orbigny, 1826

Amphistegina lessonii D´Orbigny

See Hottinger et al (1993) for synonyms

Diagnosis: Perforate, lamellar, thick-shelled, lenticular test. Peripheral outline smooth, peripheral margin angular. Chambers involute, arranged in comparatively loose, low trochospire. Ventral side of shell may be slightly more convex than dorsal side. Dorsal chamber sutures flush, sharply bent backward in a long falciform arch. Ventral chamber sutures flush, sometimes slightly depressed in the ultimate and penultimate chambers, distinctly sinusoidal, bent backward in their peripheral part. Ventral umbo larger than dorsal one. Aperture strictly interiomarginal. In front of the aperture, the unbilico-lateral walls of the first 2-3 chambers of the last whorl are covered with rows of pustules. The main chamber lumen is separated from a stellar chamberlet by an umbilical plate. The stellar chamberlet has a distinct peripheral extension bent backwards and comparatively voluminous. All cavities and the main chamber cavities are covered with egg-holder structures that house symbionts (Hottinger *et al.;*1993).

Amphistegina lobifera Larsen

See Hottinger et al (1993) for synonyms

Diagnosis: Coarsely perforate, lamellar, thick-shelled, lenticular to globular, low-trochospiral, involute test. Peripheral outline smooth peripheral margin rounded. Dorsal chamber sutures flush, bent backward in an unbroken, falciform arch. Ventral chamber sutures sigmoidal-radial, strongly lobulated. Radial, sometimes wavy hemiseptular sutures longitudinally subdivide the lateral, alar chamber wall for a third or half of its lateral extension. Aperture in ventral, interiomarginal position, forming a low but comparatively long slit. Areal supplementary apertures are irregularly spaced in between pustules covering the apertural face. The main chamber lumen´s dorsal part is posteriorly restricted by deep saddles of the lobate posterior wall. The internal, lateral wall surfaces of chamber cavities are covered with evenly spaced deep egg-holder structures (Hottinger *et al.;*1993).

Remarks: Specimens of *Amphistegina* are usually distinguished in thin section by their characteristic outline and test organization: *A. lessonii* is characterized by its bulging shape and ventrally thickened umbo with characteristically laminated thick test wall. It is also characterized by a comparatively large main chamber of the ultimate whorl. Because of the size of the chamber and the strongly backward bent main septum, in many cases not only two adjacent main chambers are cut in section but also the stellar chamberlet formed by the folded umbilical plate (Fig. 3.2.2.g). In many cases, this outer chamber has a considerably thinned wall that often postmortally breaks off. For this reason the determination of height-length ratios according to (Larsen and Drooger, 1977; Hallock and Glenn, 1986) as a measure for water depth is virtually impossible. *A.lobifera* is characterized by its subglobular shape and thick, perforate tests (Fig. 3.2.2.h). It is also the species that in the material from Crete shows the most extensive crystallization of calcite within chambers (Fig. 3.2.3.a). Crystallization of calcite is likely promoted by the irregular folding of chamber walls and large number of saddles on the chamber walls that in thin section result in an extensive subdivision of the main chambers.

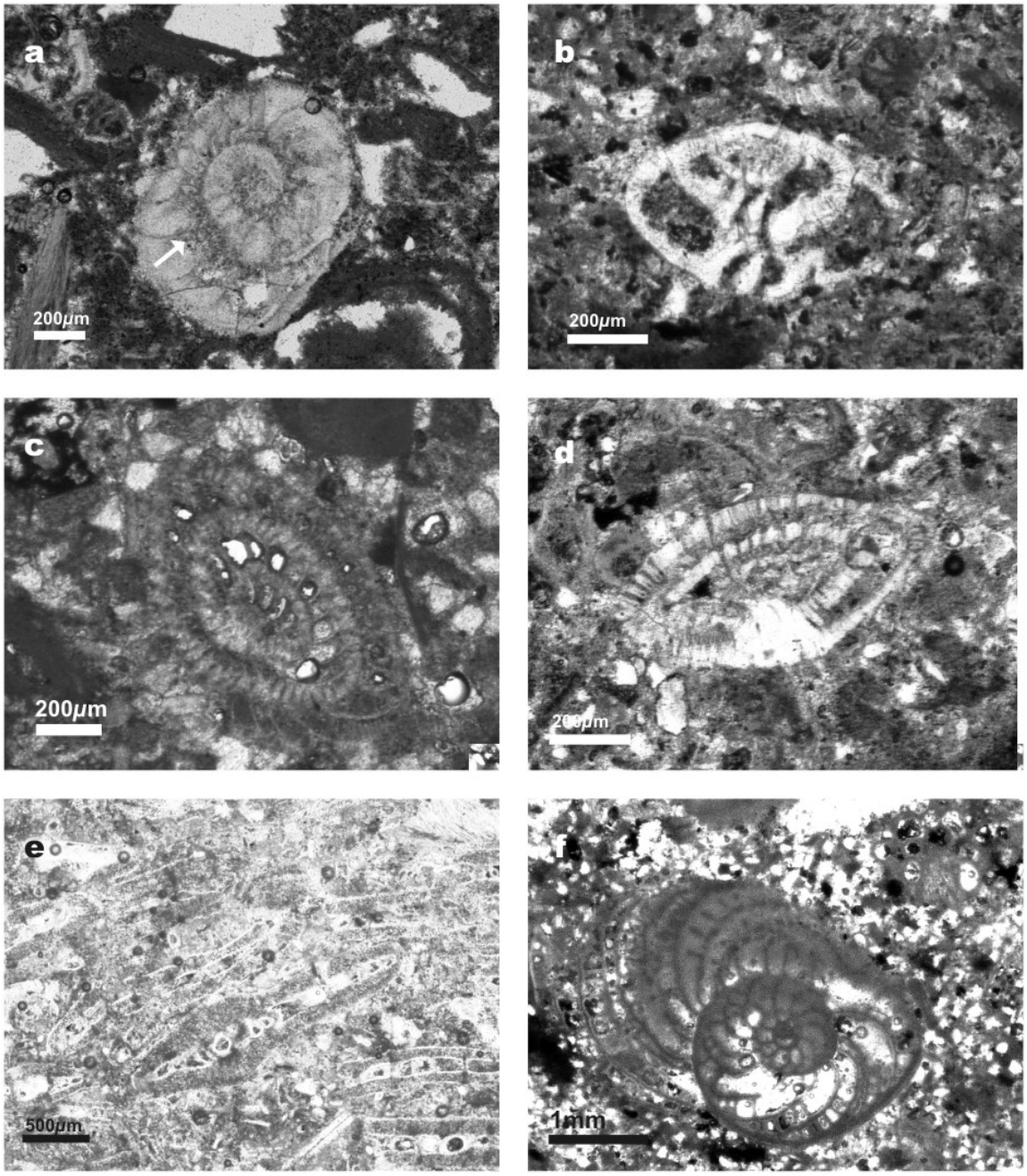

Fig. 3.2.3.: Rotaliid foraminifera
a: Equatorial section of *Amphistegina lobifera*. Note strongly folded and pustular septae (arrow) and strong calcification of chambers, VO11
b: Axial section of *Ammonia* sp., VO1
c: Oblique section of *Elphidium* sp., MO12b
d: Axial section of *Elphidium* sp., MO1b
e: Axial and tangential sections of *Heterostegina* sp., MB19
f: Equatorial section of *Heterostegina* sp., MO15

Family **Ammoniidae** (Saidova, 1981)

Genus ***Ammonia*** Brünnich, 1772

See Loeblich and Tappan (1988) for synonyms

Diagnosis: Test lamellar, moderately coarse perforate, biconvex with low trochospiral coil, both surfaces may be ornamented by pillars, coil of 3 to 4 volutions, ventrally involute and may have large umbilical plug surrounded by umbilical fissure, final whorl with deeply incised umbilical, radial and intraseptal spaces, early chambers closed toward umbilicus (Hottinger *et al.;*1993, Loeblich and Tappan; 1988).

Remarks: Specimens of *Ammonia* in the material from Crete are usually characterized by deep umbilical fissures in the ventral side, the conspicuous biconvex and ventrally involute shape and may as described by (Jorissen, 1988) from the recent Adriatic have either brownish or white tests with thin but conspicuous perforation (Fig. 3.2.3.b).

Family **Elphidiidae** Galloway, 1933

Genus ***Elphidium*** De Montfort, 1808

See Loeblich and Tappan (1988) for synonyms.

Diagnosis: Test laminar, planspiral involute or partially evolute, lenticular, biumbonate, may have umbilical plug on each side, deeply incised sutures form interlocular spaces that communicate with an umbilical spiral canal system, may have vertical umbilical canals leading from the spiral canal to the surface (Loeblich and Tappan, 1988).

Remarks: *Elphidium* is identified in thin section by its conspicuous canal system and interlocular spaces (Fig. 3.2.3.c).

Family **Numulitidae** de Blainville, 1827

Genus **Heterostegina** D´Orbigny, 1826

See Loeblich and Tappan (1988) for synonyms

Diagnosis: Test lamellar, planspiral involute to evolute, centrally thickened megalospheric proloculus followed by up to 16 operculinoid and unfolded septa, larger and relatively rare microspheric test with about thirty unfolded septa, then with chamberlets formed by complete secondary septa (Loeblich and Tappan; 1988).

Remarks: Specimens in sections from Crete (Fig. 3.2.3.d,e) are very similar to the involute *Heterostegina depressa* that is abundant in the modern Gulf of Aqaba (Reiss and Hottinger, 1984). However, since most specimens in thin sections are cut in axial direction, identification of species is difficult, especially as most sections are tangential and show only the ultimate whorl.
Heterocyclina that is very similar in axial view is not known from the pre-Holocene (Loeblich and Tappan; 1988).

Distribution

A detailed semiquantitative analysis (see chapter 1.4. for applied method) of the distribution of foraminifera in units LFA2 and LFA3 has been carried out for five sections (MO1, MS1, VO, Kl and the upper part of section Ma2, Fig. 3.2.4.). In LFA2, the most abundant foraminifera are benthic rotaliid forms such as *Amphistegina, Elphidium, Heterostegina, Ammonia, Cibicides*, including fixosessile forms such as *Victoriella* and *Homotrema.* Locally abundant are miliolinids, mostly *Quinqueloculina* and triloculine forms as well as *Borelis*. Agglutinating foraminifera are represented by the genus *Textularia*. It is widely distributed but occurs in relatively small numbers. Planktonic foraminifera (*Globigerina, Orbulina*) are rare in LFA2 but are dominating in LFA3 (section Ma2, Fig. 3.2.4.). Contents of foraminifera not shown in Fig. 3.2.4. are below 10%. Among these are a number of unidentified species and species that occur only locally and in low number such as *Sphaerogypsina, Lenticulina, Bigeneria, Spiroplectinella* , as well as various miliolid forms.
Of the benthic foraminifera in LFA2, *Amphistegina* is most abundant. It is dominant in most samples of the sections at Mount Rhodonas (KL) and Vathi (VO; Fig. 3.2.4.). In the area of Matala (sections MO1, MS), *Amphistegina* is common in the middle part of the succession (25m-65m of section MO, top 25m of section MS). It is, however, uncommon in the PS facies. The number also decreases significantly towards the top of sections MO and Ma2.

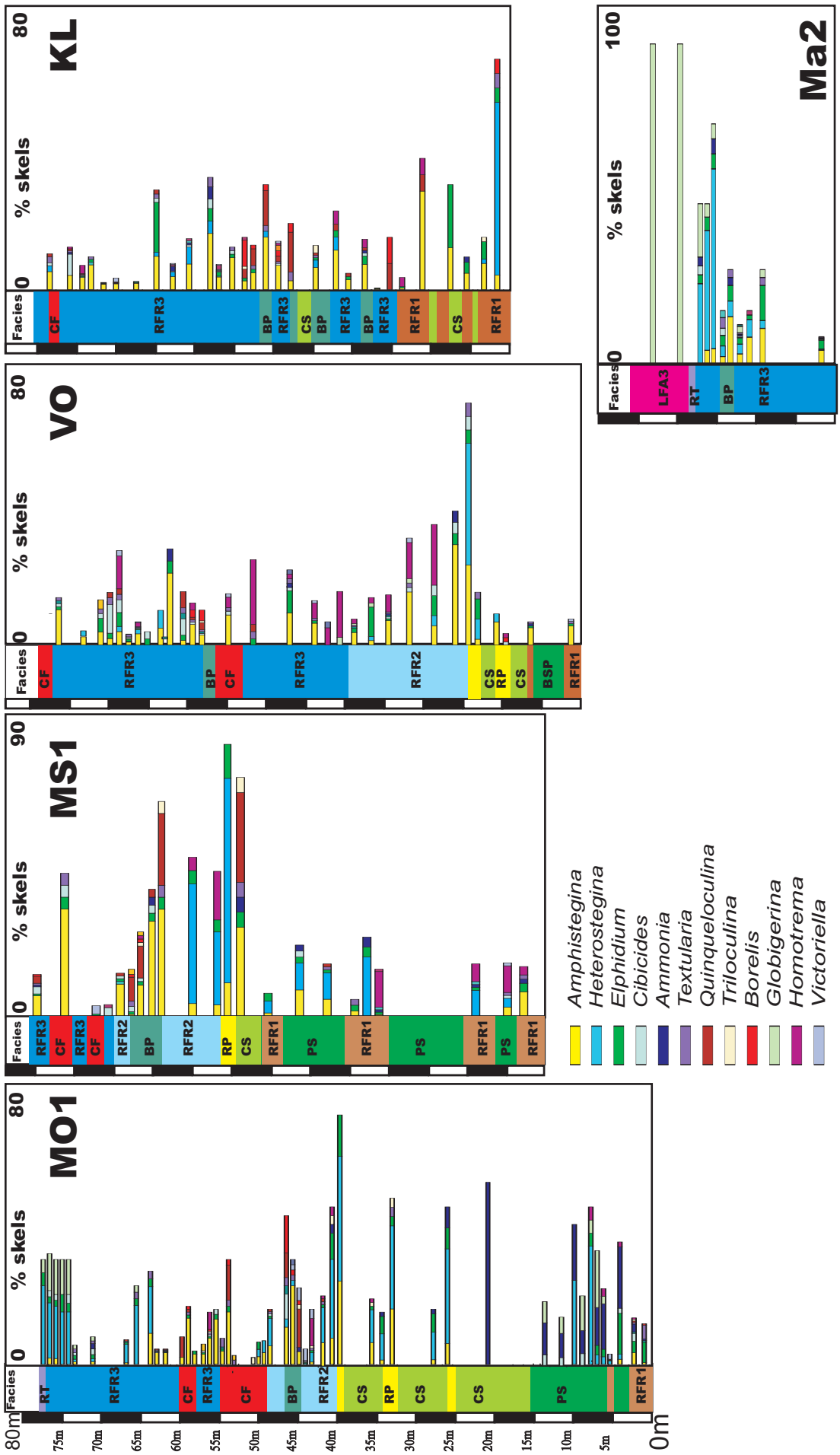

Fig. 3.2.4.: Distribution of most abundant foraminiferal genera in LFA2 in sections MO1 and MS1 near Matala, section VO (Vathi), KL (Mount Rhodonas) and Ma2 (Martsalo, section includes base of LFA3). Scale is volume percent of skeletal component total. See Fig. 1.4.1. for locations

Amphistegina is represented by dominant *A. lobifera* and *A. lessonii.* Of these, *A. lobifera* is most common in LFA2a and dominates in RFR1. A sample taken west of section MO2, however, indicates that *A. lobifera* is replaced by *A. lessonii* oceanward. *A. lessonii* is more common in LFA2b and c than *A. lobifera* and dominates in the RP and BP facies.
Heterostegina is also very common: It is dominant at the top of sections MO and Ma2 and occurs together with abundant planktonic foraminifera. *Heterostegina* also occurs in great number in the condensed horizons (CR facies). In the Matala area, it is also common or dominant in PS, RFR1 and the MRB, where it decreases in abundance upsection. In other sections, *Heterostegina* only occurs in the uppermost condensed horizon (RP facies) and in the basal bed of section KL. *Elphidium* is a minor constituent in most samples and occurs commonly together with *Amphistegina* and/or *Heterostegina*. *Cibicides* occurs usually in low proportions but is locally abundant in the PS facies (section MO) and the RFR3 facies in the upper part of sections VO and KL. *Ammonia* is abundant in the PS facies in section MO but is uncommon elsewhere. Of the miliolid foraminifera, quinqueloculid forms are most abundant in the BP facies and the CS facies (section MS1) and in the upper part of coral framestone units (section MO1). Triloculine forms are less abundant. *Borelis* is also most abundant in the BP facies but occurs as well within coral framestone and in rhodolith rudstone overlying coral framestone. Of fixosessile or incrusting foraminifera, the homotrematid forms are most common. They are mostly found on rhodoliths or intergrown with them. Fragments occur also in the BP facies. *Homotrema/Miniacina* is especially abundant in the middle part (15m-45m) of section VO (RFR2 and 3) but also common in the RFR1 facies in section MS. Planktonic foraminifera are common in section MO1 in the middle part the PS facies and at the top of the section in the RFR3 facies. They are also common in the upper part of section Ma2 at the top of LFA2 and throughout LFA3.

Paleoenvironmental implications

Benthic foraminifera are known to be valuable paleoenvironmental indicators (Chaproniere, 1975; Hallock and Glenn, 1986, Betzler et al., 1997). Most foraminifera found in great number in Neogene deposits of the WAT belong to the group commonly called “larger benthic foraminifera”. A significant property of this group of foraminifera is their housing of algal symbionts that play a large role in nutrition and formation of calcite shells. In turn, these foraminifera adapt to the environmental preferences of their symbionts in terms of light and

temperature (Lee and Anderson, 1991). This makes them valuable indicators for these parameters. The response to these parameters, however, is modified by other specific needs and preferences regarding, for example, substrate and water energy. All taxa that are abundant in Miocene sediments of the WAT are still common in modern times and their environmental preferences have been studied in detail (Hansen and Buchardt, 1977; Hottinger, 1977; Reiss and Hottinger, 1984; Hohenegger, 1995; Haunold et al., 1997; Hollaus and Hottinger, 1997; Langer and Hottinger, 2000).

The distribution of the species of *Amphistegina* in dependence of water depth and temperature is especially well known from the modern Mediterranean and the Red Sea. The absolute abundance of *Amphistegina* is greatest between 50 and 70m in the Red Sea (Hansen and Buchardt, 1977; Haunold et al., 1998). In the Gulf of Aqaba, *A.lobifera* is restricted water depth above 40m and *A. lessonii* occurs down to 80m but is gradually replaced by other species (Hottinger, 1977). In the Bay of Safaga in the Red Sea, depth distributions are very similar but *A. lobifera* is found down to 56m water depth (Haunold et al., 1998). The depth range, especially of *A. lessonii*, is considerably lower (down to no more than 50m) in other areas (Japan; Hohenegger, 1994; Hohenegger, 1995). In studies off eastern Crete, the depth range of *A. lessonii* has been found to be limited by a thermocline between 60m and 70m water depth and the associated drop of the annual minimum temperature to 16° (Hollaus and Hottinger, 1997). In the WAT, the absolute abundance of *Amphistegina* spp. and the dominance of *A.lobifera* and *A.lessonii* (Fig. 2.3.5.) suggest intermediate water depths in the order of 30-70m for most deposits (compare Reiss and Hottinger, 1984). A depth profile based on the relative abundances of *A. lobifera* and *A. lessonii,* however, is not apparent in the analysed sections since *A. lessonii* is especially abundant in BP and RP facies that were deposited in shallow environments compared to other lithologies (see chapter 2.4.). An explanation is that the distribution of *Amphistegina* spp. is also related to local parameters such as substratum: In the Gulf of Aqaba, the depth limit of seagrass coincides with the lower limit of *A. lessonii* (Hansen and Buchardt, 1977). *A. lessonii* is also an important constituent of the *Heterostegina depressa/A. lessonii/A. bicirculata* association found in the bay of Safaga on rocky surfaces with thin sand veneers and on a macroid facies (Haunold et al., 1997). This observation is in agreement with the abundance of *A. lessonii* in the RFR facies. Hohenegger et al. (1999) found that on the Island of Okinawa an umbiliconvex form of *A. lessonii* prefers soft substrates, whereas the biconvex form that is more similar to the forms found in the WAT prefers firm substrates. This explains the rarity of *A. lessonii* in the fine grained PS facies.

Modification of *Ampistegina* associations in the rock record compared to living associations by seaward transport of *A. lessonii* and *A.lobifera* especially in higher energy intervals of RFR3 also appears to be a likely reason for the absence of consistent patterns. On the other hand, important reworking and basinward transport of benthic foraminifera tests is observed neither in the modern red sea (Hansen and Buchardt, 1977) nor in Oligo-Miocene ramp environments (Pedley, 1998).

Heterostegina is most abundant in three distinct facies that are not associated with each other: The condensed RP facies, the fine grained PS facies and the RFR3 facies at the top of sections. The RP facies is interpreted to represent a mid ramp to inner ramp setting that is frequently reworked by storms while both other facies are interpreted to represent comparatively low energy mid- to outer ramp settings. The occurrence of planktonic foraminifera and increasing mud content indicate deepening in the upper part of the RFR3 facies. In this part, *Heterostegina* gradually replaces *Amphistegina*. On the other hand, *Heterostegina* rarely occurs in intervals where water depth intermediate between the high energy RP facies as is indicated by the dominance of *A.lessonii.* In modern subtropical and tropical environments, two species of *Heterostegina, H.depressa* and *H.operculinoides,* are common. These species each cover a distinct depth range: *H.depressa* in modern environments is restricted to relatively shallow water depth between 20m and 70m while *H. operculinoides* is most common at the lower limit of the photic zone (Hottinger, 1977; Hohenegger, 1994; Hohenegger, 1995). The material from the Miocene of Crete does not allow the identification of the species of *Heterostegina.* However, axial sections show that individuals are involute and therefore do not belong to *H. operculinoides.* Nevertheless, the distribution if *Heterostegina* in the facies types of the WAT suggests they are part of two distinct groups, one that prefers the shallower water and firm substrate of the RP facies and a different one that prefers soft substrate and deeper water.

Quinqueloculina spp. and *Triloculina* spp., often with *Borelis,* are especially common in sandy sediments (BP and to a lesser degree CS facies). This is in agreement with the observations of Haunold et al. (1997) in the Gulf of Safaga, where species of *Quinqueloculina* dominate on sand bottoms. There they often live epiphytic on sea grass or occur in sand patches between coral carpets where they are associated with *Borelis*. The latter observation corroborates the assumption, that some of the BP facies is connected to coral carpets or fringes that are not preserved in outcrop. The possible relation to coral carpets and the depth in which recent species of these genera live indicate water depths lower than 35m for the BP facies.

Homotrematid foraminifera and *Victoriella* commonly occur on hard substrates in water depth deeper than 90m in the modern Gulf of Aqaba (Reiss and Hottinger, 1984). They may, however, occur in shaded areas in shallower water and are common in modern beach sands. In the WAT, homotrematid foraminifera are especially common in section VO, where rhodoliths may have provided enough shadow for homotrematid growth.

Foraminifera are also reliable indicators of water temperature (Betzler et al., 1997; Hollaus and Hottinger, 1997; Langer and Hottinger, 2000). The occurrence and diversity of larger benthic foraminifera is used to define the warm temperate carbonate province (Betzler et al., 1997; Hollaus and Hottinger, 1997; Langer and Hottinger, 2000). The biogeographic distribution of larger foraminifera allows conclusions concerning minimum temperature thresholds (Langer and Hottinger, 2000): *Amphistegina* spp. occur in regions with minimum winter sea surface temperatures as low as 14°C. *Heterostegina depressa* occurs in areas with minimum winter sea surface temperatures down to 18°C and *Borelis schlumbergeri* in regions with a 21°C minimum.

The occurrence of larger benthic foraminifera is not only limited by the annual minimum temperature but also by nutrient contents: Very much like other mixotrophic symbiont bearing organisms like corals, larger benthic foraminifera are usually restricted to oligotrophic environments, so called blue deserts (Lee and Anderson, 1991; Langer and Hottinger, 2000). On the other hand, certain species of *Elphidium* and *Ammonia* may expel their symbionts and adopt heterotrophic feeding strategies in order to adapt to higher nutrient levels (Jorissen, 1988). Not surprisingly, increased numbers of *Ammonia* and *Elphidium* are therefore found in areas with fresh water input or increased content of organic matter (Jorissen, 1988; Langer and Lipps, 2003). Both genera display a characteristic inflation of chambers in with increasing trophic levels (Jorissen, 1988). In sections in the WAT, inflated forms only occur in *Ammonia* sp.. High numbers of Ammonia occur in the PS facies in section MO, indicating increased nutrient input. They are associated with *Heterostegina* that also has been attributed relatively high ecological tolerances compared to other larger benthic foraminifera (Langer and Hottinger, 2000) and with increased numbers of planktonic foraminifera that may represent plankton blooms in consequence of increased nutrient input. Increased amounts of nutrients in the lower part of LFA2a in the area of Matala is also indicated by the abundance of turitellid gastropods in the most shoreward part of the PS facies (section MO2): Turitellid

gastropods are suspension feeders that are especially abundant in high non-tropical high productivity environments (Allmon, 1988, Lukasik et al. 2000).
While nutrients are an important influence on the amount of planktonic foraminifera, their number is also limited by water depth since zooplankton layers migrate down to 40-50m below sea level in the modern Red Sea during the day (Reiss and Hottinger, 1984). The abundance of planktonic foraminifera in the PS and upper RFR3 facies is thus in accordance with a deposition in an outer ramp environment.

3.3. Non- geniculate coralline red algae

Systematic palaeontology

The taxonomy of non-geniculate coralline red algae has experienced significant revision during the past 20 years (Woelkerling, 1988). A reassessment of diagnostic criteria of vegetative and reproductive anatomy resulted in reclassification of many taxa. Taxa defined prior to this period therefore have to be treated with care.

Vegetative criteria according to Woelkerling, (1988) are: 1) dorsiventral thallus organization: the thallus can be either dimerous with two groups of filaments (primigenous or postigenous) or monomerous with only one type of filaments and lateral propagation by the formation of cores. Thalli can be both monomerous and dimerous in the same plant. Cores are either coaxial with lateral alignment of cells or plumose (absence of alignment); 2) lateral cell connection either by cell fusions or secondary pit connections; 3) relative length and shape of epithallial cells and meristematic subepithallial initials; 4) height/width relations of cells: cells that are in growth direction significantly (2-4 times) wider than high are called palisade cells. This criterion applies mainly for primigenous cells; 5) formation of specialized cell types such as haustoria and trichocytes.

Reproductive criteria according to Woelkerling (1988) are: 1) number of pores (uniporate/multiporate) of bi-/tetrasporangial conceptacles; 2) zonate or cruciate arrangement of spores; 3) tetrasporangia either borne in conceptacles or in calcified chambers that may be solitary or arranged in sori; 4) presence/absence of sporangial plugs; 5) characteristics of

conceptacle roof development and characteristics of the spermatangia (Penrose, 1992; Chamberlain and Keats, 1994; Womersley, 1996).

Thallus shape is now generally disregarded to be diagnostic. Cell and conceptacle sizes, however, are relevant on species level.

Most of the criteria described above have been shown to be applicable on fossil coralline red algae (Bosence, 1991; Braga et al., 1993; Braga and Aguirre, 1995; Rasser and Piller, 1999). However, some criteria relate to parts of the plants that do not calcify. This is the case for the interior of conceptacles. Since the identification of genera within the subfamily of the Mastophoroideae and of some genera of the Melobesioideae is largely based on these characters, separation of these genera in fossil material is problematic. Criteria that involve the shape and relative length of epitallial cells and subepitallial initials are diagnostic for the separation of *Lithothamnion* and *Phymatholithon.* However, as epithallial cells are usually poorly calcified, this requires exceptional preservation of the material.
Identification of the red algal material on Crete is mainly based on thin sections. In order to determine cell and conceptacle dimensions, photomicroscope pictures with a known magnification were taken. Measurements were performed using Corel Draw 11. Measured dimensions are cell length, cell width, height of the conceptacle chamber (excluding the pore channel) and width of the conceptacle chamber (Fig. 3.3.1.).

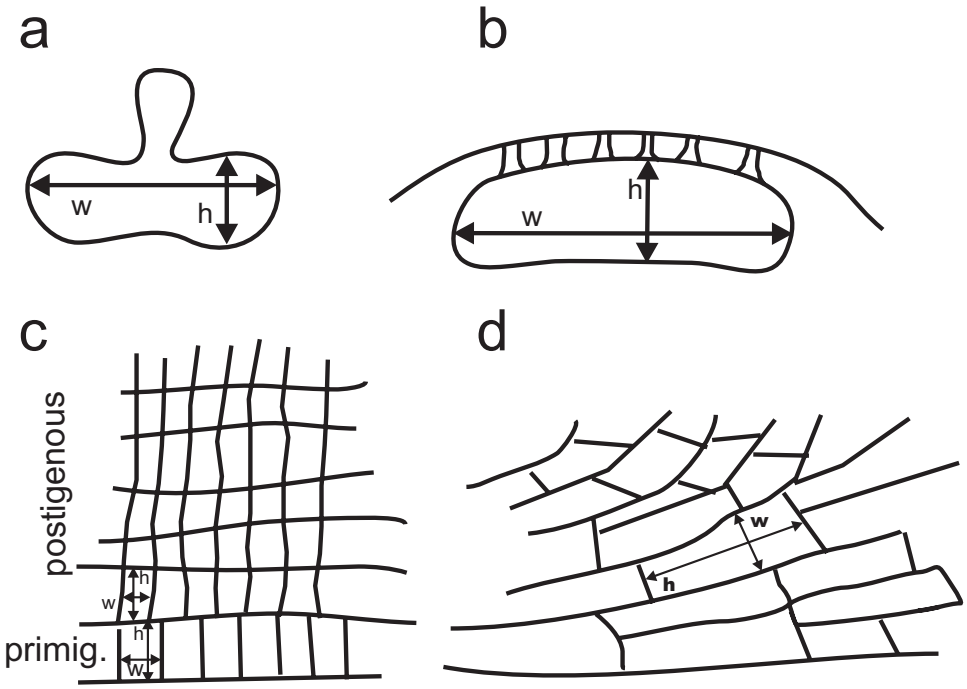

Fig. 3.3.1.: Measured dimensions in coralline red algae. a) uniporate conceptacles, b) multiporate conceptacles, c) cells in dimerous thalli (cells of primigenous and postigenous filaments), d) cells in core elements (monomerous thallus)

For description of growth-forms the terminology of Woelkerling (1993) was used: Encrusting: Plants are encrusting and flattened, ventrally attached and devoid of protuberances; foliose: plant consists of several to many lamellate branches that may have varying angles to one another and that are either free or interwoven; layered: plants that are composed of several or many flattened branches or thalli approximately parallel to each other; warty: plants with protuberances that are usually <3mm long, not swollen and unbranched; lumpy: plants with swollen protuberances that vary in length and are rarely branched; fruticose: plants with cylindrical to compressed protuberances that are usually >3mm long.
In the material from central Crete, it was possible to identify the majority of plants to genus level. The separation of *Lithothamnion* and *Phymatolithon* was not possible in all cases. Named species have all been described using the above cited criteria and have been reported from the Neogene of the Mediterranean before. Taxa that could not be referred to species previously described from the Mediterranean were treated in open nomenclature. This is reasonable since the validity of a vast number of taxa (>600), of which only a small percentage is still in use, is not yet assessed (Aguirre and Braga, 2003). Only criteria applicable for identification in thin section are included in the diagnosis. The majority of taxa found in the Miocene of central Crete are either species known from literature or newly established informal species. However, there remains a small portion of plants that could not be confidently associated with one of these species because they are either not well preserved or lack recognizable diagnostic features to delineate a species. This is especially the case within the subfamily of the Melobesioideae. The spatial distribution and locations where the various genera occur are shown and discussed in the chapter `distribution´ following the systematic section.

Division **Rhodophyta** (Wettstein, 1901)
Class **Rhodophyceae** (Rabenhorst, 1863)
Order **Corallinales** (Silva and Johansen, 1986)
Family **Corallinaceae** (Lamouroux, 1812)

Subfamily **Lithophylloideae** (Setchell, 1943)

Diagnosis: Cells of contiguous filaments are normally joined only by secondary pit connections. Cell fusions are rare or absent. All types of conceptacles are uniporate (Woelkerling, 1988).

Genus ***Lithophyllum*** (Philippi, 1837)

Diagnosis: Thallus is dimerous or dimerous and secondary monomerous in one plant. Primigenous cells are predominantly non-palisade (Braga and Aguirre, 1995). Thallus margin is multistratose (Chamberlain, 1991).

Lithophyllum dentatum Kützing (Foslie, 1898)

See Braga and Aguirre (1995) for synonyms

Description: Thallus is dimerous, encrusting to warty and up to 3mm in thickness. Cell fusions are absent. The examined material does not contain ventral core elements. Primigenous cells are non-palisade and 11 - 17µm in height and 8 - 10µm in width. Postigenous cells are short and squarish to elongate rectangular and 6 - 20µm in height and 4 - 12µm in width (Table 3.3.1.). Vertical alignment is very good due to the absence of cell fusions (Fig. 3.3.2.a) and lateral alignment is moderate. Banding is not present. Protuberances are short. Thallus may form coaxial areas with elongate cells that reach 23µm in height and 11µm in width (Fig. 3.3.2.b).
Conceptacles of bi-/tetrasporangial plants are bean shaped (Fig. 3.3.2.c) and are 127 - 165µm in height and 264 - 286µm in width (Table 3.3.1.). The conceptacle floor is raised in the

Conceptacles	Postigenous Cells			Primigenous Cells / Core Cells			Tetra-/Biosporangial		
	Σ	Height Range (µm)/MW/SD	Width Range (µm)/MW/SD	Σ	Height Range (µm)/MW/SD	Width Range (µm)/MW/SD	Σ	Height Range (µm)/MW/SD	Width Range (µm)/MW/SD
Lithophyllum									
L.dentatum	48	6-20 / 13,4 / 3,3	4-12 / 7,5 /1,8	8	11-17 / 15,6 / 3,6	8-10 / 9,3 / 0,9	5	127-165 / 150,5 / 17,8	264-286 / 272,3 / 12,1
L.incrustans	70	10-25 / 16 / 3,3	5-13 / 9,3 / 2	7	8-10 / 8,8 / 0,9	5-8 / 6,9 / 1,2	26	117-187 / 152,1 / 19,2	226-333 / 272,7 / 29,8
L.nitorum	28	6-15 / 10,5 / 2,1	3-8 / 5,6 / 1,2	2	11-13 / 11,7 / 1,3	5 / 4,9 / 0,4	4	65-106 / 98,6 / 9,7	267-381 / 272,9 / 19,7
Titanoderma									
T. pustulatum	42	5-55 / 19,4 / 9,5	3-8 / 6,5 / 1,2	10	14-44 / 22,9 / 8,4	6-10/ 7,8 / 1,1	8	65-106 / 89,3 / 15,5	267-381 / 310,9 / 37,7
Spongites									
S.albanense	155	7-18 / 12,1 / 2,8	4-11 / 5,9 / 1,4	8	10-15 / 12,4 / 1,9	4-9 / 6,3 / 1,4	31	132-232 / 180,1 / 30,8	367-602 / 472 / 59,5
Spongites sp. 1	20	8-19 / 11,2 / 3	4-10 / 5,4 / 1,7	2	8-9 / 8,7 / 0,7	5-6 / 5,4 / 0,2	7	69-109 / 94 / 13,9	179-281 / 220,1 / 32,6
Lithothamnion									
L. ramosissimum	38	6-19 / 10,9 /3,4	2-6 / 3,6 / 1	52	8-17 / 12,3 / 2,2	3-5 / 3,8 / 0,8	25	118-224 / 161,7 / 30,1	224-586 / 409,5 / 81,1
Lithothamnion sp.1	67	5-18 / 9,3 / 3,1	1-5 / 2,7 / 0,9	35	12-30 / 18,9 / 4	3-7 / 5,3 / 0,9	37	125-296 / 215,6 / 16,3	270-899 / 508,6 / 124,8
Lithothamnion / Phymatolithon									
Lith. / Phym. sp.1	73	4-13 / 7,7 / 2,4	1-4 / 2,5 / 0,8	22	7-15 / 9,8 / 2,7	1-5 / 2,8 / 0,7	15	92-165 / 121,7 / 23,6	145-388 / 250,7 / 74,2
Mesophyllum									
M. curtum	27	4-9 / 6,5 / 1,6	2-5 / 3,1 / 0,9	8	8-14 / 10,2 / 2	3-5 / 4,2 / 0,6	7	102-156 / 121,2 / 18,8	154-226 / 181,2 / 26,6
M. sancti-dionysii	42	7-20 / 12,7 / 4,2	4-8 / 5,3 / 1,6	13	11-22 / 14,1 / 5,3	5-9 / 8 / 2,8	21	151-305 / 207,4 / 49,1	220-503 / 368,4 / 78,9
Mesophyllum sp. 1	53	6-19 / 11,3 / 2,8	2-6 / 3,7 / 1	22	11-29 / 16 / 4,6	3-7 / 5,4 / 1,1	14	205-351 / 285,3 / 55,8	492-1206 / 730,8 / 179,6
Mesophyllum sp. 2	22	4-11 / 7,2 / 1,6	1-3 / 2,7 / 0,7	12	8-14 / 11 / 2,4	3-6 / 4,1 / 0,7	30	115-236 / 170,4 / 26,6	165-397 / 260 / 62,9
Sporolithon									
Sporolithon sp.1	26	10-19 / 13,5 / 2,3	3-7 / 5 / 0,9	14	10-24 / 14,9 / 4,4	3-5 / 4,2 / 0,7	31	33-79 / 56,2 / 10,8	79-133 / 104,9 / 13,1
Sporolithon sp.2	27	4-14 / 9,3 / 2,5	2-4 / 2,8 / 0,8				18	26-50 / 35,9 / 5,4	38-82 / 66,3 / 9,4

Table 3.3.1.: Dimensions measured in non-geniculate coralline red algae as indicated in Fig. 3.3.1.

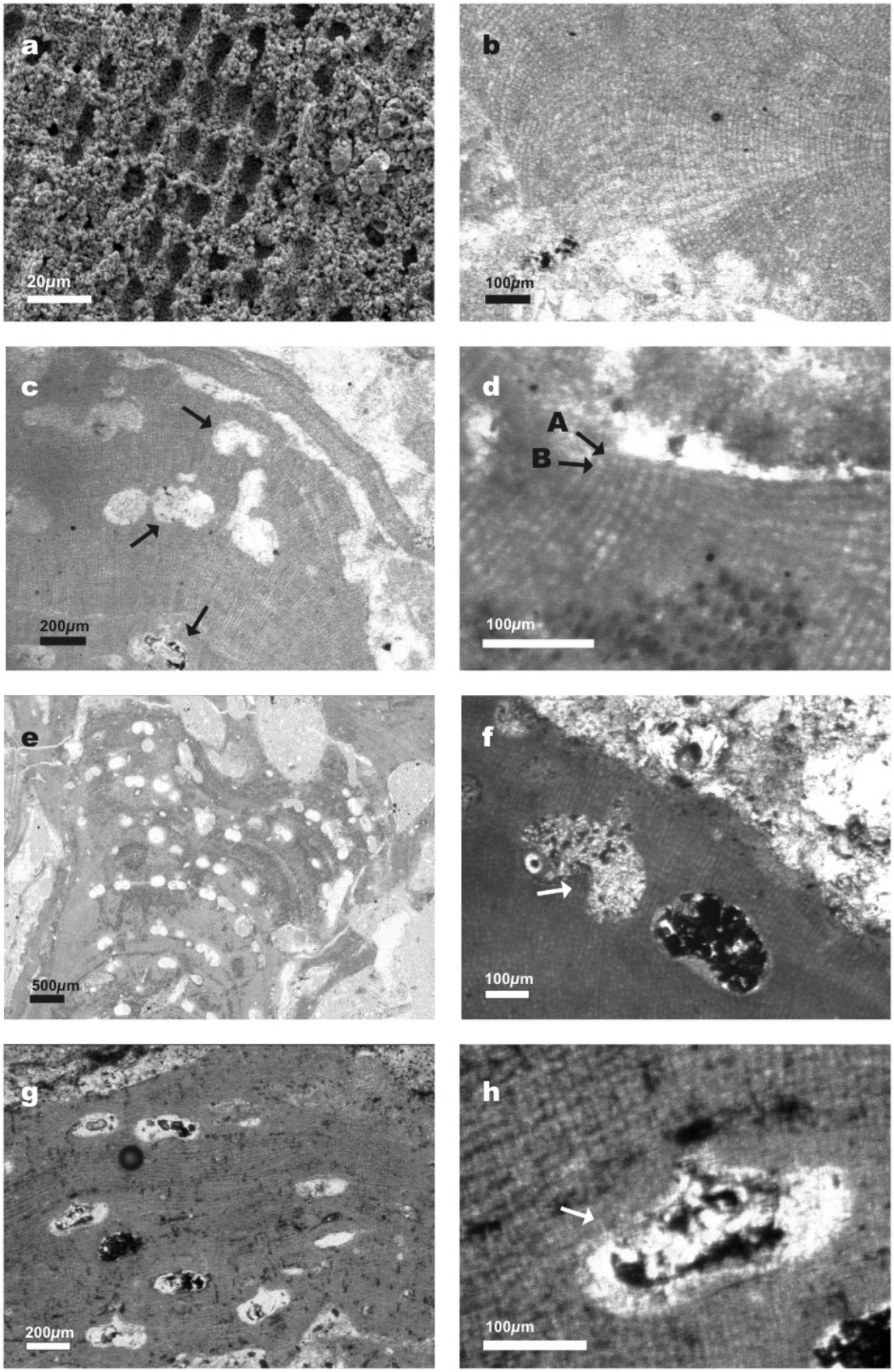
a
20μm
b
100μm
c
200μm
d
A
B
100μm
e
500μm
f
C
100μm
g
200μm
h
100μm

Fig. 3.3.2. (previous page): *Lithophyllum*
a: SEM micrograph of *Lithophyllum* sp. Note good vertical alignment of cells due to the absence of cell fusions. VO8d
b: Coaxial area within thallus of *Lithophyllum dentatum*, VA9
c: Thallus of *Lithophyllum dentatum* with bean shaped tetra-/bisporangial conceptacles (arrows), VA9
d: Dimerous thallus of *Lithophyllum incrustans*. Note non-palisade primigenous cells (A) and postigenous cells (B) and the absence of horizontal alignment, MD14
e: Swollen, bifurcated protuberance of *Lithophyllum incrustans*. Note horizontal alignment of conceptacles, MD14
f: Bean shaped tetra-/bisporangial conceptacles of *Lithophyllum incrustans* with prominent columella (arrow),VO5a
g: Thallus of *Lithophyllum nitorum*. Note oval to bean shaped tetra-/bisporangial conceptacles that do not have a pronounced columella, K11
h: Tetra-/bisporangial conceptacle of *Lithophyllum nitorum*. Note cells that form the conceptacle roof are as long as or longer than the surrounding cells. Note also good horizontal and vertical alignment of cells,K11

centre (columella). The columella can be up to 150µm high. The pore channel is dumbbell shaped and may be as long as the conceptacle height. Mature conceptacles were not raised above the thallus surface. Sexual conceptacles were not identified.
See also Braga and Aguirre (1995) for description

Lithophyllum incrustans (Philippi, 1837)

See Braga and Aguirre (1995) for synonyms

Description: Thallus is dimerous, encrusting to fruticose and >600µm in thickness. Cell fusions are absent. The examined material does not contain core elements. Primigenous cells are non-palisade (Fig. 3.3.2.d) and 8 - 10µm in height and 5 - 8µm in width. Postigenous cells are short and squarish to elongate-rectangular and 10 - 25µm in height and 5 - 13µm in width (Table 3.3.1.). Vertical alignment is very good due to the absence of cell fusions but lateral alignment is absent. Banding is not present. Protuberances are swollen and often branched (Fig. 3.3.2.e). The swollen appearance is a result of bifurcation of vertical filaments and outward curving of filaments to create space.
Conceptacles of bi-/tetrasporangial plants are usually arranged in bands parallel to the thallus surface (Fig. 3.3.2.e). They are 117 - 187µm in height and 226 - 333µm in width (Table 3.3.1.) and bean shaped (Fig. 3.3.2.f). The conceptacle floor is raised in the centre (columella). The columella can be up to 150µm high. The pore channel is dumbbell shaped and may be as long as the conceptacle height. Mature conceptacles were not raised above the thallus surface. Sexual conceptacles were not identified.

See also Braga and Aguirre (1995) and Basso et al. (1996, as Lithophyllum racemus) for description

Lithophyllum nitorum (Adey and Adey, 1973)

See Braga and Aguirre (1995) for synonyms

Description: Thallus is dimerous and encrusting to fruticose and >600µm in thickness. Cell fusions are absent. The examined material does not contain core elements. Primigenous cells are non-palisade and 11-13µm in height and around 5µm in width. Postigenous cells are short and squarish to rectangular and 6 - 15µm in height and 3 - 8µm in width (Table). Vertical alignment is good due to the absence of cell fusions and lateral alignment is good to moderate (Fig. 3.3.2.g). Banding is not present.

Conceptacles of bi-/tetrasporangial plants are oval to slightly bean shaped. They are 85 - 106µm in height and 245 - 290µm in width (Table 3.3.1.). No pronounced columella is observed. Mature conceptacles were raised above the thallus surface by one third to half of the conceptacle height. The conceptacle roof is characteristically formed by one or two rows of cells longer than the surrounding cells (Fig. 3.3.2.h). Sexual conceptacles were not identified.

See also Braga and Aguirre (1995) for description

Genus ***Titanoderma*** (Nägeli, 1858)

Diagnosis: Thallus is dimerous or dimerous and monomerous in one plant. Primigenous cells are palisade. Thallus margin is bistratose (Chamberlain, 1991).

Titanoderma pustulatum

See Irvine (1994) for synonyms

Description: Thallus is dimerous and encrusting or layered and commonly 10 - 400µm in thickness. Cell fusions are absent. Primigenous cells are dominantly palisade and 14 - 44µm in height and 6 - 10µm in width (Fig. 3.3.3.a). Irregularities in the substratum are levelled out by long, sickle-shaped cells. Postigenous cells are long and rectangular and 5 - 55µm in height and 3 - 9µm in width (Table 3.3.1.). Thallus is commonly <10 cells in thickness but multiple overgrowths by the same plant may occur. Cells are horizontally aligned and vertical alignment is absent.

Conceptacles of bi-/tetrasporangial plants are triangular in section with short conical pore channels (Fig. 3.3.3.b). They are 65 - 106µm in height and 267 - 381µm in width (Table 3.3.1.). The conceptacle floor is usually convex but no pronounced columella is observed. Mature conceptacles were almost completely raised above the thallus surface. Conceptacle walls may be formed by a row of cells larger than overlying and underlying cells. Sexual conceptacles were not identified.

Discussion: Members of the genus *Lithophyllum* are easily recognized by the absence of cell fusions and the resulting symmetric cell structure. Species of *Lithophyllum* found in the Miocene deposits of Crete are common in the modern Mediterranean. The genus *Titanoderma* has been included in the genus *Lithophyllum* by many authors, since Campbell and Woelkerling (1990) stated, that palisade cells did not occur in all species and therefore could not be used as a diagnostic criterium. The separation from *Lithophyllum* appears to be reasonable, however, not only based on the additional characteristics established by (Chamberlain and Keats, 1994) but also taking into account gene sequential analysis (Bailey, 1999). In the material from Crete, *Titanoderma pustulatum* stands out by its exceptionally large cells and is therefore easily identified.

Fig. 3.3.3. (next page): *Titanoderma, Spongites*
a: Thallus of *Titanoderma pustulatum*. Note sickle-shaped palisade primigenous cells (arrow), MD14
b: Uniporate tetra-/bisporangial conceptacle of *TItanoderma pustulatum*, K24
c: SEM micrograph of *Spongites albanensis*; the cut is perpendicular to growth direction. Note abundant multiple cell fusions (arrows) resulting in a spongy texture, VO8e
d: Protuberant branch of *Spongites albanensis* showing conspicuous radial bands, VO13c
e: Thallus of *Spongites albanensis* with ventral core. Note core filaments curving sheaf-like from the centre of the core, MO18b
f: Encrusting thallus of *Spongites albanensis* with undulating ventral core, MO18b
g: Bean shaped uniporate tetra-/bisporangial conceptacle of *Spongites albanensis*, K16
h: Flat male conceptacle of *Spongites albanensis*, K12b

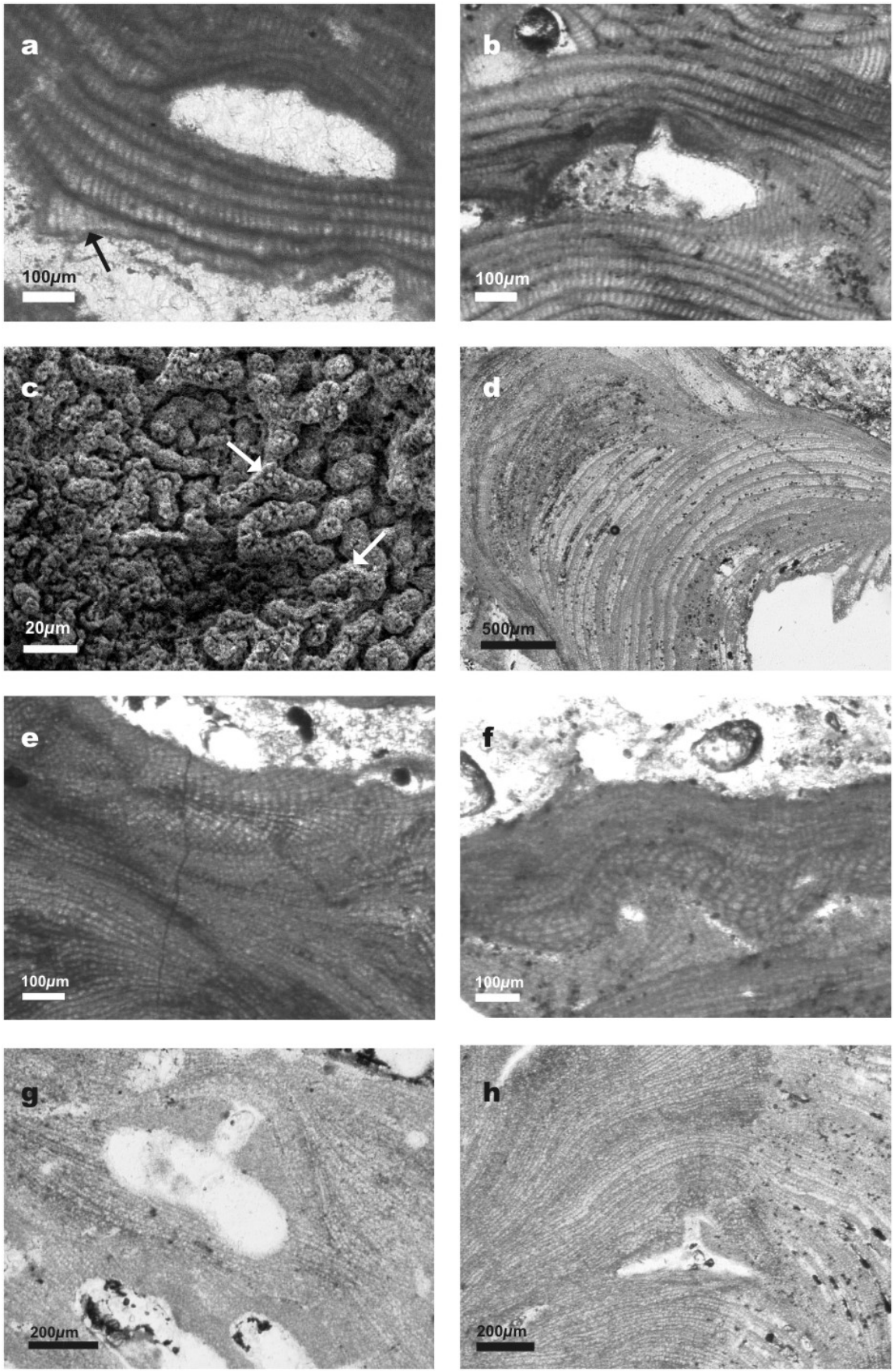
a
100μm
b
100μm
c
20μm
d
500μm
e
100μm
f
100μm
g
200μm
h
200μm

Subfamily **Mastophoroideae** (Setchell, 1943)

Diagnosis: Tetra-/bisporangial conceptacles are uniporate; cell fusions are present (Woelkerling, 1988).

Genus ***Spongites*** (Kützing, 1841)

Diagnosis: Thallus is more than 6 cells in thickness and monomerous or dimerous. Dimerous portions of the thallus lack palisade cells. (Woelkerling, 1988). Filaments around the conceptacle pore canals are subparallel to the roof surface (Penrose and Woelkerling, 1992). Coaxial core filaments are absent (Braga et al., 1993).

Spongites albanensis Lemoine (Braga et al., 1993)

See Braga et al. (1993) for synonyms

Description: Thallus is monomerous and usually warty to lumpy, more rarely encrusting, foliose or fruticose and usually >1mm in thickness. Cell fusions are numerous. Core cells are 10 - 15µm in height and 4 - 9µm in width and peripheral cells are 7 - 18µm in height and 4 - 11µm in width (Table 3.3.1.). Sections perpendicular or oblique to growth direction have a spongy texture due to multiple cell fusions (Fig. 3.3.3.c). Cell walls are usually heavily calcified. This results in a whitish appearance of fossil plants and relatively well preserved cell walls in thin section. Lateral alignment is high, vertical alignment is absent due to numerous cell fusions. Cells in the centre of protuberances are commonly enlarged (14 - 18µm in height). Protuberances have a banded appearance as a result of intermittent variation in cell length in growth direction and bands are usually concentric (Fig. 3.3.3.d). Protuberances often lack reproductive structures. Core thickness is variable and growth direction often changes. Cores are up to 300µm thick and core filaments curve sheaf-like from the central part of the core (Fig. 3.3.3.e). The core occasionally is undulating (Fig. 3.3.3.f).
Conceptacles of all fertile plants are uniporate. Conceptacles of bi-/tetrasporangial plants are usually dumbbell to bean shaped (Fig. 3.3.3.g), 132 - 232µm in height and 367 - 602µm in

width (Table 3.3.1.). When mature, more than three quarters of the conceptacle were raised above the thallus surface. Conceptacles occur either solitary at the surface of protuberances or in unordered groups within the thallus. Pore channels are conical to bulbous. Male conceptacles are flat, triangular and considerably smaller than bi-/tetrasporangial conceptacles (63 - 100µm in height and 374 - 499µm in width; Table 3.3.1.; Fig. 3.3.3.h). Female conceptacles and carposporangial conceptacles were not identified.
See also Braga et al. (1993) for description and photographs

Spongites sp.1

Description: Thallus is dimerous and layered to foliose and >300µm in thickness. Cell fusions are numerous. Primigenous cells are non-palisade and 8 - 9µm in height and 5 - 6µm in width (Fig. 3.3.4.a). Postigenous cells are 8 - 19µm in height and 4 - 10µm in width (Table 3.3.1.). Cell size is irregular and cell fusions are common. Lateral alignment is low and vertical alignment is absent. Cells are arranged in irregular arcs around 5 cells high and about 20 - 50 cells wide that intersect each other (Fig. 3.3.4.b).
Conceptacles of bi-/tetrasporangial plants are uniporate, usually oval and small compared to cell size (Fig. 3.3.4.b,c). They are 69 - 109µm in height and 179 - 281µm in width (Table 3.3.1.). Of fertile conceptacles, only the pore channel was raised above the thallus. Pore channels are as long or longer than the conceptacle height and cylindrical (Fig. 3.3.4.c). Sexual conceptacles were not identified.

Discussion: Of the Mastoporoideae, only *Lithoporella, Neogoniolithon, Pneophyllum* and *Spongites* are known as fossils (Braga 2002, *unpublished manuscript*). *Lithoporella*, characterized by dimerous thallus organization with a ventral layer of palisade cells and cell sizes of up to 80µm was not found. Mastophoroid specimens from the Miocene of Crete therefore belong to the *Pneophyllum-Spongites-Neogoniolithon* complex. Separation of genera within this complex is based on reproductive structures with very low preservation potential. In fossil material, alternatively the criteria of Braga et al. (1993) and Woelkerling (1988) can be applied: *Pneophyllum* is encrusting and forms strictly dimerous thalli usually less than 6 cells thick (Woelkerling, 1988). *Neogoniolithon* is identified by the occurrence of a coaxial core at least in some portions of the thallus. While the validity of this character has

been doubted (Penrose, 1992), it remains to be the best possibility to identify *Neogoniolithon* in fossil material. Applying these criteria, all mastoporoid individuae from Crete are included in the genus *Spongites*.

Family **Hapalidiaceae** (Harvey et al., 2003)
Subfamily **Melobesioideae** (Bizzozero, 1885)

Diagnosis: Tetra/bisporangial conceptacles are multiporate; cell fusions are common (Woelkerling, 1988).

Genus ***Lithothamnion*** (Heydrich, 1897)

Diagnosis: Plants are monomerous (Woelkerling, 1988). Cores are plumose (Braga et al., 1993). Subepithallial initials are as long or longer than their immediate inward derivates (Rasser and Piller, 2000).

Lithothamnion ramosissimum Reuss (Piller, 1994)

See Piller (1994) for synonyms

Description: Thallus is usually warty to lumpy and more rarely foliose. Foliose parts may be < 300µm in thickness. Cores reach a thickness of 200 - 250µm. Their thickness is little variable in growth direction. Cores are plumose with several filaments in the centre being (sub)parallel to growth direction (Fig. 3.3.4.d). Cores are commonly slightly undulating. Core cells are 8 - 17µm in height and 3 - 5µm in width and peripheral cells are 6 - 19µm in height and 2 - 6µm in width (Table 3.3.1.). Cell fusions are rare in the core but common in peripheral cells. Protuberances are broad (commonly several mm) and have a banded appearance due to layers of shorter, more heavily calcified cells (Fig. 3.3.4.e). Individual bands are usually up to 5 cells thick but the amount of cells is locally increased (Fig. 3.3.4.f). This results in an irregular shape and non-concentric structure of protuberances. Lateral alignment in the perithallus is usually good but poor in bulging portions of the thallus.

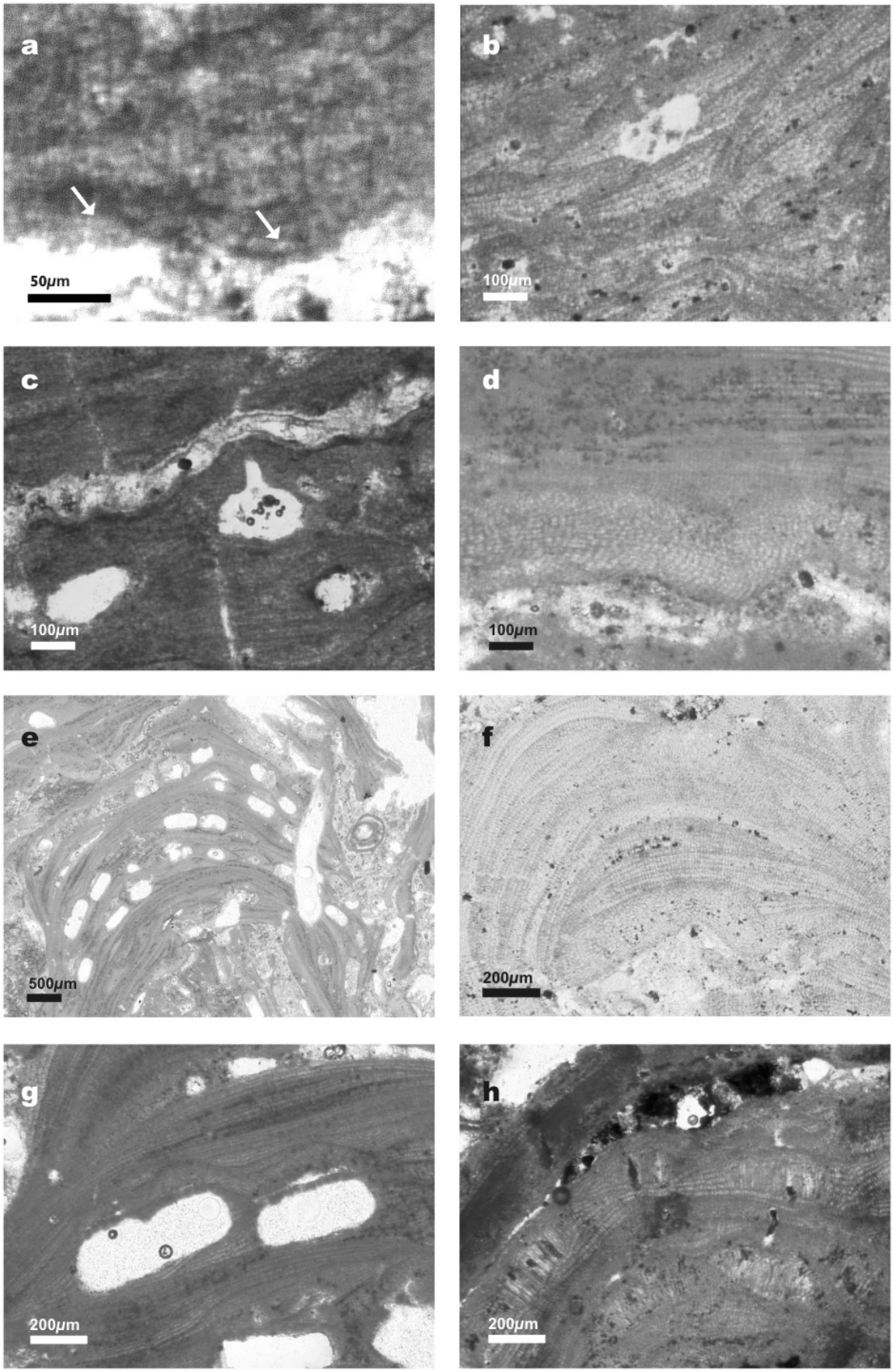
a
50μm
b
100μm
c
100μm
d
100μm
e
500μm
f
200μm
g
200μm
h
200μm

Fig. 3.3.4. (previous page): *Spongites, Lithothamnion*
a: Encrusting thallus of *Spongites* sp.1. Note non-palisade primigenous cells (arrows), V05b
b: Thallus of *Spongites* sp.1 with uniporate tetra-/bisporangial conceptacle. Note relative large cell size compared to conceptacle size. Cell size is irregular, cell fusions are common, lateral alignment is low and vertical alignment is absent. Cells are characteristically arranged in irregular arcs, VO5b
c: Uniporate tetra-/bisporangial conceptacle of *Spongites* sp.1 with long cylindrical pore channel, K25
d: Ventral core of *Lithothamniom ramosissimum.* Note elongate core cells and core filaments being arranged subparallel in the centre, VO20b
e: Warty protuberance of *Lithothamniom ramosissimum* with irregularly arranged conceptacles, VO20b
f: Warty thallus of *Lithothamniom ramosissimum*. Note irregular banding with portions of the thallus bulging upward in intervals,VO20b
g: Fused multiporate tetra-/bisporangial conceptacles of *Lithothamniom ramosissimum.* Note thon conceptacle roofs and small cores overgrowing it, VO20b
h: Multiporate tetra-/bisporangial conceptacles of *Lithothamniom ramosissimum* that are filled with prematurely calcified filaments, K28

Conceptacles occur irregularly in the thallus. Bi-/tetrasporangial conceptacles (Fig. 3.3.4.g) are 118 - 224µm in height and 224 - 586µm in width (Table 3.3.1.).
Conceptacles are commonly fused. This is the case for conceptacles wider than 400 – 450µm (Table 3.3.1.). They are rectangular with rounded edges. Conceptacle roofs are thin (usually 3 – 4 cells) and planar. They are commonly overgrown by a thin up to 80µm thick core of the same plant and a small void may remain between conceptacle roof and this core. Conceptacle walls are formed by cells that are as long as or longer than the surrounding thallus. Conceptacles are housed within an elevated area that was completely raised above the surrounding thallus by the height of the conceptacle and that has approximately two times the diameter of the conceptacle. Conceptacles are commonly situated on the wall of the raised area of an earlier conceptacle and obliquely overgrowing it. Many conceptacles are filled with vertical calcified filaments that formed prior to ripening (Fig. 3.3.4.h). For measurements only conceptacles without calcified filaments were used. Sexual conceptacles were not identified.

Lithothamnion sp.1

Description: Thallus is usually lumpy to fruticose. Cores reach a thickness of 250 - 300µm. Thickness is little variable in growth direction. Cores are plumose and filaments curve upward sheaf-like (Fig. 3.3.5.a). Upward curving filaments account for 3/4 to 4/5 of total core thickness. Core cells are large (8 - 17µm in height and 3 - 7µm in width) compared to peripheral cells that are 5 - 18µm in height and 1 - 5µm in width (Table 3.3.1.). Epithallial cells are flattened and subepithallial initials are longer than their immediate inward derivates (Fig. 3.3.5.b). Cell fusions are common but multiple fusions are rare. Protuberances are

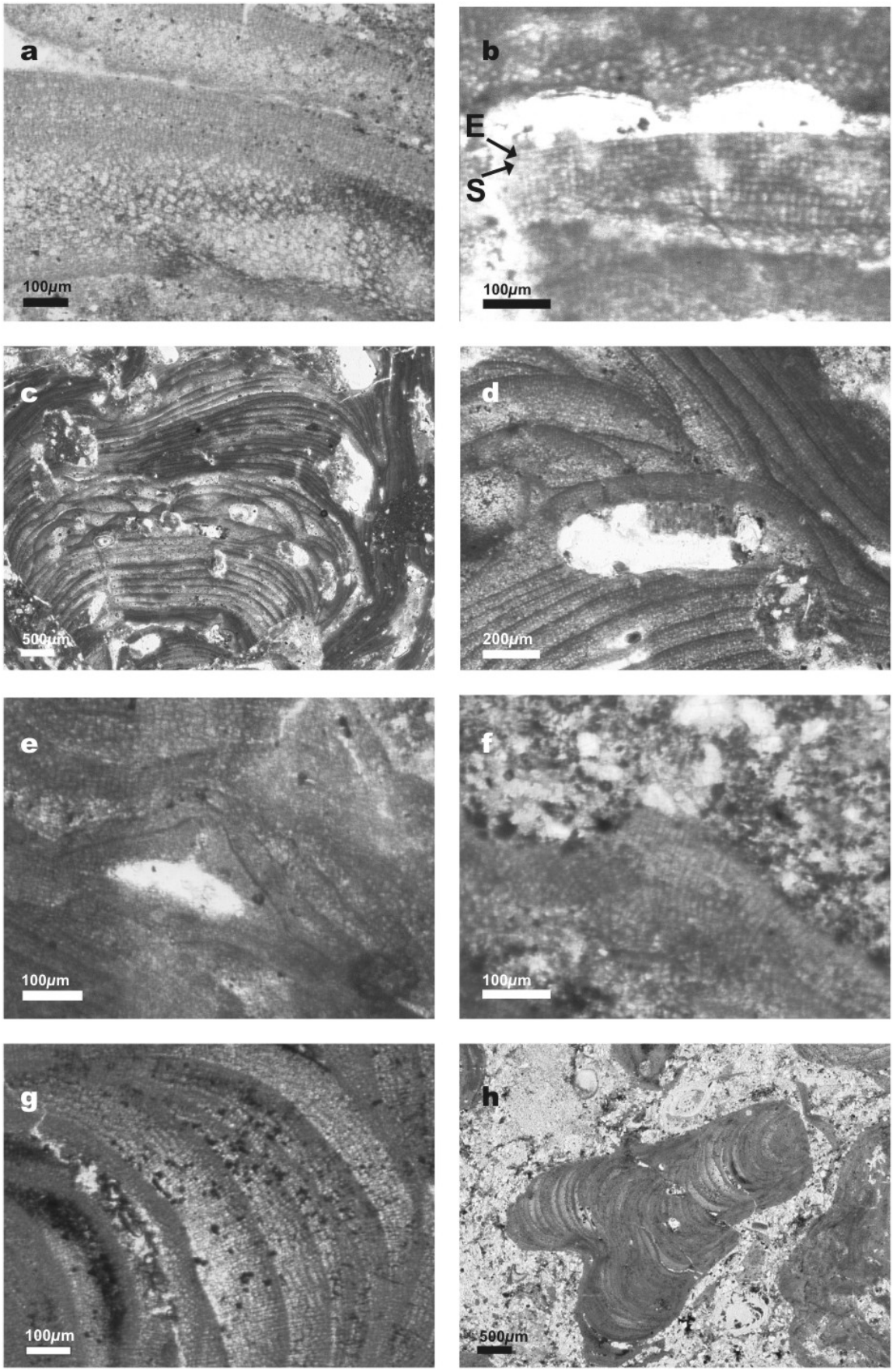
a
100μm
b
E
S
100μm
c
500μm
d
200μm
e
100μm
f
100μm
g
100μm
h
500μm

Fig. 3.3.5. (previous page): *Lithothamnion/Phymatolithon*
a: Plumose ventral core of *Lithothamnion* sp.1. Note elongate cells with cell fusions and core filaments curving upward sheaf-like, MO25
b: Thallus of *Lithothamnion* sp.1. with the complete row of epithallial (E) and subepithallial (S) cells preserved under a sessile foraminifera. Note that Epithallial cells are flattened and subepithallial initials are longer than their immediate inward derivates, K29b
c: Broad, branched and strongly banded protuberance of *Lithothamnion* sp.1. Conceptacles are situated in a certain interval of the protuberance and form thick bulges that were raised completely over the thallus surface when mature, MO26c
d: Large multiporate tetra-/bisporangial conceptacle of *Lithothamnion* sp.1 that is incised into the underlying thallus. Note considerable roof thickness, MO26c
e: Uniporate sexual conceptacle of *Lithothamnion* sp.1, MO26c
f: Plumose core of *Lithothamnion/Phymatolithon* sp.1 with core filaments that curve upward from the base of the core. VO1
g: Thallus of *Lithothamnion/Phymatolithon* sp.1 with irregular banding. Note that cells are aligned neither horizontally nor vertically, VO1
h: Branched protuberance of *Lithothamnion/Phymatolithon* sp.1, VO1

>3mm in width and in many cases branched (Fig. 3.3.5.c). They have a banded appearance due to layers of shorter, more heavily calcified cells. Bands are variable in thickness, commonly between 5 and 10 cells but may also comprise more. Bands are wavy but in protuberances usually approximately concentric. Lateral alignment in the perithallus is usually good.

Conceptacles occur in intervals within protuberances. Bi-/tetrasporangial conceptacles (Fig. 3.3.5.d) are 125 - 296µm in height and 270 - 899µm in width (Table 3.3.1.). They are rectangular with rounded edges. Conceptacle roofs are exceptionally thick (usually 8 – 10 cells) and convex. Pores are conical. Conceptacles are housed within an elevated area that has approximately two times the diameter of the conceptacle. Conceptacles may be either incised into up to 10 layers of underlying cells (Fig. 3.3.5.d) or were completely raised above the thallus surface. Conceptacles may be situated on the wall of the raised area of an earlier conceptacle and therefore obliquely overgrow it. Male conceptacles are 56 - 63µm in height and 197 - 22µm in width. They have a domed roof and a level base. The pore channel is longer than the height of the conceptacle and the mature conceptacle was completely raised above the thallus surface (Fig. 3.3.5.e).

Lithothamnion/Phymatolithon sp.1

Description: Thallus morphology is variable and ranges from encrusting and layered to fruticose. Cores reach a thickness of 165µm (Fig. 3.3.5.f). Thickness is little variable in growth direction. Cores are plumose and filaments curve upward from the ventral base of the

core. Core cells are 7 - 15µm in height and 1 - 5µm in width and peripheral cells are 4 - 13µm in height and 1 - 4µm in width (Table 3.3.1.). Horizontal and vertical alignment is usually absent (Fig. 3.3.5.g). Cell fusions are common but multiple fusions are rare. Layered portions of the thallus are irregularly banded. Protuberances are usually 1-3mm in width and often branched (Fig. 3.3.4.h). Banded appearance results from layers of shorter, more heavily calcified cells. Bands are variable in thickness, commonly between 3 and 10 cells but may also comprise more.

Conceptacles occur dispersed in the thallus. Bi-/tetrasporangial conceptacles (Fig. 3.3.6.a) are 92 - 165µm in height and 145 - 292µm in width (Table 3.3.1.). Rare fused conceptacles reach a width of 388µm. In section, conceptacles are rectangular to slightly trapezoid with rounded edges. Roofs are formed by 3 - 4 cells that may be as long as the surrounding thallus. Roofs are convex and mature conceptacles were not or only slightly raised. Identified uniporate sexual conceptacles apparently are carposporangial conceptacles. In contrast to male conceptacles, they are larger than bi-/tetrasporangial conceptacles of the same species (Womersley, 1996) and 88 - 113µm in height and 300 - 335µm in width. They are irregularly banana-shaped with a broad conical pore channel.

Genus ***Mesophyllum*** (Lemoine, 1928)

Diagnosis: Plants are monomerous (Woelkerling, 1988). Core filaments are coaxial, at least in portions of the plant (Lemoine, 1928; Braga et al., 1993; Aguirre and Braga, 1998).

Mesophyllum curtum (Lemoine, 1939)

For diagnosis of the type material and synonyms see Aguirre and Braga (1998)

Fig, 3.3.6. (next page): *Lithothamnion/Phymatolithon, Mesophyllum*
a: Multiporate tetra-/bisporangial conceptacle of *Lithothamnion/Phymatolithon* sp.1, VO1
b: Uniporate carposporangial conceptacles of *Lithothamnion/Phymatolithon* sp.1, VO1
c: Core of *Mesophyllum curtum*, VO11
d: Oblique view on warty protuberance of *Mesophyllum curtum*, MO1b
e: Multiporate tetra-/bisporangial conceptacle of *Mesophyllum curtum.* Note trapezoid shape and rim formed by additional cells at the edge of the conceptacle roof, MO1b
f: Plant of *Mesophyllum sancti dionysii* encrusting *Porites*, VO14
g: Core of *Mesophyllum sancti dionysii*, VO5a
h: Warty protuberance of *Mesophyllum sancti dionysii*. Not good lateral alignment and banded appearance due to intermittent heavy calcification of cells. Note that layers of heavily calcified cells discordantly overgrow older cells (arrows), MO12b

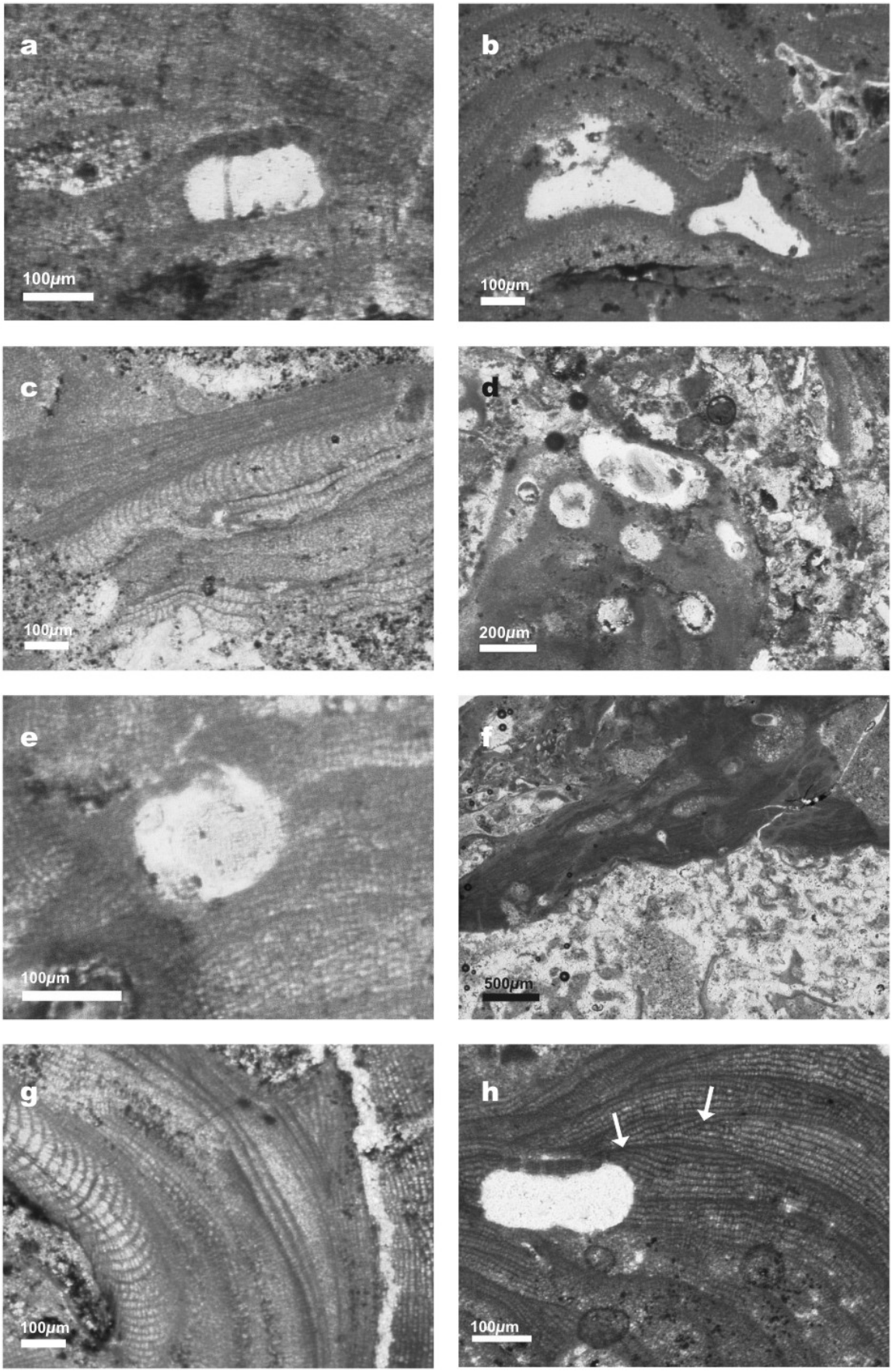
a
100μm
b
100μm
c
100μm
d
200μm
e
100μm
f
500μm
g
100μm
h
100μm

Description: Thallus is layered to foliose and partially warty and thickness is usually between 300 and 700µm. Core cells are 8 - 14µm in height and 3 - 5µm in width and peripheral cells are 4 - 9µm in height and 2 - 5µm in width (Table 3.3.1.). Cores are coaxial with good lateral alignment of filaments (Fig. 3.3.6.c). Cores are commonly straight and up to 150µm in thickness with commonly little variation in thickness in growth direction. Cell fusions are common in the core and in peripheral portions of the thallus. Protuberances are short and knobbly and are formed by irregular arcs several cells in height (Fig. 3.3.6.d). Lateral alignment is moderate to good within arcs and high in foliose portions of the thallus.
Conceptacles are usually situated within protuberances. Conceptacles of bi-/tetrasporangial plants are 102 - 156µm in height and 154 - 226µm in width (Table 3.3.1.). They usually have a conspicuous squarish to trapezoidal shape (Fig. 3.3.6.e). The upper half of the mature conceptacle was raised above the thallus surface. Conceptacle roofs are several cells thick. Many roofs have a central depression as a result of sinking and cell reduction apparently in a late stage of the evolution of the conceptacle. Sexual conceptacles were not identified.

Mesophyllum sancti-dionysii (Lemoine, 1939)

For diagnosis of the type material and synonyms see Aguirre and Braga (1998)

Description: Thallus is encrusting (Fig. 3.3.6.f) or layered to warty, more rarely foliose. The thickness of a single layer within layered portions of the thallus reaches 700-1000µm. Core thickness is up to 300µm (Fig. 3.3.6.g). Core cells are 11 - 22µm in height and 5 - 9µm in width and peripheral cells are 7 -20µm in height and 4 - 8µm in width (Table 3.3.1.). Cores are coaxial with good lateral alignment of filaments. Cell fusions are common in the peripheral portions of the thallus but less common in the core. Multiple cell fusions occur. Warty protuberances are conspicuously banded and lateral alignment of cells is good. Between orientation of lateral alignment of cells and the orientation of banding typically high angles of up to 30° - 40° occur (Fig. 3.3.6.h). This effect is a consequence of shorter and more heavily calcified cells that are responsible for the banded appearance and grow discordantly on older cells.
Conceptacles are usually situated in layered parts of the thallus, not in protuberances (Fig. 3.3.7.a). Conceptacles of bi-/tetrasporangial plants are 151 - 305µm in height and 220 - 503µm in width (Table 3.3.1.). Conceptacles are rarely fused. They are oval in shape and

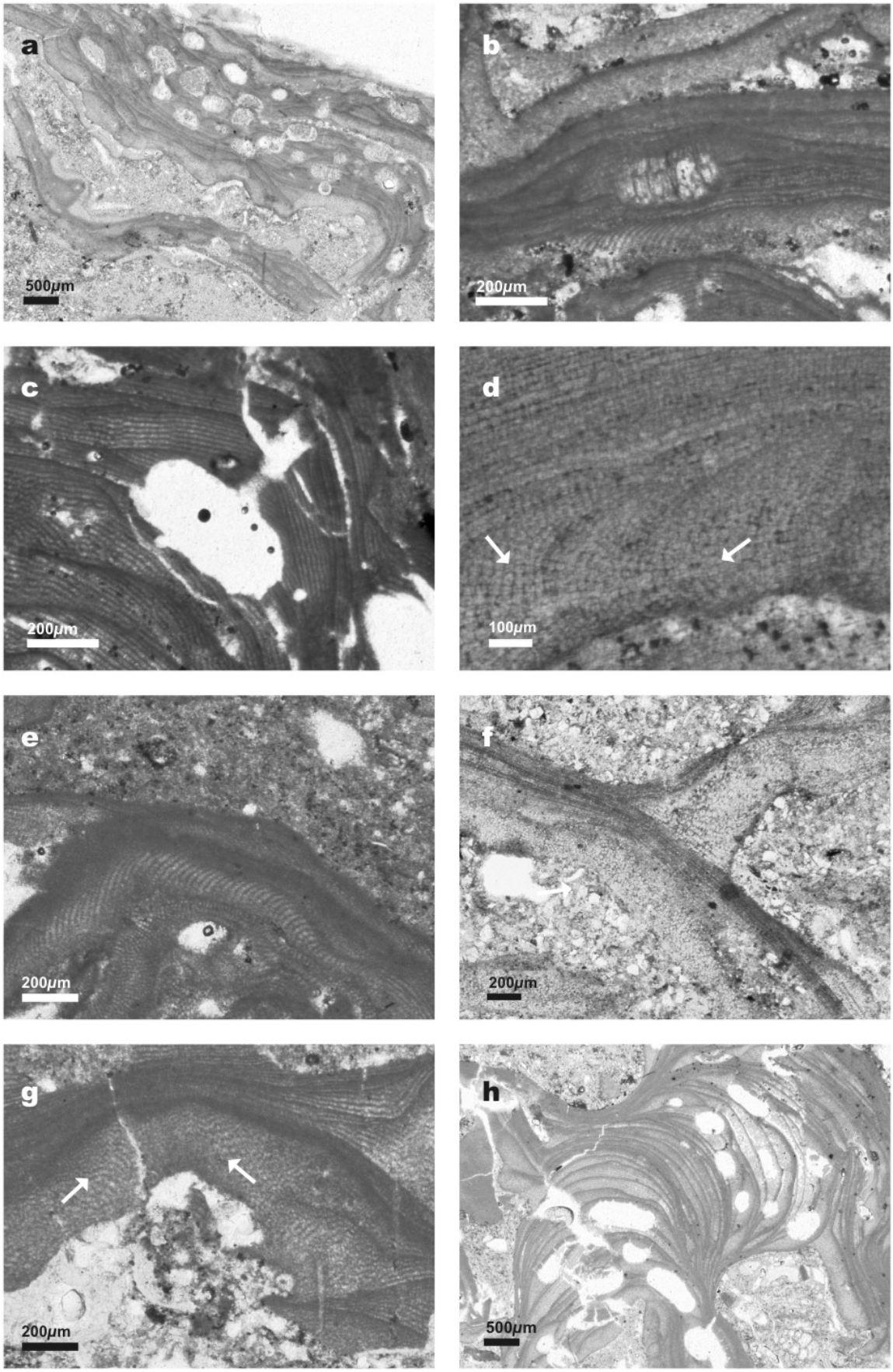
a
500μm
b
200μm
c
200μm
d
100μm
e
200μm
f
200μm
g
200μm
h
500μm

Fig. 3.3.7. (previous page): *Mesophyllum*
a: Layered and foliose thallus of *Mesophyllum sancti dionysii*, MD14
b: Multiporate tetra-/bisporangial conceptacle of *Mesophyllum sancti dionysii* characteristically filled by large cells after maturity, MO12b
c: Uniporate carposporangial conceptacle of *Mesophyllum sancti dionysii.* Note long conical to funnel shaped pore channel, MO12b
d: Broad core of *Mesophyllum* sp.1, variable in thickness and growth direction. Note paired and often fused elongate core cells (arrows) that show only moderate lateral (coaxial) alignment , VO13
e: Coaxial core of *Mesophyllum* sp.1, K21
f: Foliose thallus of *Mesophyllum* sp.1 that divides itself by formation of a new core out of peripheral cells, MS7
g: Rejoined thallus of *Mesophyllum* sp.1. Growth directions of cores are indicated by arrows, K21
h: Fruticose protuberance of *Mesophyllum* sp.1. Note conspicuous banding and variable cell length within individual bands, K21

conceptacle roofs are several cells (usually 4 – 5) thick (Fig. 3.3.7.b). The roof may be sunken, resulting in significant (up to one third) reduction of the conceptacle height. The upper half to upper third of the fertile conceptacle was raised above the thallus surface. The extent of the elevated area around the conceptacle is usually around two times the width of the conceptacle. Conceptacles are commonly filled with large secondary cells (11 - 12µm in width and 28 - 64µm in height; Fig. 3.3.7.b). Uniporate, presumably carposporangial conceptacles are also oval in shape and 158 - 215µm in height and 431- 456µm in width (Fig. 3.3.7.c). They have conical to funnel shaped pore channels that are longer than the height of the conceptacle chamber. Conceptacles were raised by more than the length of the pore channel above the thallus surface.

Mesophyllum sp.1

Description: Thallus is foliose but may also be warty to fruticose. Foliose parts consist of a relatively broad core (80 - 400µm, usually >200µm; Fig. 3.3.7.d) and a relatively thin peripheral thallus (100 - 1000µm). Cores are coaxial (Fig. 3.3.7.e) but lateral alignment of filaments may be poor in large parts of the plant (Fig. 3.3.7.f). Both, straight intervals and intervals with frequent change in growth direction and variable thickness may occur (Fig. 3.3.7.d). Plants of this species frequently form new cores at all parts of the thallus including protuberances (Fig. 3.3.7.f). Foliose parts of the thallus are often divided by formation of new cores that may rejoin with other parts of the thallus (Fig. 3.3.7.g). Core cells are 11 - 29µm in height and 3 - 7µm in width and peripheral cells are 6 - 19µm in height and 2 - 6µm in width (Table 3.3.1.). Cell fusions are common. Lateral alignment in the peripheral thallus is relatively good. Protuberances have a banded appearance as a result of intermittent variation

in cell length and calcification that is more conspicuous than the also considerable lateral variation in cell length (Fig. 3.3.7.h).

Conceptacles usually occur in protuberant parts of the plant, more rarely in foliose portions of the thallus. Bi-/tetrasporangial conceptacles (Fig. 3.3.8.a) are exceptionally large (205 - 351µm in height and 492 - 1206µm in width; Table 3.3.1.). Conceptacles larger that 700µm are most likely fused. Conceptacles are rectangular with rounded edges but may be bend parallel to the banding. Conceptacle roofs are several cells (usually 5 - 8) thick and usually parallel to the conceptacle floor. The upper half of the fertile conceptacle was raised above the thallus surface, forming a gently sloping embossment. Conceptacle walls raised above the thallus surface in many cases have approximately the same thickness as the roof. Conceptacles that are buried in the thallus may be overgrown by thin (30 - 50µm) plumose cores. Pores in the conceptacle roofs are large (up to 10µm in width) and conical (Fig. 3.3.8.a). Sexual conceptacles were not identified.

Mesophyllum sp.2

Description: Thallus is layered and reaches 650µm in thickness. Core thickness is between 110 and 260µm with little variation in growth direction (Fig. 3.3.8.b). Cores are coaxial with good lateral alignment of filaments in parts of the plant. Core cells are 8 - 14µm in height and 3 - 6µm in width and peripheral cells are 4 - 11µm in height and 1 - 3µm in width (Table 3.3.1.). Cell fusions are common. Lateral alignment in the perithallus is poor due to highly variable cell height (Fig. 3.3.8.b).

Conceptacles commonly occur in groups of three or more in lateral alignment (Fig. 3.3.8.c). Bi-/tetrasporangial conceptacles are small (115 - 236µm in height and 165 - 397µm in width; Table 3.3.1.). They are oval in shape and conceptacle roofs are several cells (usually 5 – 7) thick and usually concave (Fig. 3.3.8.d). At least the upper half to upper two thirds of the

Fig. 3.3.8. (next page): *Mesophyllum, Sporolithon*
a: Multiporate tetra-/bisporangial conceptacle of *Mesophyllum* sp.1, VO13
b: Coaxial core of *Mesophyllum* sp.2, MD14
c: Layered thallus of *Mesophyllum* sp.2 with conceptacles horizontally aligned in groups, MD14
d: Multiporate tetra-/bisporangial conceptacles of *Mesophyllum* sp.2, VO13
e: Plumose core of *Sporolithon* sp.1, K27
f: Warty banded thallus of *Sporolithon* sp.1 with tetrasporangial conceptacles arranged in sori, K27
g: Lumpy thallus of *Sporolithon* sp.2 without banding, MO23a
h: Tetrasporangial conceptacles of *Sporolithon* sp.2 that are arranged in sori, MO23a

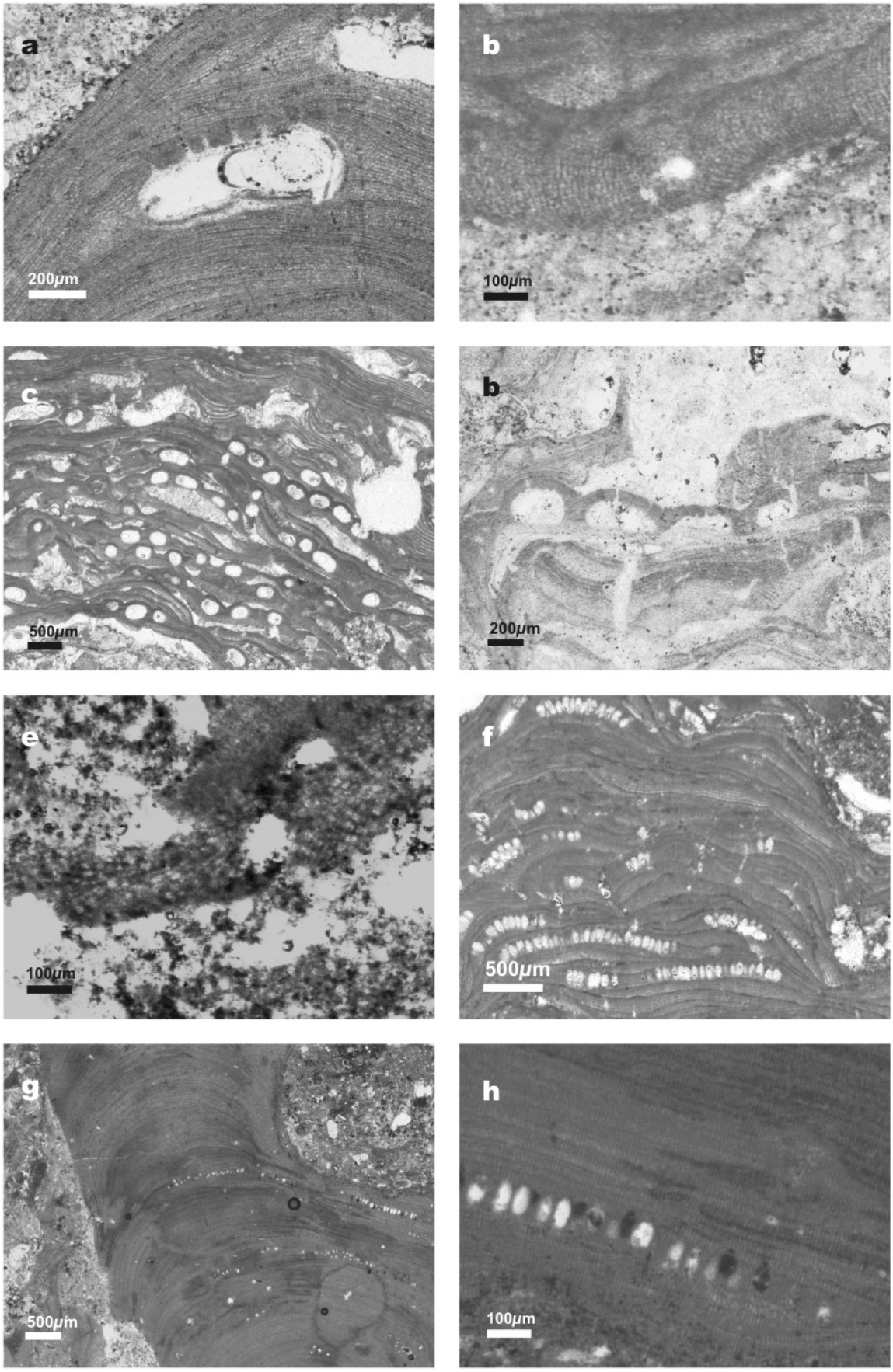
a
200μm
b
100μm
c
500μm
b
200μm
e
100μm
f
500μm
g
500μm
h
100μm

fertile conceptacle was raised above the thallus surface. Conceptacle walls that are raised above the thallus surface in many cases are not thicker than the roof. Conceptacles may be situated directly above core filaments. Sexual conceptacles were not identified.

Discussion: Among the genera of the Melobesioideae *Lithothamnion, Phymatolithon* and *Mesophyllum* are the only known to occur as fossils (Braga 2002, *unpublished manuscript*) as long as *Leptophyton* is considered as a heterotypic synonym of *Phymatolithon* (Düwel and Wegeberg, 1996). The separation of *Lithothamnion* from *Phymatolithon* based on the shape of epithallial cells and relative subepithallial initials was possible for *Lithothamnion* sp.1. *Phymatolithon,* on the other hand was not recognized but may be among the remaining melobesioid plants with a plumose core. *Mesophyllum* is in most cases defined by the persistent occurrence of a coaxial core. Only in *Mesophyllum* sp.1, plumose cores also occur. If conceptacles are present, however this species is also defined by their size that exceeds all other found in the material of central Crete.

Family **Sporolithaceae** (Verheij, 1993)

Diagnosis: Construction monomerous with a ventrally or centrally situated core and a peripheral region. Sexual reproduction occurs in uniporate cells. Tetrasporangia are borne in calcified compartments that may be solitary or are aggregated into sori (Verheij, 1993; Womersley, 1996).

*Genus **Sporolithon** (Heydrich, 1897)*

Diagnosis: Cells of adjacent filaments are usually joined by cell fusions. Tetrasporangia are borne I calcified compartments that are usually aggregated into sori of indefinite size (Verheij, 1993; Womersley, 1996).

Sporolithon sp.1

Description: Thallus is foliose to warty. Foliose parts are usually > 400µm in thickness. Cores are plumose and thickness is highly variable (110 - 240µm). Cores often change

growth direction. Core cells are elongate and of approximately the same size as peripheral cells (10 – 24µm in height and 3 - 5µm in width; Fig. 3.3.8.e; Table 3.3.1). Peripheral cells are 10 – 19µm in height and 3 – 7µm in width. Cell fusions are very common. Lateral alignment is good, vertical alignment is absent. Thallus has a banded appearance due to intermittent occurrence of more heavily calcified cell walls. Thickness of individual bands is highly variable (1-6 cells). Bands of cells are cut discordantly by younger bands (Fig. 3.3.8.f).
Tetrasporangial conceptacles are situated in warty parts of the thallus. Conceptacle chambers are arranged in sori. In a two dimensional cut, sori comprise up to 20 chambers. Individual chambers are 33 - 79µm in width and 79 – 133µm in height (Table 3.3.1.). Sexual conceptacles were not identified.

Sporolithon sp.2

Description: Thallus is lumpy and > 1000µm in thickness. The examined material does not contain core elements. Peripheral cells are 4 – 14µm in height and 2 – 4µm in width (Table 3.3.1.). Cell fusions are very common. Lateral alignment is poor to moderate in protuberant parts and vertical alignment is absent. Thallus lacks conspicuous banding (Fig. 3.3.8.g).
Tetrasporangial conceptacles are situated are arranged in sori (Fig. 3.3.8.h). In a two dimensional section, sori comprise up to 30 chambers. Individual chambers are 26 - 50µm in width and 38 – 82µm in height (Table 3.3.1.). Sexual conceptacles were not identified.

Discussion: The Sporolithaceae are easily identified in thin section due to the arrangement of conceptacle chambers in sori. This family contains only two genera of which the second genus, *Heydrichia*, is only known from the recent of southern Africa (Womersley, 1996).

Quantification of relative coralline red algal contents

The method of semiquantitative analysis using abundance classes has been discussed in chapter 1.4: Relative plant abundances and plant sizes are estimated in thin section and subdivided in three categories (common=50%, uncommon=33% and rare=16,6% of total red algal content). Using the size of cells and the height to width ratio of cells (Fig. 3.3.9.), it is possible to identify most plants and plant fragments even if cores and conceptacles are absent:

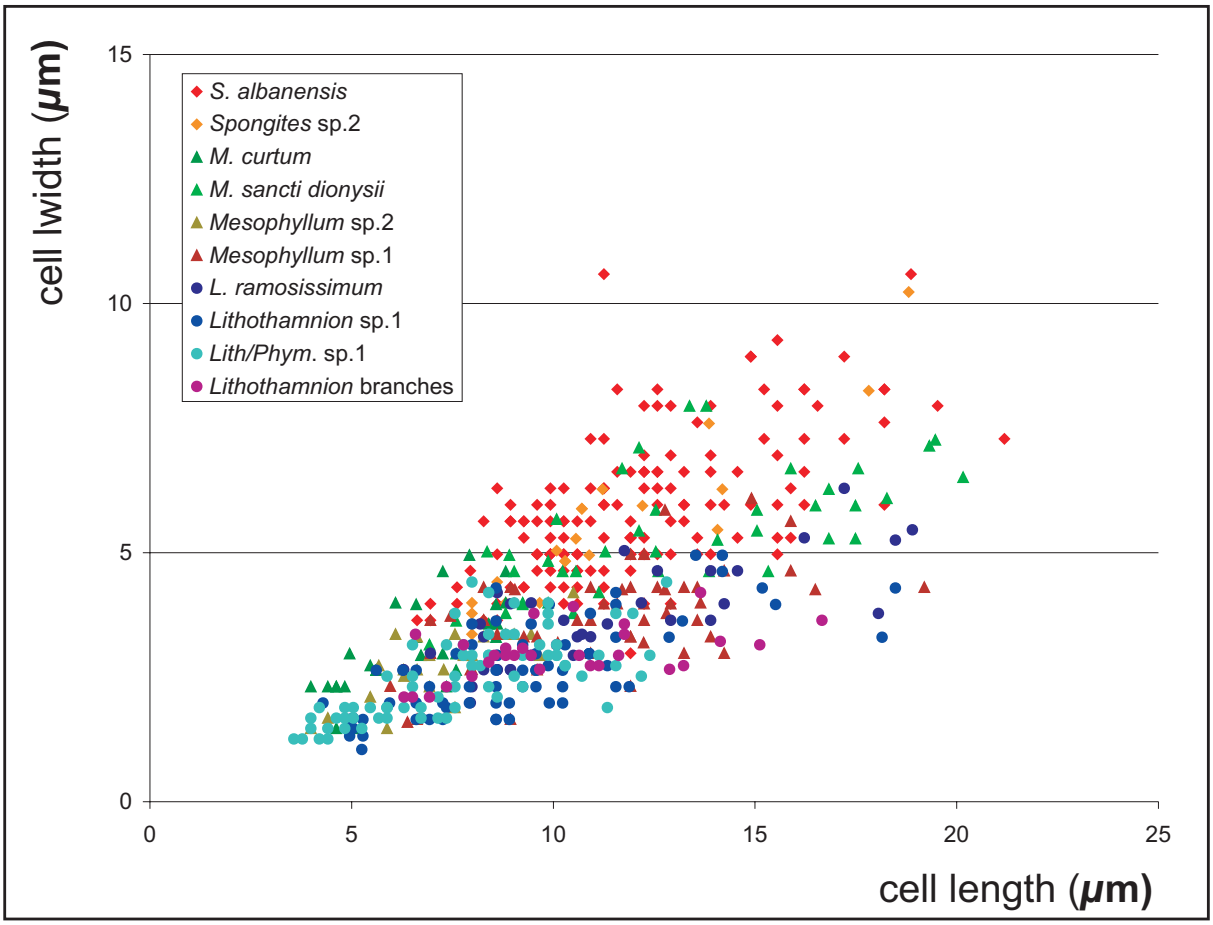

Fig. 3.3.9.: Cell height/width ratios of species of selected red algal genera from the WAT

The mean height/width ratio of *Spongites* is 2, while it is between 3 and 3,5 for *Lithothamnion*. Even plants that often form protuberances without conceptacles, which is typical in *Spongites albanensis* and *Lithothamnion* or *Phymatolithon spp.*, can be identified based on these characteristics. Mean length/width ratio of *Mesophyllum* and *Sporolithon*, however, is very similar to *Spongites.* Identification based solely on cell size characters is therefore not possible.

Results of semiquantitative analysis have been verified in the field to reflect relative abundances of coralline red algal genera in the sampled bed.

Distribution

In five sections (MO1, MS, VO, KL, Ma2), the distribution of coralline red algae in LFA2 was investigated in detail. In all sections, conspicuous patterns occur in the distribution of

corallines (Fig. 3.3.10.): Melobesioid red algae dominate in the lower part of sections MO1, MS, VO and KL in the RFR1 facies, in the PS facies and in the MRB (RFR2 facies). An exception to this is the base of section MO1, where in rhodolith rudstone, which shows evidence of elevated hydraulic energy (chapter 2.4.), *Spongites* and *Lithophyllum* are dominant. This is also the case in parts of the RP facies. The mastoporoid genus *Spongites* becomes more abundant in the upper part of the massive rhodolith bed (MRB, RFR2 facies) and is dominant in parts of the RFR3 facies while in other parts, melobesioid forms remain dominant. Among melobesioid genera, *Mesophyllum* becomes more abundant in the part of sections (LFA2c), where coral framestone and single colonies of zooxanthellate corals are abundant: In that interval both, *Mesophyllum* and *Spongites* are common. The abundance of *Lithophyllum* is generally low and it rarely occurs together with corals. It is also mostly absent in the upper 20m-30m of all sections except section MS1. The most abundant species of *Lithophyllum* is *L. incrustans* (Fig. 3.3.11.). *Titanoderma pustulatum* generally is a minor but common constituent in all sections. It is however uncommon in sediments with high siliciclastic contents, especially in the PS facies. There, it does not occur together with *Ammonia* (Fig. 3.2.4.). *Sporolithon* is very uncommon and occurrences are mostly near the top of sections. In all sections, *Spongites albanensis* is the dominant species of *Spongites*. *Spongites* is most common is section KL. The number of species is highest among melobesioid taxa and their relative abundance varies considerably from section to section: In reefs, *Mesophyllum sancti dionysii* is especially abundant and is often found to encrust corals (Fig. 3.3.6.f). *Mesophyllum* sp.2 is abundant only in the uppermost occurrence of the RFR3 facies in section MS, in the first 20m of section Vathi where the RFR3 facies occurs and in the upper part of section Ma2. In section MO1, *Mesophyllum* sp.1 is also common in the lower part of the section and the MRB and equally abundant as *Lithothamnion* and *Phymatolithon*. It is dominant between 35m and 50m of section KL (RFR3 facies) and in the RT facies at the top of section MO1. Many species of *Mesophyllum* found in the WAT lack characteristics to define a species or occur only very locally (see the taxonomy section of chapter 3.3.). *Lithothamnion* and species that belong either to *Lithothamnion* or *Phymatolithon* are most common in the lower part of sections: *Lithothamnion ramosissimum*

Fig. 3.3.10. a-d (next two pages): Relative abundance of non-geniculate coralline red algal genera in volume percent of skeletal component total; a) section Matala East (MO1), b) section Matala South (MS1), c) section Vathi (VO) and d) section Mount Rhodonas (KL). Background colouring is as in Fig. 2.2.3. – 2.2.6. (LFA2a: green, LFA2b: light blue, LFA2c: dark blue

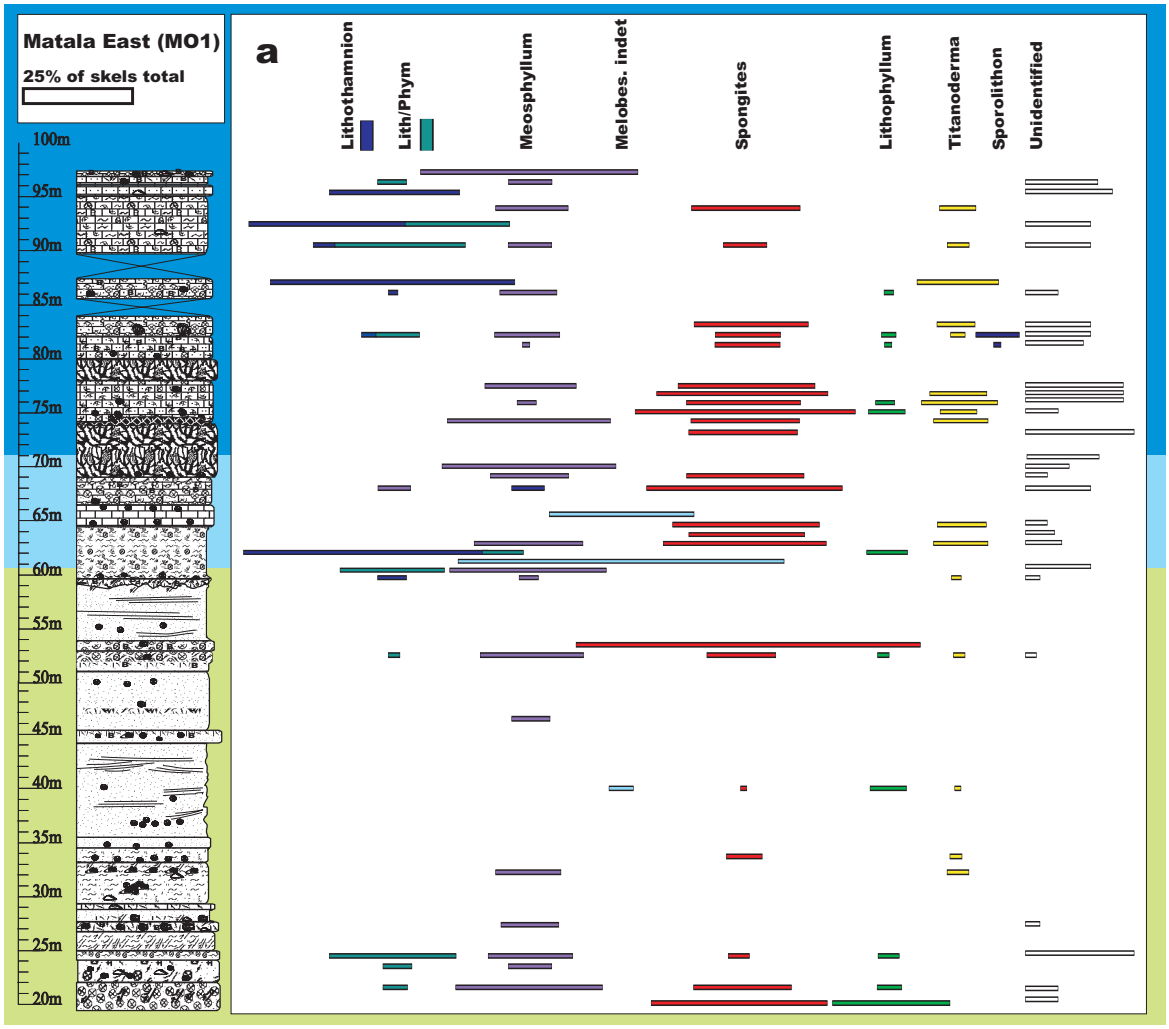
Matala East (MO1)
25% of skels total
a
Lithothamnion
Lith/Phym
Meosphyllum
Melobes. indet
Spongites
Lithophyllum
Titanoderma
Sporolithon
Unidentified
100m
95m
90m
85m
80m
75m
70m
65m
60m
55m
50m
45m
40m
35m
30m
25m
20m

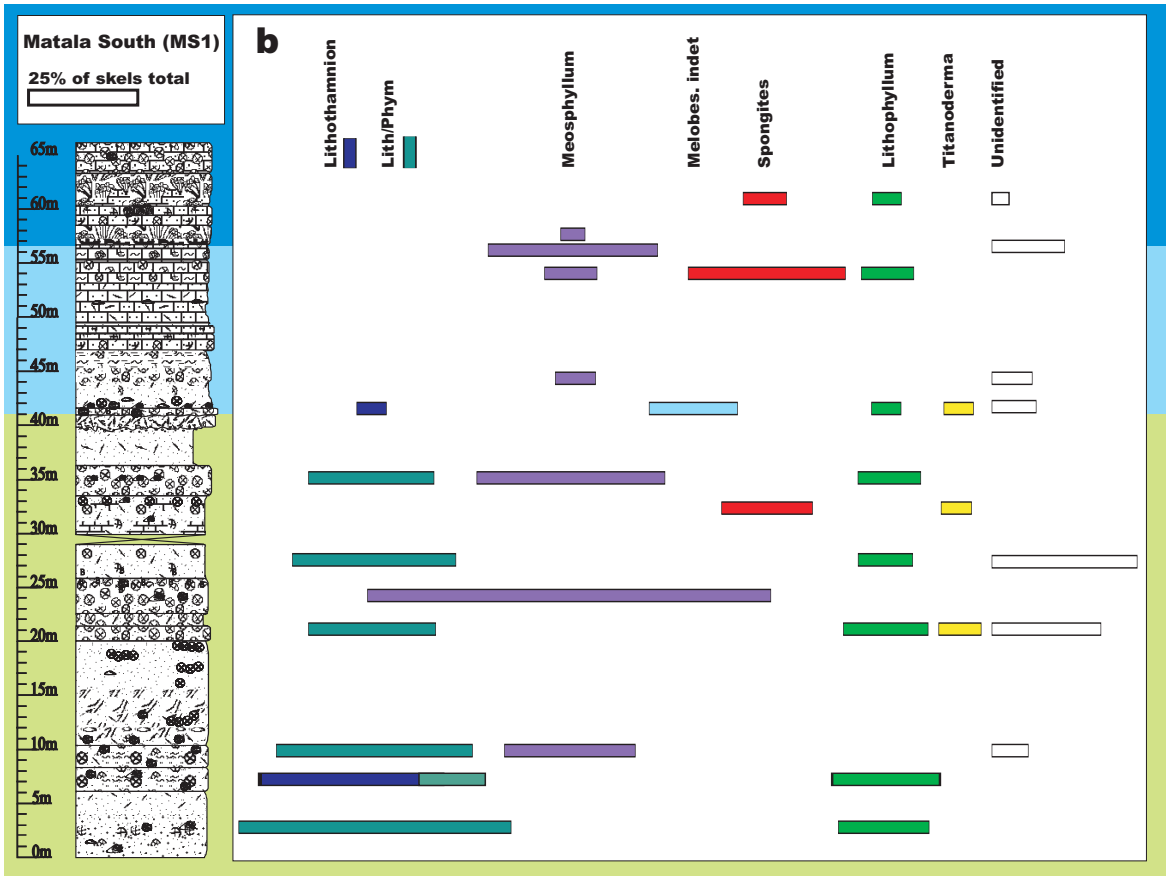
Matala South (MS1)
25% of skels total
b
Lithothamnion
Lith/Phym
Meosphyllum
Melobes. indet
Spongites
Lithophyllum
Titanoderma
Unidentified
65m
60m
55m
50m
45m
40m
35m
30m
25m
20m
15m
10m
5m
0m


Vathi (VO)
25% of skels total
c
Lithothamnion
Lith/Phym
Meosphyllum
Melobes. indet
Spongites
Lithophyllum
Titanoderma
Sporolithon
Unidentified
70m
65m
60m
55m
50m
45m
40m
35m
30m
25m
20m
15m
10m
5m
0m

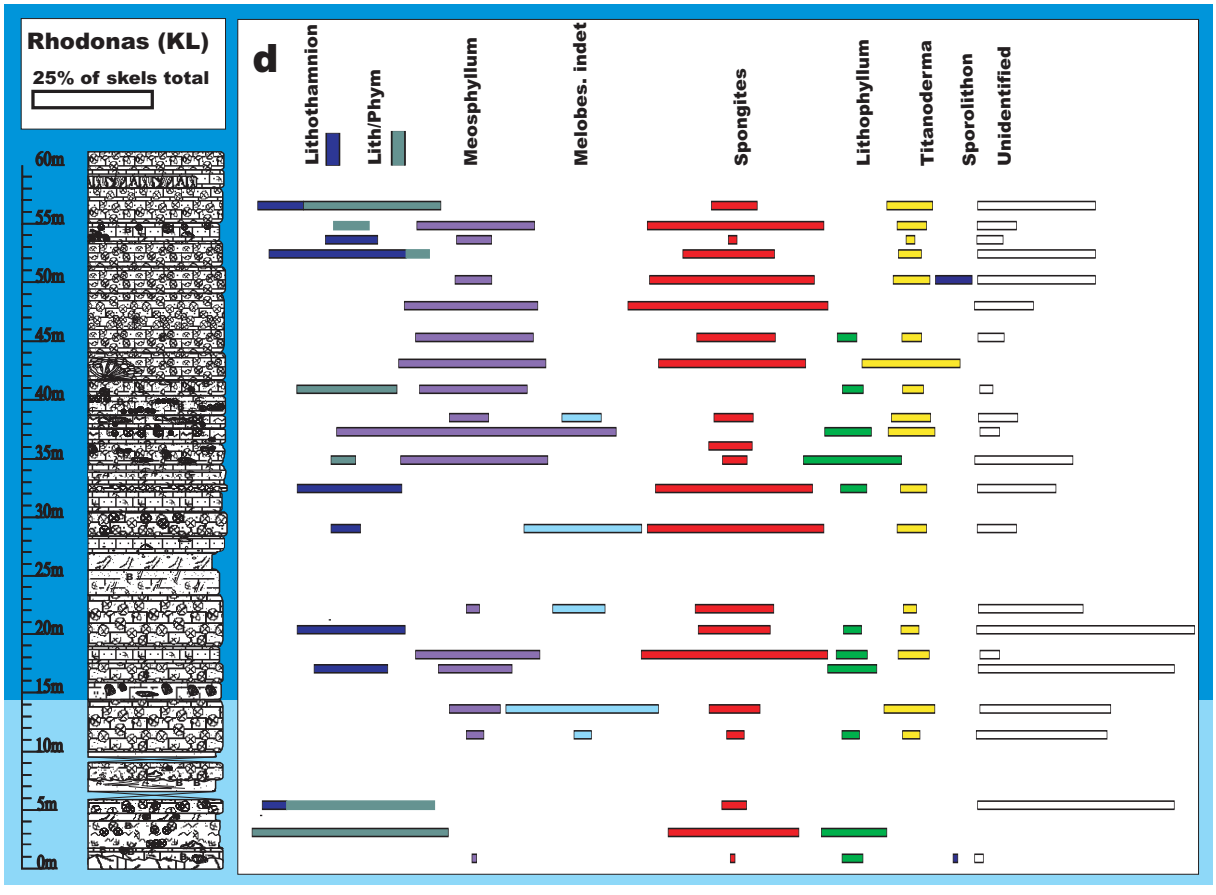
Rhodonas (KL)
25% of skels total
d
Lithothamnion
Lith/Phym
Meosphyllum
Melobes. indet
Spongites
Lithophyllum
Titanoderma
Sporolithon
Unidentified
60m
55m
50m
45m
40m
35m
30m
25m
20m
15m
10m
5m
0m

is especially abundant in the 15m thick MRB at section Vathi and in the RFR1 facies but also occurs in RFR3, for example in section KL (Fig. 3.3.11.). *Lithothamnion/Phymatolithon* sp.1 is especially abundant in RFR3 while *Lithothamnion* sp.1 occurs only in the upper 20m of section MO1 in the RFR facies. It disappears, however at the top of the section.
In samples of the RP facies, a high number of different species is recorded. While in the lower RP horizons, mostly *Spongites* and to a lesser degree *Lithophyllum* are dominant, in the uppermost RP horizon, where red algae occur only in samples from the top of the horizon *Lithothamnion/Phymatolithon* and *Mesophyllum* are more common. In a sample from the uppermost RP horizon at section MO2, however, *Spongites* sp.1 dominates with additional *Lithophyllum nitorum, Mesophyllum* sp. and *Titanoderma pustulatum* (Fig. 3.3.11.).

Paleoecological implications

The depth dependency of coralline red algae has been demonstrated earlier by Littler (1973a), Littler (1973b), van den Hoek et al. (1975) and Adey et al. (1982) and has been interpreted to be mainly a consequence of their sensitivity to light intensity (Adey et al., 1982; Minnery, 1990). After an extensive revision of the taxonomy of non-geniculate coralline red algae by Woelkerling (1988) and many others, earlier work has to be treated with caution. In a recent study in eastern Australia, however, Lund et al. (2000) have corroborated the depth dependency of the distribution of several red algal genera. Braga and Aguirre (2001) studied coralline red algal assemblages in Upper Neogene carbonates in southern Spain. They found that the distribution of red algal subfamilies is distinct in deep and shallow water environments but also differs in temperate carbonate units from those in tropical units.
The above described patterns, which are apparent in Fig. 3.3.10. can be interpreted according to published data: As in the Miocene of southern Spain (Braga and Aguirre, 2001), *Lithophyllum* occurs mainly in temperate environments that are defined by the absence of tropical foraminifera and zooxanthellate coral reefs (Betzler et al., 1997). It is also the most common genus in modern temperate shallow water environments in the northern and western Mediterranean (Adey, 1986), southern Australia (James, 1992) and the Gulf of California (Rosmena-Rodriguez et al., 1999). Mastoporoids such as *Spongites* are commonly found in shallow tropical environments (Adey et al., 1982; Bosence, 1985; Braga and Aguirre, 2001). This corresponds to the abundance of *Spongites* in intervals with zooxanthellate corals and in the BP facies that is interpreted to be associated with coral growth and the rarity of

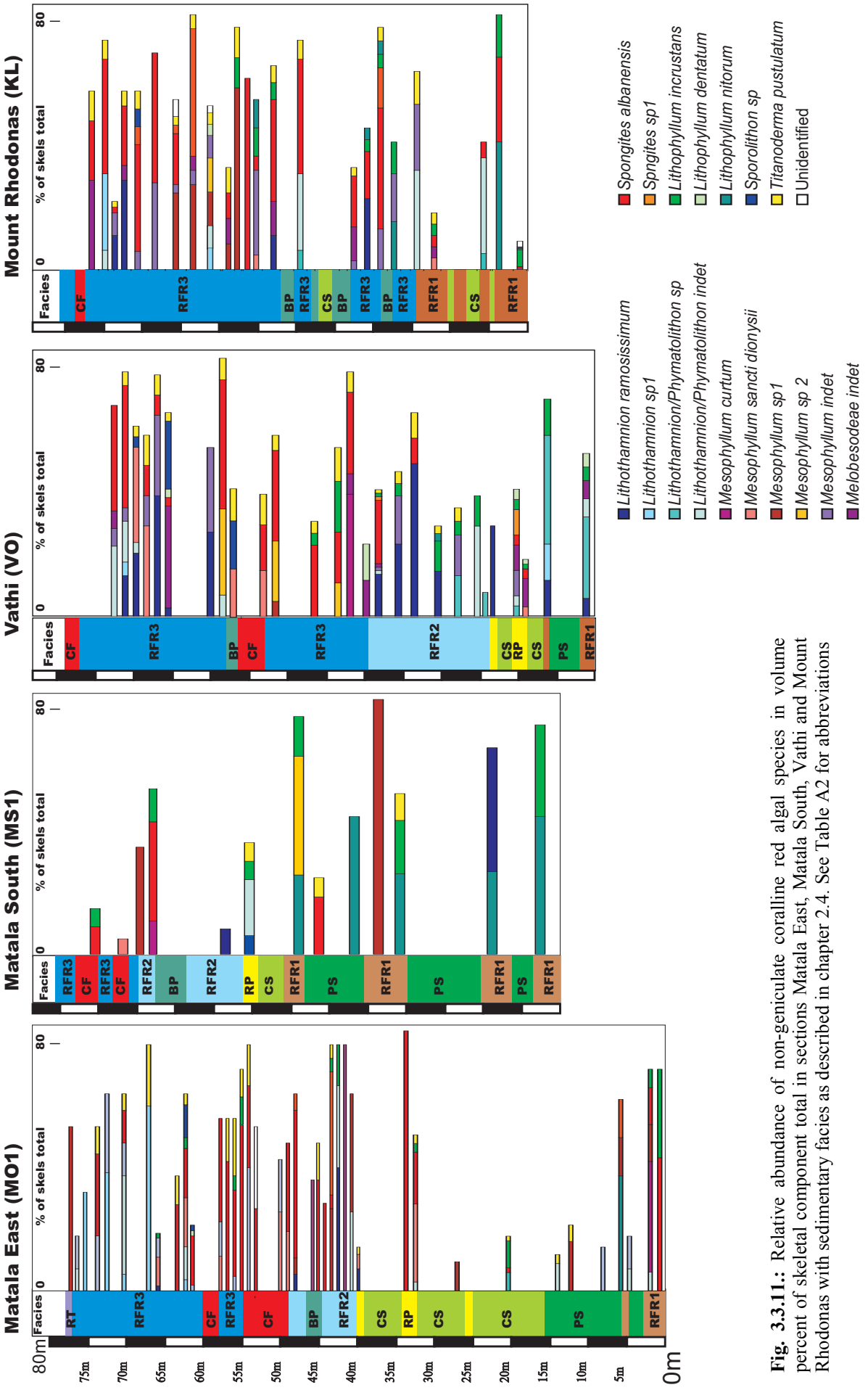

Fig. 3.3.11.: Relative abundance of non-geniculate coralline red algal species in volume percent of skeletal component total in sections Matala East, Matala South, Vathi and Mount Rhodonas with sedimentary facies as described in chapter 2.4. See Table A2 for abbreviations

Lithophyllum in these intervals. Along with the Sporolithaceae, the melobesioids are described to be the deepest taxa in recent and fossil environments (Adey et al., 1982; Lund et al., 2000; Braga and Aguirre, 2001). This is in accordance with the dominance of melobesioid taxa in the RFR facies that is interpreted to represent low to moderate energy mid- to outer ramp deposits. The dominance of melobesioids is most evident in the widespread MRB that reflects low energy conditions and therefore an increase in water depth after deposition of the RP facies (see chapter 2.4.). Similarly, melobesioid genera dominate in the uppermost 25m of sections MO1 and Ma2 where overall deepening is indicated by increasingly marly lithologies and abundant planctonic foraminifera. Of the melobesioids, *Phymatolithon* (Adey et al., 1982; Irvine and Chamberlain, 1994) and *Lithothamnion* (Freiwald and Henrich, 1994; Henrich et al., 1995) are commonly associated with arctic to warm temperate environments. This is in accordance to the abundance of *Lithothamnion/Phymatolithon* in the lower part of sections (RFR1 and 2 and PS facies) where neither corals nor foraminifera with especially low tolerances for lower temperatures occur. *Mesophyllum* on the other hand rarely occurs in cold environments. In the British Islands, for example, the occurrence of *Mesophyllum* is reduced to one species, *Mesophyllum lichenoides* (Irvine and Chamberlain, 1994) that is not identified in the material from Crete. The preferred occurrence of *Mesophyllum* together with other melobesioids in marly deeper water sediments at one hand and on corals at the other indicates that *Mesophyllum* occurs in relatively warm water as well as in relatively deep environments.

The heterogeneous red algal composition in the RP facies indicates reworking and redeposition of red algal components and reflects the amalgamated nature of the deposit. The dominance of melobesioids at the top of the uppermost condensed horizon indicates that the top represents a lag: Condensation at the top occurred in consequence of sediment starvation through transgression and not in consequence of storm events that influenced the largest part of the RP facies. A larger proportion of shallow water corallines in the same horizon in section M02 than in MO1 indicates shallowing to the east that is in accordance with an eastward increase in pebble size.

Specific preferences of coralline red algal taxa

While red algal genera and subfamilies in the WAT have general preferences, especially in terms of water temperature and water depth that connect them to a group of facies types and

stratigraphic intervals, species appear to have very individual requirements that in many cases appear to restrict them to a certain facies type in certain sedimentary sections (Fig. 3.3.11.). At present level of knowledge, the nature of many of these ecological constraints remains unresolved. However, in some cases, relationships to other environmental parameters can be established: The best example is *Titanoderma pustulatum.* It occurs in almost all samples with coralline red algae from LFA2b and c where oligotrophic conditions are indicated by the dominance of foraminifera with symbionts. It is, however very rare in samples from LFA2a where an increased siliciclastic input is observed. Moreover, it does rarely occur in samples where increased nutrient input is indicated by elevated contents of *Ammonia* with inflated chambers and rarely together with high numbers of planktonic foraminifera. *Titanoderma pustulatum* therefore may be an indicator of oligotrophic environments. *Mesophyllum sancti dionysii* preferentially occurs associated with coral framestone but also in the RFR3 facies. The association with corals corroborates the preference of the genus *Mesophyllum* for warm water. Since coral framestone in the WAT is interpreted to represent water depth shallower than 15-20m, this is in apparent contradiction to the general preference of low light intensities but can be explained by the abundance of shaded space in the framework. Preferences and limitations of other species are not established as easily: For, example, the abundance of *Lithothamnion/Phymatolithon* sp.1 in LFA2a may be related to generally elevated nutrient levels that comes with increased siliciclastic input. This species may, however, also have a tolerance for the lowest temperatures since it rarely occurs together with *Spongites* or *Mesophyllum* or it may tolerate siliciclastic rich environments of RFR1 more than other taxa. Ultimately, it can not be excluded that its abundance in section MS is a consequence of biogeographic patterns and ecological interactions that are not apparent from the fossil material.

Water depth and water temperature indices

While the distribution of the various species, especially among the Melobesioideae, appear to have specific ecological requirements, coralline red algae are shown to have certain limitations in terms of water depth and temperature that are more or less similar for all species of one genus or subfamily. In order to obtain standardized values between 0 and 1, a temperature index with *Spongites* and *Mesophyllum* as warm water taxa and *Lithophyllum* and *Lithothamnion* + *Phymatolithon* as cool water taxa is calculated:

$$T = \frac{a + d}{a + b + d + g}$$

Accordingly, a water depth index is calculated with the melobesioids and *Sporolithon* as deep water taxa and the mastoporoids and *Lithophyllum* as shallow water taxa:

$$D = \frac{a + b + c + f}{a + b + c + d + e + f}$$

In both equations ***a*** is the percentage of *Mesophyllum* of total red algal content in each sample, ***b*** of *Lithothamnion* + *Phymatolithon,* ***c*** of Melobesioideae indet., ***d*** of *Spongites*, ***e*** of *Lithophyllum* and ***f*** of *Sporolithon.*

Lithothamnion and *Phymatolithon* are treated together since no differences in preferences regarding water temperature and water depth are known or apparent from the material of Crete. *Titanoderma* is excluded because it shows no preferences in terms of water depth and water temperature and *Sporolithon* is excluded in the temperature index since its preferences in terms of water temperature are not known.

The resulting indices correlate well with data from foraminifera and with the distribution of zooxanthellate corals (Fig. 3.3.12.): Warm shallow water is indicated in the part of section MO1 where reef carpets and tropical foraminifera occur. At the top of the upper reef unit, increasing water depth indices indicate deepening (Fig. 3.3.12.a). The distribution of zooxanthellate corals and tropical foraminifera can also be linked with temperature indices in all other examined sections. In these sections, where reef carpets are absent or not as well developed as in the Matala area, water depth indices, are higher than in section MO1. Intervals with dominant *Heterostegina* that occurs together with planctonic foraminifera and that have been interpreted to represent outer ramp deposits show high water depth indices. The base of LFA2b (MRB) where deepening is reflected by the change in lithology from mid-

Fig. 3.3.12. a-d (next four pages): Water temperature and water depth indices for a) section Matala East (MO1), b) section Matala South (MS1), c) section Vathi (VO) and d) section Mount Rhodonas (KL) compared with the occurrence of zooxanthellate corals and the tropical foraminifer *Borelis* or the distribution of foraminiferal genera, respectively

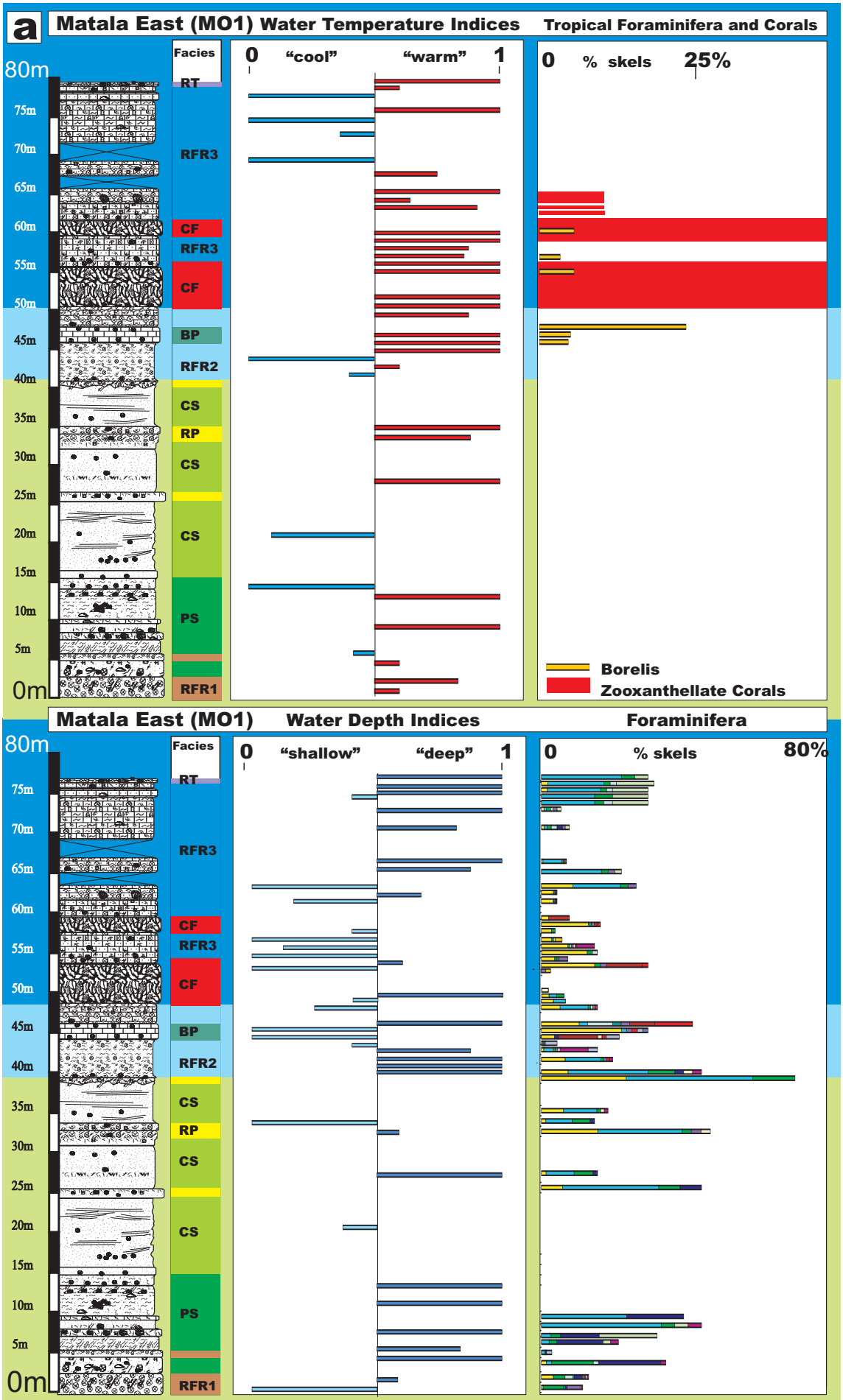
a
Matala East (MO1) Water Temperature Indices
Tropical Foraminifera and Corals
Facies
0 "cool" "warm" 1
0 % skels 25%
80m
75m
70m
65m
60m
55m
50m
45m
40m
35m
30m
25m
20m
15m
10m
5m
0m
RT
RFR3
CF
RFR3
CF
BP
RFR2
CS
RP
CS
CS
PS
RFR1
Borelis
Zooxanthellate Corals
Matala East (MO1)
Water Depth Indices
Foraminifera
Facies
0 "shallow" "deep" 1
0 % skels 80%
80m
75m
70m
65m
60m
55m
50m
45m
40m
35m
30m
25m
20m
15m
10m
5m
0m
RT
RFR3
CF
RFR3
CF
BP
RFR2
CS
RP
CS
CS
PS
RFR1

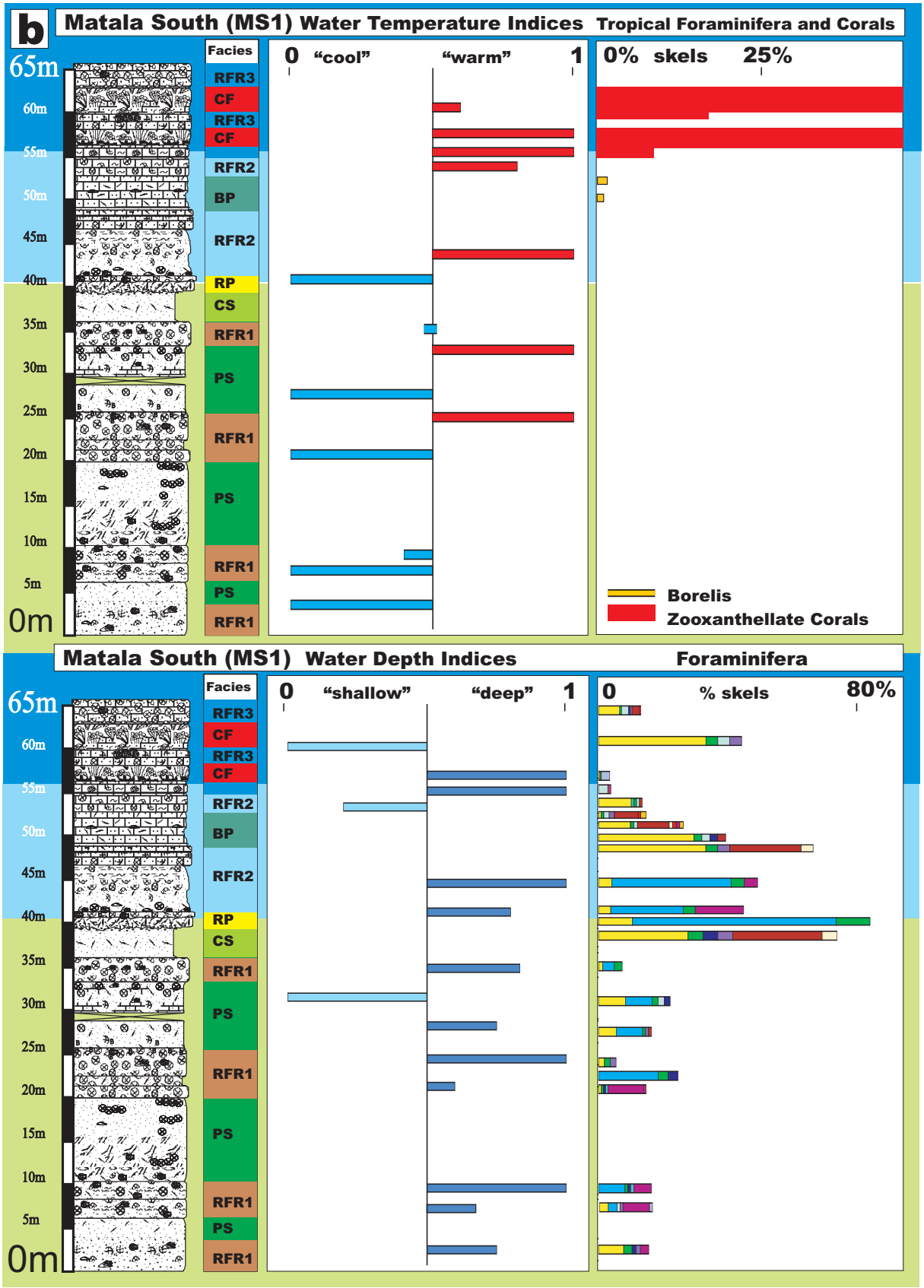
b
Matala South (MS1) Water Temperature Indices
Tropical Foraminifera and Corals
Facies
0 "cool" "warm" 1
0% skels 25%
65m
60m
55m
50m
45m
40m
35m
30m
25m
20m
15m
10m
5m
0m
RFR3
CF
RFR3
CF
RFR2
BP
RFR2
RP
CS
RFR1
PS
RFR1
PS
RFR1
Borelis
Zooxanthellate Corals
Matala South (MS1) Water Depth Indices
Foraminifera
Facies
0 "shallow" "deep" 1
0 % skels 80%
65m
60m
55m
50m
45m
40m
35m
30m
25m
20m
15m
10m
5m
0m
RFR3
CF
RFR3
CF
RFR2
BP
RFR2
RP
CS
RFR1
PS
RFR1
PS
RFR1

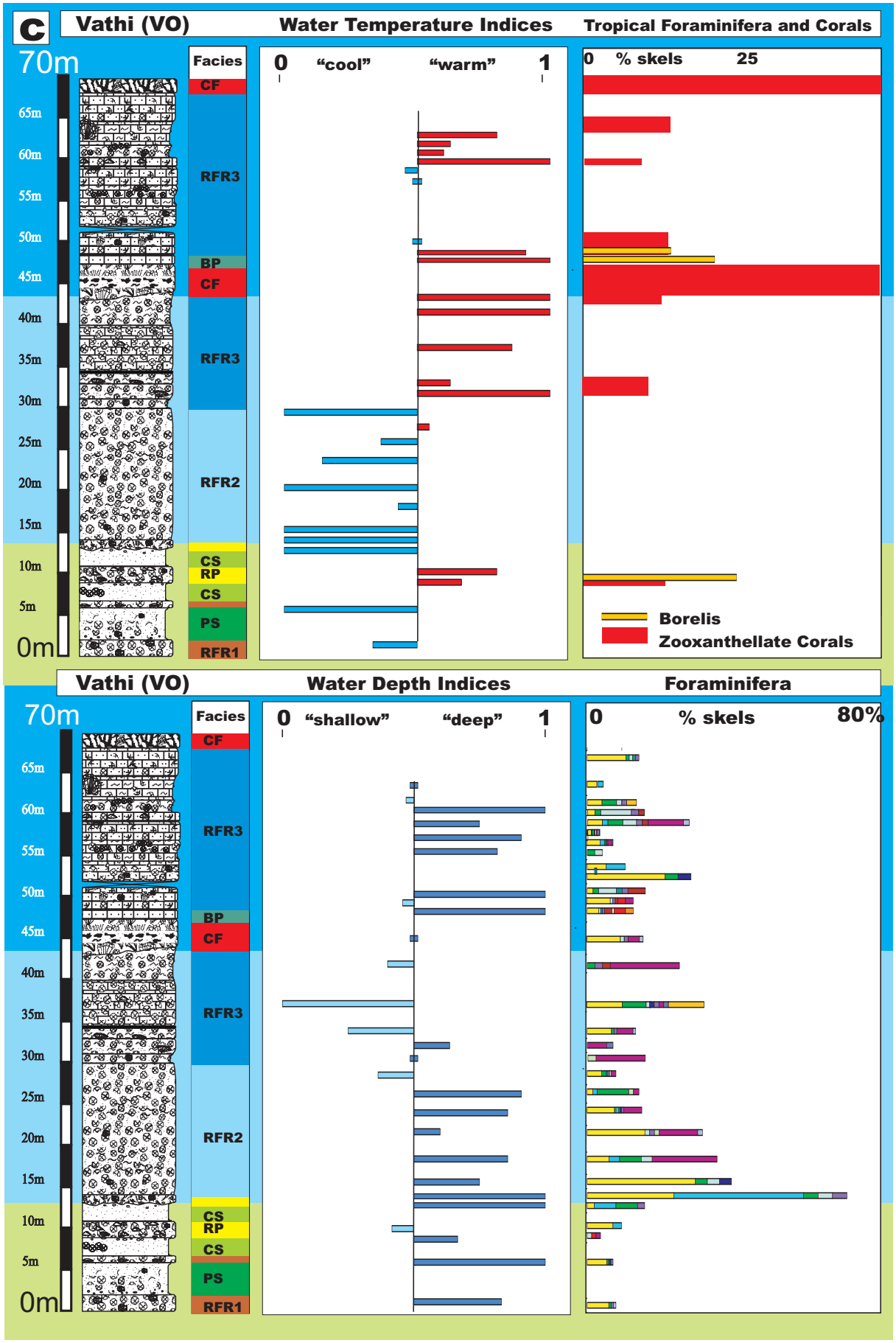
C
Vathi (VO)
Water Temperature Indices
Tropical Foraminifera and Corals
70m
65m
60m
55m
50m
45m
40m
35m
30m
25m
20m
15m
10m
5m
0m
Facies
CF
RFR3
BP
CF
RFR3
RFR2
CS
RP
CS
PS
RFR1
0 "cool" "warm" 1
0 % skels 25
Borelis
Zooxanthellate Corals
Vathi (VO)
Water Depth Indices
Foraminifera
0 "shallow" "deep" 1
0 % skels 80%

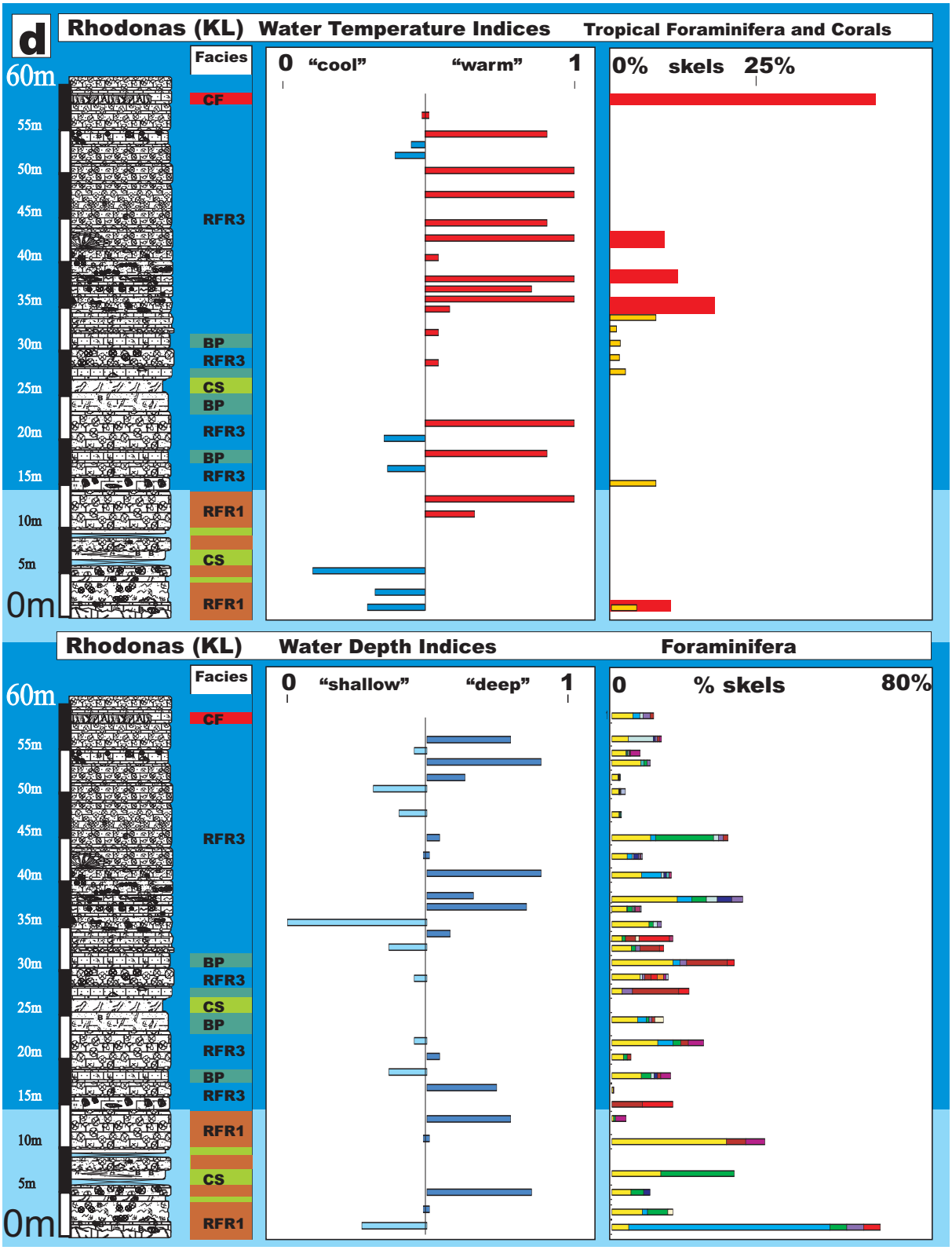
d
Rhodonas (KL) Water Temperature Indices
Tropical Foraminifera and Corals
Facies
0 "cool" "warm" 1
0% skels 25%
60m
55m
50m
45m
40m
35m
30m
25m
20m
15m
10m
5m
0m
CF
RFR3
BP
RFR3
CS
BP
RFR3
BP
RFR3
RFR1
CS
RFR1
Rhodonas (KL) Water Depth Indices
Foraminifera
Facies
0 "shallow" "deep" 1
0 % skels 80%
60m
55m
50m
45m
40m
35m
30m
25m
20m
15m
10m
5m
0m
CF
RFR3
BP
RFR3
CS
BP
RFR3
BP
RFR3
RFR1
CS
RFR1

ramp RP facies to outer ramp RFR2 facies is also generally characterized by maximum water depth index values. Few data are present for the BP facies but they largely result in low water depth indices that are in accordance with the mid- to inner ramp setting of this facies. The picture is more complex in the RP facies since red algal proportions reflect both, shallow conditions and reworking in the lower RP horizons and increasing water depth and formation of a lag deposit at the top of the uppermost condensed horizon.

Relationships between water depth- and temperature indices

In a water body, where water temperature continuously decreases with increasing water depth, organisms limited only by temperature would adjust by moving to a position in the water column where they find optimal conditions. This means, an organism that prefers cool water temperatures will be found in shallow water under cool climatic conditions and in deep water in warm climatic conditions. If the distribution of these organisms in different environments would be analysed with respect to water temperature and water depth and the values plotted against each other, a linear relationship would result. A similar relationship in non-geniculate coralline red algae is indicated by the observation that in recent environments of Brittany, Great Britain and Norway, *Phymatolithon* and *Lithothamnion* are found mostly in water depths shallower than 20m (Irvine and Chamberlain, 1994; Henrich et al., 1995), while in lower latitudes, both genera are found in relatively deep water (Adey et al., 1982; Lund et al., 2000). However, if water depth and water temperature indices based on non-geniculate coralline red algae are plotted against each other, no linear relationship emerges (Fig. 3.3.13.).

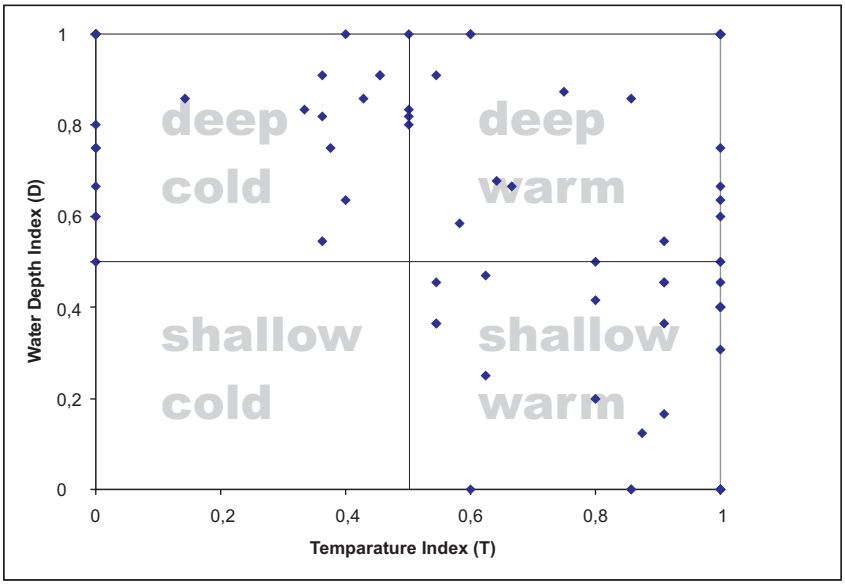

Fig. 3.3.13.: Non-linear relationship between water depth and water temperature indices of sampled sections

A non-linear relationship indicates that coralline red algae are limited by both, water temperature and water depth. This assumption is supported by the observations of Figueiredo et al. (1992) who report that specimens of *Phymatolithon* depend on shading by soft algae to survive in shallow water. Similarly, Adey et al. (1982) describe the occurrence of deep water taxa in shaded settings. These observations suggest that deep water taxa are normally not able to survive in shallow water due to their low light tolerance. Accordingly, in the material from the WAT it is not observed that *Mesophyllum,* which is interpreted to occur in deep water in areas with high surface temperatures occurs together with *Lithophyllum* in shallow cold environments. This is only the case in the red algal bindstone facies, where *Mesophyllum sancti dionysii* occurs together with *Lithophyllum incrustans. Mesophyllum sancti dionysii* is also common in coral frameworks. Thus, all shallow occurrences of *Mesophyllum* are related to frameworks with abundant shaded space. In consequence of the temperature dependency of the composition of coralline red algal associations and the different limitation in terms of light intensity of most red algal taxa, red algal associations found in warm temperate and tropical environments on Crete are subdivided into four groups (Fig. 3.3.14.): The red algal

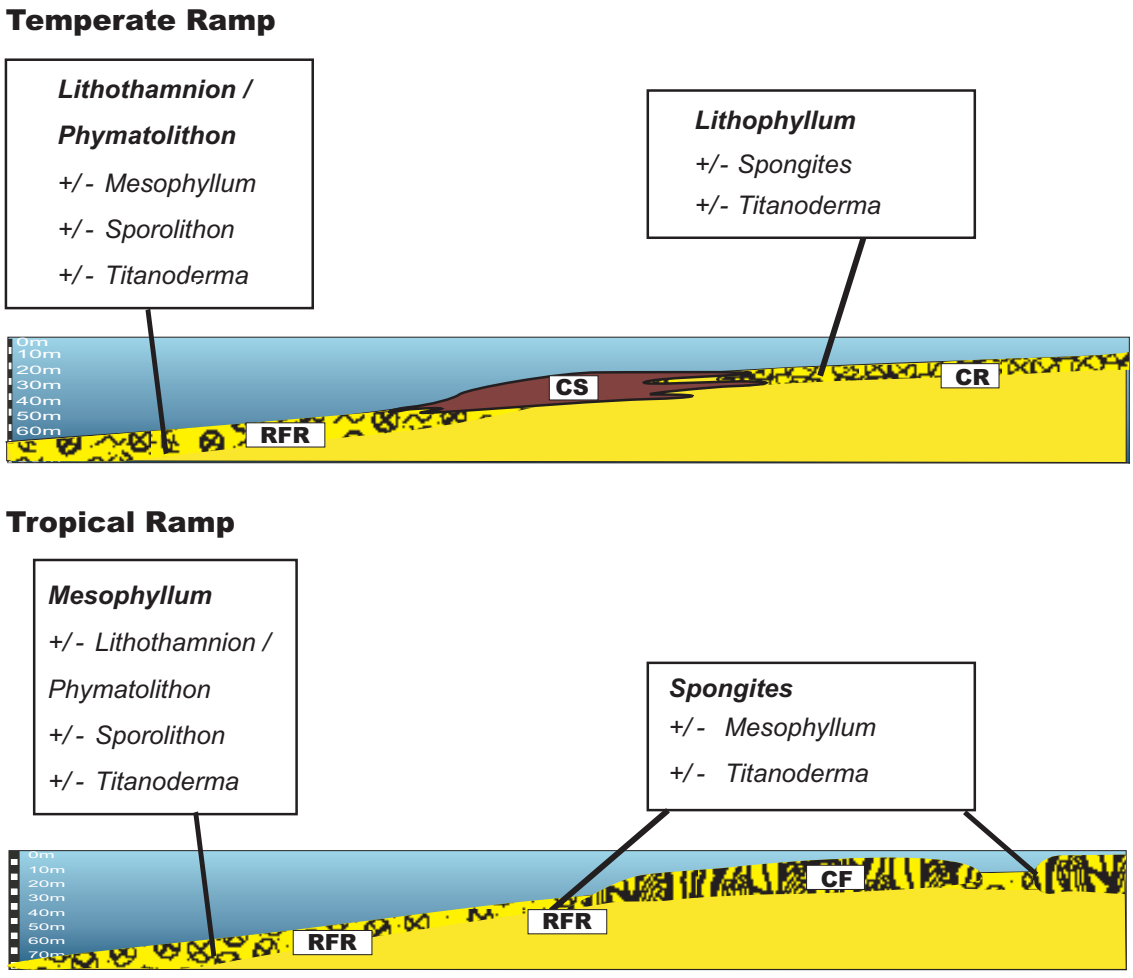

Fig. 3.3.14.: Schematic ramp profiles with coralline red algal associations typical for temperate and tropical environments as found in the analysed material from the WAT

association in shallow temperate water is replaced by a shallow tropical association in the course of climatic warming. The shallow temperate association, however, is not found in tropical deep water but the deep temperate association is replaced by an entirely different association during climatic warming. These associations can be identified in fossil material and used for plaeoclimatic reconstruction under the assumption that shading did not play an important role. Since except in the genus *Titanoderma* no dependency on other ecological parameters has been found on genus level, the application of red algal indices in paleoclimatology is expected to be possible without any further environmental information.

4. Eustasy and seawater Sr composition: application to high-resolution Sr isotope stratigraphy of Miocene shallow water carbonates

Introduction

Sr isotope stratigraphy has been established as a useful tool for chronostratigraphic correlation of marine sediments (Burke et al., 1982; Denison et al., 1993; Hodell et al., 1991; Hodell and Woodruff, 1994; Oslick, et al. 1994; Farell et al., 1995; Martin et al., 1999; Sprovieri et al., 2003). During the Neogene this method is especially effective as seawater $^{87}Sr/^{86}Sr$ isotope ratios generally increase through time. The increase, however, is not steady but periods of zero slope of an average change in Sr isotope ratios through time occur, for example in the late Miocene and Pliocene (Hodell et al., 1989). Short-term (0.2-0.5 m.y.) negative or positive $^{87}Sr/^{86}Sr$ trends deviating from the overall trend in global Sr isotope seawater evolution are common. Since some of the trends do not significantly exceed the analytical errors of Sr isotope analysis (2σ usually < $1\text{-}2x10^{-5}$), the common approach to calculate reference $^{87}Sr/^{86}Sr$ seawater curves is to smooth down short-term fluctuation by linear regression (Oslick et al., 1994), polynomial fit (Hodell and Woodruff, 1994; Martin et al., 1999) or LOWESS fit (Howarth and McArthur, 1997; McArthur et al., 2001). Errors in sedimentation ages derived from Sr isotope reference curves are > 0.5 m.y. in the early Miocene when Sr isotope ratios increased steeply and exceed 1 Ma in the late Miocene (Oslick et al., 1994).

When Sr isotope chronostratigraphy is applied in outcrop scale, ages for a certain interval that result from the comparison of measured Sr isotope ratios with published reference curves are in many cases higher than in underlying sediments (Mutti et al., 1997; Forst, 2003). Both, apparent age inversions >2 Ma and over all increasing upsection trends in age occur. An obvious interpretation is that age inversions related to condensed horizons or unconformities result from exhumation of old shell material (Mutti et al., 1997). Observed consistent decreasing upward trends in Sr isotope ratios that are not related to condensed intervals or unconformities, however, are not explained by this process. It is reasonable to assume, that instead of sedimentary processes, mechanisms inherent in the evolution of seawater Sr isotope ratios are responsible for apparent aging upward trends in sedimentary sections. Fluctuations in seawater Sr isotope ratios recorded in the Oligocene and Miocene have been interpreted to be related to glaciation (Oslick et al., 1994; Zachos et al., 1999). Consequently, fluctuations in Sr isotope ratios also link to eustatic change. Since Sr isotope ratios in the global oceanic reservoir at a given time are approximately constant (Capo and DePaolo, 1992), these

fluctuations occur contemporaneously at different sites on a global scale. Therefore, they are reproducible at different sedimentary sections of the same age interval.

In this study, a correlation of fluctuations in Sr isotope ratios is made to improve the chronostratigraphic resolution of Sr stratigraphy and to eliminate apparent age inversions. Sr isotope data sets were collected from several sections of predominantly shallow water deposits. The selected sections sample lower and middle Miocene sediments in southern Portugal (Algarve) and Upper Miocene sediments in Greece (central Crete). Several prerequisites were met to obtain a high-resolution dataset for confidential correlation of fluctuations in the $^{87}Sr/^{86}Sr$ record: 1) an original low magnesium calcite mineralogy of the analysed bivalve shells; 2) small sample intervals; 3) good lithological control on intra-basin correlation of sections; 4) information on relative water depth to link the $^{87}Sr/^{86}Sr$ record to eustasy and 5) high-resolution seawater $^{87}Sr/^{86}Sr$ reference datasets.

The study was carried out in two steps: The first step encompassed the correlation of measured sections independently from Sr isotope analysis by lithological marker horizons and the establishment of a sequence stratigraphic framework. During the second step, the results of Sr isotope measurements in the various sections were linked to a global Sr isotope reference curve and thus to absolute age. The correlation of measured Sr isotope values with the global reference curve is verified in two ways: 1) intervals of sections that are correlated by lithological markers should plot on the same intervals of the global reference curve, 2) samples that plot on minima of the global reference curve should be from beds that represent lowstand deposits since Sr isotope minima are assumed to be related to eustatic minima.

This approach provides not only high-resolution chronostratigraphic information, but is also a tool to compare sedimentological models with sequence stratigraphical information and thus to link sedimentology with climatological processes.

Sampled sections

Algarve, Portugal

Five sections up to 45 m thick were chosen for Sr isotope analysis (Algar Sêco Ost – ASO, Leixão do Ladrão – LDL, Marinha West – MW, Praia da Galé – PDG and Praia da São Rafael – PSR; Fig. 4.1.a; 4.2.) representing the Lagos Portimão Formation (Antunes et al., 1997; Antunes et al., 2000; Forst, 2003). The sediments consist of limestone rich in siliciclastics and

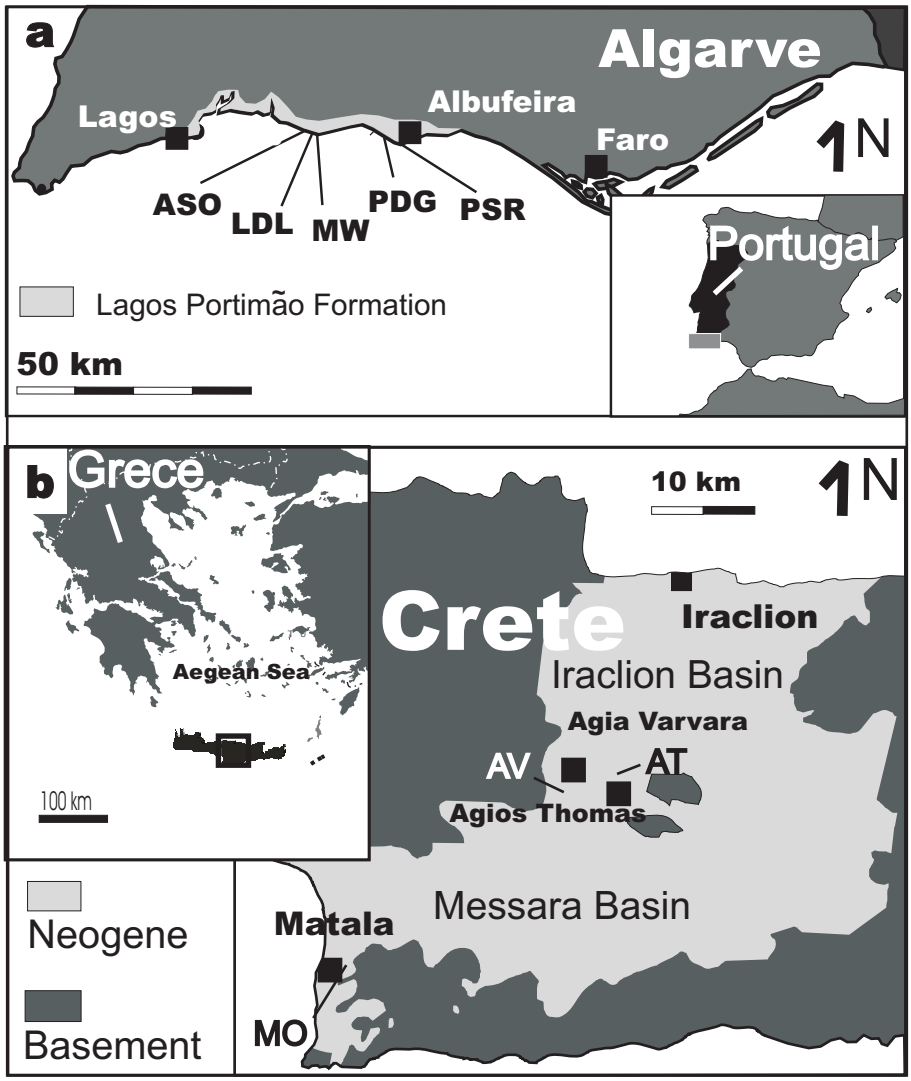

Fig. 4.1.: Map of a) southern Portugal and b) central Crete with locations of measured sections

intercalated sandstone of Burdigalian to Serravallian age derived from planktonic foraminifera and $^{87}Sr/^{86}Sr$ data (Antunes et al., 1997; Antunes et al., 2000). The Lagos Portimão Formation unconformably overlies limestone of Mesozoic age (Fig. 4.2.). The stratigraphically highest section (PDG, Fig. 4.2.) samples the base of the so called "laminated sands" unit that unconformably overlies limestone and sandstone of the Lagos Portimão Formation (Forst, 2003). This up to 20m thick unit is regarded to be of Serravallian age (Antunes et al., 1997; Antunes et al., 2000).

The stratigraphic correlation of the sampled sections relies on three lithological marker beds composed of sandstone with unique bryozoan faunas (Forst *et al*., 2000; Fig. 4.2.). The lowermost marker bed is characterized by mass occurrences of the bryozoa *Calpensia* and the second by mass occurrences of the large benthic foraminifer *Heterostegina* together with bryozoans. The uppermost marker bed is a horizon formed by two sandstone beds with a characteristic *Celleporaria palmata – Culizia parasitica* bryozoan-coral association

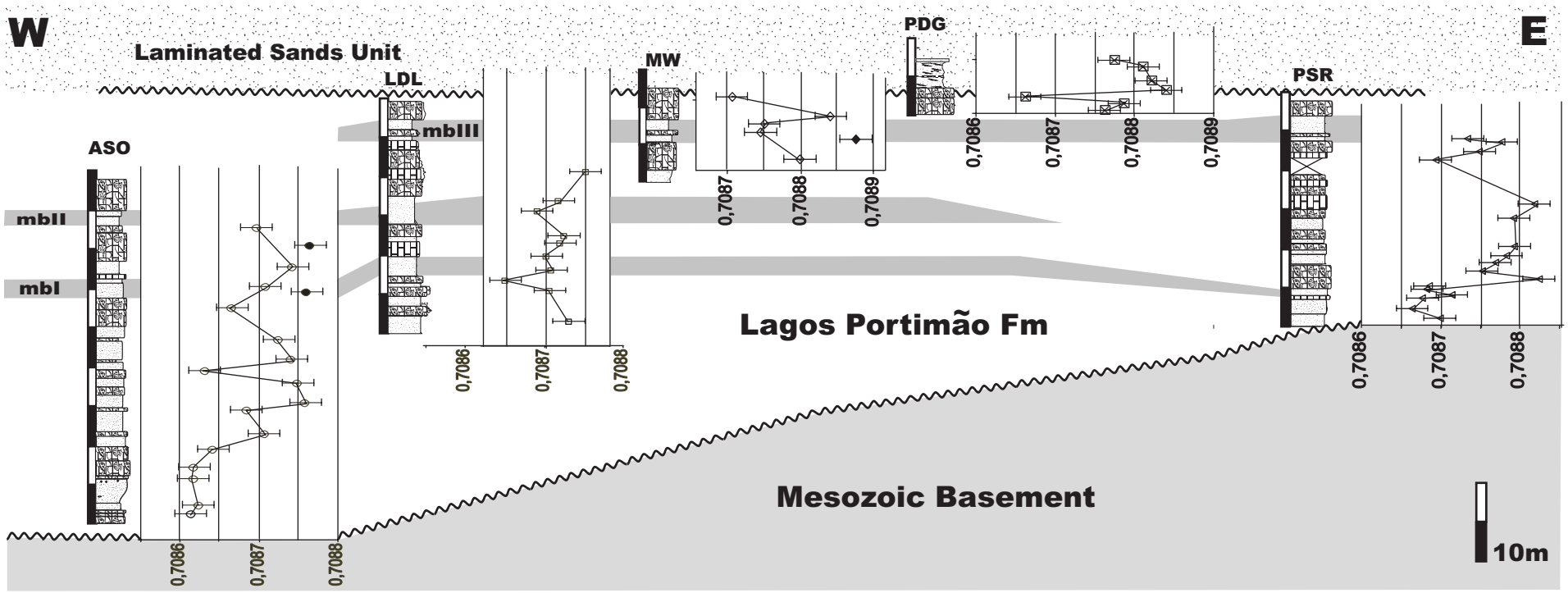

Fig. 4.2.: Measured sections along the Algarve Coast (southern Portugal) with Sr ratios. Marker beds I-III (mb I-III) were used to correlate sections. Open symbols represent Sr ratios of bivalve shells, black symbols represent whole rock samples. See Fig.4.1.a for locations and Fig. 4.3 for lithological signatures

subdivided by an intercalated limestone bed. Sediments of the Lagos Portimão Formation were deposited in a high energy shelf setting and are rich in bivalves, bryozoans, red algae and large benthic foraminifera (*Heterostegina*). During low sea-level, faunal elements were reworked to form shell beds whereas sandstone beds were deposited during high sea-level. This interpretation is in agreement with elevated bryozoan/bivalve ratios (bryozoan index of James *et al.*; 2001) in sandstone relative to condensed limestone beds (Brachert et al., 2003, Forst, 2003). The easternmost section (PSR) is condensed relative to the other sections due to the synsedimentary movements of the salt diapir of Albufeira (Forst, 2003; Fig. 4.1., 2).

Central Crete, Greece

Sediments of the 25-100m thick sampled sections (Matala Ost – MO, Agia Varvara – AV, Agios Thomas – AT; Fig. 4.1.b; 4.3) grade upsection from fluviatile sediments (base of MO section) into shallow marine sandstone and limestone and are overlain by marine marls and calciturbidites in the AV section. The AV section overlies 60 m of marine sandstone and

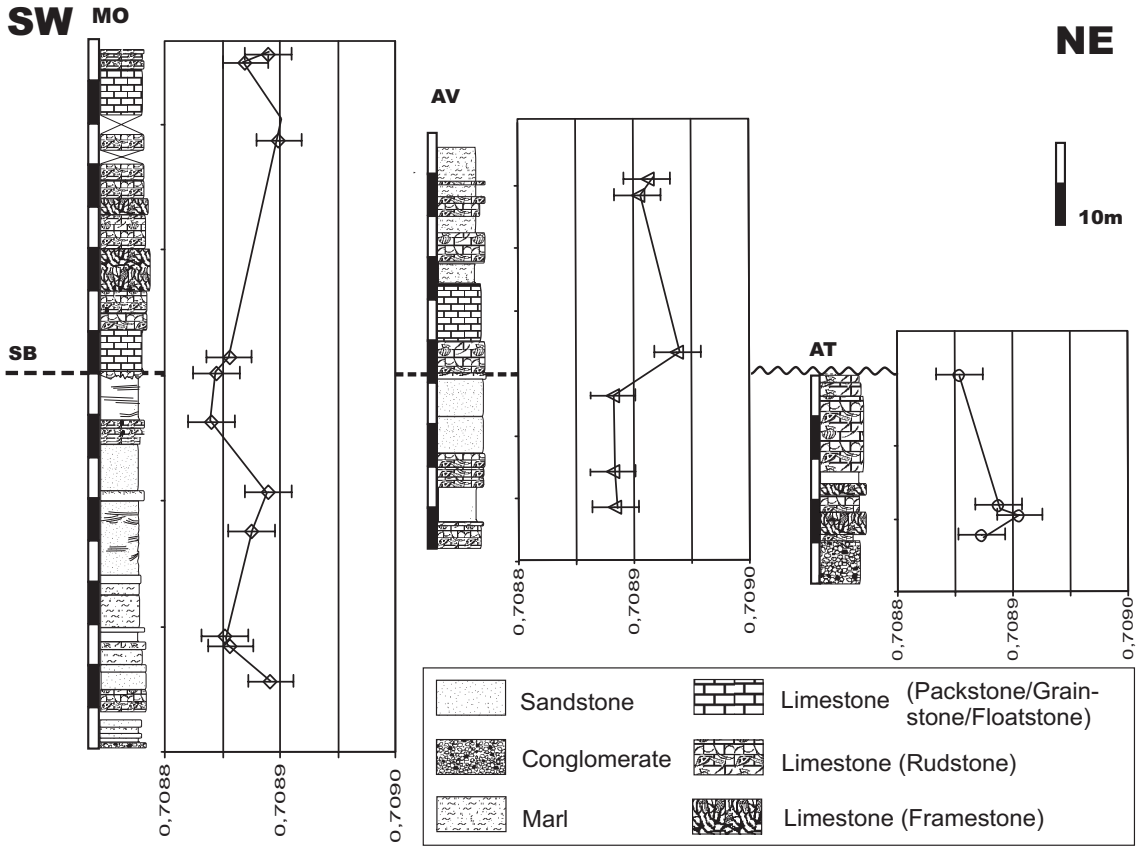

Fig. 4.3.: Measured sections in central Crete with Sr ratios. Sections are correlated by 3rd order Sequence boundary (SB). Dashed line represents type 2 unconformity, wave line represents type 1 unconformity. See Fig. 4.1b for locations

claystone, the AT section overlies 40m of similar deposits. In the central Messara Basin (Fig. 4.1.b), offshore sediments (marls and clays) have been determined to be of late Tortonian to Messinian age based on biostratigraphic, magnetostratigraphic and astronomical dating (Zachariasse, 1975; Langereis et al., 1984; Hilgen et al., 1995; Krijgsman et al., 1995). In the eastern Messara Basin, a late Seravallian biostratigraphic age of early marine deposits has been found (Meulenkamp, 1979).

Sections are characterized by a lower part formed by limestone rich in siliciclastics with intercalated sandstone and an upper part consisting of limestone with little siliciclastic content. In nearshore settings (sections MO and AT), both parts are separated by a conspicuous sedimentary surface that is a flooding surface characterized by a lag in the Matala area and an angular unconformity in the Agios Thomas area (Fig. 4.3.). For its large spatial extent this correlative surface is interpreted to relate to a 3rd order sequence boundary. In MO section, limestone overlying the surface contains red algal assemblages with abundant *Lithothamnion* and *Mesophyllum* that indicate increasing water depth.

Methodology

Sampling

Five sections along the southern coast of Portugal (Algarve) between Portimão and Albufeira were measured in detail and sampled (Fig. 4.1.a). Bivalve shells and shell fragments of *Pecten* and *Chlamys* were selected. Based on their stable low magnesium calcite mineralogy, they can be expected to record the original seawater Sr isotope composition. Vertical sample intervals were kept close to 2 m and a total of 70 samples were taken. In Greece (central Crete), 3 sections were measured and a total of 21 samples was taken (Fig. 4.1.b). *Pecten* and *Chlamys* shells in these sections were less frequent and sample density is therefore lower (1 sample /8 m in average) than in the sections investigated in Portugal.

Sr isotope analysis

Samples from the Algarve were measured at the Max Planck-Institute for Chemistry/Mainz. Samples from Crete were measured at Georg August University, Geowissenschaftliches

Zentrum/Göttingen. All samples were thoroughly cleaned mechanically and ultrasonically and washed with suprapure HCl before grinding. Approximately 300 mg of each cleaned Algarve bivalve sample was dissolved in LD-PE bottles with multi-distilled HNO_3. Decomposition took place immediately at room temperature without any visible residue. Ion exchange column technique with resin AG 50W-X12 (200-400 mesh) was used for Sr separation. For measurement, the dried Sr fractions were dissolved with suprapure HCl and loaded on outgassed W single-filaments with TaF_5 to enhance ionization. Sr isotope ratios were measured on a Finnigan MAT 261 mass spectrometer with static multicollection.

Approximately 30-50 mg from each sample from Crete was dissolved under high-pressure in sealed Savillex-PFA reaction vessels enclosed in Teflon beakers with a mixture of concentrated suprapure HF and double distilled HNO_3. Samples were completely decomposed in 15 hours at a temperature of 200°C. Sr was separated using the ion exchange technique described above. The dried Sr fractions were dissolved in HNO_3 and loaded with H_3PO_4 on an outgassed Re double filament. Isotope ratios were measured on a Finnigan MAT 262 RPQ II+ mass spectrometer with multi collectors operating in static mode.

For all samples, measured Sr isotope ratios have been normalized for mass fractionation to $^{86}Sr/^{88}Sr = 0.1194$ and to a recommended value of $^{87}Sr/^{86}Sr = 0.710248$ for NBS standard $SrCO_3$ 987 in order to minimize instrumentally caused bias and to ensure external comparability of our data.

On all samples, trace elements were measured by ICP-OES in order to control possible diagenetic alteration. Additionally, on selected samples from Algarve, cathodoluminescence analysis was used for optical detection of possible alteration effects.

Results of Sr isotope analysis

Sr isotope ratios between 0.7086 and 0.70883 in the Portuguese Algarve sections are in agreement with published reference data (Fig. 4.4.) of late Burdigalian to Serravallian seawater Sr isotope ratios and thus fit into the biostratigraphic and chronostratigraphic time frame established by Antunes et al. (1997) and Antunes et al. (2000). Measured Sr curves show pronounced positive and negative trends (Fig. 4.2.). The amplitude of these trends is well above the average 2σ analytical error of Sr isotope analysis. Trends in Sr isotope ratios are in phase in the stratigraphical interval of the Lagos Portimão Formation that is defined by marker beds I-III. A minimum occurs below marker bed I in sections ASO, LDL and PSR. A

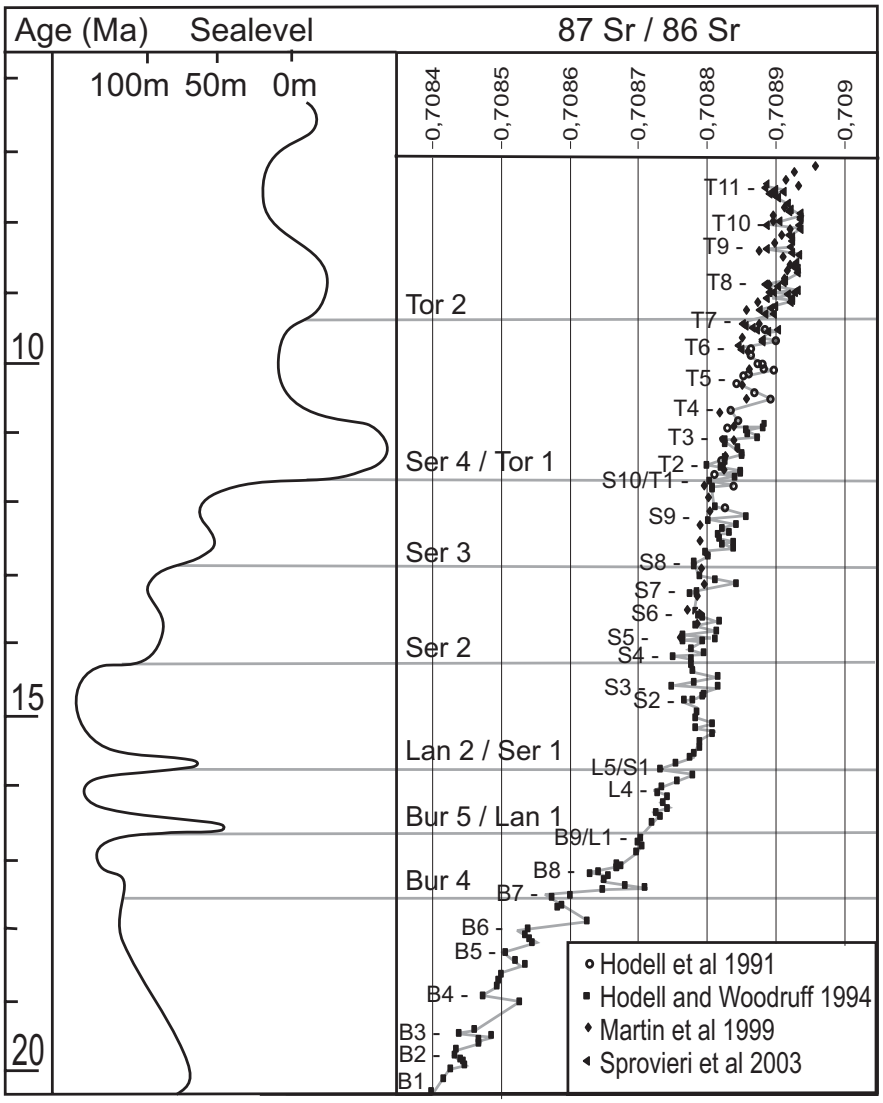

Fig. 4.4.: Reference seawater Sr isotope curve from published data and sealevel curve and sequence boundaries of Haq et al (1988) with sequence boundaries named after Hardenbol et al. (1998). All ages are calibrated to Cande and Kent (1992). Note that the data of Martin et al. (1999) that have ages calculated from the polynomial fit of Hodell and Woodruff (1994) tend to deviate from the curve. Negative Sr events at 3rd order sequence boundaries and within sequences are informally labelled using a combination of a letter, representing the stage and a figure, representing the number of events within each stage

second minimum occurs below marker bed II (section ASO) and within marker bed II (section LDL). In each case, the minimum is followed by a consistent rise in Sr isotope ratios. Also, within and above marker bed III in sections MW and PDG a rise in Sr isotope ratios is observed. It is followed by a minimum close to the overlying unconformity at the base of the "laminated sands" unit.

Strontium isotope ratios of whole rock samples are elevated, compared to ratios measured on bivalve shells (Fig. 4.2.).

Sr isotope ratios in the Cretan sections (Fig. 4.3.) are between 0.70884 and 0.70894 and comparison with reference seawater Sr ratios (Fig. 4.4.) indicates a Tortonian age. Trends are less pronounced than in the Algarve sections. A minimum occurs at the correlative surface in section AT and, respectively, 3m - 6m below this surface in sections AV and MO, which is

interpreted to relate to a 3rd order sequence boundary. Upsection in both sections, AV and MO, a rise in Sr isotope ratios and a second minimum at the top is observed.

Concepts for high-resolution Sr isotope chronostratigraphy

Control on seawater Sr isotope ratios

Seawater Sr isotope ratio is mainly a function of input of strontium with low $^{87}Sr/^{86}Sr$ from hydrothermal alteration of ocean ridge basalt (mantle source) and with high $^{87}Sr/^{86}Sr$ from continental weathering (Palmer and Edmond, 1989; Richter et al., 1992). While the input from hydrothermal alteration of ocean ridge basalt has been regarded to be constant by the authors, the continental input fluctuates in time, resulting in significant changes of seawater Sr isotope ratios. The amount of Sr residing seawater is 7 orders of magnitude higher than annual riverine input (Richter *et al*., 1992). Therefore, considerable variation in continental input is necessary to affect seawater Sr isotope ratios. Main factors controlling continental Sr flux are tectonic uplift, climate induced changes in weathering rates and -mechanisms as well as glaciation (Armstrong, 1971; Raymo et al., 1988; Hodell et al., 1989; Capo and DePaolo, 1990; Dia et al., 1992; Edmond, 1992; Richter et al., 1992; Derry and France-Lanord, 1996; Blum, 1997). A main source of continent derived radiogenic ^{87}Sr that results from the decay of ^{87}Rb are silicate minerals. The exposure of large quantities old silicate rocks to weathering therefore can result in significant increase in seawater Sr isotope ratios. Important processes that increase the weathering of old silicate rocks are the denudation of large areas by either tectonic uplift such as the Himalayan uplift or glacial erosion by continental ice shields and following deglaciation (Derry and France-Lanord, 1996; Blum, 1997). Major increases of the seawater Sr ratio in Cenozoic times have been related to the Indian-Tibetian continental collision beginning 40 Ma ago with a peak uplift of the Himalaya between 15 and 20 Ma (Richter et al., 1992) and to the appearance of continental ice-sheets on Antarctica from the Eocene-Oligocene transition onward (Zachos et al., 1999). Short-term variability in the Sr record has been found for the past 450 ka to respond to global climate cycles, glaciation and related changes in rainfall (Dia et al., 1992; Clemens et al., 1993). While some of these results that indicate a relationship between Sr isotope variation and 41ka and 100ka cycles have later been attributed to analytical artefacts (Clemens et al., 1995), short-term trends over a period of $\leq$ 1 m.y. are recorded in the Miocene as well as in the early Oligocene that correlate

between boreholes (Oslick et al., 1994; Zachos et al., 1999). Additionally, sharp increases of Ca fluxes and opal accumulation rates, which indicate increased Si fluxes in the earliest Oligocene imply both, a total increase of weathering and a high proportion of silicate weathering (Zachos et al., 1999). Blum and Erel (1995) and Blum (1997) demonstrate that, depending on the extent of glaciation, the global amount of silicate weathering would increase fivefold in the first 1000 years after deglaciation, if deglaciation was an instantaneous process. In consequence, the release of radiogenic Sr mainly from fresh biotite would increase dramatically. This process potentially causes Sr isotope ratios to increase after the glacial maximum. Towards the glacial maximum a decrease in Sr isotope ratios is to be expected for several reasons: Continental weathering declines due to reduced precipitation during glacial-ages (Clemens et al., 1993). Weathering is also reduced in ice covered areas were little CO_2 can reach the rock surface (Blum, 1997). The rate of weathering and erosion in these areas is further reduced if glaciers are frozen to the ground (Zachos et al., 1999). Moreover, sea-level fall related to glacial maxima exposes recent and young shelf carbonates with low Sr isotope ratios to weathering. Erosion of these carbonates buffers or even reduces seawater $^{87}Sr/^{86}Sr$ (Zachos et al., 1999). However, mass balance calculations have shown that neither intensified weathering due to deglaciation nor reduction of riverine input during glacial maxima can in all cases account for the magnitude of the $^{87}Sr/^{86}Sr$ shift correlated with glaciation (Blum and Erel, 1995; Blum, 1997). Nevertheless, glaciation is regarded to be responsible for the fine structure superimposed on long-term tectonically driven trends in global seawater Sr isotope variation (Hodell and Woodruff, 1994; Oslick et al., 1994; Blum and Erel, 1995; Blum, 1997).

High-resolution Sr stratigraphy

Since the mixing time of ocean water (<1ka) is much shorter than the residence time of Sr in the oceans (ca. 3Ma), $^{87}Sr/^{86}Sr$ at a given time is homogeneous in the world oceans (McArthur, 1994; Richter and Liang 1993). Even oceanic water masses with relatively restricted marine circulation possess this global oceanic signature (DePaolo and Ingram, 1985). Sr isotope ratios in shells of biota that are restricted to normal marine salinities such as *Pecten* therefore record the global oceanic signature.

As has been discussed above, fluctuations in the seawater Sr curve correspond to climatic processes. Thus, minima in the Sr curves that relate to glacial maxima can be treated as "Sr events" comparable to oxygen isotope stages of Shackleton and Opdyke (1973) or SPECMAP

oxygen isotope events based on the work of Imbrie et al. (1984). While SPECMAP events represent minima in ^{16}O in the world ocean that relate to glacial maxima, Sr events correspond to reduced input of ^{87}Sr during glaciation and therefore globally reduced Sr isotope ratios. For a better reference in the text, we informally label negative Sr events in the combined reference curve, for example B1 – B9 for the Burdigalian (Fig. 4.4.). Additional age information comes from the long-term rise in Sr isotope ratios (Fig. 4.4.). Since minima in $^{87}Sr/^{86}Sr$ relate to glacial maxima, they also relate to eustatic minima. Minima in Sr isotope ratios at 3rd order sequence boundaries are however not more pronounced than minima that lie within 3rd order sequences (Fig. 4.4.). Thus there is apparently no direct relationship between magnitude of sea-level fall and the amplitude of the Sr curve. The relationship between Sr isotope ratios and glacial cycles however suggests that minima in Sr isotope ratios within 3rd order sequences relate to higher order eustatic fluctuation.

Shallow-water sediments are sensitive to eustatic change that is reflected in the stratigraphical architecture of shelf deposits. Eustatic change is also reflected by changes in lithology and biotic associations (Brachert et al., 2003).

Due to the variability in sedimentation rate and the possible occurrence of hiatuses within the measured sections, the calculation of a depth – age model is not possible in shallow-water sediments. To obtain absolute age information it is therefore necessary to tie the Sr curve of the measured section point by point to a reference seawater Sr curve (Fig. 4.5.; 4.6). This is possible by combination of Sr event stratigraphy with outcrop information on eustatic change.

The resolution of this method depends on several factors: 1) internal error of Sr isotope analysis and sample density; 2) accuracy of the age model on which the Sr reference curve is based: age models from different drill sites vary in the magnitude of several 100k.y. The resulting error in age of the reference curve can become close to the duration of intervals between Sr events. For this reason it is sensible in many cases to use only one reference dataset for a given time interval to avoid a phase shift that blurs out Sr events; 3) accuracy of the age of the sequence boundaries.

Reference Sr curves and absolute age

Several high-resolution data sets of Miocene Sr isotope ratios have been published. Since no dataset from a single site has the required stratigraphic range, we use a composite reference curve by splicing the data of Hodell and Woodruff (1994), Hodell et al. (1991) and Sprovieri

et al., (2003); (Fig. 4.4.). All chosen datasets base on the analysis of planktonic foraminifera tests from deep marine sediments. The data of Hodell and Woodruff (1994) from site 289 cover the period from 18 Ma to 10,7 Ma while the curve of Sprovieri et al. (2003) ranges from 9,7 Ma to 7,5 Ma. The data of Hodell et al. (1991) fill the gap between 10,7 Ma and 9,7 Ma. However, the Sr isotope ratios from DSDP site 588A (Hodell et al., 1991) do not show trends as clearly as the data from Hodell and Woodruff (1994). On the other hand the data from DSDP site 588 (Hodell et al., 1991) are in phase with the curve of Sprovieri et al. (2003) except for those younger than 9,5 Ma which appear to be offset by up to 0,3 Ma. While Hodell et al. (1991), Hodell and Woodruff (1994) and Sprovieri et al. (2003) use independent age models, the Sr ages of Martin et al. (1999) are based on the reference curve of Hodell and Woodruff (1994). Long-term trends found in the combined data of Hodell et al. (1991), Hodell and Woodruff (1994) and Sprovieri et al. (2003) are well represented in the dataset of Martin *et al*. (1999), whereas short-term trends are not clearly recognizable and commonly offset (Fig. 4.4.). The age/depth model of Hodell and Woodruff (1994) is based on biostratigraphy and tied into the magnetostratigraphic time scale of Cande and Kent (1992) by carbon isotope stratigraphy. Hodell et al. (1991) use the magnetostratigraphic age model of Barton and Bloemendal (1986) while Sprovieri et al. (2003) use the astronomical polarity time scale of Hilgen et al. (1995).

All age data used in this paper were calibrated to the time scale of Cande and Kent (1992; = CK92) and thereby adjusted to the reference curve of Hodell and Woodruff (1994) which has the longest age range. The sea-level curve and sequence boundaries are taken from Haq et al. (1988) and sequence boundaries are named according to Hardenbol et al. (1998). Ages of sequence boundaries have also been calibrated to the CK92 scale.

Application of high-resolution Sr isotope chronostratigraphy

To determine the age of the measured sections from Portugal and Crete, Sr isotope curves (Fig. 4.2.; 4.3.) are correlated point by point with the reference Sr curve (Fig. 4.4.). This technique converts the vertical scale of measured sections (m) to absolute age. The resulting time referenced data points combined with the reference datasets are shown in Fig. 4.5. and Fig. 4.6.

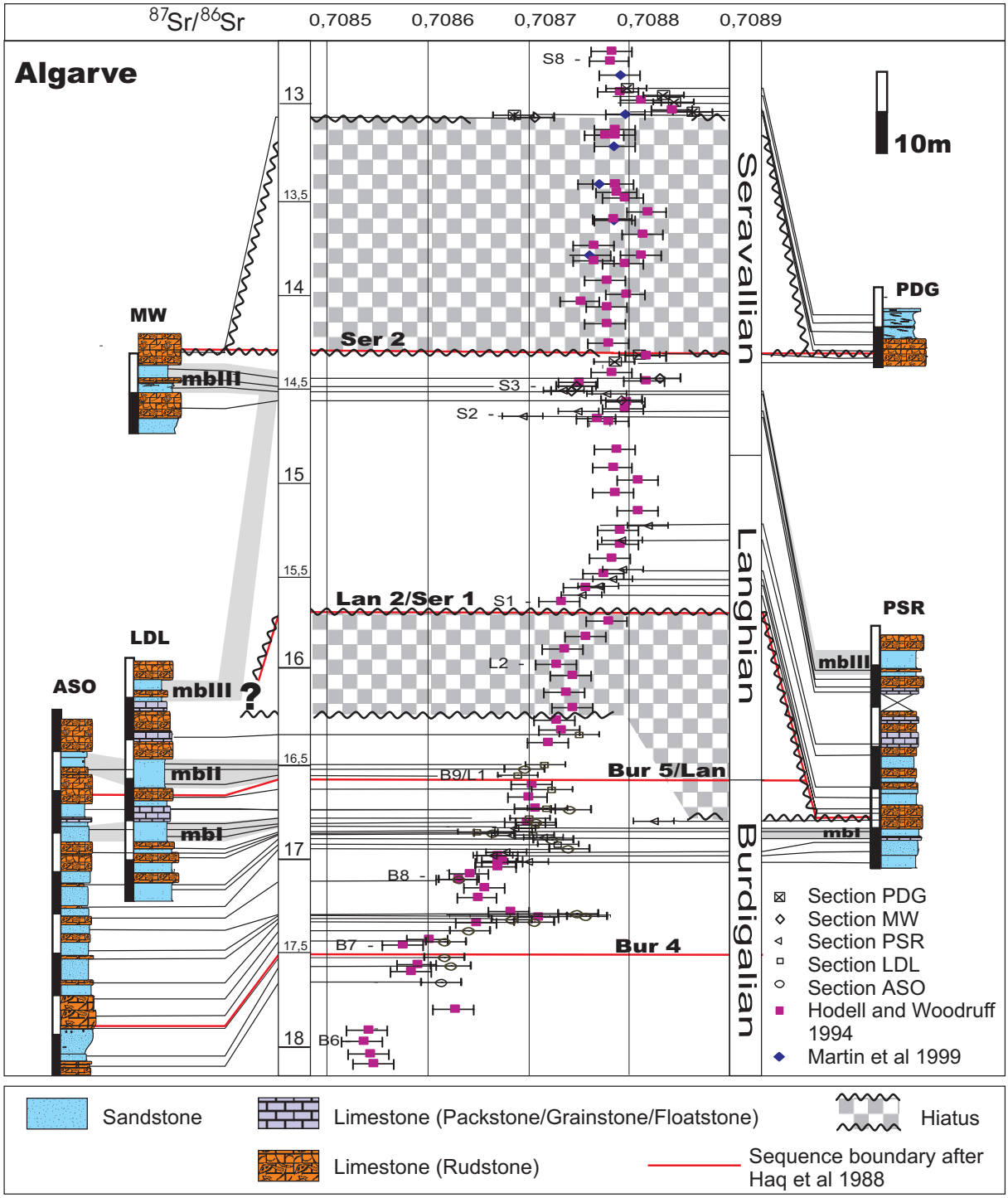

Fig. 4.5.: Sections in southern Portugal (see Fig. 1a for locations) and measured Sr ratios in the sections plotted on the reference data of Fig. 4.4. in order to obtain absolute age of the sections. Note that for measured sections vertical scale is meters, and for the Sr ratios it is time. Marker beds are abbreviated mb I – III. Sr events are labelled as in Fig. 4.4.

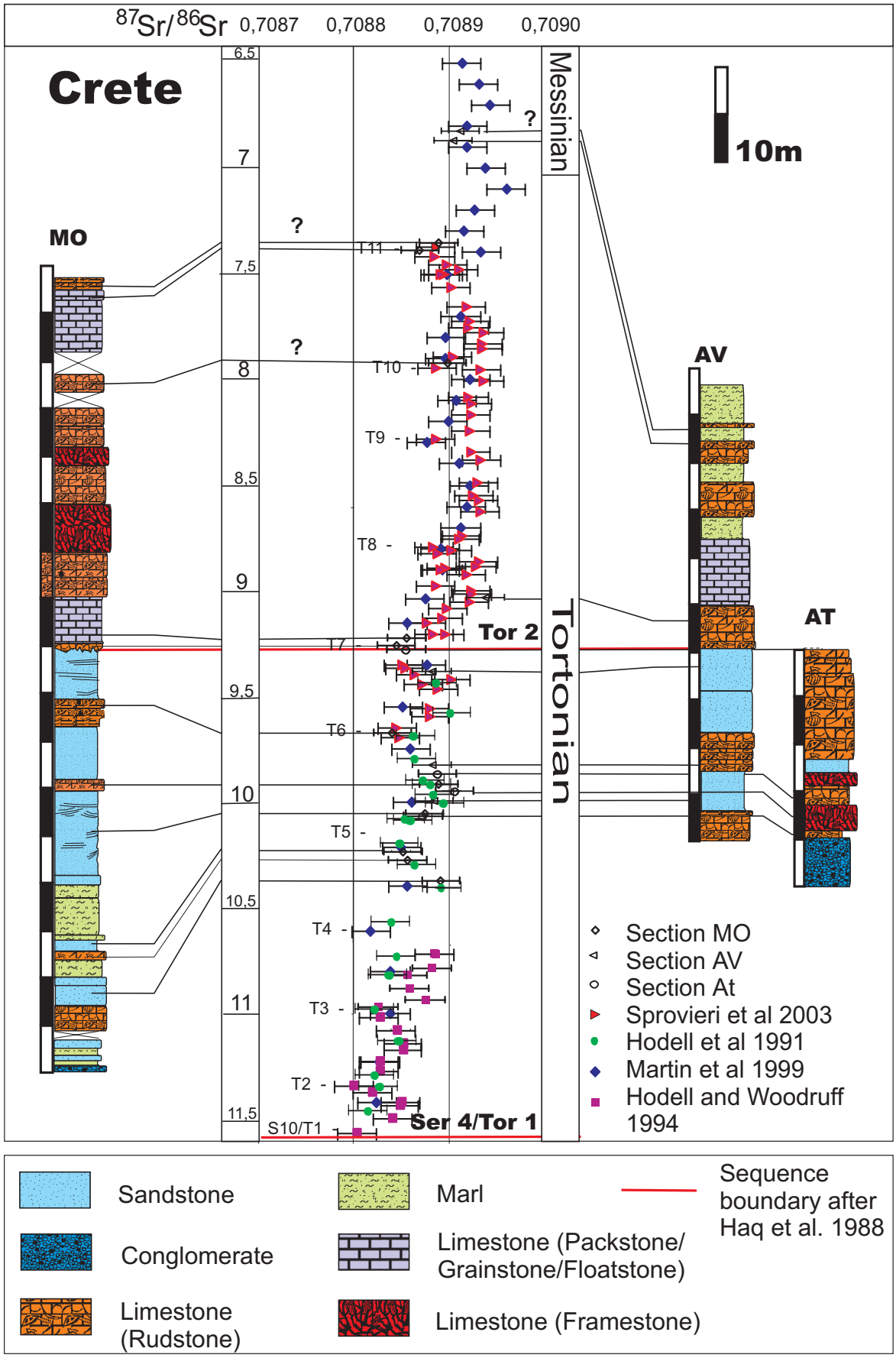

Fig. 4.6.: Sections in central Crete (see Fig. 1b for locations) and measured Sr ratios in the sections plotted on the reference data of Fig. 4.4. in order to obtain absolute age of the sections. Note that for measured sections vertical scale is meters, and for the Sr ratios it is time. Sr events are labelled as in Fig. 4.4. Note cyclic occurrence of T2-T8 events

Portugal

Trends in the sections from Portugal (Fig. 4.2.) correlate with Sr events in the reference Sr seawater curve (Fig. 4.5.). Minima in the combined Sr curve (Fig. 4.5.) are predominantly located within condensed shell beds. This is the case for B7-B9 events in section ASO, B9 event in section LDL, S1-S3 events in section PSR and S3 event in section MW. Of these, B7, B9 and S1 events have the same age as the Bur 4, Bur 5/Lan 1 and Lan2/ Ser 1 sequence boundaries after Haq et al. (1988). With exception of the PDG section, sandstone intervals overlying the condensed shell beds, including marker beds I-III are characterized by increasing Sr isotope ratios (Fig. 4.5.).

Three values deviate significantly from the reference curve, at 6m of the PSR section, at the base of PDG section and at top of MW section. The latter two are located at the unconformity at the base of the laminated sands unit.

Average sedimentation rates derived from the conversion of thickness into absolute age in Fig. 4.5. are up to 6 cm/ka in the intervals with the highest accumulation rate.

The age of the base of the Lagos Portimão Formation is defined by the prominent B7 event at the Bur 4 sequence boundary (Fig. 4.5., section ASO). The sequence boundary lies at the base of a conspicuous stack of shell beds at 6 m – 12 m. The age of the base of the Lagos Portimão Formation is therefore approximately 17,7 Ma (Fig. 4.5.). Towards the salt dome of Albufeira in the east, the age of the base of the Lagos Portimão Formation decreases and forms an onlap on Cretaceous basement. Close to Albufeira, marker bed II is absent due to a 1 m.y. hiatus (section PSR, Fig. 4.5.). The “laminated sands” unit also overlies a >1 m.y. hiatus and its base has an age of 13,1 Ma.

Crete

The $^{87}Sr/^{86}Sr$ minimum at the proposed 3rd order lowstand can be linked to the T7 event that has the same age as the Tor 2 sequence boundary after Haq et al. (1988; Fig. 4.3; 4.6). Rudstone beds at 39 m, 45 m, 73 m and 83 m of the MO section correspond to minima T6 and T7 in the Sr isotope curve as well as to two of T8, T9, T10 or T11 events. A connection to T10 and T11 is most likely because the resulting sedimentation rate then averages 2,5 cm/k.y., which is a realistic value for carbonate sediments (James, 1997). Sr isotope ratios of samples

from sandstone beds are mostly elevated. Noticeably, in the early to middle Tortonian, minima are sinuous with a frequency of 400-450ka (T2-T8 events, Fig. 4.6.).

The age of the base of the AT and AV sections is defined by the T5 event (10,2 Ma, Fig. 4.6.). The top of the AT section corresponds in age to the T7 event (9,3 Ma). Since both sections overlie thick successions of siliciclastic marine deposits, these ages are to be taken as minimum age of marine transgression in central Crete. This is in agreement with the late Seravallian age of early marine deposits found by Meulenkamp (1979). The base of marine sediments at Matala (MO section) is around 10,5 Ma (Fig. 4.6.) and overlies fluviatile sediments. It follows that marine transgression occurred earlier in the Agia Vavara – Agios Thomas area than in the Matala area. Strontium values of the youngest shallow marine sediments in the Matala area (top of MO section) are interpreted to correspond to T10 and T11 events. The resulting age of the top of the MO section is 7,4 Ma. Deep marine sediments at the top of the AV section plot into the late Tortonian to Messinian part of the reference Sr seawater curve. Off-shore marls in the central Messara Basin are dated by Zachariasse (1975), Langereis et al. (1984), Hilgen et al. (1995) and Krijgsman et al. (1995) to be of the same age.

Discussion

Diagenesis

Not much is known about diagenetic processes affecting Sr isotope ratios. In the measured samples diagenetic modification of Sr isotope ratios is unlikely for several reasons: 1.) Trace element composition does not co-vary with Sr isotope ratios and low concentrations of Mn (10-40 ppm) and Fe (10-180 ppm) do not indicate diagenesis. Cathodolumenescence analysis also does not indicate diagenetic alteration. 2.) Diagenetic alteration should level out fluctuations in Sr isotope ratios. 3.) In the case of selective alteration by meteoric diagenesis the more permeable sediments can be expected to be preferentially affected. Cementation destroys pore space and significantly reduces permeability. Diagenesis by circulating meteoric waters leads to an increase of Sr isotope ratios. Shell beds that represent minima in the Sr curve, however are not generally better cemented than sandstone that contains shells with comparatively high Sr isotope ratios. 4.) Whole rock samples have Sr isotope ratios consistently higher than bivalve shells from the same part of the section and therefore indicate diagenetic alteration of the original sea-water signal.

Sedimentary processes

Trends in Sr isotope ratios in the Miocene of Portugal and Crete have been shown to correlate between different sections and with trends in published Sr curves. Therefore, apparent age inversions are explained by changes in Neogene seawater Sr isotope ratios. Only two negative outliers that lie above a >1m.y. hiatus are most likely from exhumed shells. This shows, that even on the high-energy shelf of the Neogene Algarve area, deep exhumation of coarse skeletal material plays only a minor role. Shell beds are therefore formed mostly by winnowing out of fine material and to a lesser degree by exhumation and redistribution. The latter process would level out short-term fluctuations in the Sr composition. Moreover, in order to produce negative Sr isotope trends it is necessary that only material consistently increasing in age was exhumed. The negative trend between T4 and T5 events at section MO on Crete cannot result from exhumed shell material as marine sediments in the area of Matala conformably overlie fluviatile sediments. Exhumation of shell material can therefore be excluded as a main reason for negative Sr trends in shallow marine sediments.

Sequence stratigraphy

By applying Sr stratigraphy, sequence boundaries in the measured sections were correlated with sequence boundaries of Haq et al. (1988; Fig. 4.5.; 4.6.; 4.7.). Of these, only the Lan 2/Ser 1 and the Ser 2 boundaries in the Portuguese sections and the Tor 2 boundary at the Top of AT section on Crete are clearly represented by erosional unconformities. Sequence boundaries lie always within or directly below condensed beds. These are overlain by sandstone or limestone that is interpreted to reflect increased water depth based on faunal elements. Shell beds are interpreted to represent lowstand deposits that formed through winnowing out of the fine material during sea-level minima. Accordingly, sandstone overlying shell beds was deposited during the following transgression and highstand. The succession of stacked shell bed - sandstone couplets in the sections from Portugal suggests a high frequency eustatic control on water depth.

The comparison of fluctuations of the Sr isotope curves from the analysed sections calibrated to absolute time (Fig. 4.5.; 4.6.) with the sea-level curve of Haq et al. (1988; Fig. 4.7.) shows that a 3rd order sequence comprises several fluctuations which are related to limestone-sandstone couplets. A 3rd order sequence is thus composed of several successive transgressive

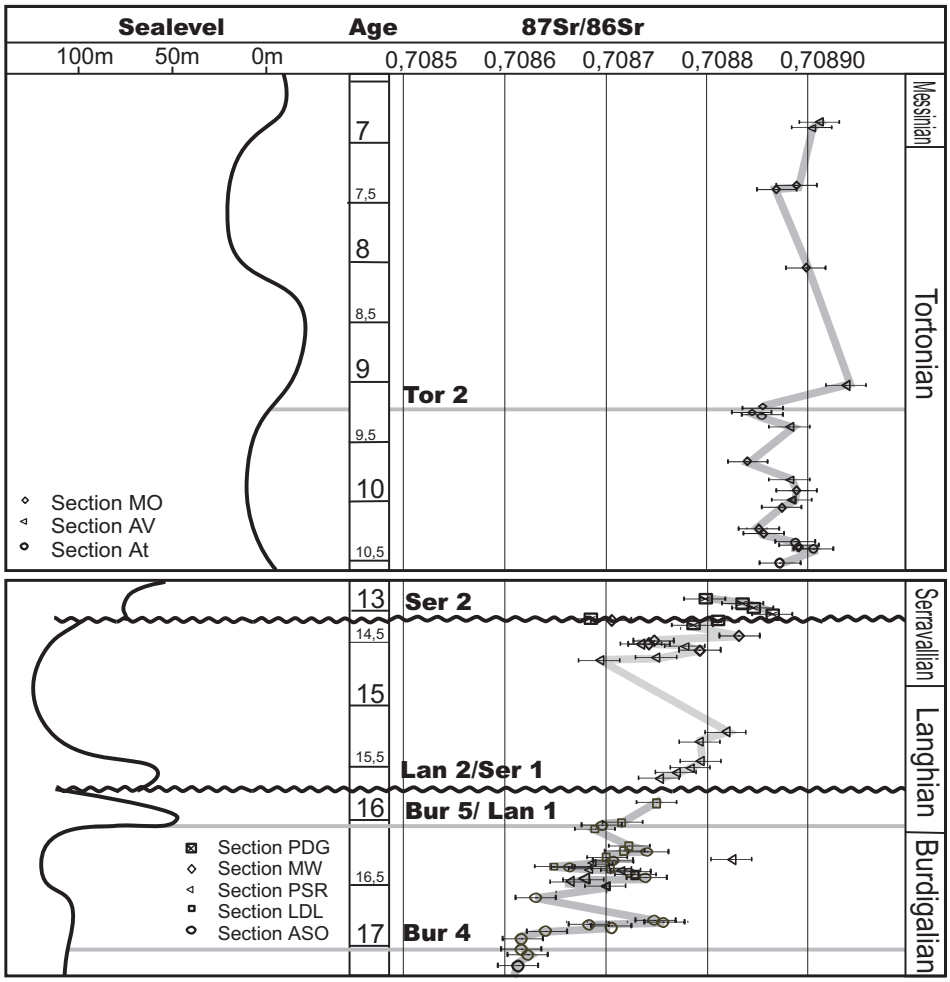

Fig. 4.7.: Measured Sr ratios and absolute age in correlation with relevant intervals of the sealevel curve of Haq et al. (1988). Note the rise in Sr ratios above Bur 4, Bur 5/Lan 1, Lan 2/Ser 1 and Tor 2 sequence boundaries and higher order fluctuation of the Sr trend between sequence boundaries.

and highstand systems tracts (sandstone or limestone) separated by lowstand systems tracts (carbonate shell beds) that are in most cases forming a conformable sedimentary succession. This interpretation is in agreement with the lowstand carbonates – highstand sandstones model of Brachert et al. (2003).

In the sections from Crete, the influence of high frequency sea-level change on lithology appears to be less pronounced. Nevertheless, Sr isotope ratios in rudstone beds correlate with minima in the reference Sr curve and therefore are related to eustatic minima. In the AV section, in contrary to the other sections, shell beds that are related to turbidites do not necessarily represent a response to sea-level change.

Sr isotope ratios and eustasy

Glaciation and deglaciation are interpreted to control the fine structure of the global seawater Sr isotope record. In the Tortonian, minima in Sr isotope ratios exhibit a 400 to 450 ka

periodicity over an interval of more than 2,5 M.y. The cyclicity may correspond to the 406 ka eccentricity period found in late Oligocene and early Miocene $\delta^{18}O$ records by Zachos et al. (2001). If the 406 ka period is verified to occur in seawater Sr isotope ratios, an indirect orbital forcing on seawater Sr isotope ratios can be inferred. Variability in $\delta^{18}O$ records changes in water temperature and global ice volume and is thought to reflect eustatic change. This relationship has been established by Miller et al. (1991) for several Oligocene and Miocene sequence boundaries of Haq et al. (1988) and by Abreu and Haddad (1998) for sequence boundaries of Hardenbol et al. (1998). However, trends in Sr isotope ratios do not directly depend on ice volume but on the process of deglaciation. They can therefore not be expected to be proportional to eustatic change. Thus, the amplitude of Sr isotope fluctuation is different from the amplitude of eustatic fluctuation. This is especially true for long time intervals. On the other hand, fluctuation in the Sr isotope record is related to lithologic change. This is the case because a change in lithology in conformable successions is related to eustatic change rather than to absolute values of sea-level. Therefore, the relationship between higher order eustasy expressed in lithologic change and Sr isotope ratios has the capacity of high-resolution dating of shallow water sediments. The chronostratigraphic record of eustatic change thus can be mapped down to the resolution of high frequency sea-level fluctuations that are best recorded in neritic sediments. The influence of climate on the Sr signal links sedimentary data directly with climate change. The Sr isotope system is therefore an alternative and supplement to $\delta^{18}O$ and $\delta^{13}C$ analysis.

Conclusions

Several studies document the influence of global climate and glaciation on the Sr isotope record that must therefore also be linked to eustatic changes. This relationship can be used all over the world at any time as the residence time of Sr in seawater significantly exceeds circulation rate of the world oceans. The correlation of Sr-events related to glaciation therefore provides a powerful tool for high-resolution chronostratigraphy in sections that contain calcite shells. It is especially effective in shallow water sediments that best record sea-level changes. The combination of information from Sr isotope ratios with sequence stratigraphic outcrop information further improves age resolution. In contrast to stable isotope stratigraphy, results are not influenced by local parameters such as water temperature or bioproductivity. For these reasons high-resolution Sr stratigraphy is a unique method to

determine the age of shallow water sediments with an accuracy that is commonly only met in deep water sediments.

While the relationship between global sea-level and Sr isotope ratios is only qualitative, it has nevertheless to be assumed, that the presence of continental ice masses is crucial for this method and thus limits it to ice house periods.

5. Structural Geology

Introduction

Depositional environments in the WAT and the southern Messara Basin are influenced by tectonic movements. This is reflected by the variability in thickness of the sedimentary units described in chapter 2. and by their spatial extent that is defined by fault bounded horsts and basin margins. In most cases however, synsedimentary faults are difficult to detect since they are covered by younger sediments. As will be demonstrated below, late Miocene faults do not necessarily correspond to the modern postsedimentary fault system and the orientation of faults and tectonic setting considerably changed during the course of the late Miocene to recent.

Structural framework

The WAT is dissected by a conjugate set of SW-NE (40°-50°) and NW-SE (130°-140°) oriented normal faults that define the limits of uplifted basement blocks and the limits of outcrops of Neogene sediments towards the Asteroussia Mountains (Fig. 2.2.1.). To the west and northwest, the orientation of faults gradually changes to WSW-ENE (70°) and NNW-SSE (160°) directions that also define the southern margin of the Messara Plain to the east. This change can be identified on satellite images by a change in orientation of valleys and bays (Fig. 5.1.). The most noticeable structure is the boundary between the WAT and the Messara Plain north of Matala and Pitsidia and finds its continuation north of Sivas (Fig. 2.2.1.). It is also oriented 70° and juxtaposes lithologically very different units against each other: the siliciclastic succession overlain by the carbonate succession typical for the WAT in the south (LFA1 and 2; see chapters 2.3. and 2.4.) and marl deposits of LFA3 (see chapter 2.5.) in the north. No facies transition between coarse grained mid- to outer ramp sediments to the south and offshore marl to the north is visible. The actual fault, however, has not been identified in outcrop. In general, due to the low degree of lithification of Neogene deposits and the brittle character of the underlying Flysch, fault planes are poorly preserved.

The most prominent structural feature of the WAT is the steep 399m high fault bounded block of Mount Kristo Kefali at the southwestern tip of the WAT (Fig. 1.2.2.b, 2.2.1). Orientation of normal faults is distinct from elsewhere in the WAT: To the east, the uplifted block is

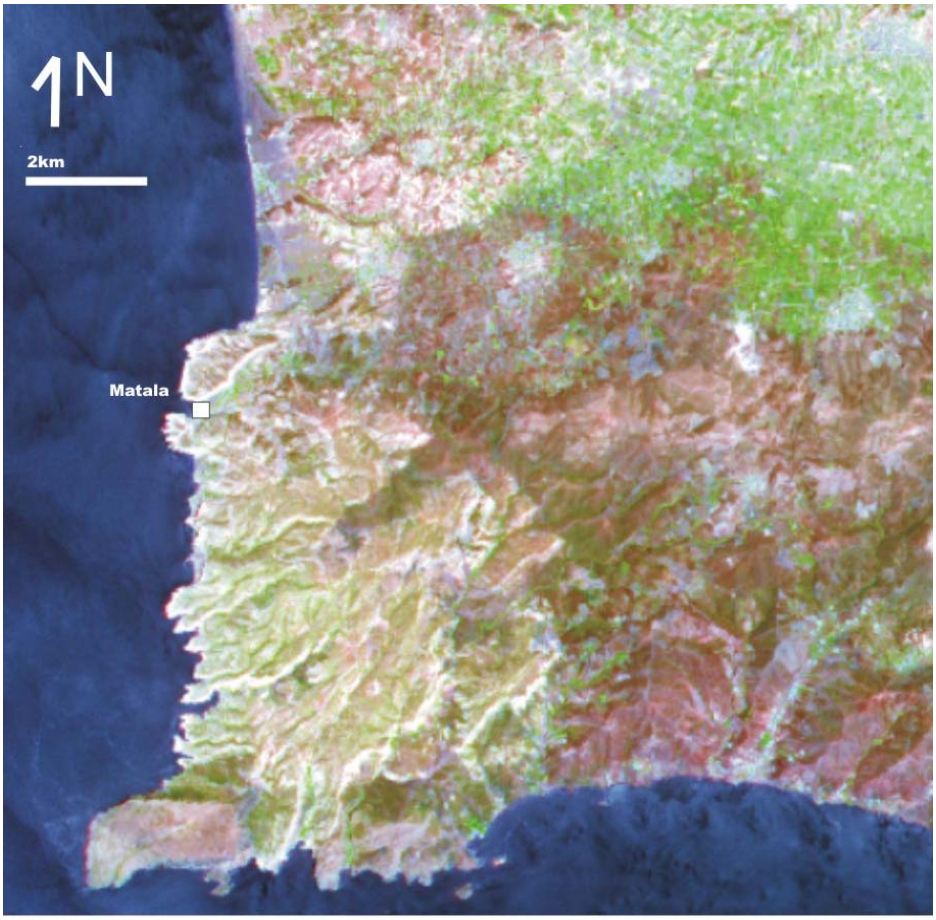

Fig. 5.1.: Rectified satellite image of the WAT and south-western Messara Plain. Bright green colours indicate moist soil of irrigated fields in the Messara Plain, darker brownish to greenish colours are characteristic for basement areas and some siliciclastic deposits of LFA1. Lighter greenish to reddish colours indicate distribution of LFA2 and 3 deposits. Valleys are indicated by whitish colours due to a maximum in reflected energy to the S - SW. Note change in orientation of valleys that reflects the orientation of normal faults from SW - NE in the south to WSW - ENE in the north

bounded by a set of 0° - 20° oriented normal faults. Fault planes show fresh surfaces due to recent activity. The northern side is bounded by 70/50 NW (Fig. 5.2.a) and 115/50 NE (Fig. 5.2.b) oriented normal faults with strongly curved fault planes. Of these, the 70/50 NW oriented fault cuts only pre-Neogene sediments. On the hanging wall side, Flysch occurs on top of Tripolitza Limestone while on the footwall block (Kristo Kefali) Flysch is absent. The 115/50 NE oriented fault also cuts Neogene deposits north of Kristo Kefali. A set of 50/40 and 80/50 NW oriented normal faults that does not cut through Neogene deposits with Flysch on the hanging wall side and Tripolitza Limestone on the foot wall side can also be traced between Kristo Kefali and Moni Martsalo (Fig. 5.3.).

Strike-slip faulting is identified by subhorizontal slickenside lineation is found at western Martsalo Bay along with slight folding of Neogene sediments on the hanging wall side. Neogene limestone on the foot-wall side of the fault contains abundant clasts of Tripolitza Limestone (sections Ma1 and Ma2, Fig. 2.2.3.) that are absent on the hanging wall side where coral horizons occur. Dextral offset of 40°-50° faults along a 130°-140° oriented fault by no more than a few 100m is observed between Matala and Moni Odhiyitria (Fig. 2.2.1). The persistence of facies and thickness of sedimentary units across faults north of Kristo Kefali, however shows that transcurrent faulting does not play an important role in the WAT.

In the WAT, thrust faulting is observed only at one location, 1km to the southwest of Pitsidia Fig. 5.2.c,d). Its orientation is 60/30 to 50/70NE and the fault plane is steepening to the southwest. Fault vergence is to the S-SSE. At the southern rim of the Messara Plain, 1,5km south of Plora, at the road to Lentas, small scale southward thrusting is also observed.

Fig. 5.2.:
a: 70/50° NW oriented fault on the northern side of Kristo Kefali. Fault plane is on Tripolitza Limestone (dark grey). Beige sediments on the hanging wall side are weathered Flysch. The fault can be traced to the horizon were it is expressed by the decrease in slope to the north due to the change from limestone to Flysch along the fault. View is to the WSW
b: 115/50° NE oriented fault on the northern side of Kristo Kefali. Fault plane is on Tripolitza Limestone. Picture is taken 3m to the east of Fig. 5.2.a, east of the intersection with to 70° oriented fault. To the right of the road is an outcrop of Neogene limestone on the hanging wall side of the fault. View is to the west
c: Outcrop of a fresh rock surface with trust fault southwest of Pitsidia. Note slickenside lineation on the faultplane above trace of the fault that is marked by gravel
d: Small thrust sheet of Neogene limestone on top of Neogene sandstone (LFA1). Direction of movement is indicated by arrow

Synsedimentary faults

Most faults found in the WAT cut through Neogene deposits and sedimentary units have the same thickness on both sides of the fault. Therefore most faults found in the WAT are postsedimentary. Synsedimentary faulting is hard to identify since faults are usually covered

by younger Neogene sediments or overprinted by later reactivation of faults. Synsedimentary faulting during deposition of LFA1 is best seen in the Vasiliki area: South of Kandhila, the lower part of the LFA1 succession including three reef horizons is in tectonic contact with basement (Fig. 2.3.3.). The fault is covered by cobble conglomerate that passes into sandstone, indicating increase in water depth on the hanging wall side of the fault (see chapter 2.3.). Uplift and erosion on the footwall side is indicated by erosion and redeposition of reef limestone (Fig. 2.3.7.h). Angular cobbles and blocks in the outcrop south of Plora described in chapter 2.3. also suggest tectonic activity.

Significant local increase in thickness of single units, such as the lagoon deposits at section MS2 indicates local subsidence of fault blocks. Small synsedimentary faults in LFA1 in the Matala area (Fig. 2.3.1.g) also suggest tectonic control on subsidence. While the braid delta systems appear to have prograded westward to southward (Fig. 2.3.11a), the coarser grained fan delta systems found south of Kandhila have prograded northward (Fig. 2.3.11b). Most Fan deltas form as a result of tectonically increased and controlled relief (Dabrio, 1990). Therefore, the Kandhila fan delta complex most likely formed on a steep, tectonically induced relief, while the braid delta system in the Pitsidia – Sivas area indicates a coastline with relatively low relief (Fig. 2.3.11.). Since fan deltas are interpreted to form late during deposition of LFA1, relief intensification and increasing tectonic activity through time can be inferred that eventually led to marine ingression covering most of the area of the modern Messara Plain (Fig. 2.3.11.b). South of Kandhila and Vasiliki, sediments wedge out rapidly towards the basement to the south across the synsedimentary active fault. In the WAT, sediments more gradually wedge out towards the south. An asymmetric fault system with a steep footwall scarp in the south, where coarse grained fan deltas formed and with a gently southward dipping hanging wall to the north as described in Leeder and Gawthorpe (1987) best explains facies distribution found along the southern margin of the Messara Plain and the WAT. The fault system was oriented east – west and separated a basinal area that extended only a few 100m to kilometres further to the south than the limits of the modern Messara Basin from an elevated hinterland in the south (Fig. 2.3.11.). Relief and tectonic offset increased eastward.

The best example for tectonic activity during deposition of LFA2 is found around Mount Kristo Kefali (Fig. 5.3.). Fresh fault surfaces and faults cutting Neogene deposits show that this basement block was uplifted after deposition of sediments. The set of faults to the north of Kristo Kefali (Fig. 5.2.a,b), however, indicates that uplift of the Tripolitza Unit also

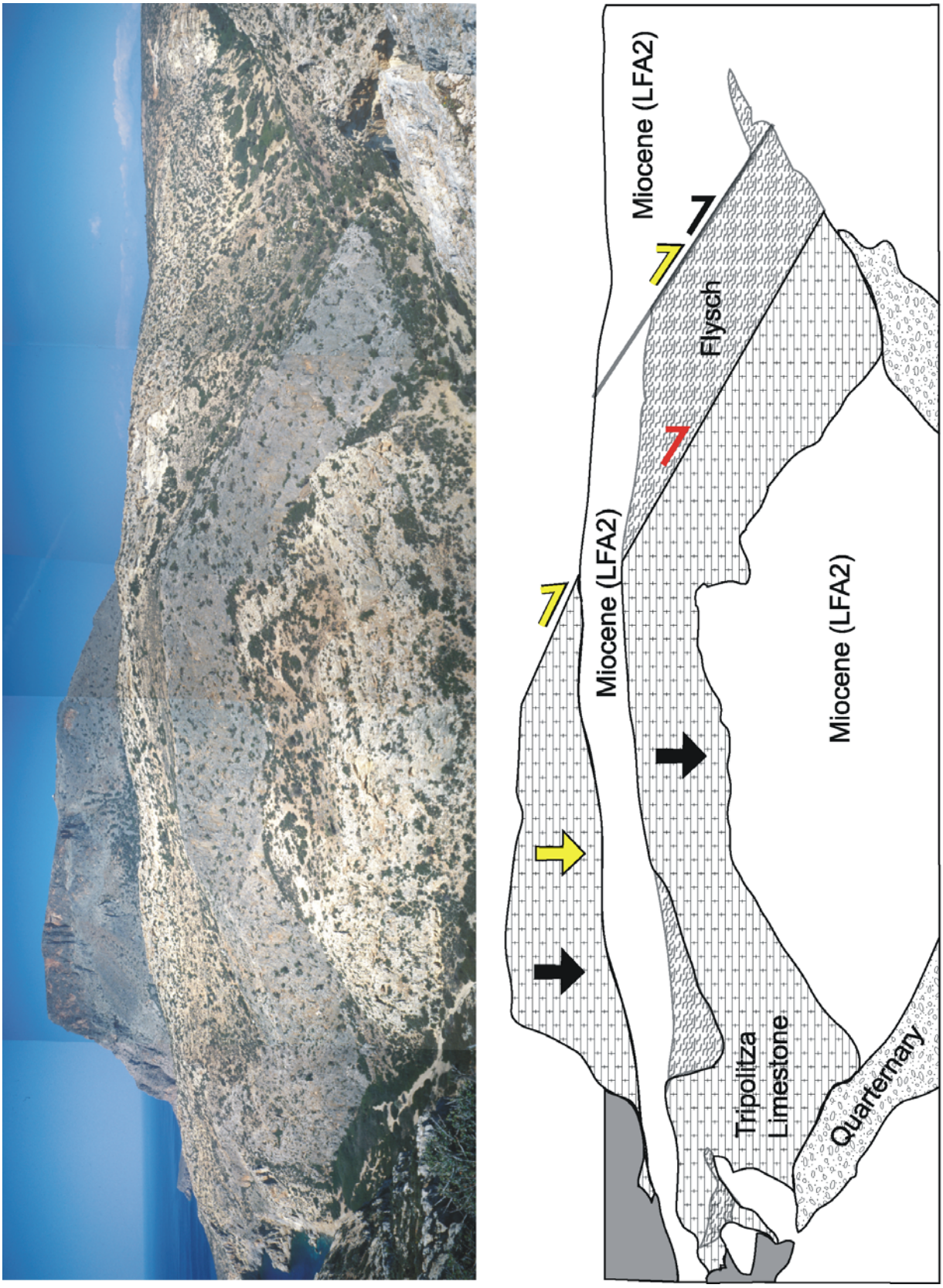

Fig. 5.3.: View of the Kristo Kefali (background) area from the east of Moni Martsalo. The area is dissected by pre-sedimentary (red), synsedimentary (yellow) and postsedimentary (black) active faults

occurred prior to and/or during sedimentation of LFA2. Thereby, Flysch on top of the Tripolitza Unit was eroded on the footwall block. Carbonates of LFA2 with coarse conglomerate at the base (chapter 2.4., Fig. 2.4.2.c,e; section KN, Fig. A1) and the presence of Tripolitza cobbles and boulders (Fig. 2.4.6.h) in the rhodolith floatstone and rudstone facies indicate high submarine relief related to a paleocliff formed by Tripolitza Limestone. Intervals with abundant Tripolitza gravel indicate intermittent tectonic activity. The decrease in grainsize to the east (east of Martsalo Bay, east of the strike slip-fault bounded block, Fig. 2.2.1.) and the presence of sandstone pebbles instead of Tripolitza clasts indicates a position of the paleocliff to the west in a very similar position as the steep modern eastern flank of the approximately 400m high Kristo Kefali (Fig. 5.4.b). This assumption is corroborated by the constant thickness of basal conglomerate in north-south direction. Coastal conglomerates on the northern side of Kristo Kefali (section KN) were deposited on top of the Flysch on the hanging wall side of the 50°- 80° faults that defined the northern limits of a late Miocene basement high. The Neogene extent of the uplifted block to the west and south, however, is unknown. While the modern uplift of the Kristo Kefali block in the north clearly is controlled by faults that are oriented differently from the late Miocene faults (WNW-ESE instead of WSW-ENE), late Miocene faults controlling the formation of the N-S oriented paleocliffs may have corresponded to the orientation of recent faults.

In most cases, synsedimentary faulting is not as evident as around Kristo Kefali. Modern exposures of basement west of Knarkokefala and north of Martsellos Ridge (Fig. 2.2.1.) correspond only partially to Neogene basement highs. The existence of a Neogene basement high around Knarkokefala (Knarkokefala Horst) in a similar position as the large modern exposures of basement is however evidenced by wedging out of Neogene sediments to the north at Martsellos ridge (section Mart, Fig. 2.2.3.; 2.4.2.b) and to the east of Sidheropetra Bay (Fig.2.4.2.a). The rapid change in thickness of the Neogene sedimentary units across Knarkokefala Horst suggests a fault control on basin subsidence. These synsedimentary faults were situated between Martsellos Ridge (section Mart) and Moni Martsalo (section MaN) and east of Vathi and Sidheropetra Bay, defining the limits of the marine basin between Knarkokefala Horst and the Kristo Kefali block. Thus, the southern limits of the Knakokefala Horst apparently were controlled by E-W oriented faults and the western limits by north-south oriented faults. The conjugate fault set controlling Knarkokefala Horst therefore is interpreted to have been oriented similar as the one observed at Kristo Kefali. On the other hand, a change of thickness of Neogene deposits is not observed across SW-NE oriented faults that

control the extent of modern basement outcrops near Knarkokefala (Fig. 2.2.1.; 2.2.3.). The position and orientation of Tortonian faults in the WAT therefore was different from the postsedimentary system.

Synsedimentary uplift in the area around Sivas and Pitsidia that was a depocentre during deposition of LFA1 is indicated by the occurrence of a hiatus between sediments of LFA2a and LFA2c (Fig. 2.2.4). In the Moni Odhiyitria area, LFA2c is absent and LFA2b is represented only by 15m of bioclastic packstone. While the absence of the RP facies or RFR3 facies with corals may be related to a position close to the shoreline, the low thickness compared to LFA1 and LFA2a indicates low subsidence or even uplift of the area similar as in the Sivas area (Fig. 2.2.1; 2.2.5). Generally, differences in thickness of sedimentary units between the north of the WAT (section MO1, MS3) and the south (sections VO, MN) suggest differential subsidence in consequence of synsedimentary tectonics.
The basin margin to the east is not preserved in outcrop due to the recent uplift of the Asteroussia Mountains. East of Moni Martsalo, where Neogene sediments appear to thin out gradually, a strong structural control is not indicated. At the southern margin of the Messara Plain (Vasiliki area), a similar situation as in the Sivas - Pitsidia area is indicated since LFA2 is represented only by calcareous sands (CS facies) capped by a rudstone with pebbles (LFA2c equivalent).

The timing and sense of tectonic activity along the 70° oriented structure that forms the boundary between the WAT and the Messara Plain and that offsets marl of LFA3 described in chapter 2.5. against carbonate deposits of LFA2 described in chapter 2.4. appears to be enigmatic. While the fault plane is nowhere visible, it has been interpreted by ten Veen and Kleinspehn (2003) to represent an important sinistral strike slip system. In fact, the apparently large extent of the possible fault and the juxtaposition of lithologically very different units that are interpreted to have been deposited in different water depths and the absence of any facies transition suggest considerable postsedimentary offset. On the other hand, at the eastern flank of the Ida Massif, very rapid lateral facies change from coarse sediments to laminated marl due to synsedimentary tectonics is observed (Reuter, in prep.). Moreover, lithoclasts found at the top of section KO (Fig. A5) are very similar to Neogene limestone found in the area of Matala (Fig. 2.5.1.c. see chapter 2.5.). In this context, large scale postsedimentary sinistral offset is unlikely, since in the central Messara Plain similar limestone rarely occurs along strike of the fault. Therefore, the presence of a synsedimentary fault system, which

defined the oceanward limit of the outer ramp sedimentary environment to the north and eventually resulted in uplift and exposure of the limestone during deposition of the marls is indicated. Thus, if the lithoclasts originate from the Matala area, post-Neogene movement of this fault should be in the order of the now observed vertical offset of about 50m.

Stress fields, their evolution through time and control on paleogeography

Late Seravallian – earliest Tortonian

The orientation of the sedimentary basin during deposition of LFA1 clastics was E-W (Fig. 2.3.11.). Synsedimentary normal faults controlling the southern margin of the basin have a similar orientation. The focus of sedimentation in the resulting half-graben was along the margin of the modern Messara Plain and in the north of the WAT. Extension was predominantly N-S and controlled the southward extent of siliciclastic deposits (Fig. 5.4.a; see Chapter 2.3.). The age of the base of the overlying carbonates in the Matala area, defined by Sr chronostratigraphy (see chapter 4) is early Tortonian (10,5 Ma). Therefore synsedimentary extension oriented N-S and related deposition of siliciclastic deposits occurred in late Seravallian to early Tortonian times. According to (Mercier et al., 1989), due to the weight of thickened crust in the southern Aegean arc, the maximum stress σ_1 can be assumed to be equal the vertical stress σ_z. N-S extension in the Seravallian – early Tortonian therefore indicates a stress field with $\sigma_1 > \sigma_2 > \sigma_3$ and with σ_3 being oriented N-S. These results are in agreement with early N-S extension resulting in E-W oriented basins that parallel basement folds found in various parts of Crete (Meulenkamp et al., 1988; ten Veen and Postma, 1999; Fassoulas, 2001). Early N-S extension has been interpreted to be a consequence of decompaction of the thickened crust of Crete in the process of exhumation of HP/LT rocks (Jolivet et al., 1996; Fassoulas, 1999).

Early to middle Tortonian

The orientation of fault bounded horsts in the WAT shows that extension during the deposition of LFA2 carbonates in the Tortonian was N-S as well as WSW-ENE to W-E (Fig. 5.4.b). This can be described as a consequence of σ_2 becoming equal to σ_3 and resulted in

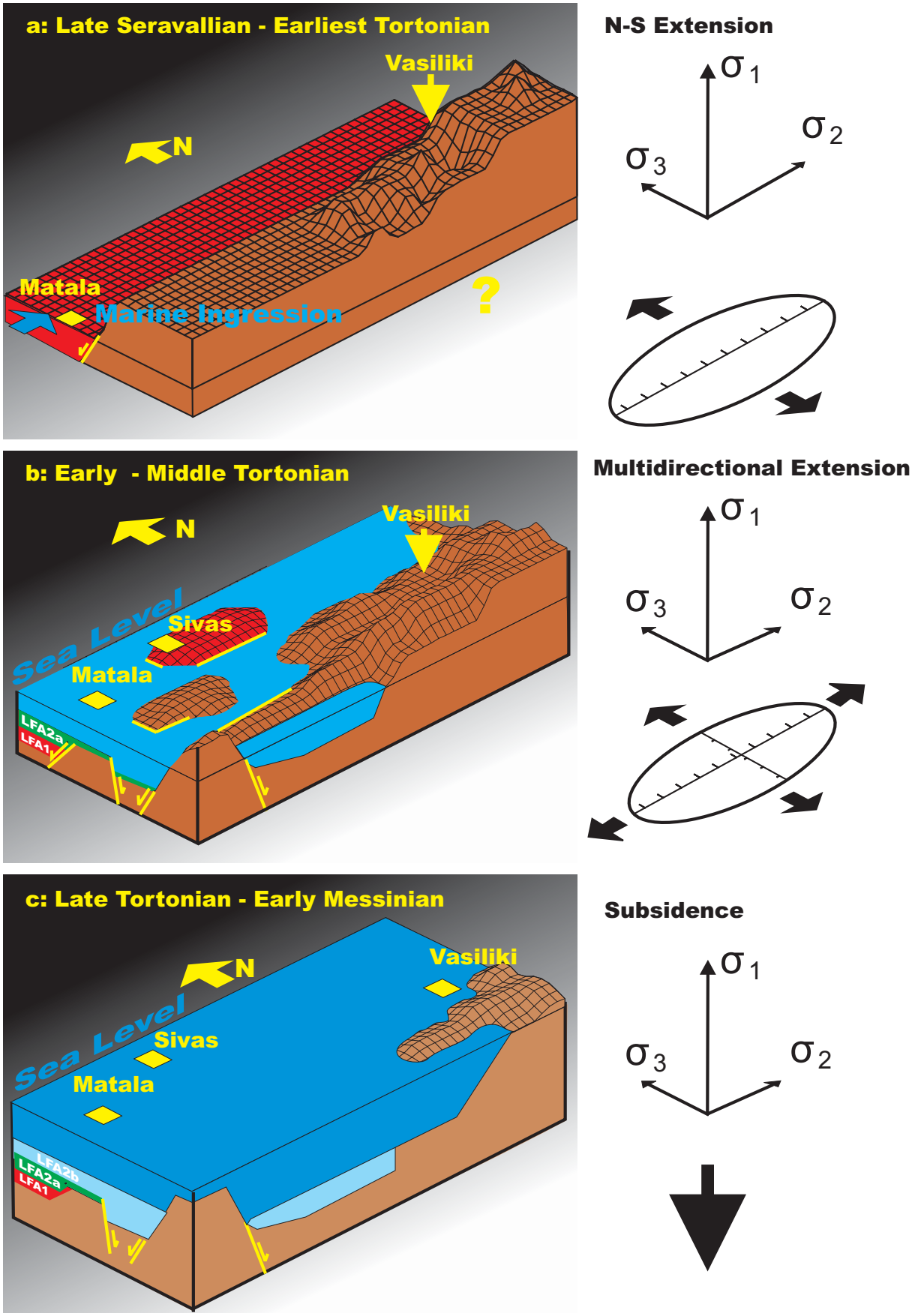

Fig. 5.4.: Models of tectonic control on the paleogeography of the WAT and the southern Messara Plain in the course of the late Seravallian to early Messinian

progressive fragmentation of the sedimentary basin. Especially in the south of the WAT, faulting lead to the formation of considerable relief: Relative crustal movements resulted in uplift of the Tripolitza Unit that is covered by Flysch in other parts of the WAT and in local subsidence and uplift of parts of the WAT reflected by differential thickness of sedimentary units. Since in the southern WAT, sediments of LFA2 overlying basement can be correlated with LFA2 in the Matala area, the age of the sedimentary basins in the south is early Tortonian or younger. While the thickness of LFA2a is highest in the Matala area, LFA2b has the highest thickness in the Vathi-Martsalo area. This indicates a shift of the area of maximum subsidence to the south after 9,5Ma. Fragmentation of the originally E-W- oriented basin is also observed in the northern part of the WAT, where in the area around Sivas and Pitsidia in contrast to the Matala area, synsedimentary uplift is indicated by an unconformity separating LFA2a and LFA2c.

An increasing structural fragmentation of central Crete during the Tortonian has also been observed by Meulenkamp et al. (1979), Angelier et al. (1982) and ten Veen and Postma (1999). The character and orientation of synsedimentary faulting in the WAT resembles the 100° and 20° fault system found by ten Veen and Postma (1999) that resulted in an egg box pattern of horsts and grabens in central Crete. However, the 115° fault north of Kristo Kefali was active after deposition of Neogene sediments while synsedimentary faulting occurred in WSW - ENE direction.

Multidirectional extension with $\sigma_2 = \sigma_3$ has been interpreted to be a consequence of the roll back of the Helenic Subduction zone during the upper Miocene and related southward expansion and curvature of the Hellenic Arc (Le Pichon and Angelier, 1979; Angelier et al., 1982; Meulenkamp et al., 1988; Mercier et al., 1989; ten Veen and Postma, 1999; ten Veen and Postma, 1999; Fassoulas, 2001).

Outcrops along the southern rim of the Messara Plain and in the Kandhila - Vasiliki area show that the input of coarse clastic material has stopped after the deposition of the siliciclastic succession. Therefore, this region in contrast to other parts of central Crete (Reuter, *in prep*.) appears to have been characterised by relief reduction. Similarly, the fact that siliciclastic input was considerably reduced in the WAT after deposition of the RP horizon which is related to the Tor2 sequence boundary of Haq et al. (1988), (Fig. 4.6.) indicates that at least from the middle Tortonian onward, fragmentation did not lead to the uplift of large hinterland areas that would likely have been the source of clastic input. Additionally, eustatic sea level rise potentially led not only to sediment starvation at the coast but also to reduction of the subaerially exposed hinterland area. A different reason for reduction of siliciclastic input may

have been increasingly arid climatic conditions that favoured the deposition of carbonate sediments instead of siliciclastic deposits. A shift to predominantly carbonate deposition in the Upper Tortonian is observed not only all over Crete (Meulenkamp et al., 1979) but also in many other parts of the Mediterranean (Buchbinder, 1996; Esteban et al., 1996).

Late Tortonian – early Messinian

Compared to the area of the Central Iraclion Ridge (Reuter *in prep*.) and the southern margin of Crete (Kristo Kefali area), relative tectonic motions were insignificant in the WAT. The area was then gradually subsiding in the late Tortonian and carbonate sediments were deposited on the basement horsts (Fig. 5.4.c). Increasing water depth is indicated all over the WAT during the deposition of the upper part of the carbonate succession by the distribution of foraminifera and red algae as well as by the finer-grained lithologies at the top of the succession. Eventually, in the course of the Tortonian, even in the Kristo Kefali area, where the relative highest uplift occurred in the WAT, local input of lithoclasts stopped and off-shore marl (LFA3) was deposited. At section FN, marl, which is interpreted to represent basinal deposits (chapter 2.5.) overlies near-shore sandstone (LFA1) and 4m of limestone of LFA2 that in its fossil content is very similar to the limestone found in the WAT. The low thickness of limestone below marl indicates high rates of subsidence in the area of the central Messara Plain. In the area of the Central Iraclion Ridge and southern Iraclion basin, however, continuing tectonic activity is observed (Reuter *in prep*). Nevertheless, backstepping of near-shore marine facies in response to over all subsidence also occurs in this area.

On a regional scale, overall subsidence is observed in Late Tortonian sediments. Rates of subsidence are moderate in the WAT except in the Kristo Kefali area in the south of the WAT. High subsidence rates are indicated in the area of the Messara Plain, where between Komos and Festos, thick successions of LFA3 where deposited. High relief and tectonic activity is indicated in the north of the Messara Plain. The Central Iraclion Ridge area is therefore interpreted to have formed an E-W oriented fault scarp that found its continuation along the modern southern rim of the Ida massif. Accordingly, the WAT and the Messara plain are interpreted to represent the dip slope ramp of a half-graben system on the hanging wall side to south of the scarp. This interpretation is corroborated by the northward increase of subsidence to from the WAT to the Messara Plain. Additional to the southward dipping main fault north of the Messara Basin, the dip slope ramp was also dissected by northward

dipping synsedimentary faults such as the 70° fault that controlled the rapid facies change between the WAT and the Messara basin. High subsidence at the southern margin of the WAT may have been related to a fault scarp to the south of Crete, a precursor of the modern trench system. Marl of LFA3 deposited in consequence of half-graben formation and high rates of subsidence has been dated to be Upper Tortonian to Messinian by Zachariasse (1975), Langereis et al. (1984) and Hilgen et al. (1995). In the late Tortonian, a return to dominant N-S extension is thus observed.

Messinian - Recent

Coarse turbidites or slumps are found at the top of successions of offshore marl in the Messara Plain (LFA3, chapter 2.5.). Increase in grain size indicates relief intensification and higher transport energy or a more proximal source of the turbidites. The coarsest deposits are found at the northern margin of the Messara Plain at Faneromeni (Fig. 2.5.1.f). Extensive slump masses (Fig. 2.5.1.e) occur 2km south of Timbaki (Fig. 1.4.1.) on top of thin bedded marl but the stratigraphic relationship is not well established. Lower grain sizes to the east and south indicate more distal positions of these areas to the source of turbidites. These turbidites contain rounded polimict pebbles and gravel and angular fragments of Neogene sediments including corals, red algae and large foraminifera (Fig. 2.5.1.c). Besides lithoclasts, these turbidites also contain bioclasts of various fossils, including *Porites, Halimeda,* vermetids, bivalves and planktonic foraminifera. This reflects two processes: The uplift and lithification of older Neogene deposits and the continuing formation of shallow water sediments at the basin margins. These basin margins apparently were instable and episodically collapsed. Instability may have been a consequence of increased relief and/or tectonic events. The exact timing of these events and begin of relief intensification is not known. Abundant *Porites* fragments found among components unlithified prior to deposition in the turbidites, however, indicate a Pre-Pliocene age since from the Pliocene on, hermatypic coral reefs are unknown from the Mediterranean (Esteban, 1996). In accordance to Sr isotope ages (chapter 4) of marl deposits in the Agia Varvara area, a Messinian age of the mass flow deposits is therefore plausible. Slumps, reworking and formation of breccias in the northern Iraclion basin have been interpreted to be a consequence of the Messinian salinity crisis (Meulenkamp et al., 1994). On the other hand, coarse conglomerate overlying mass flow deposits at Faneromeni may correlate to coarse conglomerate of the Galini Fan to the west that is of Pliocene age and

younger (ten Veen and Kleinspehn, 2003). The fan is interpreted by the authors to represent the onset of extensive basin scale faulting (ten Veen and Kleinspehn, 2003). Since the age of the mass flow deposits is not well defined, their origin remains unresolved. Events that may have increased relief of the shorelines and triggered the deposition of coarse grained mass flow deposits are 1) sea level fall during the Messinian salinity crises, 2) onset of extensive faulting or 3) coastal erosion associated with the Lower Messinian sea-level lowstand (Fig. 4.1.).

Late Pliocene – Holocene faulting has been found by ten Veen and Kleinspehn (2003) to have occurred dominantly along 70° oriented sinistral strike-slip faults. The orientation of some major faults in the northwest of the WAT has a similar orientation. However, as demonstrated before, most postsedimentary faults found in the WAT have low strike-slip components. It is also unlikely that the uplift of central Crete from low elevations in Upper Miocene times to the present elevations of up to 2500m occurred mainly along strike slip fault systems. A reactivation of Upper Miocene E-W striking half graben systems oriented similar as the modern north rim of the Messara Plain appears to be a better explanation.

6. Paleoecological factors in Miocene carbonates of Crete: an evaluation

Introduction

In order to evaluate the influence of climate change on depositional environments in the Neogene of central Crete, the response of two biotic groups, foraminifera and non-geniculate coralline red algae to ecological factors has been examined in detail (see chapter 3.). Foraminiferal associations appear to be controlled by a variety of ecological parameters. Preferences of certain taxa, however, reflect the preferences of their symbionts that may be very specific and can be used to evaluate environment conditions. Nevertheless, in combination with the preferences of their host, the picture may become very complex and may be best described by specific facies associations as in Haunold et al. (1997). On the other hand, non-geniculate coralline red algae have proved to be invariably limited in their occurrence by light intensity and water temperature. While this response is clearly visible on genus-level, the response of taxa to other factors such as nutrients and substrate is more individual for each species and much harder to evaluate. Applying the results of analysis of skeletal associations found in the WAT, three ecological parameters, temperature, water depth and nutrients and their relationship to global climate change will be discussed in detail below. Other parameters such as sediment input, turbulence and hydraulic energy are linked to these parameters.
Salinity is a limiting factor in some environments of LFA1 but the absence of typical brackish or hypersaline associations in LFA2 and 3 suggests that salinity was normal marine. The influence of biotic interactions is hard to evaluate but is important regarding the effects of shading or for epiphytic organisms and therefore potentially influences the distribution of certain foraminifera and coralline red algae. Other influences such as predation are out of scope of this study.

Temperature

Since the recognition of non-tropical carbonates in modern and in ancient settings (Lees and Buller, 1972; Carannante et al., 1988; Nelson et al., 1988; Brachert et al., 1996), temperature is known to be a key factor controlling the character of carbonate sedimentation. For many reasons, however, it is difficult to relate changes in sedimentary environments and skeletal

associations to absolute temperature values. The best approach is, to use temperature-sensitive organisms as markers for the crossing of certain temperature thresholds. The most important threshold with the greatest impact on sedimentary environments is between (warm) temperate and tropical environment when framework-forming zooxanthellate corals occur (Lees and Buller, 1972; Betzler et al., 1997). Healthy coral reefs are found in areas were minimum temperatures do not fall below 18°C (Veron, 1995). Another marker is the occurrence of large benthic foraminifera that define a temperature threshold of 11°C-12°C and separate cold temperate environments from warm temperate environments (Betzler et al., 1997). Faunal markers as a measure whether water temperatures exceed certain levels have to be treated with care for the following reasons: 1) it may not be the annual minimum temperature that is limiting the occurrence of certain biotic elements; 2) measured temperature values usually relate to surface temperatures, whereas the critical organisms may live at various water depths and water temperature may not gradually decline with water depth; 3) the minimum temperature at which the organisms thrive depends on various ecological factors other than water depth. For example, the threshold temperature at which coral reefs occur may be elevated due to increased nutrient levels (Hallock and Schlager, 1986).

In the present study, non-geniculate coralline red algae have been employed as an indicator for water temperature. The advantages of their non-linear limitation by water temperature and light intensity have been discussed in chapter 3.3. Water temperature and water depth indices calculated from coralline distribution have been compared to the occurrence of large benthic foraminifera and framework forming zooxanthellate corals. An index > 0,5 correlates with the occurrence of zooxanthellate corals and foraminifera with low tolerance for cold minimum temperatures. High indices, however, are also found in intervals without zooxanthellate corals (Fig. 3.3.12.a-d). In this case the absence of corals may relate to water depth or to a threshold temperature that is lower for the occurrence of “tropical” red algal associations than for the formation of zooxanthellate coral reefs. Therefore, high temperature indices may indicate both, warm temperate and tropical conditions. “Shallow” warm-temperate associations that are close to the threshold of the tropical biotic association correspond to the rhodozoan association of Halfar et al. (2000) where red algae are abundant together with non-framework forming zooxanthellate corals. Indices in intervals with abundant large benthic foraminifera are between 0 and 0,5 and therefore also indicative of warm temperate environments. Indices based on coralline red algae thus are a high resolution palaeo-thermometer for warm temperate environments.

As discussed before, using a combination of coralline genera for the calculation of water temperature indices largely eliminates the influence of other ecological factors such as water depth and nutrients. Due to annual variability of surface water temperatures and non linear temperature profiles in the water column, the index can be only an approximation for absolute surface temperatures: According to the data from Crete, a water depth index of 0 relates to an annual minimum surface temperature of 14°C or lower, as defined by the annual minimum temperature that *Amphistegina lessonii* tolerates (Langer and Hottinger, 2000). On the other hand, a water temperature index of 1 can be related to an annual minimum surface temperature of a little less than 18°C or higher, as defined by the occurrence of zooxanthellate corals.

It appears to be even more difficult to use these indices as indicators for global climate and to evaluate the influence of global climate on depositional environments since global influence is likely overprinted by local factors (see discussion in the following chapters). Nevertheless, comparison of water temperature indices with the $\delta^{18}O$ record of Hardenbol et al. (1998) which displays a combined record of change in global water temperature and sea level (Abreu and Anderson, 1998) shows striking similarities (Fig. 6.1.): To be comparable with data on global climate, red algal temperature indices were calibrated to absolute time by Sr chronostratigraphy. Althoug resolution of correlation by Sr chronostratigraphy is low above the Tor2 sequence boundary, the two independent datasets, time calibrated red algal indices and global $\delta^{18}O$ values show similar patterns. Change in red algal indices thus can be linked to global change in water temperatures. Coralline red algae therefore are not only indicators for ecological parameters in the depositional environment but also for global climate. Consequently they can be used for climatically tuned high resolution chronostratigraphy (Brachert et al., 2001). Correlation of sections of the WAT based on temperature indices (Fig. 6.2.) is in agreement with lithostratigraphic correlation (Fig. 2.2.3.-2.2.6.). During deposition of LFA2, there are two intervals, between 10 and 9,5 Ma and between 9 and 8Ma when persisting high temperature indices and $\delta^{18}O$ values below 2 indicate temperatures favourable for zooxanthellate corals. In the largest part of the WAT, the twin unit of coral carpets in LFA2c marks the longest interval between 9 and 8Ma. The gap in coral carpet formation between both units can be related to a climatic detoriation at 8,4Ma expressed by an increase in $\delta^{18}O$ and lower temperature indices. The older warm interval in LFA2a is characterized by local formation of single colonies of zooxanthellate corals (section Vathi) in the WAT and by the formation of coral reefs elsewhere in central Crete (section AT, Fig. 4.5.; Reuter *in prep.*). Thus, in the lower interval, the occurrence of framework forming zooxanthellate corals in the

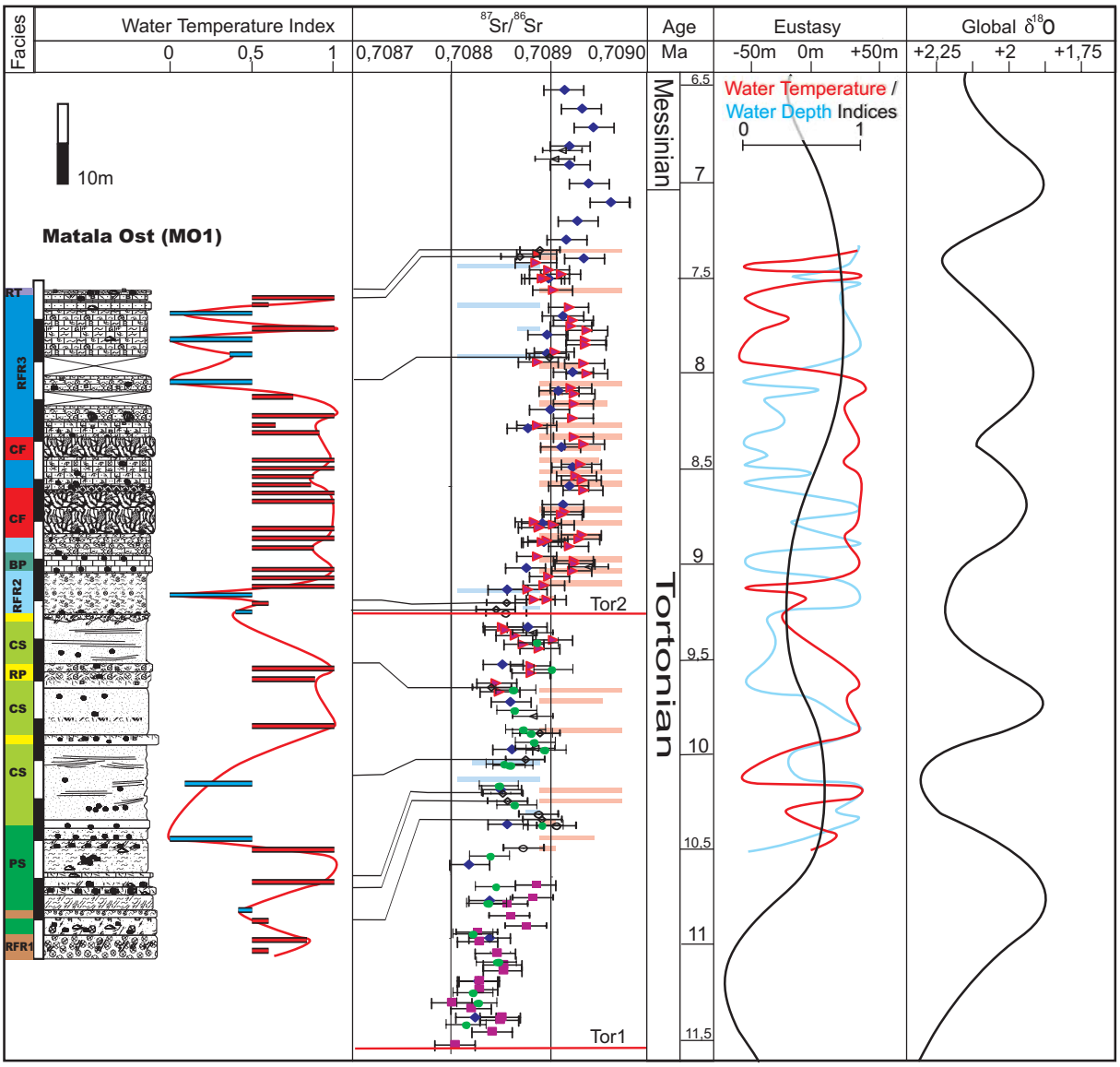

Fig. 6.1.: Water temperature and water depth indices based on analysis of coralline red algae in section MO1 are calibrated to the absolute time scale for section MO1 established in chapter 4 by correlation of fluctuations in the global Sr isotope record and measured Sr isotope values in section MO1. Temperature (red) and water depth (blue) indices are converted into curves for comparison with global oxygen isotope record taken from Hardenbol et al. (1998). Sequence boundaries Tor1 and 2 (red line) are also from Haq et al. (1987) but named according to Hardenbol et al. (1998). All data are calibrated to CK92

WAT apparently is limited by other ecological factors. A third warm interval beginning in the latest Tortonian is indicated by the occurrence of single coral colonies and thin carpets or patches of corals in the Matala area and at the top of sections MaN and KL. It relates to a high water depth index at the top of section MO1 and decreasing $\delta^{18}O$ values after 7,5Ma. No coral reefs that that can be unequivocally related to the 9-8Ma climatic optimum are found in central Crete (Reuter *in prep.*); a fact that is possibly related to high subsidence of this area during this period and the non-preservation of shallow water sediments in the geological record due to later uplift. However, extensive barrier reef formation on Mallorca (Llucmajor

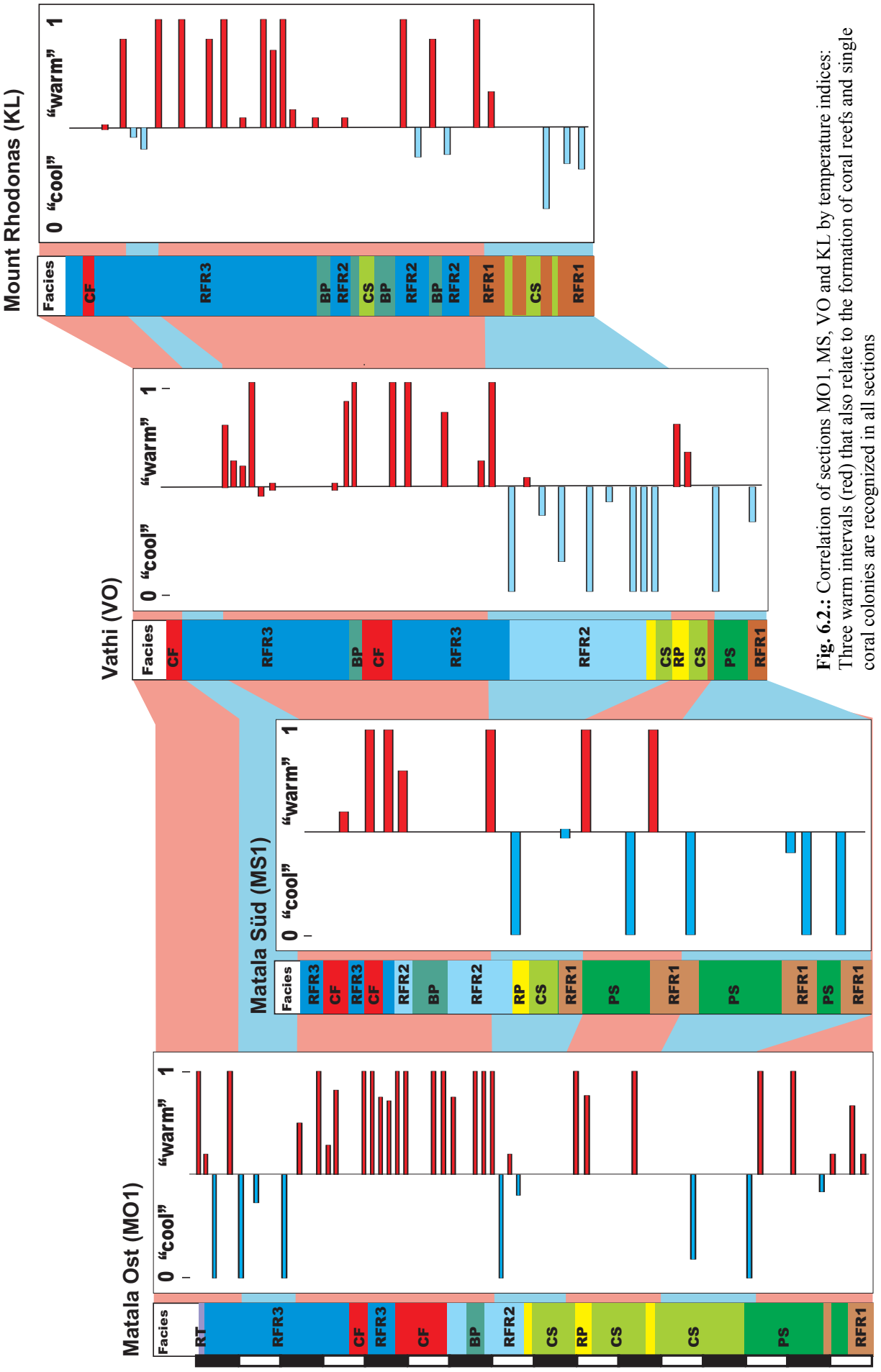

Fig. 6.2.: Correlation of sections MO1, MS, VO and KL by temperature indices: Three warm intervals (red) that also relate to the formation of coral reefs and single coral colonies are recognized in all sections

Platform) falls into this time (Pomar et al., 1996). The occurrences of zooxanthellate corals and coral reefs in LFA1 and 3 can also be related to minima in the $\delta^{18}O$ record (Fig. 6.1.): Some of the coral reefs of LFA1 may relate to the low $\delta^{18}O$ interval between 11 and 10,5 Ma. The youngest warm interval recorded in LFA2 deposits of the WAT may relate to the late Tortonian warm period when coral reefs were common in the Mediterranean (Esteban, 1996).

Water depth

As recognized by Lees and Buller (1972) and Carannante et al. (1988), tropical deep water sediments may resemble non-tropical shallow water sediments in their biotic makeup. To draw a conclusion on climatic conditions, it is therefore usually necessary that to know the depositional depth of the analysed sediments. This is not the case if coralline red algae are used as climate indicators: As discussed before, the red algal association in deep warm environments differs from the association in cold shallow environments. Therefore water depth indices can be regarded independent from temperature indices. Similar as for water temperature, however, it is difficult to draw quantitative conclusions on water depth at times of deposition: Since the amount of light that is needed or tolerated is the controlling factor on red algae and other biotic water depth indicators, various factors might influence the water depth in which a certain association is found: Water turbidity is most important but shading by other organisms or reflectivity of the sea floor are also key factors.
Nevertheless, by comparison with recent occurrences of the analysed coralline red algae, water depth ranges can be defined: Data from eastern Australia (Lund et al., 2000) suggest that *Lithothamnion* and *Mesophyllum*, which are the most important deep water genera in the analysed material from the WAT, are most abundant at water depths below 40m. This is in agreement with the abundance of *Amphistegina lessonii* in sediments of the WAT with high water depth indices. It also agrees with the hydrodynamic interpretation that sediments with high water depth indices are relatively low energy outer ramp deposits: The upper limit of the outer ramp is defined by the position of the storm wave base (Burchette and Wright, 1992) which is at 30-40m water depth in the modern Mediterranean (Betzler et al., 1997). Water depth indices between 0 and 0,5 are typical for the CF facies, which represents a similar environment as *Porites* carpets that are reported from water depths of no more than 25m in the modern Red Sea. Occasional higher water depth indices in the lower coral horizon in section MO1 are a consequence of the occurrence of *Mesophyllumm sancti dionysii* in shaded

environments within the carpet. Single tabular coral colonies occur in intervals with intermediate water depth indices. These intervals therefore can be linked to the most shoreward reaches of RFR3 facies and may thus correspond to water depth between 25m and 40m. Large funnel shaped single colonies with diameters >50cm occur where shallowing is indicated.

More than temperature, water depth is a function of local parameters such as tectonically controlled subsidence and sediment accumulation. Climatically tuned chronostratigraphy based on water temperature indices shows that thickness of time-equivalent sedimentary packages is variable in different sections (Fig. 6.2.). Thickness of time-equivalent stratigraphic intervals depends on the combined effects of subsidence, eustasy and sediment input. Sediment accumulation is limited by accommodation space, which is defined by storm wave abrasion depth. Thus, in conformable successions, the amount of sediment accumulated between two units that were deposited at storm wave base is a measure for the amount of subsidence and eustatic rise (relative sea-level rise). In the WAT, facies that are deposited at or close to the lower limit of storm wave abrasion are the CS, RP and BP facies (see chapter 2.4.) while the CF facies is formed within water depths affected by storm wave abrasion. Differences in thickness of RFR (for example the MRB, see chapter 2.4.; RFR2; Fig. 6.2.) and PS units therefore are, as has been discussed in chapter 5, the result of differential tectonic subsidence. Widespread shallowing reflected by the deposition of the coupled CS-RP facies and CF facies and deepening reflected by widespread deposition of the MRB on top of the RP facies on the other hand is interpreted to reflect a eustatic signal (sections MO1, MS1, VO). The formation of stacked sandstone (CS) – limestone (RP) couplets has been interpreted to reflect higher order eustatic change (see chapter 4). The eustatic signal, however, appears to be superimposed by local influences in the Rhodonas area (section KL) since none of the widespread sedimentary horizons (RP, CF, MRB) interpreted to relate to eustatic change are found in this area.

Although sedimentary units in the WAT are thought to reflect eustatic sea level, the correlation of water depth indices with the $\delta^{18}O$ curve of Abreu and Anderson (1998) is poor (Fig. 6.1.). This is a consequence of smoothing the oxygen isotope records in the process of the calculation of the curve to reflect fluctuations in the order of about 1m.y. (Abreu and Anderson, 1998). Correlation with the global seawater Sr isotope record on the other hand is well in the part of the section older than 9,1 Ma (Fig. 6.1). As discussed in chapter 4, conformable sedimentary sections reflect short term eustatic fluctuation in the order of few 100k.y. This is reflected by the facies change from CS to RP and RP to RFR2 that

corresponds to fluctuation in Sr isotope and water depth index values (Fig. 6.1.). Additionally, however, the sedimentary succession in the WAT reflects long-term change in water depth: During 3rd order sea level fall, stacked CS-RP horizons are deposited across the WAT whereas during long-term sea-level rise, rhodolith rudstone or thickly bedded packstone is deposited. Widespread coral carpet formation occurs during late 3rd order transgression and highstand. Correlation between water depth indices and Sr-isotope values is poor in the upper part of MO1 younger than 9,1Ma. This is partially due to insufficient Sr isotope data points for high resolving correlation between Sr isotope values and water depth index values. However, since carbonate sediment accumulation is mainly a function of carbonate production and shifting loci of the site of maximum carbonate production (carbonate factory) in dependence of ecological factors (Pomar, 2001), it is not surprising, that the siliciclastic rich interval (CS-CR lithofacies) better reflects eustatic sea-level change than the overlying intervals (LFA2b and c) with pure carbonate sedimentation. It will be discussed in more detail in chapter 7, in which ways carbonate producers take part in shaping depositional environments in response to ecological parameters.

Nutrients

The influence of the availability of nutrients on a carbonate sedimentary environment has been overlooked for a long time. Therefore the problem why in otherwise favourable areas coral reefs are not present or poorly developed remained unresolved. Hallock and Schlager (1986) found that elevated nutrient levels lead to poisoning and bacterial infestation of corals on one hand and favour smaller fast growing organisms in the competition for space and light on the other. This applies also to other organisms that have comparatively slow growth rates and have adapted to oligotrophic environments by symbiosis with zooxanthellate. Another way of adaptation is the specialized life cycle of large benthic foraminifera that produce relatively few and large offspring (Hallock and Schlager, 1986).

Nutrients essential for the existence of living organisms are ionic phosphate, nitrogen, iron and silicon. Of these, phosphate is a limiting factor especially in ecosystems of enclosed marine basins such as the Mediterranean and the Red Sea. Eutrophication by both nitrate or phosphorous brings stress to these phosphate limited communities (Brasier, 1995)

Recently, much importance has been attached to nutrients as a factor controlling biotic associations in the Mediterranean during Miocene times (Brandano and Corda, 2002; Pomar

et al., 2004). Based on datasets on terrestric climate from Spain and Germany and apparent diachrony in the occurrence of reefs in the Mediterranean, Pomar et al. (2004) concluded that tropical conditions prevailed in the Mediterranean during the entire Miocene and that therefore other factors than temperature such as nutrients must have controlled biotic associations. Data from Crete presented here with an improved resolution, however, show that this is not the case during the Tortonian when zooxanthellate corals were restricted to warm periods. Rhodalgal or foramol sediments with larger benthic foraminifera are common in the Mediterranean in Miocene times. Since most larger benthic foraminifera occur only in oligotrophic environments (Langer and Hottinger, 2000), most Mediterranean sediments are not likely to have been deposited under high nutrient conditions. Little is known about the trophic tolerances of non-geniculate coralline red algae. The studied material from Crete indicates that the response to increased nutrient levels is individual on species level. A lower proportion of red algae in the PS facies, where increased nutrient input is indicated by foraminiferal associations (see chapter 3), however suggests that non-geniculate coralline red algae are generally susceptible to nutrient input. It is also unlikely that slow growing red algae profit from high nutrient input, which promotes fast growing organisms in competition for space. Nevertheless, data of (Halfar et al., 2004) suggest that red algae tolerate short periods of annual eutrophication in consequence of upwelling. Besides upwelling, the sources of nutrients in seawater are mainly continental runoff and advection (Hallock and Schlager, 1986). Upwelling as a source of nutrients depends on the availability of cold, nutrient rich deep-sea waters. In the modern Mediterranean, the availability of nutrients in deep water is limited by the Mediterranean circulation pattern (anti-estuarine circulation, Seibold (1970): Relatively warm and nutrient poor Atlantic surface water flowing in across the Strait of Gibraltar sinks and forms Mediterranean deep water. If the Strait of Gibraltar in the Tortonian was equally limited in depth a situation similar to the modern Mediterranean is indicated. Therefore, a general eutrophication of the Mediterranean appears to be unlikely. Nutrient input by continental runoff, on the other hand, may have locally played an important role, especially if increased by orogenetic processes. In central Crete, decrease in siliciclastic deposition at both, the LFA1-LFA2 and LFA2a-2b transitions reflects a decrease in continental runoff in consequence to relief reduction in the hinterland. Data shown in (Pomar, 2001) indicate a period of increased humidity in the early Tortonian and an arid period in the later Tortonian. This indicates that the decrease in siliciclastic input observed in the WAT and elsewhere on Crete (Meulenkamp et al., 1979) in the course of the Tortonian also reflects a change from humid to arid climatic conditions.

The longer oligotrophic and warm interval between 9Ma and 8 Ma with widespread coral growth in the WAT correlates with the arid period shown in (Pomar, 2001). A change from arid to humid conditions may, however occur in much shorter intervals than indicated by (Pomar, 2001): An interval of warm and during the winter humid climate is indicate by floral associations from the Upper Tortonian of the Ierapetra Basin (Sachse and Mohr, 1996). Similarly, the presence of coral reefs and larger benthic foraminifera in LFA1 indicates that despite of over all humid climatic conditions, nutrient levels were relativily low in intervals. An arid interval in the late Seravallian- early Tortonian may be reflected by widespread occurrence of the laminated marly limestone facies deposited in a hypersaline lagoon southeast of Matala.

7. Depositional environments and their response to climate- and sea-level change

7.1. Evolution of depositional environments in the Neogene of central Crete

Late Seravallian (?) to early Tortonian extensional basin (LFA1)

Sedimentation during this period was strongly controlled by pre-existing topography and tectonic activity. During deposition of LFA1 increasing tectonic influence is observed (chapter 5). It resulted in the formation of a steep footwall scarp that limited the Neogene basin to the south and a hanging wall dip slope ramp to the north of the WAT (Fig. 2.3.11.; 5.4.a). Initial half-graben formation is reflected by an east-west orientation of the area of maximum subsidence. On the southward inclined dip slope ramp, braid river deltas evolved. This system shed high amounts of siliciclastics into a low relief shallow marine basin that formed in the area of the highest subsidence. The largely sand sized material was transported along shore and behind resulting sand bar systems, extensive, predominantly estuarine lagoons formed (Fig. 2.3.11.a). Carbonate production was low compared to siliciclastic input. In the course of increasing tectonic activity fan deltas formed at the footwall scarp, which was more pronounced in the Vasiliki area than in the northern WAT. Contemporaneously, marine ingression occurred over the largest part of the basin and resulted in deposition of marine sands in the basin and the formation of coral reefs along its shorelines. Sedimentation rate kept up with relative sea-level rise and was maximal in the area of maximum subsidence north of the footwall scarp. Biotic associations show that the basin floor remained within the photic zone. Common trough cross-bedding suggests reworking by waves and thus deposition above storm- or fair weather wave base. High sedimentation rates and substrate instability in shallow sandy environments prevented the formation of coralline red algal dominated deposits.

Floral associations typical for humid environments and the dominance of estuarine deposits indicate that high siliciclastic input was not only a consequence of high relief but also of humid climatic conditions. It was likely related to high rates of chemical weathering and high nutrient input. However, the widespread occurrence of hypersaline lagoons at a certain stratigraphic level indicates intermittent arid conditions. Floral associations and benthic foraminifera imply warm temperate to tropical conditions. The *Crassostrea – Terebralia* association likely related to the occurrence of mangroves indicate tropical conditions even before the first coral reefs formed. In the upper part of LFA1, formation of coral reefs on

abandoned delta lobes and abundant limestone in coarse coastal deposits indicate a return to (semi-) arid conditions.
Complete and conformable facies successions including delta, estuary and shallow marine deposits suggest that subsidence was high enough to prevent erosion of older deposits. This implies that high rates of subsidence overprinted eustatic influence in the sedimentary record. Persitent warm climatic conditions may be related to the warm interval before 10,5 Ma indicated by low oxygen isotope ratios (Fig. 6.1.).

Tortonian ramp deposits (LFA2)

Compared to LFA1 deposits, tectonic influence decreases in most parts of the WAT during deposition of LFA2 when the E-W oriented fault in the north of the WAT becomes inactive and the area eventually becomes part of a northward inclined dip slope ramp (chapter 5). Overall subsidence was high enough to preserve conformable successions even during long term sea-level fall. Differential subsidence occurred at low rates, so that laterally extensive lithologies formed in response to eustatic change, allowing high resolution correlation of sedimentary units and comparison with global Sr isotope curves (chapter 4; 6). The lithologies however, differ also in their biotic makeup that modified response to sea level change and reflects the influence of global climate change.
Five stages of depositional environment evolution are recognized: The initial stage formed during late 3rd order sea-level rise in early Tortonian times (Fig. 6.1.) that was enhanced by high subsidence rates in the northern part of the WAT. It is characterized by homoclinal ramp geometries. Both, siliciclastic-rich deposits and pure limestone deposits formed during this stage. The second stage represents the development of a distally steepened ramp with flat topped shelf character in the mid- and inner ramp in response to the middle Tortonian 3rd order sea-level fall. The middle Tortonian eustatic rise that follows the Tor2 sequence boundary caused a landward shift of facies belts, deposition of monotonous RFR2 sediments on the vast flat topped area and development of a carbonate ramp. The late Tortonian warm interval associated with the coeval late Tortonian sea-level highstand was characterized by the reestablishment of a ramp with a flat topped inner part, stabilized by extensive coral carpets. The last stage is represented by extensive deposition of RFR3 that covered the largest part of a re-established carbonate ramp. Tortonian off-shore equivalents may be represented by the lower part of LFA3.

Early Tortonian ramp (LFA2a)

Early Tortonian (10,5Ma to 10Ma) ramp deposits include sediments of the RFR1 and PS lithofacies as well as CS shoreface deposits (Fig. 2.4.4.; 7.1.aI). To the southwest of Matala and in the Moni Odhyitria area, the PS facies is substituted by rhodolith rudstone of the RFR3 facies with coralline bindstone (RB facies). Sedimentary successions and analysed biota indicate deepening (see chapter 2 and 3). Sedimentary architecture reflects an aggradational mode of deposition implying persistent availability of accommodation space (Fig.7.1.a). This is in accordance with the curve of Haq et al. (1988), that indicates late 3rd order sea level rise and highstand during deposition of early Tortonian ramp deposits and with Sr isotope ratios that indicate pronounced higher order sea level rise during this time interval (Fig. 4.6.; 6.1.). It was also a time of high subsidence rates in the north of the WAT (chapter 5). At approximately 10Ma, a higher order sea-level lowstand is indicated by low Sr ratios. It marks the facies change from PS to CS and the transition to the following flat topped ramp stage (see below).

During deposition of LFA1, most of the siliciclastic input originated from the northeast (Fig. 2.3.11.). High siliciclastic contents in early Tortonian ramp deposits in the northeast of the WAT show that of siliciclastic sediment input remained highest in this area during deposition of LFA2a. Parts of the ramp further to the south (sections MS3 and Moni 1,2) apparently were protected from siliciclastic input due to their position south of the basement high east of Sivas (Fig. 5.4.b). Here a facies rich in red algae (RFR3) occupied the mid- to outer ramp environment (Fig. 7.1.aII), replacing gastropod and bivalve rich sands that were deposited in the Matala area. High siliciclastic input is likely related to relatively humid conditions in the early Tortonian indicated by data shown in Pomar (2001a).

Fig. 7.1. (next page): Models of the evolution of ramp geometries in the course of the Tortonian. Abbreviations on top of the models indicate approximate positions of sections where the shown lithology is found. Small maps to the left indicate orientation of the model ramp in the WAT. **aI:** lower Tortonian ramp in the Matala area with high siliciclastic input and oceanward decrease in grain size, **aII:** lower Tortonian ramp southeast of Matala with low siliciclastic input and oceanward increase in grainsize from inner- to mid-ramp, **b:** middle Tortonian flat-topped high energy ramp with prograding CS facies that is protected by RP facies from storm wave abrasion. Stacking of prograding units results in characteristic sandstone-limestone couplets, **c:** homoclinal ramp morphology is re-established during sea-level rise after Tor2 sequence boundary through aggradation of massive rhodolith rudstone and high carbonate production in the outer ramp, **d:** bioclasitc packstone and aggraded rhodolith rudstone is colonized and stabilized by coral carpets during the late Tortonian highstand and associated climatic optimum, **e:** high subsidence results in drowning of the carpets and deposition of RFR3 rhodolith rudstone that covers mid- and outer ramp

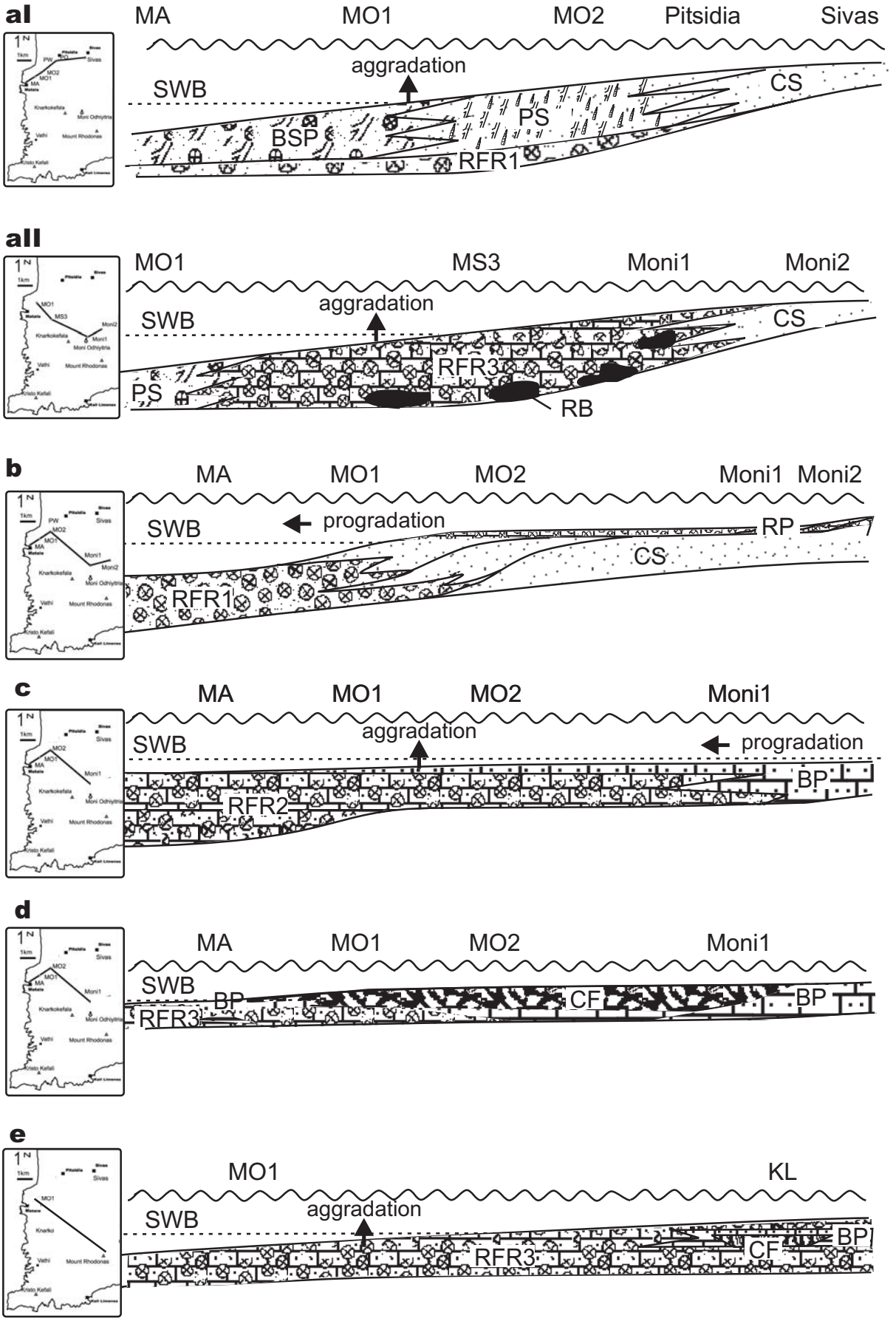
al
MA
MO1
MO2
Pitsidia
Sivas
aggradation
SWB
CS
PS
BSP
RFR1
all
MO1
MS3
Moni1
Moni2
aggradation
SWB
CS
RFR3
PS
RB
b
MA
MO1
MO2
Moni1
Moni2
SWB
progradation
RP
CS
RFR1
c
MA
MO1
MO2
Moni1
aggradation
SWB
progradation
BP
RFR2
d
MA
MO1
MO2
Moni1
SWB
BP
CF
BP
RFR3
e
MO1
KL
aggradation
SWB
BP
CF
RFR3

The early Tortonian ramp interval formed during a time of climatic cooling that followed the early Tortonian temperature maximum. It is indicated by a maximum in $\delta^{18}O$ and a decrease of water temperature indices in section MO1 (Fig. 6.1.) and low water temperature indices in section MS1 and VO (Fig. 3.3.12.)

The early Tortonian depositional system represents a homoclinal ramp system sensu Read (1985) and Burchette and Wright (1992) with high energy inner shelf sandstone and continuously decreasing hydraulic energy towards the outer ramp. Where siliciclastic input was low, facies belts of the mid- to outer ramp are very similar to ramp environments described by Pedley (1998) from the Oligo-Miocene of the central Mediterranean. These are characterized by a mid ramp rhodolith rudstone facies with algal build-ups and outer ramp mollusc and echinoid rich larger foraminifera facies (Pedley, 1998). In this depositional environment, the sediment budget is approximately constant along the ramp profile. This is the prerequisite to maintain an equilibrium ramp system sensu strictu (Walkden and Williams, 1998).

Red algal build-ups in this stage appear to be typical for initial deepening and transgression under non-tropical conditions in areas far from sources of siliciclastic input.

Middle Tortonian high energy ramp (LFA2a)

This interval is characterized by deposition of mid- and inner ramp sandstone-rudstone couplets of the CS and RP facies and an associated rhodolith rudstone belt (RFR1 facies) in the outer ramp (Fig. 2.4.4.; 7.1.b). The stacked couplets reflect a strongly prograding system. The upper mid ramp was occupied by extensive blankets of rhodolith rudstone with pebbles (RP facies) that were replaced by cross stratified sandstone towards the outer ramp composed of sediment that was winnowed out from the RP facies (see chapter 2.4.). Close to the shoreline, in the surf zone, a belt of crossbedded rhodolith rudstone and conglomerate developed. As discussed before, this interval deposited between 10-9,3Ma reflects both, the long-term (3^{rd} order) sea-level fall and superimposed higher order eustatic change indicated by Sr isotope ratios (Fig. 6.1.). Subsidence remained in the order of eustatic sea-level fall and therefore no unconformity was developed except in the Sivas-Pitsidia area. Nevertheless, due to longterm eustatic fall, accommodation space below storm wave abrasion remained low and was filled up quickly by siliciclastics.

A relatively short warm interval is indicated by a minimum in $\delta^{18}O$ between 9,7 and 9,8 Ma (Fig. 6.1.) that is reflected by high water temperature indices and local growth of single coral colonies (sections VO and MS3).

In consequence of low accommodation space and constant winnowing out of siliciclastic material from the inner ramp and mid-ramp, the sediment budget was in strong disequilibrium along the ramp profile. Virtually all sediment was exported to the outer mid ramp where it was moved along shore and deposited close to the shoreward boundary of the outer ramp where current and wave energy induced by storms dropped. Carbonate production in the unstable substratum of this environment was low. Since only the finest material was further exported to the outer ramp, the sediment budget was characterized by a large sediment input and a small production and output. Carbonate production by red algae was shifted to the outer ramp where substrate stability was higher and sediment input was low. Due to the positive sediment budget in the outer mid ramp, sediments were quickly building up to the shelf equilibrium surface, the minimum water depth at which sediment accumulation occurs. It is defined by the ratio between sediment input and fluid power to move it (Swift and Thorne 1991). This surface was stabilized by coarse grained in situ carbonate production of rhodoliths and bivalve shells and thus was resistant to storm wave abrasion even during relative sea-level fall. Boring and the high proportion of apparently relict red algal components suggest that residence times were long and that the surface potentially was stable over geologic time intervals (see chapter 2.4.). The strongly prograding system resulted in a depositional profile with a marked break in slope, similar to, if smaller as a flat topped high energy shelf [James, 1994 #189]. Higher order sea level rise results in almost instantaneous shoreward jump of facies belts. Sandstone-limestone couplets are the result of repeated higher order eustatic fluctuation. These couplets are stacked into an over all prograding unit. In contrast to the lower Tortonian ramp, shore parallel belts of shallow water carbonates (RP facies) and deeper water calcareous sandstone (CS facies) developed according to the lowstand carbonate, highstand sandstone model of Brachert et al. (2003) that is typical for high energy mixed siliciclastic – carbonate shorelines such as the Miocene Algarve coast (Forst, 2003). This environment is comparable to the Holocene high energy environment of the southern Australian shelf (shaved shelf model, James et al. 1994). The fundamental difference between these high energy coasts and the middle Tortonian environment on Crete, however, lies in the depth of the storm wave base: Wave abrasion depth exceeds 100m in the southern Australian shelf area (James et al.,1992; Collins 1988) whereas it is between 30-40m in the Mediterranean (Betzler et al.,1997). The resulting dimensions are very different: The

Australian shelf is up to 300km wide whereas the Miocene Cretan "shelf" is only a few kilometres wide. For the analysis of sedimentary environments, however, the most important aspect is that in environments with shallow storm wave abrasion depth, the depositional environment basinward of the slope is still within the photic zone. Carbonate accumulation by benthonic foraminifera and red algae in the lower part of the photic zone is considerable (Pomar, 2001a; Pomar, 2001b). Therefore, the basinal red algae dominated environment keeps pace with relative sea-level rise and transgresses shoreward as soon as the "wave base razor" (James and von der Borch, 1991; Sonnefeld and Cross 1993) is lifted due to eustatic rise. At this time the process of massive seaward export of sand sized material ceases and homoclinal ramp geometry is reinstalled.

Middle Tortonian ramp (LFA2b)

This approximately 0,5m.y. interval is characterised by the widespread deposition of unbedded rhodolith rudstone to floatstone (RFR2, MRB) on top of the uppermost RP horizon (see chapter 2.4.) and associated near-shore bioclastic packstone (BP facies, Fig. 7.1.c). Both, lithologies and biotic associations (temperature index) reflect pronounced deepening (Fig. 3.3.12.). The widespread occurrence of this horizon corroborates formation in response to pronounced higher order eustatic rise after the Tor2 sequence boundary (chapter 4,6; Fig. 6.1.). The interval also marks the beginning of climatic warming that led to the late Tortonian climatic optimum between 9 and 8Ma.

Rapid transgression resulted in initial sediment starvation of the depositional environment and almost instantaneous transgression of the red algae dominated outer ramp facies across the underlying flat topped shelf topography (Fig. 2.4.4.; 7.1.c). The top of the uppermost RP layer was modified from a high energy facies to a transgressional lag deposit. In the southern part of the WAT (Vathi, Moni Martsalo), transgression falls into a phase of increased tectonic subsidence and therefore the massive MRB reaches the greatest thickness in that area (see chapter 5; Fig. 2.2.3.; 5.4.b). The change in profile of the depositional environment from flat-topped shelf system in the middle- to inner ramp to a more homoclinal ramp system was thus related to eustatic sea-level rise that increased accommodation space and resulted in an aggradational mode of deposition following initial transgression and onlap on the basement horsts. Most of the ramp remained below the level of frequent abrasion by storm waves that would have caused export of bioclastic sand towards the outer ramp. This period was also

characterized by increasingly arid climate (see chapter 6) and a decrease in siliciclastic sediment input. Therefore, in the course of climatic warming, siliciclastic sedimentation was replaced by extensive production of nearshore carbonate sands.

Late Tortonian coral carpets (LFA2c)

This interval is characterised by the widespread formation of two coral carpet horizons (CF, Fig. 7.1.d) in the WAT (chapter 2.4.) on top of rhodolith rudstone (RFR2 facies) and bioclastic sands (BP facies). The calibration of sections to absolute time by Sr chronostratigraphy (chapter 4) shows that, according to the sea-level curve of Haq et al. (1988), coral carpet formation occurred during late Tortonian late 3rd order sea-level rise and early highstand between 9Ma and 8Ma (Fig. 6.1.). Persistent water temperature indices of 1 in all sections indicate a climatic optimum that is also reflected by minima in $\delta^{18}O$. It is interrupted by a short period of cooling with an oxygen isotope maximum at about 8,4Ma coeval with the gap between coral carpet horizons.

Widespread colonization by zooxanthellate corals suggests that the ramp was built up to a water depth shallower than 25m by extensive carbonate production and decreasing accommodation space during (higher order) sea-level highstand in the area of Matala. In the south of the WAT (Vathi – Martsalo Bay), rates of tectonic subsidence and eustatic rise remained higher than sediment accumulation. Therefore, initially, water depth was too deep for coral frameworks to develop. In the area of Pitsidia/Sivas, relative tectonic uplift resulted in erosion or non-deposition of upper LFA2a deposits and LFA2b ramp deposits. Coral framestone therefore directly overlies a bed of condensed rudstone. Landward (Moni Odhyitria area) and seaward, coral carpets pass into carbonate sands (BP facies). Carbonate sand belts oceanward of coral carpets, however, are only a few hundred meters in width (Fig. 2.4.4.) and pass into marly rhodolith rudstone to floatstone (RFR3 facies) that may contain large single colonies of *Porites* and *Tarbellastrea*.

Similar as in the Middle Tortonian distally steepened ramp, the sedimentary surface was build up towards a shelf equilibrium surface within wave abrasion depth by prograding sand sized deposits (BP facies, Fig. 2.4.4.; 7.1.c). In this case, however, elevated water temperature permitted colonization by coral carpets that stabilized the sedimentary surface instead of rhodolith – mollusc pavements. The fundamental difference between coral carpets and rhodolith pavements lies in their ability to trap sediment: While from rhodolith pavements,

sand-sized material was partially winnowed out, coral carpets are more effective bafflers (Riegl and Piller, 1999) that trap most of the sediment. Therefore in this setting, progradation by winnowing out of fine sediment and transport towards the outer ramp was insignificant. Consequently, coral carpets formed an extensive platform in the inner ramp with the ability to build up close to sea-level. Since carpets prevent a distal steepening of the ramp, no relief is created. Therefore coral carpets may not necessarily evolve into coral reefs that form a platform rim. Progradation does however occur through accumulation of mid- to outer ramp rhodolith rudstone until water depth is shallow enough for the formation of coral carpets. In the area of Matala, two stages of coral carpet formation occur that are separated by a rhodoliths rudstone interval. Low temperature indices and a coeval maximum in $\delta^{18}O$ indicate that the gap in coral growth was related to climatic cooling. Increasing water depth indices in the sediments above the upper carpet interval on the other hand indicate that the upper carpet was drowned before climatic cooling between 8 and 7,5 Ma (Fig. 6.1.). This reflects a limited capability of coral carpets in marginal tropical environments to keep up with sea-level rise.

Late Tortonian ramp (LFA2c)

Late Tortonian ramp formation between 8 and 7Ma was characterized by extensive deposition of RFR3 rhodolith rudstone (Fig. 2.4.4.; Fig. 7.1.e). It is coeval with late 3rd order highstand (Fig. 6.1.) and occurs during an interval of overall subsidence of the WAT (chapter 5). Consequentially accommodation space below wave abrasion depth was constantly present, resulting in largely aggradational deposition. A global climate related temperature minimum is indicated around 7,5Ma by a minimum in water temperature indices and a maximum $\delta^{18}O$ values (Fig. 6.1.). After 7,5Ma, renewed warming is reflected by the formation of coral carpet patches and associated bioclastic packstone (section KL) and single *Porites* colonies (uppermost warm interval, Fig. 6.2.). In consequence of over all subsidence, however, water depth was relatively high in most sections as is indicated by high water depth indices (Fig. 3.3.12.), inhibiting the formation of extensive coral carpets.

The ramp had built into an extensive, gently dipping surface typical for mature ancient ramp systems that stretched for tens of kilometres with an oceanward dip <2° (Burchette and Wright, 1992). Since, at this time, uplifted fault blocks in the southwest of the WAT, such as Kristo Kefali and possibly other basement highs subsided, the ramp became more open to storm induced waves, resulting in more effective wave abrasion and deepening of the storm

wave base. Consequently parts of the RFR3 facies now were in a mid-ramp position explaining higher degrees of reworking in the RFR3 facies compared to RFR1 and 2 (chapter 2.4.).

7.2. Controls on ramp systems and facies successions

Pre-existent topography

In contrast to LFA2, LFA1 represents a depositional environment that was controlled to a large degree by local factors such as the structural framework and sedimentation rate. This results in facies zonations that reflect local topography and tectonism rather than global influences. Nevertheless, where local conditions were appropriate, coral reefs formed in response to warm climate and biota reflect tropical conditions. In the course of the Tortonian, when local tectonic influence on paleogeography became smaller in the WAT and most of the precedent relief was filled with sediments, influence of global climate change and related eustatic change became more pronounced.

Nutrients, a local resource

Facies associations on homoclinal ramp systems observed in the WAT show considerable differences between each other: While on the early Tortonian ramp (Fig. 7.1.aI), an oceanward decrease in grain size is observed, in the middle and late Tortonian ramps, an oceanward increase in grainsize due to the production of little fragmented large carbonate skeletons such as rhodoliths occurs (Fig. 7.1.c and e). The comparison between areas with high siliclastic input and areas protected from large scale sediment input in the early Tortonian (Fig. 7.1.aII) suggests that this pattern is a consequence of the amount and distribution of continent derived material: Where siliciclastic input was low, a facies (RFR3) similar to rhodolith rudstone in the late Tortonian environment develops on the mid- to outer ramp. Bioclastic sand produced during middle Tortonian transgression and early 3rd order sea-level highstand prograded quickly across the ramp prior to the formation of coral carpets when the rate of eustatic rise decreased. This indicates that the rate of carbonate sand production in the Upper Tortonian was comparable to the input of siliciclastic sand in the Lower Tortonian. Therefore the difference in mid- to outer ramp facies between the Lower

Tortonian (PS facies) and Upper Tortonian (RFR3 facies) ramp is not a consequence of difference in sediment input. On the other hand, foraminiferal associations indicate that in the PS facies, nutrient levels were significantly increased compared to other LFA2 facies. This indicates that lower carbonate production on the siliclastic rich early Tortonian ramp is mainly a consequence of nutrient input. As has been discussed before, upwelling is not an important source of nutrients in the Mediterranean since Mediterranean deep waters are not significantly enriched. Therefore, the main nutrient source is continental runoff that is mostly restricted to river mouths. The nutrient content of continental runoff is related to the rate of chemical weathering and therefore to humidity of climate. Consequently, nutrient content is not necessarily related to silicilastic sediment accumulation: The amount in siliciclastic input may still be considerable if a high relief hinterland is present. Moreover, siliclastic material may be effectively transported long shore for a long time while nutrients are rapidly taken up by phytoplankton and benthic algae (Hallock and Schlager, 1986) and thus may be fixed rapidly close to the location of input. Such a bias between siliciclastic sediment accumulation and nutrient contents is observed in the Tortonian (LFA2b; Fig 7.1.b), when siliclastic sediment accumulation was high while biotic associations indicate oligotrophic conditions and rhodolith rudstone was deposited in the outer ramp. Similar as in LFA2a sediments, the presence of larger benthic foraminifera and zooxanthellate corals in LFA1 may not only be explained by a high frequency variability in humidity (see chapter 6) but also by the distribution of nutrients and a discrepancy between siliciclastic content and nutrient availability.

Dynamic ramp models – response to sea-level change

According to the general definition by Wright and Burchette (1998), ramps are platforms with a continuous depositional slope in contrast to shelves which are flat topped structures with a defined margin determined by a steep slope. The definition of a ramp therefore includes a wide variety of profiles between two end members: homoclinal ramps and (rimmed) shelves. Ramps with an offshore break in slope are termed distally steepened ramps. These breaks in slope may occur in consequence of offshore faulting, progradation of nearshore deposits (Read, 1985) or a significant oceanward gradient in carbonate productivity (Pomar, 2001a). In other terms, deviations from the homoclinal ramp profile in response to sedimentary processes can be described as a state of disequilibrium that is in disagreement with the original

definition of a ramp (Walkden and Williams, 1998). Since the depositional system is oscillating between approximately homoclinal morphologies and morphologies that are closer to an open shelf system without establishing a stable flat-topped shelf, the Cretan system may be described as a self-perpetuating ramp system *sensu* Walkden and Williams (1998). It is therefore in equilibrium if longer time intervals are considered. Therein, this system is distinct from many modern "ramps" that may never evolve into self-perpetuating systems due to high amplitudes of glacioeustatic sea-level change (Walkden and Williams, 1998). Nevertheless, the three observed homoclinal ramp intervals on Crete are genetically distinct and fundamentally different from the Middle Tortonian distally steepened ramp interval and the late Tortonian coral carpet interval: Homoclinal ramp morphologies are related to eustatic rise and/or high rates of subsidence that provided enough accommodation space for continuous sediment accumulation and prevented significant progradation of mid- to inner ramp facies. Thus the homoclinal ramp profile is a consequence of chiefly aggradational sediment accumulation while progradation leads to the formation of flat-topped morphologies.

Flat-topped ramps in tropical and temperate environments

The middle Tortonian distally steepened ramp interval and the late Tortonian coral carpet interval are very different from the homoclinal ramp intervals. While the distally steepened ramp interval is also very distinct from the coral carpet interval, they show important similarities: Both developed in periods with little rise in relative sea-level and in response to strong progradation of facies belts. Progradation resulted in the formation of shallow flat topped platforms in the inner- to mid ramp. The fundamental morphological difference between both systems, however is, that the middle Tortonian distally steepened ramp continued to prograde over approximately 1Ma, forming a more and more pronounced break in slope and would eventually have prograded over the part of the outer ramp that was still within the photic zone and producing carbonate sediments. Thus, one might imagine that, if progradation had continued long enough, the Cretan ramp may have developed into an open high energy shelf very similar to the southern Australian shelf (Collins, 1988; James et al. 1994; James et al. 2001). Progradation of the Cretan "shelf", however was ended by eustatic rise after the Tor2 sequence boundary that lifted storm wave abrasion depth above almost the entire "shelf" surface. Progradation of carbonate sands during late Tortonian early 3rd order highstand, on the other hand, was limited by the formation of coral carpets. These structures

have the ability to cover vast shelf areas and to grow close to sea-level and to trap most of the sediment produced on the shelf. Reasons why coral carpets did not evolve into rimmed shelves were already discussed above: They are either related to the position at the outer reaches of the tropical province where global climate change related cooling would result in drop of water temperatures below the threshold of reef formation and where corals can not as easily keep up with sea-level rise or they are related to the difference between coral carpets and actual reefs: By trapping most of the sediment produced in the shallow carbonate factory, coral carpets prevent the formation of a pronounced slope break. Thus the formation of a barrier reef that depends on shelf edge currents which are important for the nourishment and stabilization through early cementation of the reef may also be prevented. If higher order sea-level fluctuation is taken into account, it appears to be even more unlikely that carpet systems develop into platform since carpet growth may be ended by both, higher order sea-level fall that leads to subaerial exposure of the whole carpet or high order rise that may drown the carpet. On the other hand, the example of the Llucmajor Platform on Mallorca shows, that the formation of a barrier reef complex on a carbonate ramp is also possible in marginal tropical settings: This platform formed during the second 3rd order eustatic highstand of the Tortonian and existed through higher order sea-level fluctuation (Pomar et al., 1996).

For the reasons discussed above both, the temperate and the tropical flat-topped ramps are transitory systems: Both develop in time intervals of little long term (3rd order) change of sea-level or long-term sea-level fall, respectively. The siliciclastic dominated flat topped shelf interval in the early Tortonian (Fig. 7.1.b) clearly persists during most of the falling sea level stage of the early Tortonian 3rd order eustatic cycle until the Tor2 sequence boundary (Fig. 6.1.). The tropical system on the other hand is limited to the warm interval during eustatic highstand. Therefore the flat-topped systems occur only during a limited time interval and thus are part of a self-perpetuating, dynamic ramp system.

7.3. Implications for climate related sedimentological models

Mechanisms found to control the Cretan ramp system are related to both, global climate and geographical position. In carbonates of the WAT, global influence is most evident during the interval between the first Tortonian 3rd order sea-level highstand and late highstand of the second Tortonian 3rd order cycle (Fig. 6.1.). Since the succession of facies developed in response to a 3rd order sea-level cycle (Fig. 7.2.), comparable successions are expected to

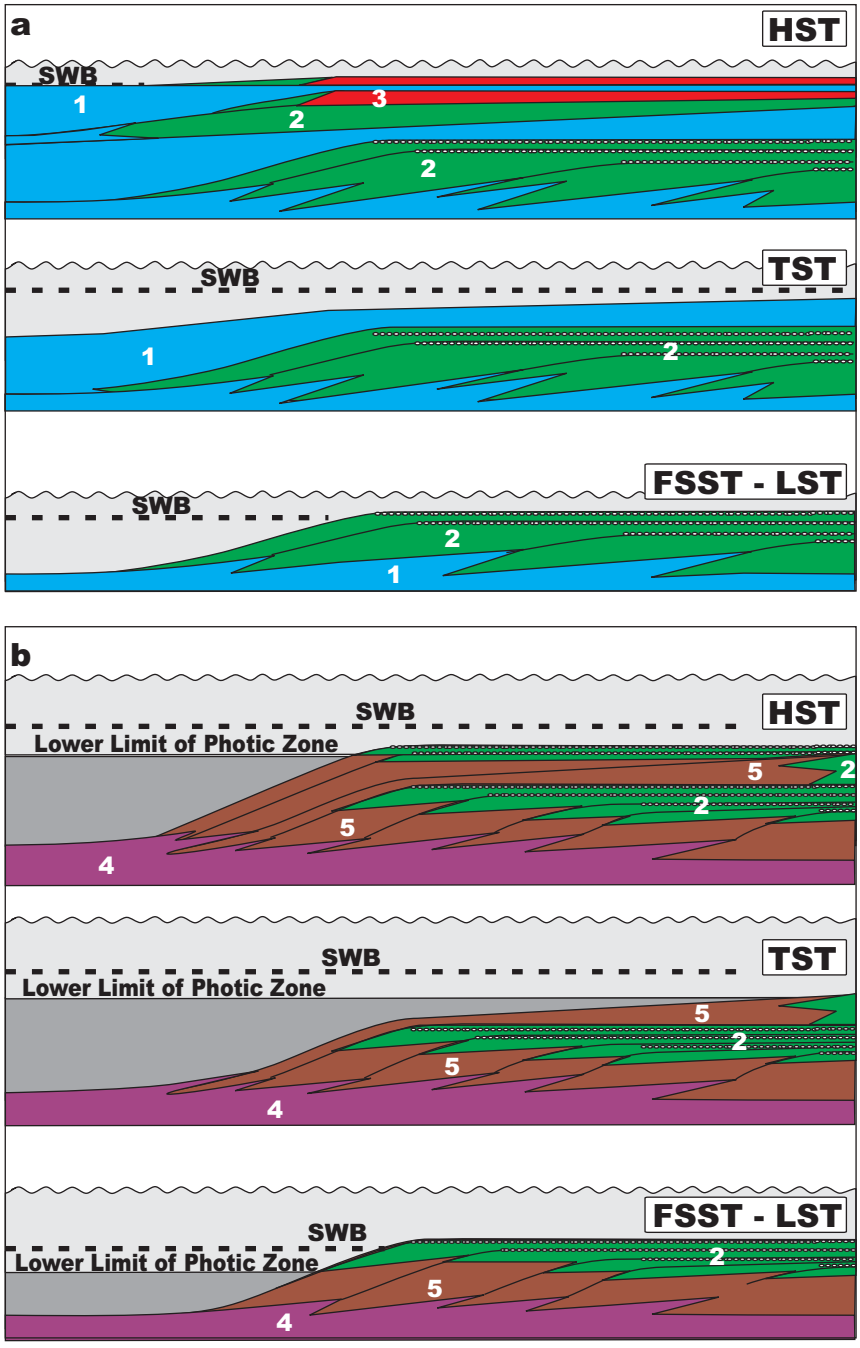

Fig. 7.2.: Schematic sections of depositional environments in the course of a 3rd order sea-level cycle in a high subsidence setting that is intermediate between the temperate and tropical province
a: In a setting where the range of the photic zone (light grey) is considerably deeper that storm wave abrasion depth (dashed line), a self-perpetuating ramp system develops since the outer ramp fully remains within the photic zone. The flat-topped shelf interval that develops in consequence of high sediment export to the outer ramp, hampering carbonate production, remains transitory.
b: In a setting where the outer "ramp" is mostly below the lower limit of the photic zone, a flat topped shelf becomes stable since too little sediment is accumulated in the outer ramp environment to re-install a ramp profile.
Colours indicate (1) outer ramp sediments formed within the photic zone, (2) sandy slope deposits formed within the photic zone with intercalated coarse grained (carbonate) beds formed by event condensation, (3) inner- to mid-ramp frameworks (coral carpets), (4) outer ramp or basinal sediments deposited below the photic zone, (5) slope deposits formed below the photic zone.

have evolved in a similar setting: Interbedded mixed carbonate-siliciclastic sediments represent the falling stage of a 3rd order eustatic cycle that is also related to polar ice accumulation due to long term climatic cooling. During long term eustatic rise following a 3rd order sequence boundary, an aggradational red algal dominated carbonate ramp forms. Late transgression and highstand is related to an interval of little polar ice accumulation and therefore the warmest interval of a 3rd order cycle. During this interval, ramps build up close to sea-level and climatic conditions are most likely to allow coral reef or carpet formation. Mixed sandstone-limestone successions that are observed to have formed during 3rd order eustatic fall and lowstand in the WAT are common in the rock record. The conventional

interpretation is that siliciclastic sediments preferentially form during sea-level lowstand either as fluvial or shore face sediments prograding across a carbonate platform or as siliciclastic lowstand wedges in front of the platform, if the platform is above sea-level. During highstand, on the other hand, carbonates are produced on the platform (carbonate factory) and exported into the basin (Davies et al., 1989). Brachert et al. (2003) have shown, that on an open, mixed carbonate-siliciclastic temperate high energy shelf the pattern is inverted: Carbonates preferentially form during lowstand as condensed beds while during sea-level rise and early highstand and coeval uplift of the wave abrasion depth, sandstone is deposited. It appears that in the Cretan system, the conventional model of Davies et al. (1989) applies, because intervals with calcareous sandstone formed during 3rd order sea-level fall and lowstand while carbonates formed during 3rd order highstand. The system, however, behaves analogous to the model of Davies et al. (1989) only if it is regarded at a long time scale (several M.y.). In a shorter time scale, if only parts of 3rd order sea-level cycles are considered, such as the period between 10 and 9,3Ma in the WAT, a pattern similar as described in Brachert et al., (2003) develops: During higher order lowstand, condensed carbonate sediments are deposited while during higher order sea-level rise, mid ramp calcareous sandstone transgresses across the platform, resulting in the formation of characteristic sandstone-limestone couplets. Similar as in the sections from the Portuguese Algarve coast, these can be linked to fluctuation in Sr isotope values (see chapter 4).

The fact that in the regarded setting, different models apply in different time scales is a consequence of wave abrasion depth in relation to the depth of the photic zone: No outer ramp carbonate factory develops if the outer “ramp” is largely below the photic zone (Fig. 7.2.b). Consequently, the aggradational ramp system is not re-established during sea-level rise and the depositional system becomes an ever building up high energy shelf similar to the southern Australian shelf or the Miocene Algarve coast. Therefore a depositional system that remains in the high energy shelf mode most of the time and retains a topography with a marked shelf break can be termed a stable system. Depositional systems found on Crete suggest, that a homoclinal ramp with an equilibrium supported by a balanced sediment budget across the ramp is not likely to be stable in geological time scales. The data from Crete, however, also show that a system which systematically switches between flat topped shelf and homoclinal ramp geometries can be self perpetuating and therefore stable if longer time intervals are considered. The system remains stable as long as parameters such a wave abrasion depth in relation to the depth of the photic zone and rates of eustatic change remain unchanged. If the rate of eustatic change significantly surmounts the rate of subsidence, ramps are unlikely to

reach a state of equilibrium and to preserved in the geologic record. This is the reason why no equilibrium ramp systems are known from the Quaternary, which is characterized by unstable climate and related rapid glaciation and deglaciation resulting in high frequency eustatic change (Walkden and Williams, 1998). In the rock record, stable ramp systems are expected from times when eustatic change was more gradual and in deposits of ancient enclosed or epeiric seas where wave abrasion depth was low. A characteristic complete 3rd order cycle can only be preserved in areas with high subsidence rates and low rates of relative tectonic movements. Ramps do also not form when effective framework builders are present and climatic and ecological conditions allow them to build rimmed platforms. An ideal cycle with mixed siliciclastic-carbonate deposition during the long term falling sea-level stage and pure carbonate deposition during transgression and highstand is most likely to form if the system fluctuates between temperate and tropical conditions and is not perturbed by high siliciclastic or nutrient input from the hinterland. Under these conditions, symbiont-bearing framework constructors are likely restricted to the late transgression- and highstand interval. Cycles with siliciclastic lowstand deposits, transgressive red algal deposits and highstand reefs are regarded by Esteban et al. (1996) to be typical for the Miocene of the Mediterranean. In this setting, rimmed shelves such as the Llucmajor platform on Mallorca (Pomar, 2001b) are an exception. Coral carpets are also uncommon in the Mediterranean but can be expected to occur, when low-relief ramps are present. Carpets however form only if the ocean floor is shallow enough. They are therefore more likely to be found in marginal seas than in open ocean settings with deep wave abrasion where the shelf platform remains in water depths too deep for coral carpet formation. Since in settings where climatic conditions allow framework builders to thrive only during warm intervals, biostromes are expected to be more common than reef platforms, it follows, that biostromes such as coral carpets may occur in higher latitudes than platform forming reefs. This relationship may be important for the interpretation of many ancient environments when epeiric seas and framework constructors that build biostromes rather than reefs were common.

8. Conclusions

- Neogene deposits of southern central Crete show a marked transition from predominantly siliciclastic coastal deposits to near-shore marine limestone and off-shore marl deposition. Distributions and facies associations of siliciclastic deposits were controlled by pre-existent topography and tectonic movements. The siliciclastic sedimentary basin was limited to the south by an east-west trending fault scarp that shed coarse clastic material. Reduction of hinterland relief and more arid climatic conditions in the course of the Tortonian led to a decrease in siliciclastic input and to the deposition of pure limestone. Contemporaneously, a change from predominantly N-S extension to multidirectional extension led to basin fragmentation. While differences in accommodation space are apparent in sections of the WAT, the tectonic influence on sedimentation remained low compared to the northern rim of the Messara Basin and the Central Iraclion Ridge. Towards the end of the Tortonian, over-all subsidence is observed in the southern part of central Crete until, in Messinian times, relief intensification led to basin margin instability and reworking of Tortonian limestones.

- Studies of the distribution of biota carried out in Neogene deposits of central Crete have shown that the most valuable information on environmental and climatic condition comes from the analysis of certain groups of organisms that react very specifically environmental variation. Non-geniculate coralline red algae have proven to be ideal indicators for water temperature and water depth: In contrast to other organisms such as foraminifera, red algal genera show a predictable response to either one of these factors while foraminiferal associations respond to a variety of interdependent factors. On species level, however, both, coralline red algae and foraminifera may also provide useful information on other environmental factors: *Titanoderma pustulatum* is an indicator for strictly oligotrophic conditions and is absent as soon as nutrient levels are slightly increased.
From the distribution of coralline red algae, water depth and water temperature indices can be calculated. Although both indices are difficult to express as absolute values, they can be used as indicators for temperature and water depth thresholds similar as zooxanthellate corals and larger benthic foraminifera, which are used to define the limits of the warm temperate and tropical faunal provinces. On Crete, high water depth indices above 0,5 have been found to define the transition from mid- to outer ramp deposits. The occurrence of high water temperature indices of 1 have been found to mark a temperature threshold that is slightly lower than the threshold for the formation of zooxanthellate coral reefs. Coralline red algae

thus are especially suitable to map temperature conditions within the warm temperate province.

- In order to analyse the relationship of climate data from Crete to global climate change, a high resolving time frame was established using fluctuations in $^{87}Sr/^{86}Sr$ isotope ratios in the global oceanic record: Change in Sr isotope ratios that respond to processes of glaciation and deglaciation and therefore sea-level is represented in all deposits of the world ocean. In shallow water deposits reflecting eustatic fluctuation, Sr isotope stratigraphy therefore can be used for high resolution chronostratigraphy. High energy-mixed-carbonate-siliciclastic sediments as found in the Miocene Algarve and the lower Tortonian of southern central Crete are closely related to higher order eustatic fluctuation and therefore especially suitable for this method. Ages found for Neogene limestone of the WAT are between 10,5 and 7,3Ma.

- Applying the absolute time scale established by Sr isotope chronostratigraphy for sections on Crete, water depth and water temperature indices based on the distribution of non-geniculate coralline red algae were correlated with data on global sea-level change and oxygen isotope variation. The correlation of water depth indices with the Sr isotope curve is good in the lower part of the limestone succession (LFA2a and b) when mixed-silicilastic-carbonate sediments were deposited, but low during limestone deposition. In water depth indices, especially in carbonates, global influences therefore appear to be overprinted by local processes. Temperature indices, on the other hand, correlate with the global oxygen isotope curve. This correlation shows that water temperature in the Mediterranean was directly related to global climate and that Sr chronostratigraphy is a reliable method for high resolution dating of shallow water sediments.

- The close relationship of temperature indices with the global oxygen isotope curve shows that temperature was the main factor controlling the biotic makeup of the sediments. The observed fluctuation between warm temperate and tropical conditions therefore was a consequence of global climate change. Nutrient levels did not significantly influence the general pattern since oligotrophic conditions are indicated by the dominance of larger benthic foraminifera and non-geniculate coralline red algae in Upper Tortonian limestone of the WAT. In an enclosed sea with an anti-estuarine circulation likely governing nutrient distribution in the Tortonian in a similar way as in the recent Mediterranean, nutrient input is mainly controlled by weathering and continental runoff and thus also linked to climate.

Four tropical intervals were identified on Crete during the Tortonian: An early Tortonian warm interval is evidenced by the occurrence of tropical biota in the siliciclastic half-graben deposits (LFA1) during initial marine ingression. In central Crete, the subsequent interval between 10 and 9,5Ma led to extensive formation of coral reefs. In southern central Crete (WAT), the longer interval ("Tortonian climatic optimum") between 9 and 8Ma led to widespread formation of coral carpets. The most extensive formation of coral reefs in the Miocene of the Mediterranean, the Llucmajor Platform on Mallorca is apparently also related to this interval. The youngest identified Tortonian tropical interval can be related to the spatially most extensive occurrence of coral reefs in the Mediterranean.

- Although biotic associations reflect change in water temperature related to global climate change, eustatic change that is also related to climate change is a main controlling factor on the geometry of sedimentary environments: The depositional environment of the WAT can be described as a self-perpetuating ramp system that oscillates between a homoclinal ramp system and a distally steepened or flat-topped high energy ramp system. The system was controlled by the availability of accommodation space below storm wave abrasion related to eustatic change. Homoclinal ramps were characteristic for intervals of relative rise in sea-level when sediment accumulation is mostly aggradational. During highstand and lowstand, prograding depositional systems developed. As a result of differences in water temperature, these were very different from each other: During sea-level fall and lowstand under non-tropical climatic conditions, characteristic deposition of (higher order) lowstand carbonate and highstand sandstone couplets similar to those found on high energy shelves occurred. Under tropical conditions, on the other hand, on a low relief carbonate ramp, coral carpets develop that prograded less than the mixed-carbonate-siliciclastic temperate system and therefore did not develop a pronounced shelf break.
In general, factors that favour a stable high energy shelf system in non-tropical or marginal tropical environments, are deep storm wave abrasion and low amplitude and frequency in eustatic change. Self-perpetuating ramp systems that switch from a flat-topped system to a homoclinal system are favoured in areas with shallow storm wave abrasion depths. The evolution of a stable flat-topped shelf is further limited in warm temperate environments with effective outer ramp carbonate factories. These allow the maintenance or reestablishment of homoclinal ramp profiles. On marginal-tropical ramps, the development of coral carpets is favoured over the formation of morphological reefs due to the absence of a marked relief and the limited duration of tropical intervals. Self-perpetuating ramp systems may have been very

common in the geologic past, especially in marginal tropical environments and during geological periods with widespread epeiric seas where shallow storm wave abrasion depths prevailed.

9. References

Abreu, V. S. & Anderson, J. B. (1998) Glacial eustasy during the Cenozoic: Sequence stratigraphic implications. *AAPG Bulletin*, **82**(7), 1385-1400.

Abreu, V. S. & Haddad, G. A. (1998) Glacioeustatic fluctuations: the mechanism linking stable isotope events and sequence stratigraphy from the Early Oligocene to Middle Miocene. In: *Mesozoic and Cenozoic sequence stratigraphy of European basins* (Ed. by P.-C. de Gracianski, J. Hardenbol, J. Thierry and P. R. Vail), pp. 245-259. Society for Sedimentary Geology, Tulsa. *SEPM special publication, Vol. 60.*

Adey, W. H., Adey, P. J. (1973) Studies on the biosystematics and ecology of the epilithic crustose corallinaceae of the British Isles. *British Phycological Journal*, **8**, 343-408.

Adey, W. H., Townsend, R.A., Boykins, W. T. (1982) The crustose coralline algae (Rhodophyta, Corallinaceae) of the Hawaiian Islands. *Smithonian Contributions to Marine Sciences*, **15**, 75.

Adey, W. H. (1986) Coralline red algae as indicators of sea-level. In: *Sea level research: a manual for the collection and evaluation of data.* (Ed. by O. van de Plassche), pp. 229-279. Free University Amsterdam, Amsterdam.

Ager, D. V. (1974) Storm deposits in the Jurassic of the Maroccan High Atlas. *Paleogeography, Paleoclimatology, Paleoecology*, **15**, 83-93.

Aguirre, J. & Braga, J. C. (1998) Redescription of Lemoine´s (1939) types of coralline algal species from Algeria. *Paleontology*, **41**, 489-507.

Aguirre, J. & Braga, J. C. (2003) Impact of fossil species (Rhodophyta, Corallinales). Implications for present day taxonomic practise. In: *8th International Symposium on Fossil Algae* (Ed. by J. Aguirre and J. C. Braga), pp. 1-2, Granada, Spain.

Aigner, T. (1982) Calcareous tempestites: Storm-dominated stratification in Upper Muschelkalk limestones. In: *Cyclic and event Stratification* (Ed. by G. Einsele and A. Seilacher), pp. 180-198. Springer, Heidelberg.

Allmon, W. D. (1988) Ecology of Recent turitelline gastropods (Prosobranchia, Turritellidae): current knowledge and paleontological implications. *Palaios*, **3**, 259-284.

Angelier, J., Lyberis, N., Le Pichon, X., Barrier, P. & Huchon, P. (1982) The tectonic development of the Hellenic Arc and the Sea of Crete: A synthesis. *Tectonophysics*, **86**, 159-196.

Antunes, M. T., Elderfield, H., Legoinha, P. & Pais, J. (1997) The Neogene of Algarve. In: *2nd Congress of R.C.A.N.S. (Regional Commitee on Atlantic Neogene stratigraphy)*, *Field Trip Guide* (Ed. by J. A. Gonzalez-Delgado, F. J. Sierro and J. Pais), pp. 55, Salamanca, Spain.

Antunes, M. Z., Pais, J., Legoinha, P., Elderfield, H., Sousa, L. & Estevens, M. (2000) The Neogene of Algarve (Portugal). *Ciencias da Terra*, **14**, 1-22.

Armstrong, R. L. (1971) Glacial erosion and the variable isotopic composition of strontium in seawater. *Nature*, **230**, 132-133.

Athersuch, J., Horne, D. J. & Whittaker, J. E. (1989) *Marine and brackish water ostracods*. The Linnean Society of London, Avon, 343 pp.

Bailey, J. C. (1999) Phylogenetic positions of *Lithophyllum incrustans* and *Titanoderma pustulatum* (Corallinaceae, Rhodophyta) based on 18S rRNA gene sequence analyses, with revised classification of the Lithophylloideae. *Phycologia*, **38**, 208-216.

Barton, C. E. & Bloemendal, J. (1986) Paleomagnetism of sediments collected during Leg 90, southwest Pazific. In: *Initial reports DSDP*, *Vol. 90* (Ed. by J. P. Kennet and v. d. B. C.C), pp. 1273-1315. U.S. Govt. Printing Office, Washington.

Basso, D., Fravega, P. & Vanucci, G. (1996) Fossil and living Corallinaceans related to the Mediterranean endemic species *Lithophyllum racemus*. *Facies*, **35**, 275-292.

Basso, D. (1998) Deep rhodolith distribution in the Pontian Islands, Italy: a model for the paleoecology of a temperate sea. *Paleogeography, Paleoclimatology, Paleoecology*, **137**, 173-187.

Betzler, C., Brachert, T. C. & J., N. (1997) The warm temperate carbonate province, a review of the facies, zonations, and deliminations. *Cour. Forsch.-Inst. Senckenberg*, **201**, 83-99.

Berggren, W. A., Kent, D. V., Swisher, C. C. I. & Aubry, A.-P. (1995) A revised Cenozoic geochronology and chronostratigraphy. In: *Geochronology, time scales and global stratigraphic correlation* (Ed. by W. A. Berggren, D. V. Kent, M.-P. Aubry and j. Hardenbohl), pp. 129-212. Society for Sedimentary Geology, Tulsa. *SEPM Special Publications*, *Vol. 54*.

Bizzozero, G. (1885) *Flora Veneta Crittogamica*, Padova, 255 pp.

Blanc, J. J. (1972) Observation sur la sédimentation bioclastique en quelques points de la marge continentale de la Méditérranée. In: *The Mediterranean Sea* (Ed. by D. J. Stanley), pp. 225-240. Dowden, Hutchinson&Ross, Stroudsburg.

Blum, J. D. (1997) The effect of late Cenozoic glatiation and tectonic uplift on silicate weathering rates and the marine 87Sr/86Sr record. In: *Tectonic uplift and climate change* (Ed. by W. F. Ruddiman), pp. 259-288. Plenum Press, New York.

Blum, J. D. & Erel, Y. (1995) A silicate weathering mechanism linking increases in marine 87Sr/86Sr with global glaciation. *Nature*, **373**, 415-418.

Bonneau, M. (1984) Correlation of the Hellenic nappes in the south-east Aegean and their tectonic reconstruction. In: *The geological evolution of the eastern Mediterranean* (Ed. by J. E. Dixon and A. H. F. Robertson), pp. 517-527. Blackwell Sci. Publications, Oxford. *Special Publications of the Geological Society of London*.

Borrego, J., Morales, J. A. & Pendon, J. G. (1995) Holocene estuarine facies along the mesotidal coast of Huelva, south-western Spain. In: *Tidal signatures in modern and ancient sediments*, (Ed. by B. W. Flemming and A. Bartholomä), pp. 151-170. Blackwell, Oxford. *IAS special publications, Vol. 24*

Bosence, D. W. J. (1976) Ecological studies on two unattached coralline algae from western Ireland. *Paleontology*, **19**, 365-395.

Bosence, D. W. J. & Pedley, M. (1982) sedimentology and palaeoecology of a Miocene coralline algal biostrome from the Maltese Islands. *Palaeogeography, Palaeoclimatology, Palaeoecology*, **38**, 9-43.

Bosence, D. W. J. (1983) Description and classification of rhodoliths (rhodoids, rhodolites). In: *Coated grains* (Ed. by T. M. Peryt), pp. 217-224. Springer, Berlin.

Bosence, D. W. J. (1985) The morphology and ecology of a mound building coralline alga (*Neogoniolithon strictum)* from the Florida Keys. *Paleontology*, **28**, 189-206.

Bosence, D. W. J. (1991) Coralline Algae: Mineralogy, taxonomy and palaeoecology. In: *Calcareous algae and stromatolites* (Ed. by R. Riding), pp. 98-113. Springer, Heidelberg.

Brachert, T. C. (1996) Klimasteuerung von Karbonatsystemen: Fallbeispiele zur Biofazies ozeanischer und flachmariner Ökosysteme im Känozoikum. Habilitation, Johannes Gutenberg Universität.

Brachert, T. C., Betzler, C., Braga, J. C. & Martin, J. M. (1996) Record of climatic change in neritic carbonates: Turnover in biogenic associations and depositional modes (Late Miocene, southern Spain). *Geologische Rundschau*, **85**, 327-337.

Brachert, T. C., Betzler, C., Braga, J. C. & Martin, J. M. (1998) Microtaphofacies of a warm-temperate carbonate ramp (Uppermost Tortonian/Lowermost Messinian, southern Spain). *Palaios*, **13**, 459-475.

Brachert, T. C., Hultzsch, N., Knoerich, A. C., Krautworst, U. M. R. & Stückrad, O. M. (2001) Climatic signatures in shallow-water carbonates: high-resolution stratigraphic markers in structurally controlled carbonate buildups (Late Miocene, southern Spain). *Palaeogeography, Palaeoclimatology, Palaeoecology*, **175**, 211-237.

Brachert, T. C., Forst, M. H., Pais, J. J., Legoinha, P. & Reijmer, J. J. G. (2003) Lowstand carbonates, highstand sandstones? *Sedimentary Geology*, **155**, 1-12.

Braga, J. C., Martin, J. M. & Alcala, B. (1990) Coral reefs in coarse-terrigenous sedimentary environments (Upper Tortonian, Granada Basin, southern Spain). *Sedimentary Geology*, **66**, 135-150.

Braga, J. C., Bosence, D. W. J. & Steneck, R. S. (1993) New anatomical characters in fossil coralline algae and their taxonomic implications. *Palaeontology*, **36 (3)**, 535-547.

Braga, J. C. & Aguirre, J. (1995) Taxonomy of fossil coralline algal species: Neogene Lithophylloideae (Rhodophyta, Corallinaceae) from southern Spain. *Review of Palaeobotany and Palynology*, **86**, 265-285.

Braga, J. C. & Aguirre, J. (2001) Coralline algal assemblages in upper Neogene reef and temperate carbonates in southern Spain. *Palaeogeography, Palaeoclimatology, Palaeoecology*, **175**, 27-41.

Brandano, M. & Corda, L. (2002) Nutrients, sea level and tectonics: constraints for the facies architecture of a Miocene carbonate ramp in central Italy. *Terra Nova*, **14**, 257-262.

Brasier, M. D. (1995) Fossil indicators of nutrient levels. 1: Eutrophication and climate change. In: *Marine palaeoenvironmental analysis from fossils* (Ed. by D. W. J. Bosence and Allison, P.A.), pp. 113-132. Alden Press, Oxford. *Geological Society Special Publications*, *Vol. 83*.

Bromley, R. G. (1999) *Spurenfossilien*. Springer, Berlin, 347 pp.

Buchbinder, B. (1996) Middle and Upper Miocene reefs and carbonate plattforms in Israel. In: *Models for carbonate stratigraphy from Miocene reef complexes of Mediterranean regions*, (Ed. by E. K. Franseen, M. Esteban, W. C. Ward and J.-M. Rouchy), pp. 333-347. SEPM, Tulsa. *Concepts in Sedimentology and Paleontology, Vol. 5*.

Burchette, T. P. & Wright, V. P. (1992) Carbonate ramp depositional systems. *Sedimentary Geology*, **79**, 3-57.

Burke, W. H., Denison, R. E., Hetjerington, E. A., Koepnick, R. B., Nelson, H. F. & Otto, J. B. (1982) Variation of seawater $^{87}Sr/^{86}Sr$ throughout phanerozoic time. *Geology*, **10**, 516-519.

Burne, R. V. & Colwell, J. B. (1982) Temperate carbonate sediments of northern Spencer Gulf, South Australia: a high salinity `foramol ´ province. *Sedimentology*, **29**, 223-238.

Cande, S. C. & Kent, D. V. (1992) A new geomagnetic polarity time scale for the Late Cretacious and Cenozoic. *Journal of Geophysical Research*, **97**(B10), 13917-13951.

Capo, R. C. & DePaolo, D. J. (1990) Seawater strontium isotopic variations from 2,5 Million years ago to the present. *Science*, **249**, 51-54.

Capo, R. C. & DePaolo, D. J. (1992) Homogeneity of Sr isotopes in the oceans. *Eos, Transactions, American Geophysical Union*, **73**, 272.

Carannante, G., Esteban, M., Milliman, J. D. & Simone, L. (1988) Carbonate lithofacies as paleolatitude indicators: problems and limitations. *Sedimentary Geology*, **60**, 333-346.

Carannante, G. & Simone, L. (1996) Rhodolith facies in the central-southern Appennines Mountains, Italy. In: *Models for carbonate stratigraphy from Miocene reef complexes of Mediterranean regions* (Ed. by E. K. Franseen, M. Esteban, W. C. Ward and J.-M. Rouchy), pp. 261-277. SEPM, Tulsa. *Concepts in Sedimentology and Paleontology*, *Vol. 5*.

Caulet, J. P. (1972) Recent biogenic calcareous sedimentation on the Algerian shelf. In: *The Mediterranean Sea* (Ed. by D. J. Stanley), pp. 261-278. Dowden, Hutchinson&Ross, Stroudsburg.

Campbell, S. J. & Woelkerling, W. J. (1990) Are *Titanoderma* and *Lithophyllum* (Corallinaceae, Rhodophyta) distinct genera ? *Phycologia*, **29**(114-125).

Chamberlain, Y. M. (1991) Historical and taxonomic studies in the genus *Titanoderma* (Rhodophyta, Corallinales) in the British Isles. *Bulletin of the British Museum (Natural History), Botany Series*, **21**, 1-80.

Chamberlain, Y. M. & Keats, D. W. (1994) Three melobesoid crustose coralline red algae from south Afrika: *Leptophytum acervatum* (FOSLIE) comb. nov., *L. foveatum* sp. nov. and *L. ferox* (FOSLIE) comb. nov. *Phycologia*, **33**, 111-133.

Chapman, F. & Crespin, I. (1930) Rare foraminifera from deep borings in the Victorian Tertiaries - *Victoriella,* gen. nov., *Cycloclypeus communis* Martin, and *Lepidocyclina borneensis* Rovale. *Proceedings of the Royal Society of Victoria, new ser.*, **42**, 110-115.

Chaproniere, G. C. H. (1975) Paleoecology of Oligo-Miocene larger foraminiferida, Australia. *Alcheringa*, **1**, 37-58.

Clemens, S. C., Farrell, J. W. & Gromet, L. P. (1993) Synchronous changes in seawater strontium isotope composition and global climate. *Nature*, **363**, 607-610.

Clemens, S. C., Gromet, L. P. & Farrell, J. W. (1995) Artefacts in Sr isotope records. *Nature*, **373**, 201.

Colella, A. (1988) Pliocene-Holocene fan deltas and braid deltas in the Crati basin, southern Italy: a consequence of varying tectonic conditions. In: *Fan deltas: sedimentology and tectonic settings* (Ed. by W. Nemec and Steel R.J). Blackie and Son, London.

Collins, L. (1988) Sediments and history of the Rottnest Shelf, southwest Australia: a swell dominated, non-tropical carbonate margin. *Sedimentary Geology*, **60**, 15-49.

Cowardin, L. M., Carter, V., Golet, F. C. & LaRoe, E. T. (1979) Classification of wetlands and deepwater habitats of the United States. U. S. Department of the Interior, Fish and Wildlife Service, Washington, D.C. Jamestown, ND: Northern Prairie Wildlife Research Center Online, http://www.npwrc.usgs.gov/resource/1998/classwet/classwet.htm

Creutzburg, N. (1975) Zum Stand der Geologie des Präneogens auf Kreta. *N. Jb. Geol. Paläont. Abh.*, **149**, 363-383.

Cushman, J. A. (1927) An outline of a re-classification of the Foraminifera. *Contributions from the Cushman Laboratory for Foraminiferal Research*, **3**, 1-105.

Cushman, J. A. (1937) A monograph of the subfamiliy Virgulinidae of the foraminiferal family Buliminidae. *Contributions from the Cushman Laboratory for Foraminiferal Research*, **9**, 1-228.

Dabrio, C. J. & Polo, M. D. (1988) Late Neogene fan deltas in the Almanzora Basin, Almería Province, southeastern Spain. In: *Fan deltas: sedimentology and tectonic settings* (Ed. by W. Nemec and Steel R.J), pp. 354-367. Blackie and Son, London.

Dabrio, C. J. (1990) Fan-delta facies associations in late Neogene and quarternary basins of southeastern spain. In: *Coarse-grained deltas* (Ed. by A. Colella and D. B. Prior), pp. 91-111. Blackwell, Oxford. *Special Publication of the International Association of Sedimentologists*, *Vol. 10*

Dalrymple, R. W. (1992) Tidal depositional systems. In: *Facies models* (Ed. by R. G. Walker and N. P. James), pp. 195-218. Geological Association of Canada, St. John´s.

Dalrymple, R. W., Zaitlin, B. A. & Boyd, R. (1992) Estuarine facies models: conceptual basis and stratigraphic implications. *Journal of Sedimentary Petrology*, **62**, 1030-1055.

Davies, P. J., Symonds, P. A., Feary, D. A. & Pigram, C. J. (1989) The evolution of the carbonate platforms of northeast Australia. In: *Controls on carbonate platform and basin development*, *Vol. 44* (Ed. by P. D. Crevello, J. L. Wilson, J. F. Sarg and J. F. Read), pp. 233-258. SEPM special publication, Tulsa.

Delage, Y. & Hérouard, E. (1896) *La cellule et les protozoaires*. Schleicher Frères, Paris.

Denison, R. E., Koepnick, R. B., Fletcher, A., Dahl, D. A. & Baker, M. C. (1993) Reevaluation of early Oligocene, Eocene and Paleocene seawater stronium isotope ratios using outcrop samples from the U.S. Gulf Coast. *Paleoceanography*, **8**, 101-126.

DePaolo, D. J. & Ingram, B. L. (1985) High resolution stratigraphy with strontium isotopes. *Science*, **227**, 938-941.

Derry, L. A. & France-Lanord, C. (1996) Neogene Himalayan weathering history and river $^{87}Sr/^{86}Sr$: impact on the marine Sr record. *Earth and Planetary Science Letters*, **142**, 59-74.

Dia, A. N., Cohen, A. S., O´Nions, R. K. & Shackleton, N. J. (1992) Seawater Sr isotope variation over the past 300kyr and influence of global climate cycles. .

Düwel, L. & Wegeberg, S. (1996) The typification and status of *Leptophytum* (Corallinaceae, Rhodophyta). *Phycologia*, **35**, 470-483.

Edmond, J. M. (1992) Himalayan tectonics, weathering processes, and the strontium isotope record in marine limestones. *Science*, **258**, 1594-1597.

Ehrenberg, C. G. (1839) Über die Bildung der Kreidefelsen und des Kreidemergels durch unsichtbare Organismen. *Physikalische Abhandlungen der Königlichen Akademie der Wissenschaften zu Berlin*, 59-147.

Eichwald, C. E. v. (1830) *Zoologia specialis*. D.E. Eichwaldus, Vilnae, 323 pp.

Ellison, A. M., Farnsworth, E. J. & Merkt, R. E. (1999) Origins of mangrove ecosystems and the mangrove biodiversity anomaly. *Global Ecology and Biogeography*, **8**, 95-115.

Esteban, M. (1996) An overview of Miocene reefs from Mediterranean areas: general trends and facies models. In: *Models for carbonate stratigraphy from Miocene reef complexes of*

Mediterranean regions (Ed. by E. K. Franseen, M. Esteban, W. C. Ward and J.-M. Rouchy), pp. 3-55. SEPM, Tulsa. *Concepts in Sedimentology and Paleontology*, *Vol. 5*.

Esteban, M., Braga, J. C., Martin, J. & Santisteban, C. (1996) Western Mediterranean reef complexes. In: *Models for carbonate stratigraphy from Miocene reef complexes of Mediterranean regions* (Ed. by E. K. Franseen, M. Esteban, W. C. Ward and J.-M. Rouchy), pp. 55-73. SEPM, Tulsa. *Concepts in Sedimentology and Paleontology*, *Vol. 5*.

Farell, J. W., Clemens, S. C. & Gromet, L. P. (1995) Improved chronostratigraphic reference curve of late Neogene seawater $^{87}Sr/^{86}Sr$. *Geology*, **23**, 403-406.

Fassoulas, C., Kilias, A. & Mountrakis, D. (1994) Post-nappe stacking extension and exhumation of the HP/LT rocks in the island of Crete, Greece. *Tectonics* **13**, 127-138

Fassoulas, C. (1999) The structural evolution of central Crete: insight into the tectonic evolution of the south Aegean (Greece). *Journal of Geodynamics*, **27**, 23-43.

Fassoulas, C. (2001) The tectonic development of a Neogene basin at the leading edge of the active European margin: the Heraklion basin, Crete, Greece. *Journal of Geodynamics*, **31**, 49-79.

Figueiredo, M., Kain, J. M. & Norton, T. A. (1992) Crustose coralline algae responses to epiphytic cover. *British Phycological Journal*, **27**, 89.

Flügel, E. (1978) *Mikrofazielle Untersuchungsmethoden von Kalken*. Springer, Heidelberg, 454 pp.

Fornos, J. J. & Ahr, W. M. (1997) Temperate carbonates on a modern, low-energy, isolated ramps: the Balearic platform, Spain. *Journal of Sedimentary Research*, **67**, 364-373.

Forst, M. H., Brachert, T. C. & Pais, J. J. C. (2000) High-resolution stratigraphic correlation of coastal cliff sections in the Lagos Portimao Formation (Lower-Middle Miocene, central Algarve, Portugal). *Ciencias da Terra*, **14**, 289-296.

Forst, M. H. (2003) Zur Karbonatsedimentologie, Biofazies und sequenzstratigraphischen Architektur eines fossilen Hochenergie-Schelfs aus dem Neogen der Algarve (Miozän, Südportugal). Doctoral, Johannes Gutenberg Universität.

Foslie, M. (1898) List of species of the lithothamnia. *K. Nor. Vidensk. Selsk. Skr.*, **3**, 1-7.

Freiwald, A. & Taviani, M. (in prep.) Warm-temperate carbonate sediments on structural highs in the Strait of Sicily, Mediterranean Sea. .

Galloway, J. J. (1933) *A manual of foraminifera*. Principia Press, Bloomington, Indiana, 483 pp.

Gómez-Pérez, I., Fernández-Mendiola, C. A. & García-Mondéjar, J. (1998) Constructional dynamics of a Lower Cretacious carbonate ramp (Gerbea Massif, north Iberia). In: *Carbonate ramps*, (Ed. by V. P. Wright and T. P. Burchette). London, *Geological Society Special Publications*, *Vol. 149*.

Halfar, J., Godinez-Orta, L. & Ingle JR, J. C. (2000) Microfacies analysis of recent carbonate environments in the southern Gulf of California, Mexico - a model for warm-temperate to subtropical carbonate formation. *Palaios*, **15**(4), 323-342.

Halfar, J., Godinez-Orta, L., Mutti, M., Valdez-Holguín, J. E. & Borges, J. M. (2004) Nutrient and temperature controls on modern carbonate production: An example from the Gulf of California, Mexico. *Geology*, **32**(3), 213-216.

Hall, R., Audley-Charles, M. G. & Carter, D. J. (1984) The significance of Crete for the evolution of the eastern Mediterranean. In: *The geological evolution of the eastern Mediterranean* (Ed. by J. E. Dixon and A. H. F. Robertson), pp. 517-527. Blackwell Sci. Publications, Oxford. *Special Publications of the Geological Society, Vol. 17*.

Hallock, P. & Glenn, E. C. (1986) Larger foraminifera: a tool for paleoenvironmental analysis of Cenozoic carbonate depositional facies. *Palaios*, **1**, 55-64.

Hallock, P. & Schlager, W. (1986) Nutrient excess and the demise of coral reefs and carbonate platforms. *Palaios*, **1**, 389-398.

Hansen, H. J. & Buchardt, B. (1977) Depth distribution of *Amphistegina* in the Gulf of Elat, Israel. *Utrecht Micropaleontological Bulletin*, **15**, 205-224.

Haq, B. U., Hardenbol, J. & Vail, P. R. (1988) Mesozoic and Ceonozoic chronostratigraphy and cycles of sea-level change. In: *Sea-level changes: An integrated approach* (Ed. by K. C. Wilgus, B. S. Hastings, C. G. S. C. Kendall, H. W. Posamentier, C. A. Ross and J. C. V. Wagoner), pp. 71-108. Society for Sedimentary Geology, Tulsa. *SEPM special publications*, *Vol. 42*

Hardenbol, J., Thierry, J., Farley, M. B., Jacquin, T., de Graciansk, P.-C. & Vail, P. R. (1998) Mesozoic and Cenozoic sequence stratigraphic framework of European Basins. In: *Mesozoic and Cenozoic sequence stratigraphy of European basins* (Ed. by P.-C. de Graciansk, J. Hardenbol, J. Thierry and P. R. Vail), pp. 3-14. Society for Sedimentary Geology, Tulsa. *SEPM special publications*, *Vol. 60*.

Hart, B. S. & Plint, A. G. (1995) Gravelly shoreface and beachface deposits. In: *Sedimentary facies analysis*, *Vol. 22* (Ed. by A. G. Plint), pp. 75-99. Blackwell, Oxford. *Special Publicaton of the International Association of Sedimentologists*.

Harvey, A. S., Broadwater, S. T., Woelkerling, W. J. & Mitrovski, P. J. (2003) *Choreonema* (Corallinales, Rhodophyta): 18S rDNA phylogeny and resurrection of the Hapalidiaceae for the subfamilies Choreonematoideae, Austrolithoideae, and Melobesioideae. *Journal of Phycology*, **39**, 988-998.

Haunold, T. G., Baal, C. & Piller, W. E. (1997) Benthic foraminiferal associations in the northern Bay of Safaga, Red Sea, Egypt. *Marine Micropaleontology*, **29**, 185-210.

Haunold, T. G., Baal, C. & Piller, W. E. (1998) Larger Foraminifera. In: *The northern Bay of Safaga (Red Sea, Egypt): An actuopalaeontological approach V. Foraminifera* (Ed. by T. G. Haunold and W. E. Piller), pp. 155-180. Frankfurt a. M. *Abhandlungen der Senckenbergischen Naturforschenden Gesellschaft, Vol. 548*

Hayward, A. B. (1982) Coral reefs in a clastic sedimentary environment: Fossil (Miocene, s.w. Turkey) and modern (recent, Red Sea) analogues. *Coral Reefs*, **1**, 109-114.

Henrich, R., Freiwald, A., Betzler, C., Bader, B., Schäfer, P., Samtleben, C., Brachert, T. C., Wehrmann, A., Zankl, H. & Kühlmann, D. H. H. (1995) Controls on modern carbonate sedimentation on warm-temperate to arctic coasts, shelves and seamounts in the northern hemisphere: implications for fossil counterparts. *Facies*, **32**, 71-108.

Heydrich, F. (1897a) Corallinaceae, insbesondere Melobesieae. *Berichte der Deutschen Botanischen Gesellschaft*, **15**, 34-71.

Heydrich, F. (1897b) Melobesiae. *Berichte der Deutschen Botanischen Gesellschaft*, **15**, 403-420.

Hilgen, F. J., Krijgsman, W., Langereis, C. G., Lourens, L. J., Santarelli, A. & Zachariasse, W. J. (1995) Extending the astronomocal (polarity) time scale into the Miocene. *Earth and Planetary Science Letters*, **136**, 495-510.

Hodell, D. A., Mueller, P. A., McKenzie, J. A. & Mead, G. A. (1989) Strontium isotope stratigraphy and geochemistry of the late Neogene ocean. *Earth and Planetary Science Letters*, **92**, 165-178.

Hodell, D. A., Mead, G. A. & Mueller, P. A. (1990) Variation in the strontium isotopic composition of seawater (8 Ma to present); implications for chemical weathering rates and dissolved fluxes to the oceans. *Chemical Geology*, **80**, 291-307.

Hodell, D. A., Mueller, P. A. & Garridano, J. R. (1991) Variations in the strontium isotopic composition of seawater during the Neogene. *Geology*, **19**, 24-27.

Hodell, D. A. & Woodruff, F. (1994) Variations in the strontium isotope ratio of seawater during the Miocene: Stratigraphic and geochemical implications. *Paleoceanography*, **9**, 405-426.

Hohenegger, J. (1994) The distribution of living larger Foraminifera NW of Sesoko-Jima, Okinawa, Japan. *Marine Ecology*, **15**, 291-334.

Hohenegger, J. (1995) Depth estimation by proportions of living larger foraminifera. *Marine Micropaleontology*, **26**, 31-47.

Hohenegger, J., Yordanova, E., Yoshikatsu, N. & Tatzreiter, F. (1999) Habitats of larger foraminifera on the upper reef slope of Sesoko Island, Okinawa, Japan. *Marine Micropaleontology*, **36**, 109-168.

Hollaus, S. S. & Hottinger, L. (1997) Temperature dependance of endosymbiontic relationships? *Eclogae geol. Helv.*, **90**, 591-597.

Hottinger, L. (1977) Distribution of larger Peneroplidae, *Borelis*, and Numulitidae in the Gulf of Elat, Red Sea. *Utrecht Micropaleontological Bulletin*, **15**, 35-109.

Hottinger, L., Halicz, E. & Reiss, Z. (1993) *Recent Foraminiferida from the Gulf of Aqaba, Red Sea*. Slovenska Akademija Znanosti in Umetnosti, Ljubljana, 179 pp.

Howard, J. D. & Frey, R. W. (1973) Characteristical physical and biogenic sedimentary structures in Georgia estuaries. *AAPG Bulletin*, **57**, 1159-1184.

Howarth, R. J. & McArthur, J. M. (1997) Statistics for strontium isotope stratigraphy: A robust LOWESS fit to the marine Sr-isotope curve for 0 to 206 Ma, with look-up table for derivation of numeric age. *Journal of Geology*, **105**, 441-456.

Hubbard, J. A. E. B. & Pocock, Y. P. (1972) Sediment rejection by recent scleractinian corals; a key to palaeo-environmental reconstruction. *Geologische Rundschau*, **61**(2), 598-626.

Imbrie, J., Hays, J. D., Martinson, D. G., McIntyre, A., Mix, A., Morley, J. J., Pisias, N. G., Prell, W. L. & Shackleton, N. J. (1984) The orbital theory of Pleistocene climate: Support from a revised chronology of the marine $D^{18}O$ record. In: *Milankovitch and Climate*, *Part I* (Ed. by A. L. Berger), pp. 269-305. D. Reidel Publishing Company.

Ingram, R.L. (1954) Terminology for the thickness of stratification and parting units in sedimentary rocks. *Geol. Soc. Am. Bull.*, **65**, 937-938.

Irvine, L. M. & Chamberlain, Y. M. (1994) *Seaweeds of the British Isles Volume 1: Rhodophyta Part 2B: Corallinales Hildebrandiales*. The Natural History Museum, London, 276 pp.

Jacquotte, P. (1962) Etude des fonds de maerl de la Méditerranée. *Receuil des Travaux de la Station Marine D´Endoume*, **26**, 141-235.

Jakobsagen, V. (1986) *Geologie von Griechenland*. Bornträger, Berlin, Stuttgart. *Beitr. Regionalen Geologie Erde*; **19** 1-363,

James, D. W. (2000) Diet, movment, and covering behavior of the sea urchin Toxopneustes roseus in rhodolith beds in the Gulf of California. *Marine Biology*, **137**, 913-923.

James, N. P. & von der Borch, C. C. (1991) Carbonate shelf edge off southern Australia. *Geology*, **19**, 1005-1008.

James, N. P. & Bone, Y. (1992) Synsedimentary cemented calcarenite layers in Oligo-Miocene shelf limestones, Eucla Plattform, southern Australia. *Journal of Sedimentary Petrology*, **62**, 860-872.

James, N. P., Boreen, T. D., Bone, Y. & Feary, D. A. (1994) Holocene carbonate sedimentation on the west Eucla Shelf, Great Australian Bight: a shaved shelf. *Sedimentary Geology*, **90**, 161-177.

James, N. P. (1997) The cool-water carbonate depositional realm. In: *Cool-water cabonates* (Ed. by N. P. James and J. A. D. Clarke), pp. 1-22., Tulsa. *SEPM Special Publication*, *Vol. 56*.

James, N. P., Bone, Y., Collins, L. B. & Kyser, T. K. (2001) Surficial sediments of the Great Australian Bight: facies dynamics and oceanography on a vast cool-water carbonate shelf. *Journal of Sedimentary Research*, **71**, 549-567.

Jolivet, L., Goffé, B., Truffert-Luxey, C., Patriat, M. & Bonneau, M. (1996) Miocene detachment in Crete and exhumation P-T-t paths of high-pressure metamorphic rocks. *Tectonics*, **15**, 1129-1153.

Jorissen, F. J. (1988) *Benthic foraminifera from the Adriatic Sea. Principles of phenotypic Variation*, Utrecht, 157 pp.

Kahle, H. G., Straub, C., Reilinger, R., McKlusky, S., King, R., Hurst, K., Veis, G., Kastens, K. & Cross, P. (1998) The strain rate field in the eastern Mediterranean region, estimated by repeated GPS measurements. *Tectonophysics*, **294**, 237-252.

Kennet, J. P. & Barker, P. F. (1990) Latest Cretaceous to Cenozoic climate and oceanographic developments in the Weddel Sea, Antarctica: An ocean-drilling perspective. In: *Proceedings ODP, scientific results, 113: College Station* (Ed. by P. F. Barker and J. P. Kennet). *Proceedings of the Ocean Drilling Program, Vol. 113*.

Kershaw, S. (1994) Classification and geological significance of biostromes. *Facies*, **31**, 81-92.

Kissel, C. & Laj, C. (1988) The Tertiary geodynamical evolution of the Aegean Arc: A paleomagnetic reconstruction. *Tectonophysics*, **146**, 183-201.

Krijgsman, W., Hilgen, F. J., Langereis, C. G., Santarelli, A. & Zachariasse, W. J. (1995) Late Miocene magnetostratigraphy, biostratigraphy and cyclostratigraphy in the Mediterranean. *Earth and Planetary Science Letters*, **136**, 475-494.

Kützing, F. T. (1841) *Ueber die die `Polyphers calcifères` des Lamouroux*. Nordhausen, 34 pp.

Lamouroux, J. V. F. (1812) Classification des Ploipyers coralligènes. *Bulletin philosophique*, **3**, 181-188.

Langer, M. R. & Hottinger, L. (2000) Biogeography of selected "larger" foraminifera. *Micropaleontology*, **46 (1)**, 105-126.

Langer, M. R. & Lipps, J. H. (2003) Foraminiferal distribution and diversity, Madang Reef and Lagoon, Papua New Guinea. *Coral Reefs*, **22**, 143-154.

Langereis, C. G., Zachariasse, W. J. & Zidjderveld, J. D. A. (1984) Late Miocene magnetostratigraphy of Crete. *Marine Micropaleontology*, **8**, 261-281.

Larsen, A. R. & Drooger, C. W. (1977) Relative thickness of the test in the *Amphistegina* species of the Gulf of Elat. *Utrecht Micropaleontological Bulletin*, **15**, 225-233.

Lee, J. J. & Anderson, O. R. (1991) Symbiosis in foraminifera. In: *Biology of foraminifera* (Ed. by J. J. Lee and O. R. Anderson), pp. 157-220. Academic Press, London.

Leeder, M. R. & Gawthorpe, R. L. (1987) Sedimentary models for extensional tilt-block/half - graben basins. In: *Continental extensional tectonics* (Ed. by M. P. Coward, J. F. Dewey and P. L. Hancock), pp. 139-152. Blackwell, Oxford. *Geological Society Special Publication*, *Vol. 28*.

Lees, A. & Buller, A. T. (1972) Modern temperate-water and warm-water shelf carbonate sediments contrasted. *Marine Geology*, **13**, M67-M73.

Lees, A. (1975) Possible influence of salinity and temperature on modern shelf carbonate sedimentation. *Marine Geology*, **19**, 159-198.

Lemoine, P. (1910) Repartition et mode de vie du maerl (*Lithothamnium calcareum*) aux environs de Concarneau (Finistère). *Ann Inst Oceanogr Monaco*, **1**, 1-28.

Lemoine, M. P. (1928) Un nouveau genre de Mélobésiées: *Mesophyllum*. *Bulletin de Société Botanique de France*, **75**, 251-254.

Lemoine, M. P. (1939) *Algues calcaires fossiles de l ´Algerie*, 128 pp.

Le Pichon, X. & Angelier, J. (1979) The Hellenic arc and trench system: A key to the neotectonic evolution of the eastern Mediterranean area. *Tectonophysics*, **60**, 1-42.

Le Pichon, X., Chamot-Rooke, N. & Lallemant, S. (1995) Geodetic determination of the kinematics of central Greece with respect to Europe : Implications for eastern Mediterranean tectonics. *Journal of Geophysical Research*, **100**, 12675-12690.

Littler, M. (1973a) The distribution, abundance and communities of deepwater Hawaiian crustose Corallinaceae (Rhodophyta, Cryptonemiales). *Pacific Sciences*, **27**, 281-289.

Littler, M. (1973b) The population and community structure of Hawaiian fringing reef crustose Corallinaceae (Rhodophyta, Cryptonemiales). *Journal of Experimental Marine Biology*, **11**, 103-120.

Loeblich, A. R. j. & Tappan, H. (1988) *Foraminiferal genera and their classification*. Van Nostrand Reinhold Company, New York, 970 pp.

Lukasik, J. J., James, N. P., McGowran, B. & Bone, Y. (2000) An epeiric ramp; low-energy, cool-water carbonate facies in a Tertiary inland sea, Murray Basin, South Australia. *Sedimentology*, **47**(4), 851-881

Lund, M., Davies, P., J. & Braga, J. C. (2000) Coralline algal nodules off Fraser Island, eastern Australia. *Facies*, **42**, 25-34.

Martin, J. M., Braga, J. C. & Rivas, P. (1989) Coral successions in Upper Tortonian reefs in SE Spain. *Lethaia*, **22**, 271-286.

Martin, E. E., Shackleton, N. J., Zachos, J. C. & Flower, B. P. (1999) Orbitally-tuned Sr isotope chemostratigraphy for the late middle to late Miocene. *Paleoceanography*, **14**, 74-83.

Massari, F. & Colella, A. (1988) Evolution and types of fan-delta systems in some major tectonic settings. In: *Fan deltas: sedimentology and tectonic settings* (Ed. by W. Nemec and Steel R.J), pp. 103-122. Blackie and Son, London.

Massari, F. & Parea, G. C. (1990) Wave-dominated Gilbert-type gravel deltas in the hinterland of the Gulf of Taranto (Pleistocene, southern Italy). In: *Coarse-grained deltas* (Ed. by A. Colella and D. B. Prior), pp. 311-331. Blackwell, Oxford. *IAS special publications*, *Vol. 10.*

McArthur, J. M. (1994) Recent trends in strontium isotope stratigraphy. *Terra Nova*, **6**, 331-358.

McArthur, J. M., Howarth, R. J. & Bailey, T. R. (2001) Strontium isotope stratigraphy: LOWESS version 3. Best-fit line to the marine Sr- isotope curve for 0 to 509 Ma and accompanying look-up table for deriving numerical age. *Journal of Geology*, **109**, 155-169.

McKlusky, S., Balassanian, S., Barka, A., Demir, C., Ergintav, S., Georgiev, I., Gurkan, O., Hamburger, M., Hurst, K., Kahle, H., Kastens, K., Kekelidze, G., King, R., Kotzev, R., Lenk, O., Mahmoud, S., Mishin, A., Nadariya, M., Ouzounis, A., Paradissis, D., Peter, Y., Prilepin, M., Reilinger, R., Sanli, I., Seeger, H., Tealeb, A., Toksöz, M. N. & Veis, G. (2000) Global Positioning System constraints on plate kinematics and dynamics in the eastern Mediterranean and Caucasus. *Journal of Geophysical Research*, **105**, 5695-5719.

McPherson, J. G., Shanmugam, G. & Moiola, R. J. (1987) Fan-deltas and braid deltas: varieties of coarse grained deltas. *Geol. Soc. Am. Bull.*, **99**, 331-340.

Mercier, J. L., Sorel, D. & Vergeley, P. (1989) Extensional tectonic regimes in the Aegean basins during the Ceonozoic. *Basin Research*, **2**, 49-71.

Meulenkamp, J. E., Georgiadou-Dikeoulia, E., Jonkers, H. A. & Böger, H. (1979a) Field guide to the Neogene of Crete. *Publications of the Department of Geology & Paleontology University of Athen*, **32**, 1-32.

Meulenkamp, J. e., Jonkers, A. & Spaak, P. (1979b) Late Miocene to Early Pliocene developement of Crete. *Proc VI Coll. Geol. Aegean Region (Athens)*, 137-149.

Meulenkamp, J. E., Wortel, M. J. R., Van Wamel, W. A., Spakman, W. & Hoogerduyn Strating, E. (1988) On the Hellenic subduction zone and the geodynamic evolution of Crete since the late Middle Miocene. *Tectonophysics*, **146**, 203-215.

Meulenkamp, J. E., van der Zwaan, G. J. & van Wamel, W. A. (1994) On the Late Miocene to Recent vertical motions in the Cretan segment of the Hellenic Arc. *Tectonophysics*, **234**, 53-72.

Miall, A. D. (1992) Alluvial deposits. In: *Facies models* (Ed. by R. G. Walker and N. P. James), pp. 119-142. Geological Association of Canada, St. John´s.

Miller, K. G., Wright, J. D. & Fairbanks, R. G. (1991) Unlocking the ice house, Oligocene-Miocene oxygen isotopes, eustasy and margin erosion. *Journal of Geophysical research*, **96**(B4), 6829-6848.

Minnery, G. A. (1990) Crustose coralline algae from the Flower Garden Banks, northwestern Gulf of Mexico. In: *Paleoalgology: Contemporaory Research and Applications* (Ed. by D. F. Toomey and M. H. Nitecky), pp. 237-247. Springer Verlag, Berlin.

Mutti, M., Bernoulli, D. & Stille, P. (1997) Temperate carbonate platform drowning linked to Miocene oceanographic events: Maiella Platform margin, Italy. *Terra Nova*, **9**(3), 122-125.

Nägeli, C. (1858) Die Stärkekörner. In: *Pflanzenphysiologische Untersuchungen* (Ed. by C. Nägeli and C. Kramer), pp. x+624. Friedrich Schulthess, Zürich.

Nelson, C. S. (1988) An introductory perspective on non-tropical shelf carbonates. *Sedimentary Geology*, **60**, 3-12.

Oslick, J. S., Miller, K. G., Feigenson, M. D. & Wright, J. D. (1994) Oligocene-Miocene strontium isotopes: Stratigraphic revisions and correlations to an inferred glacioeustatic record. *Paleoceanography*, **9**, 427-444.

Palmer, M. R. & Edmond, J. M. (1989) The strontium isotope budget of the modern ocean. *Earth and Planetary Science Letters*, **92**, 11-26.

Pedley, H. M. (1976) A palaeoecological study of the Upper Coralline Limestone, *Terebratula-Aphelesia* bed (Miocene, Malta) based on bryozoan growth-form studies and brachiopod distributions. *Paleogeography, Paleoclimatology, Paleoecology*, **20**, 209-234.

Pedley, M. (1998) A review of sediment distributions and processes in Oligo-Miocene ramps of southern Italy and Malta (Mediterranean divide). In: *Carbonate Ramps* (Ed. by V. P. Wright and T. P. Burchette), pp. 163-179., London. *Geological Society Special Publications*, *Vol. 149*.

Penrose, D. (1992a) Hydrolithon cymodoceae (Foslie) comb. nov. (Corallinaceae, Rhodophyta) in southern Australia and its relationships to Fosliella. *Phycologia*, **31**(1), 89-100.

Penrose, D. (1992b) *Neogoniolithon fosliei* (Corallinaceae, Rhodophyta), the type species of *Neogoniolithon*, in southern Australia. *Phycologia*, **31**, 338-350.

Penrose, D. & Woelkerling, W. J. (1992) A reappraisal of *Hydrolithon* and its relationship to *Spongites* (Corallinaceae, Rhodophyta). *Phycologia*, **31**(1), 81-88.

Pérès, J. N. & Picard, J. (1964) Nouveau manuel de bionome benthique de la Mer Méditerranée. *Receuil des Travaux de la Station Marine D´Endoume*, **31**, 5-137.

Peterman, Z. E., Hedge, C. E. & Tourtelot, H. A. (1970) Isotopic composition of strontium in seawater throughout the Phanerozoic time. *Geochimica et Cosmochimica Acta*, **34**.

Pastorino, P. & Guineri, P. (2000) Gli orizzonti ad ostreacea della "Formazione Di San Paolo" (San Michele di Mondovì, Sottobianco delle Langhe, Italia nord-occidentale. *Atti Ticinensi di Scienze della Terra*, **41**, 11-16.

Philippi, R. (1837) Beweis dass die Nulliporen Pflanzen sind. *Arch. Naturgesch.*, **3**, 387-393.

Piller, W. E. (1994) *Nullipora ramosissima* Reuss, 1847. *Beiträge zur Paläontologie*, **19**, 181-189.

Piller, W. E. (1994) The northern Bay of Safaga (Red Sea, Egypt): an actuopalaeontological approach. *Beiträge zur Paläontologie*, **18**, 1-73.

Pomar, L., Ward, W. & Green, D. G. (1996) Upper Miocene reef complex of the Llucmajor area, Mallorca, Spain. In: *Models for carbonate stratigraphy from Miocene reef complexes of Mediterranean regions* (Ed. by E. K. Franseen, M. Esteban, W. C. Ward and J.-M. Rouchy), pp. 191-227. SEPM, Tusla. *Concepts in Sedimentology and Paleontology*, *Vol. 5*.

Pomar, L. (2001a) Types of carbonate platforms: a genetic approach. *Basin Research*, **13**, 313-334.

Pomar, L. (2001b) Ecological control of sedimentary accomodation: evolution from a carbonate ramp to rimmed shelf, Upper Miocene, Balearic Islands. *Paleogeography, Paleoclimatology, Paleoecology*, **175**, 249-272.

Pomar, L., Obrador, A. & Westphal, H. (2002) Sub-wavebase cross-bedded grainstones on a distally steepened carbonate ramp, Upper Miocene, Menorca, Spain. *Sedimentology*, **49**, 139-169.

Pomar, L., Brandano, M. & Westphal, H. (2004) Environmental factors influencing skeletal grain sediment associations: a critical review of Miocene examples from the western Mediterranean. *Sedimentology*, **51**(3), 627-652.

Postma, G. & Roep, T. B. (1985) Resedimented conglomerates in the bottom sets of Gilbert-type gravel deltas. *Journal of Sedimentary Petrology*, **55**, 874-885.

Purser, B. H. (1983) *Sédimentation et diagenèse des carbonates néritiques récents*, Paris, 389 pp.

Rabenhorst, L. (1863) *Die Kryptogamen-Flora von Sachsen, der Ober-Lausitz, Thüringen und Nordböhmen*. Krummer, Leipzig, 653 pp.

Racey, A. (2001) A review of Eocene nummulite accumulations: Structure, formation and reservoir potential. *Journal of Petroleum Geology*, **24(1)**, 79-100.

Raffi, I., Mozzato, C., Fornaciari, E., Hilgen, F. J. & Rio, D. (2003) Late Miocene calcareous nannofossil biostratigraphy and astrobiochronology for the Mediterranean region. *Micropaleontology*, **49**, 1-26.

Rasser, M. W. & Piller, W. E. (1999) Aplication of neontological taxonomic concepts to Late Eocene coralline algae (Rhodophyta) of the Austrian Molasse Zone. *Journal of Micropaleontology*, **18**, 67-80.

Rasser, M. W. & Piller, W. E. (2000) Designation of *Phymatolithon* (Corallinaceae, Rhodophyta) in fossil material and its paleoclimatological indications. *Micropaleontology*, **46**(1), 89-95.

Rasser, M. W. & Piller, W. E. (2004) Crustose algal frameworks from the Eocene Alpine Foreland. *Paleogeography, Paleoclimatology, Paleoecology*, **206**, 21-39.

Raymo, M. E., Ruddiman, W. F. & Froehlich, P. N. (1988) Influence of late Cenozoic mountain building on ocean geochemical cycles. *Geology*, **16**, 649-653.

Raymo, M. E. & Ruddiman, W. F. (1992) Tectonic forcing of late Cenozoic climate. *Nature*, **359**, 117-122.

Read, J. F. (1985) Carbonate platform facies model. *AAPG Bulletin*, **69**(1), 1-21.

Reading, H. G. & Collinson, J. D. (1996) Clastic coasts. In: *Sedimentary environments: processes, facies and stratigraphy*, (Ed. by H. G. Reading). Blackwell, Oxford. 154-231

Reilinger, R. E., McClusky, S. C., Oral, M. B., King, R. W., Toksoz, M. N., Barka, A. A., Kinik, I., Lenk, O. & Sanli, I. (1997) Messinian pre-evaporite sapropels and precession-induced oscillations in western Mediterranean climate. *Marine Geology*, **153**, 137-146.

Reinson, G. E. (1992) Transgressive barrier island and estuarine systems. In: *Facies models* (Ed. by R. G. Walker and N. P. James), pp. 179-194. Geological Association of Canada, St. John´s.

Reiss, Z. & Hottinger, L. (1984) *The Gulf of Aqaba*. Springer, New York, 454 pp.

Reuter, M. (*in prep.*) Klimastratigraphie flachmariner Karbonate des Ober-Miozän (Heraklion-Becken, Kreta/Griechenland): Eine neue sedimentologische Gliederungsmethode tektonisch mobiler Becken?

Richter, F. M., Rowley, D. B. & DePaolo, D. J. (1992) Sr isotope evolution of seawater: the role of tectonics. *Earth and Planetary Science Letters*, **109**, 11-23.

Richter, F. M. & Liang, Y. (1993) The rate and consequences of Sr diagenesis in deep-sea carbonates. *Earth and Planetary Science Letters*, **117**, 553-565.

Riegl, B. & Piller, W. E. (1997) Distribution and environmental control of coral assemblages in northern Safaga Bay (Red Sea, Egypt). *Facies*, **36**, 141-162.

Riegl, B. & Piller, W. E. (1999) Coral frameworks revisted-reefs and coral carpets in the northern Red Sea. *Coral Reefs*, **18**, 241-253.

Riegl, B. & Piller, W. E. (2000) Biostromal coral facies-a Miocene example from the Leitha Limestone (Austria) and its actualistic interpretation. *Palaios*, **15**(5), 399-413.

Robertson, A. H. F. & Party, S. S. (1996) Tectonic Introduction. *Proceedings of the Ocean drilling Program, Initial Reports*, **160**, 5-20.

Rosmena-Rodriguez, R., Woelkerling, W. J. & Foster, M. S. (1999) Taxonomic reassessment of rhodolith-forming species of Lithophyllum (Corallinales, Rhodophyta) in the Gulf of California, Mexico. *Phycologia*, **38**, 401-417.

Sachse, M. & Mohr, B. A. R. (1996) Eine obermiozäne Makro- und Mikroflora aus Südkreta (Griechenland), und deren paläoklimatische Interpretation.-Vorläufige Betrachtungen. *N. Jb. Geol. Paläont. Abh.*, **200**(1), 149-182.

Sachse, M. (1997) Die Makrilia-Flora (Kreta, Griechenland) - Ein Beitrag zur neogenen Klima- und Vegetationsgeschichte des östlichen Mittelmeergebietes. Dissertation, Eidgenössische Technische Hochschule.

Saidova, K. H. (1981) *O sovremennom sostoyanii sistemy nadvidovykh taksonov Kaynozoyskikh benthosnykh foraminifer*. Institut Okeanologii P.P. Shirshova, Akademyia Nauk SSSR, Moskow.

Santisteban, C. & Taberner, C. (1988) Sedimentary models of silicalastic deposits and coral reefs interaction. In: *Carbonate-clastic transitions* (Ed. by L. J. Doyle and R. H.H.), pp. 35-76. Elsevier, Amsterdam. *Developments in Sedimentology*.

Schulze, M. S. (1854) *Über den Organismus der Polythalamien (Foraminiferen), nebst Bemerkungen über die Rhizopoden im Allgemeinen*. Wilhelm Engelmann, Leipzig.

Schwager, C. (1876) Saggio di una classificazione dei foraminiferi avuto riguardo alle loro famiglie naturali. *Bolletino R. Comitato Geologico d´Italia*, **8**, 18-27.

Seibold, E. (1970) Nebenmeere im humiden und ariden Klimabereich. *Geologische Rundschau*, **60**, 73-105.

Seilacher, A. (1984) The Jeram Model: event condensation in a modern intertidal environment. In: *Sedimentary and evolutionary cycles* (Ed. by Bayer, U.), Springer, Heidelberg, 336-341.

Setchell, W. A. (1943) Mastophora and the Mastophorae: genus and subfamily of the Corallinaceae. *Proceedings of the National Academy of Science*, **29**, 127-135.

Shackleton, N. J. & Opdyke, N. D. (1973) Oxygen isotope and paleomagnetic stratigraphy of equatorial Pazific core V28-238: oxygen isotope temperatures and ice volumes on a 10^5 year and 10^6 year scale. *Quarternary Research*, **3**(39-55).

Silva, P. C. & Johansen, H. W. (1986) A reappraisal of the Order Corallinales (Rhodophyceae). *British Phycological Journal*, **21**, 245-254.

Smith, A. M. & Nelson, C. S. (1996) Differential abrasion of bryozoan sceletons: taphonomic implications for paleoenvironmental interpretation. In: *Proceedings of the 10th International Bryozoology Conference Wellington New Zealand* (Ed. by D. P. Gordon, A. M. Smith and J. A. Grant-Mackie), pp. 305-313. National Institute of Water & Atmospheric Research Ltd, Wellington.

Sonnefeld, M. D. & Cross, T. A. (1993) Volumetric partitioning and facies differentation within the Permian Upper San Andres Formation of Last Chance Canyon, Guadalupe Mountains, New Mexiko. In: *Carbonate sequence stratigraphy: recent developements and applications* (Ed. By Loucks, B., Sarg, R.G.) Tulsa, *AAPG Memoir Vol. 57*, 435-474.

Spjeldnaes, N. & Moisette, P. (1997) Celleporid (bryozoan) thickets from the upper Pliocene of the island of Rhodes, Greece. In: *Cool water carbonates*, *Vol. 56* (Ed. by N. P. James and J. A. D. Clarke), pp. 263-270, Tulsa. *SEPM special publications*.

Sprovieri, M., Barbieri, M., Bellanca, A. & Neri, R. (2003) Astronomical tuning of the Tortonian $^{87}Sr/^{86}Sr$ curve in the Mediterranean Basin. *Terra Nova*, **15**(1), 29-35.

Swift, D.J.P., Thorne, J.A. (1991) Sedimentation on continental margins, I: a general model for shelf sedimentation. In: *Shelf sand and sandstone bodies; geometry, facies and sequence stratigraphy* (Ed by Swift, D.J. P., Oertel, G.F. & Tillman, R.W.), Blackwell, Oxford, *IAS special publications, Vol. 14.*

ten Veen, J. H. & Postma, G. (1999a) Neogene tectonics and basin fill patterns in the Hellenic outer-arc (Crete, Greece). *Basin Research*, **11**, 223-241.

ten Veen, J. H. & Postma, G. (1999b) Roll-back controlled vertical movements of outer-arc basins of the Hellenic Subduction Zone (Crete, Greece). *Basin Research*, **11**, 243-266.

van den Hoek, C., Cortel-Breeman, A. M. & Wanders, J. B. W. (1975) Algal zonation in the fringing coral reef in Curacao, Netherlands, Antilles, in relation to zonation of corals and gorgonians. *Aquatic Botany*, **1**, 269-308.

Veizer, J. & Compston, W. (1974) $^{87}Sr/^{86}Sr$ composition of seawater during the Phanerozoic. *Geochimica et Cosmochimica Acta*, **38**, 1461-1484.

Veron, J. E. N. (1995) *Corals in space and time*. Comstock/Cornell, Ithaca, 321 pp.

Verheij, E. (1993) The genus *Sporolithon* (Sporolithaceae fam. nov., Corallines, Rhodophyta) from the Spermonde Archipelago, Indonesia. *Phycologia*, **32**, 184-196.

Walkden, G. & Williams, A. (1998) Carbonate ramps and the Pleistocene - recent depositional systems of the Arabian Gulf. In: *Carbonate Ramps*, (Ed. by V. P. Wright and T. P. Burchette), pp. 43-53, London. *Geological Society Special Publications, Vol. 149*.

Wettstein, R. R. (1901) *Handbuch der systhematischen Botanik*. Deuticke, Leipzig, 201 pp.

Wilson, J. L. (1975) *Carbonate facies in geologic history*. Springer, Berlin-Heidelberg-New York, 471 pp.

Woelkerling, W. J. (1988) *The coralline red algae, an analysis of genera and subfamilies of nongeniculate Carallinaceae*. Oxford University Press, London, 268 pp.

Womersley, H. B. S. (1996) *The marine benthic flora of southern Australia*. Australian Biological Research Study, Canberra, 392 pp.

Woodroffe, C. D., Chappel, J. M. A., Thom, B. G. & Wallensky, E. (1989) Depositional model of a macrotidal estuary and floodplain, South Alligator River, Northern Australia. *Sedimentology*, **36**, 737-756.

Wright, V.P, Burchette, T.P. (1998) Carbonate ramps: an introduction. In: *Carbonate Ramps*, (Ed. by V. P. Wright and T. P. Burchette), pp. 1-7, London. *Geological Society Special Publications, Vol. 149*.

Yokoyama, Y., Lambeck, K., De Deckker, P., Johnston, P. & Fifield, L. K. (2000) Timing of the last glacial maximum from observed sea-level minima. *Nature*, **406**, 713-716.

Zachariasse, W. J. (1975) *Planctonic foraminiferal biostratigraphy of the Late Neogene of Crete /Greece)*, *Utrecht Micropaleontological Bulletin, Vol. 11*. 143 pp.

Zachos, J. C., Opdyke, B. N., Quinn, T. M., Jones, C. E. & Halliday, A. N. (1999) Early Cenozoic glaciation, Antarctic weathering, and seawater $^{87}Sr/^{86}Sr$: Is there a link? *Chemical Geology*, **161**, 165-180.

Zachos, J., Pagani, M., Sloan, L., Thomas, E. & Billups, K. (2001) Trends, rhythms and aberrations in global climate 65 Ma to present. *Science*, **292**, 686-693.

Zachos, J. C., Shackleton, N. J., Revenaugh, J. S., Pälike, H. & Flower, B. P. (2001) Climate response to orbital forcing across the Oligocene-Miocene boundary. *Science*, **292**, 274-287.

Section Kandhila 1 (Ka1)

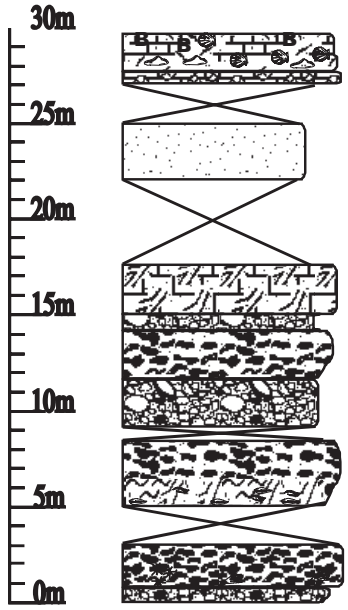

Section Kandhila 2 (Ka2)

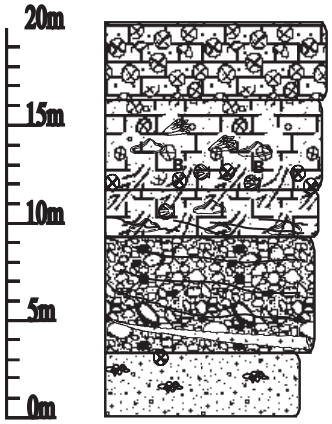

Section Kristo Kefali Nord (KN)

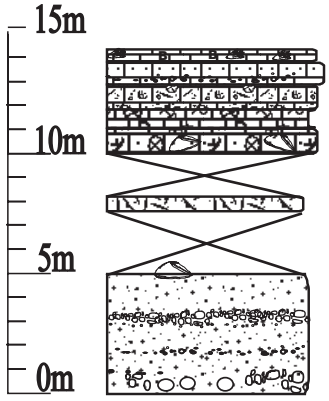

Fig. A1: Sections southwest of Kandhila and section north of Kristo Kefali (see Fig. 1.4.1. for locations and Fig. 2.2.2. for legend)

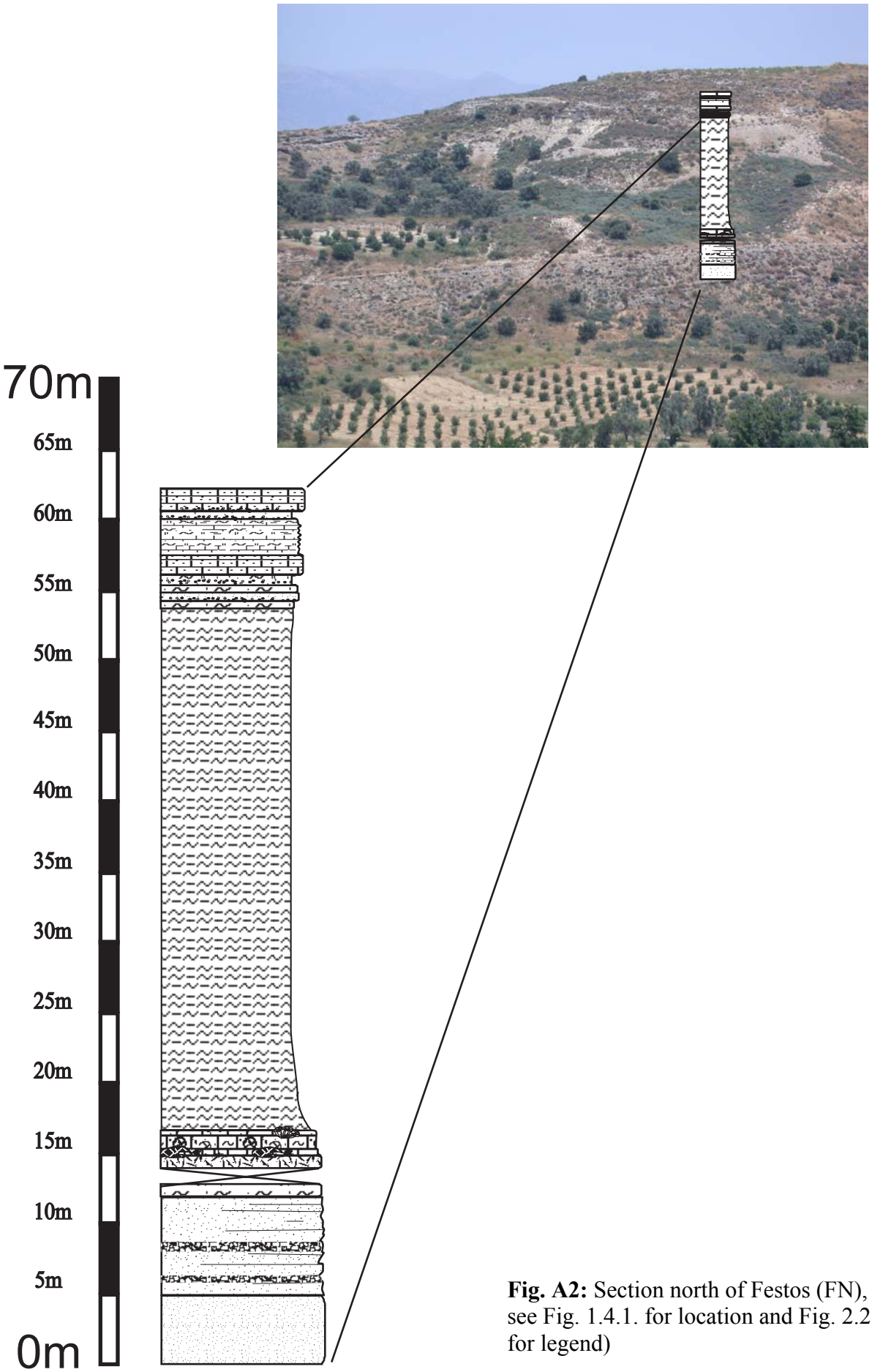

Fig. A2: Section north of Festos (FN), see Fig. 1.4.1. for location and Fig. 2.2.2. for legend)

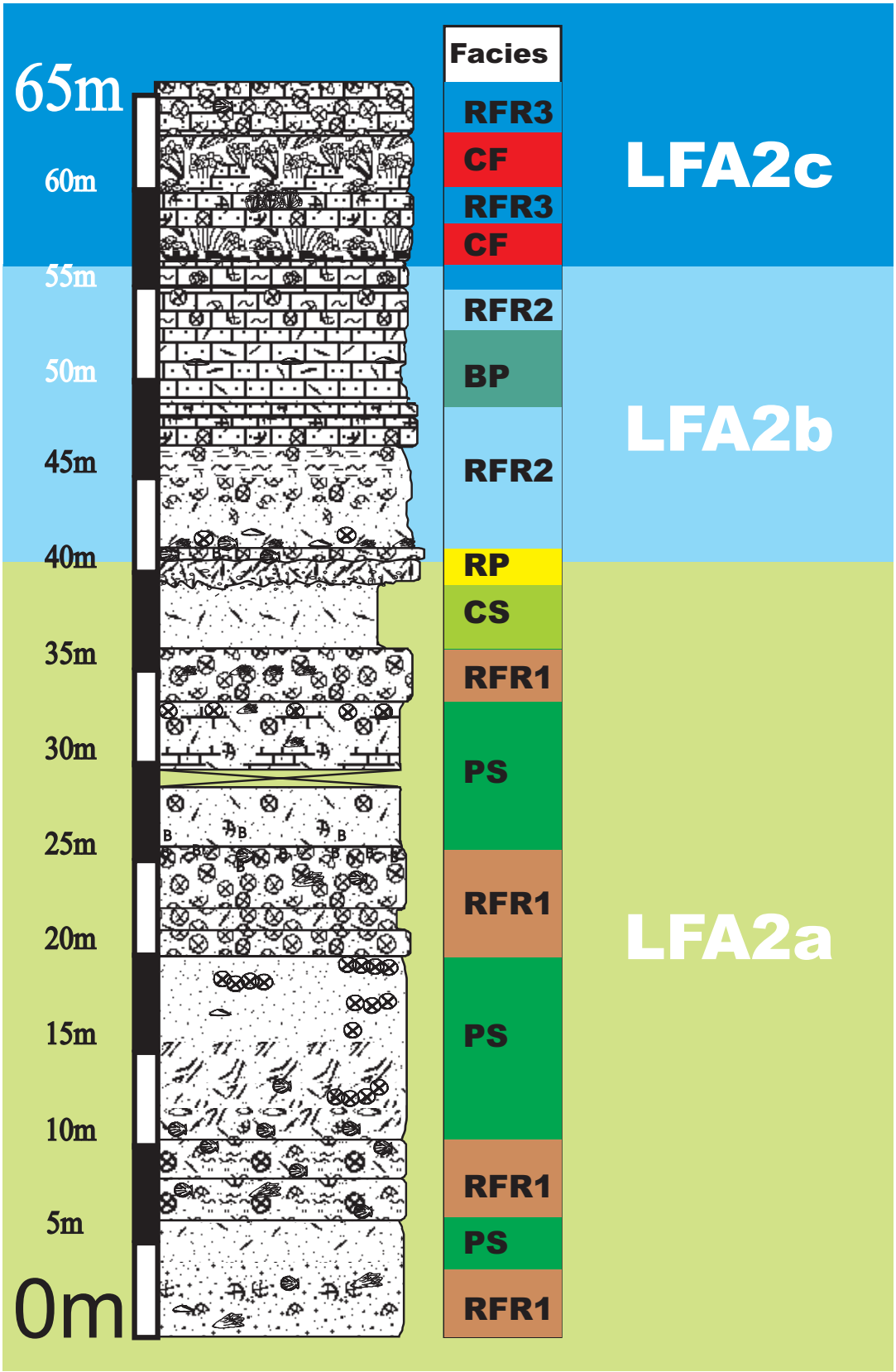

Fig. A3: Section Matala South (MS1) with facies units described in chapter 2.4. (see Fig. 2.2.1. for location and Fig. 2.2.2. for legend)

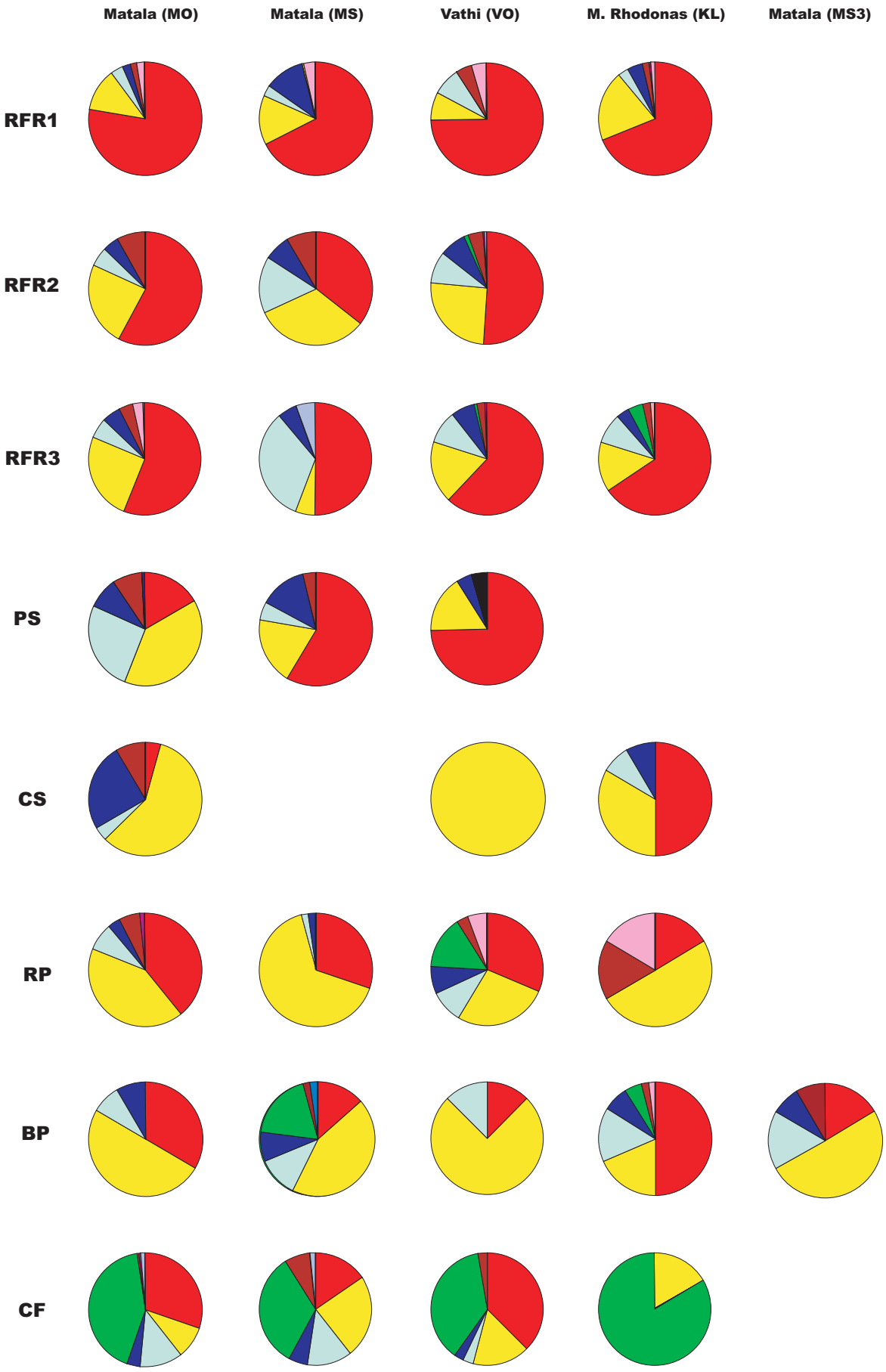

Fig. A4: Results of semiquantitative biofacies analysis for lithological units described in chapter 2.4. Results are shown separate for each of sections MO1, MS1, VO, KL and one sample of section MS3. Results are shown in volume percent of skeletal elements total

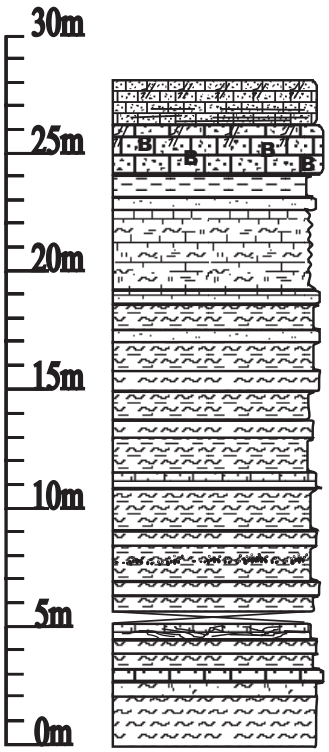

Fig. A5: Section Komos (Ko, see Fig. 2.2.1. for location and Fig. 2.2.2. for legend)

Section	Abbr.	Samples	X-Coordinates	Y-Coordinates	Lithofacies
Ayios Andreas	AA		29862	387344	LFA1
Festos Nord	FN		*24.8223°	*35.05723°	LFA1-LFA3
Kandhila 1	Ka1		*24.9759°	*34.9914°	LFA1-LFA2
Kandhila 2	Ka2		n.a.	n.a.	LFA1-LFA2
Kefali Nord	KN		29524	386852	LFA2b-c
Komos	KO	KO	29564	387635	LFA3
Martsalo Nord	MaN		29656	386853	LFA2a-c
Martsalo Bay 1	Ma1	MA	29610	386746	LFA2b-c
Martsalo Bay 1	Ma2	MB	29567	386718	LFA2b-LFA3
Martsellos	Mart		29750	387085	LFA2b
Matala Archeological Site	MA		29479	387480	LFA2a-c
Matala East (Ost) 1	MO1	MO	29565	387545	LFA1-LFA2-c
Matala East (Ost) 2	MO2	OK	29615	387575	LFA1-LFA2c
Matala South 1	MS1	MS	29508	387463	LFA2a-c
Matala South 2	MS2		29601	387378	LFA1
Matala South 3	MS3	MD	29667	387393	LFA1-LFA2c
Moni Odhiyitria1	Moni1		29953	387263	LFA1-LFA2b
Moni Odhiyitria2	Moni2		30013	387294	LFA2a-b
Mount Rhodonas	KL	KL	30068	387039	LFA2b-c
Pitsidia East (Ost)	PO		29793	387652	LFA1-LFA2c
Pitsidia South	PS		29768	387399	LFA1
Pitsidia West	PW		29762	387678	LFA1
Sivas	Sivas	S	29971	387667	LFA1-LFA2c
Vathi	VO	VO	29571	387003	LFA2a-c

Table A1: Locations of measured sections

BP	Bioclastic Backstone	
CS	Calcareous sandstone	
CF	Coral Framestone	
LFA1	Lithofacies association 1 (siliciclastics)	
LFA2	Lithofacies association 2 (carbonates)	
LFA3	Lithofacies association 3 (marl)	
MRB	Massive Rodolith Bed	
PS	Packstone with Sand	
RB	Red Algal Bindstone	
RFR	Rhodolith Floatstone to Rudstone	
RP	Rudstone with Pebbles	
RT	Rudstone with Terebratula	
SB	Sequence Boundary	
SWB	Storm wave Base	
WAT	West Asteroussia Tabellands	

Table A2: Abbreviations used in the text

Facies	Sample	Abundance of skeletal components in volume percent of skeletal content total							
		Rotalgen	Forams	Echinoids	Bryozoans	Corals	Bivalves	Serpulids	Crustaceans
PS	MO								
	8c	11	33,3	33,3	11		11		
	8b	20	20	20	20		20		
	7		50	33,3	5,5		5,5		
	6a	33,3	33,3	11	11		11		
	4b	5,5	50	33,3	5,5		5,5		
	4a	33,3	33,3	33,3					
	2	16,6	50	16,6	8,3		8,3		
	average	17,10	38,56	25,83	8,76	0,00	8,76	0,00	0,00
	MS								
	1	75	16,6	2,8	2,8		2,8		
	9	25	25	8,3	33,3		8,3		
	8	75	16,6	4,2	4,2				
	average	58,33	19,40	5,10	13,43	0,00	3,70	0,00	0,00
	VO								
	2	75	16,6		4,5				
CS	MO								
	9c		100						
	11b	8,8	16,6	8,8	50		16,6		
	average	4,4	58,3	4,15	25	0	8,3	0	0
	VO								
	V06		100						
	KL								
	5	50	33,3	8,3	8,3				
RFR1	MO								
	1b	75	16,6	2,1	2,1		2,1	2,1	
	1a	75	16,6	4,5	4,5				
	3	83,3	4,2	4,2			4,2	4,2	
	average	77,77	12,47	3,60	2,20	0,00	2,10	2,10	0,00
	MS								
	3	75	16,6		2,8		2,8	2,8	
	7	83,3	5,5		5,5			5,5	
	6	25	25	8,4	33,3			8,4	
	5	75	16,6		8,4				
	10	77,7	7,4	7,4	7,4				
	average	67,2	14,22	3,16	11,48	0	0,56	3,34	0
	VO								
	Vo1	75	8,3	8,3			4,5	4,5	
	Vo3	75	8,3	8,3			4,5	4,5	
	average	75	8,3	8,3	0	0	4,5	4,5	0
	KL								
	8b	83,3	5,5	5,5	5,5				
	8a	41,65	41,65	5,5	5,5		5,5		
	4	75	16,6	2,1	2,1		2,1	2,1	
	2	75	16,6		4,5				
	average	27,50	8,04	1,31	1,76	0,00	0,76	0,21	0,00
RFR2	MO								
	18b	75	16,6	2,8	2,8			2,8	
	16e	33,3	33,3	11	11		11		
	16d	83,3	5,5	5,5			5,5		
	16c	75	16,6		4,5		4,5		
	16b	75	16,6	4,5			4,5		
	16a	16,6	50	8,3	8,3		16,6		
	average	59,7	24,4	5,86	4,76	0	8,42	0	0
	MS								
	14	16,6	50	16,6			16,6		
	19	54,1	15,2	15,2	15,2				
	average	35,35	32,6	15,9	7,6	0	8,3	0	0
	VO								
	V08f	50	8,3	16,6	16,6	8,3			
	Vo8e	50	16,6	16,6	8,3		8,3		
	Vo8d	75	16,6	2,8	2,8				2,8
	Vo8c	50	33,3	5,5	5,5		5,5		
	Vo8b	37,5	37,5	8,3	8,3		4,5	4,5	
	Vo8a	41,65	41,65	5,5	5,5		5,5		
	average	50,69	25,66	9,22	7,83	1,38	3,97	0,75	0,47

Table A3: Results of semiquantitative facies analysis in measured sections listed separately for each facies type

Table A3 continued

RFR3	MO								
	20d	75	8,3	8,3	4,5			4,5	
	20c	75	16,6	4,5	4,5				
	20b	75	16,6	2,1	2,1		2,1	2,1	
	29	50	33,3	5,5	5,5		5,5		
	28b	50	33,3	8,3	8,3				
	28a	33,3	33,3	8,3	8,3		8,3	8,3	
	27	50	33,3	5,5	5,5		5,5		
	26d	50	33,3	8,3			8,3		
	26c	75	5,5	5,5	5,5		2,8	2,8	2,8
	26a	75	8,3	8,3	2,8		2,8	2,8	
	25	75	8,3	2,8	2,8		2,8	8,3	
	24	25	25	8,3	8,3		16,6	16,6	
	23b	50	33,3	5,5	5,5		5,5		
	23a	75	5,5	4,5	5,5		4,5	5,5	
	15	10,4	79,2	10,4					
	17a	50	33,3		16,6				
	average	55,86	25,40	6,01	5,36	0,00	4,04	3,18	0,18
	MS								
	20	50	5,5	33,3	5,5				5,5
	VO								
	VO23	75	16,6	4,5	4,5				
	VO22	77,2	7,7	7,7	7,7				
	VO21b	75	16,6	2,1	2,1	2,1	2,1		
	VO21a	75	16,6	2,1	2,1	2,1	2,1		
	VO20c	50	33,3	8,3	8,3				
	Vo20b	83,3	4,2	4,2	4,2		4,2		
	Vo20a	75	8,3	4,5	8,3	4,5			
	Vo19	50	5,5	33,3	5,5		5,5		
	Vo18b	66,6	11	11	11				
	Vo18a	50	33,3	5,5	5,5		5,5		
	Vo17	58,3	21	21					
	V016	75	16,6	4,5		4,5			
	Vo13	50	33,3	5,5	5,5		5,5		
	Vo12	37,5	37,5	4,5	16,6		4,5		
	Vo11	58,3	14	14	14				
	Vo10	75	8,3	8,3	8,3				
	Vo9	25	16,6	25	16,6		8,3	8,3	
	average	62,13	17,67	9,76	7,07	0,78	2,22	0,49	0,00
	KL								
	30	75	16,6	4,5				4,5	
	29b	75	8,3	8,3	8,3				
	28	75	2,8	16,6	2,8		2,8		
	27	75	4,5	16,6	4,5				
	26b	75	2,8	16,6	2,8		2,8		
	26a	50	33,3	8,3	8,3				
	25	75	8,3	8,3	4,5		4,5		
	24	50	16,6	16,6	8,3			8,3	
	22	37,5	37,5	16,6	4,5		4,5		
	21	75	8,3	8,3	4,5		4,5		
	20b	8,3	8,3			83,3			
	20a	75	16,6	2,1	2,1		2,1	2,1	
	18	75	16,6	2,1	2,1		2,1		
	16	75	16,6	2,8	2,8		2,8		
	12b	50	33,3	5,5	5,5		5,5		
	12a	83,3	8,3	8,3					
	11	75	16,6	2,8			2,8	2,8	
	10	75	2,1	16,6	2,1		2,1	2,1	
	average	65,51	14,30	8,94	3,51	4,63	2,03	1,10	0,00

Table A3 continued

RP	**MO**								
	15	10,4	79,2	10,4					
	13b	79,2	20,8						
	12b	50	16,6	5,5	5,5		16,6	5,5	
	10	16,6	50	16,6	8,3		8,3		
	average	39,05	41,65	8,125	3,45	0	6,225	1,375	0
	MS								
	13	45,6	45,6	4,2	4,2				
	12	14,6	85,4						
	average	30,1	65,5	2,1	2,1	0	0	0	0
	VO								
	V07b	8,3	75	8,3	2,8		2,8	2,8	
	V07a	50	16,6	8,3	16,6			8,3	
	V05b	50	11	5,5	11	11	5,5	5,5	
	Vo5a	16,6	5,5	16,6		50	5,5	5,5	
	average	31,225	27,025	9,675	7,6	15,25	3,45	5,525	0
	Sivas								
	S6	16,6	50				16,6	16,6	
BP	**MO**								
	17b	33,3	50	8,3	8,3				
	MS								
	16	8,4	75	8,4	8,4				
	17	16,6	50	8,4	16,6			8,4	
	18b	4,3	16,6	4,3		75			
	18a	25	33,3	25	8,4		8,4		
	average	13,575	43,725	11,525	8,35	18,75	2,1	2,1	0
	VO								
	15	12,5	75	12,5					
	KL								
	17	50	33,3	16,6					
	MD								
	26	8,4	75	16,6					
	MO2								
	1	16,6	50	16,6	8,4		8,4		
	KL								
	31	58,3	14	14	14				
	29a	25	11	11	8,3	25	11	8,3	
	13	58,3	14	14	14				
	17	50	33,3	16,6					
	15	58,3	21	21					
	average	62,475	23,325	19,15	9,075	6,25	2,75	2,075	0
CF	**MO**								
	20a	75	8,3	2,8	2,8		2,8	8,3	
	19i	50	33,3	5,5	5,5	5,5			
	19g	50	33,3	5,5	5,5				5,5
	19f	50	5,5	33,3	5,5				5,5
	19e					100			
	19d					100			
	19c	16,6	2,8	2,8	2,8	76			
	19b	50	8,3	33,3	8,3				
	19a	50	8,3	33,3	8,3				
	22e					100			
	22d	33,3	5,5	5,5	5,5	50			
	22c					100			
	21c	50	8,3	33,3	8,3				
	21b	25	16,6	16,6	5,5	25	5,5		5,5
	21a	5,5	5,5	5,5		83,3			
	average	30,36	9,05	11,83	3,87	42,65	0,55	0,55	1,10
	MS								
	23	25	16,6	16,6	8,3	25	8,3		
	22	16,6	50	16,6	8,3		8,3		
	21	5	5	5		75	5		5
	average	15,53	23,87	12,73	5,53	33,33	7,20	0,00	1,67
	VO								
	Vo14a	37,5	16,6	2,8	2,8	37,5	2,8		
	KL								
	9		16,6			83,3			

Sample	Amphistegina	Heterostegin	Elphidium	Cibicides	Ammonia	Textularia	Quinqueloculir	Triloculina	Borelis	Globigerina	Homotrema	Victoriella
VO23	11,21	0,00	0,93	0,93	0,00	0,93	0,00	0,00	0,00	0,00	0,00	0,00
VO22	2,10	0,35	0,00	0,00	0,00	0,00	0,00	0,00	0,00	0,00	0,00	0,00
VO21b	3,74	0,00	3,74	1,25	0,00	1,25	0,00	0,00	0,00	0,00	0,00	0,00
VO21a	1,66	0,00	1,25	7,47	0,00	1,66	1,25	0,00	0,00	0,00	0,00	0,00
VO20c	3,33	1,25	3,33	3,33	0,00	1,25	1,25	0,00	0,00	0,00	7,49	1,25
Vo20b	0,38	0,00	0,38	0,38	0,00	0,38	0,00	0,00	0,00	0,00	0,00	0,00
Vo20a	3,74	1,25	0,25	0,25	0,00	0,25	0,00	0,00	0,00	0,00	1,25	0,00
Vo19	0,00	0,00	2,20	2,20	0,00	0,00	0,00	0,00	0,00	0,00	0,00	0,00
Vo18b	5,50	5,50	0,00	0,00	0,00	0,00	0,00	0,00	0,00	0,00	0,00	0,00
Vo18a	22,48	0,00	3,75	0,00	3,75	0,00	0,00	0,00	0,00	0,00	0,00	0,00
Vo17	1,68	0,00	1,68	5,04	0,00	1,68	5,04	0,00	0,00	0,00	0,00	0,00
V016	6,64	0,00	0,00	0,74	0,00	0,74	0,74	0,00	2,21	0,00	2,21	0,00
V015	3,32	0,00	0,00	0,55	0,00	0,55	2,21	0,55	3,32	0,00	0,00	0,00
Vo14a	7,47	0,00	0,00	0,83	0,00	0,83	0,00	0,00	0,00	0,00	2,49	0,83
Vo13	0,00	0,00	2,22	0,00	0,00	2,22	2,22	0,00	0,00	0,00	19,98	0,00
Vo12	8,44	0,00	5,63	1,13	1,13	1,13	0,00	0,00	0,00	0,00	1,13	0,00
Vo11	7,00	0,00	0,78	0,00	0,00	0,78	0,00	0,00	0,00	0,00	4,67	0,78
Vo10	0,00	0,00	0,00	0,00	0,00	0,00	0,00	0,00	0,00	0,00	5,60	0,00
Vo9	0,00	0,00	0,00	0,00	0,00	0,00	0,00	0,00	0,00	2,08	12,45	0,00
V08f	4,15	0,00	1,38	0,00	0,00	0,46	0,00	0,00	0,00	0,46	1,38	0,00
Vo8e	1,66	1,25	7,47	0,00	0,00	0,00	0,00	0,00	0,00	1,25	1,66	0,00
Vo8d	7,89	0,00	0,53	0,53	0,53	0,53	0,00	0,00	0,00	0,00	5,26	0,00
Vo8c	16,65	0,00	0,00	1,39	0,00	1,39	0,00	0,00	0,00	1,39	11,10	1,39
Vo8b	6,25	3,13	6,25	3,13	0,00	0,00	0,00	0,00	0,00	0,00	18,75	0,00
Vo8a	31,24	0,00	3,47	3,47	3,47	0,00	0,00	0,00	0,00	0,00	0,00	0,00
V07b	25,00	37,50	4,17	4,17	0,00	4,17	0,00	0,00	0,00	0,00	0,00	0,00
V07a	2,08	6,23	6,23	0,00	0,00	2,08	0,00	0,00	0,00	0,00	0,00	0,00
V05b	7,43	2,48	0,00	0,00	0,00	0,00	0,00	0,00	0,00	0,00	0,00	0,00
Vo5a	0,00	0,00	0,00	1,28	0,00	0,00	0,00	0,00	1,28	0,00	1,28	0,00
Vo3	5,60	0,00	0,62	0,00	0,62	0,62	0,00	0,00	0,00	0,00	0,00	0,00
Vo1	6,23	0,00	0,69	0,00	0,00	0,69	0,00	0,00	0,00	0,00	0,00	0,69
KL												
K31	5,69	1,90	0,00	0,95	0,00	1,90	0,95	0,00	0,00	0,00	0,00	0,00
30	4,50	0,00	0,00	6,74	0,56	0,56	0,56	0,00	0,00	0,00	0,56	0,00
29b	3,84	0,26	0,26	0,26	0,00	0,26	0,26	0,00	0,00	0,00	2,56	0,00
29a	7,84	0,87	0,87	0,00	0,00	0,87	0,00	0,00	0,00	0,00	0,00	0,00
28	1,71	0,00	0,00	0,00	0,09	0,09	0,00	0,00	0,09	0,09	0,09	0,00
27	1,83	0,00	0,00	0,12	0,00	0,12	0,12	0,00	0,12	0,12	0,00	0,00
26b	1,94	0,22	0,22	0,00	0,00	0,00	0,00	0,00	0,00	0,22	0,00	0,00
26a	10,55	1,32	15,82	1,32	0,00	1,32	1,32	0,00	0,00	0,00	0,00	0,00
25	4,15	1,38	0,00	0,35	1,38	0,35	0,00	0,00	0,00	0,00	0,00	0,35
24	8,09	5,40	0,00	0,67	0,67	0,00	0,00	0,00	0,00	0,67	0,00	0,67
22	17,81	3,96	3,96	2,97	3,96	2,97	0,00	0,00	0,00	0,00	0,00	0,00
21	3,99	0,27	1,33	0,27	0,00	0,27	0,00	0,00	0,00	0,27	0,00	1,33
20a	10,12	0,00	1,12	1,12	0,00	1,12	0,00	0,00	0,00	0,00	0,00	0,00
19	2,77	0,00	0,92	0,00	0,00	0,00	2,77	0,92	8,30	0,00	0,00	0,92
18	5,29	0,00	1,18	0,00	0,00	1,18	5,29	0,00	1,18	0,00	0,00	0,00
17	16,65	1,85	0,00	0,00	0,00	1,85	11,10	0,00	1,85	0,00	0,00	0,00
16	7,68	0,00	0,00	0,64	0,00	0,64	1,71	0,00	1,71	0,00	0,64	0,00
15	2,80	0,00	0,00	0,00	0,00	2,80	12,60	0,00	2,80	0,00	0,00	0,00
13	7,00	2,33	0,78	0,00	0,00	0,78	0,78	2,33	0,00	0,00	0,00	0,00
12b	12,49	4,16	2,08	0,00	0,00	0,00	2,08	0,00	0,00	0,00	4,16	0,00
12a	3,11	0,00	1,04	0,00	0,00	0,00	1,04	0,00	0,00	0,00	0,00	0,00
11	7,99	0,00	2,66	0,89	0,89	0,00	0,89	0,00	0,00	0,00	2,66	0,00
10	0,32	0,00	0,11	0,00	0,00	0,00	0,00	0,00	0,00	0,00	0,11	0,00
9	0,00	0,00	0,00	0,00	0,00	0,00	8,30	0,00	8,30	0,00	0,00	0,00
8b	0,48	0,00	0,48	0,00	0,00	0,00	0,00	0,00	0,00	0,00	2,89	0,00
8a	31,24	0,00	0,00	0,00	0,00	0,00	5,21	0,00	0,00	0,00	5,21	0,00
5	13,32	0,00	19,98	0,00	0,00	0,00	0,00	0,00	0,00	0,00	0,00	0,00
4	5,19	0,00	3,46	0,00	1,73	0,00	0,00	0,00	0,00	0,00	0,00	0,00
2	8,30	1,38	5,53	0,00	0,00	0,00	0,00	1,38	0,00	0,00	0,00	0,00
1a	4,57	54,84	4,57	0,00	0,00	4,57	0,00	0,00	4,57	0,00	0,00	0,00
MS1												
23	6,64	0,00	0,55	2,21	0,55	0,55	2,21	0,00	0,55	0,00	0,00	0,00
22	33,75	0,00	3,75	3,75	0,00	3,75	0,00	0,00	0,00	0,00	0,00	0,00
21	0,44	0,00	0,44	0,00	0,00	0,00	0,00	0,00	0,00	0,00	0,00	0,00
20	0,00	0,00	0,00	2,89	0,00	0,00	0,00	0,00	0,00	0,00	0,00	0,96
19	10,26	0,86	0,86	0,86	0,00	0,00	0,86	0,00	0,00	0,00	0,00	0,00
18b	0,83	0,00	0,83	1,66	0,00	1,66	7,47	0,00	0,83	0,00	0,00	0,00
18a	9,99	0,00	1,11	1,11	0,00	0,00	9,99	1,11	1,11	0,00	1,11	0,00
17	30,00	0,00	2,50	2,50	2,50	0,00	2,50	0,00	0,00	0,00	0,00	0,00
16	33,75	0,00	3,75	0,00	0,00	3,75	22,50	3,75	0,00	0,00	0,00	0,00
14	4,17	37,50	4,17	0,00	0,00	0,00	0,00	0,00	0,00	0,00	4,17	0,00
13	3,80	22,80	3,80	0,00	0,00	0,00	0,00	0,00	0,00	0,00	15,20	0,00
12	10,68	64,05	10,68	0,00	0,00	0,00	0,00	0,00	0,00	0,00	0,00	0,00
11c	28,13	0,00	4,69	0,00	4,69	4,69	28,13	4,69	0,00	0,00	0,00	0,00
10	1,23	3,70	2,47	0,00	0,00	0,00	0,00	0,00	0,00	0,00	0,00	0,00
9	8,44	8,44	1,88	1,88	1,88	0,00	0,00	0,00	0,00	0,00	0,00	0,00
8	5,53	8,30	0,92	0,00	0,00	0,92	0,92	0,00	0,00	0,00	0,00	0,00
7	1,83	0,00	1,83	0,00	0,00	1,83	0,00	0,00	0,00	0,00	0,00	0,00
6	0,00	18,75	3,13	0,00	3,13	0,00	0,00	0,00	0,00	0,00	0,00	0,00
5	0,75	0,00	0,75	0,00	0,75	0,00	0,00	0,00	0,00	0,75	11,21	0,75
3	0,00	8,30	0,92	0,00	0,92	0,00	0,00	0,00	0,00	0,92	5,53	0,00
2	2,77	2,77	0,00	0,92	0,00	0,92	0,00	0,00	0,00	0,00	8,30	0,00
1	7,89	0,00	2,63	0,00	1,31	1,31	0,00	0,00	0,00	0,00	2,63	0,00
MO1												
29	0,00	22,48	3,75	0,00	0,00	0,00	0,00	0,00	0,00	3,75	0,00	0,00
28b	1,76	15,82	1,76	1,76	0,00	0,00	0,00	0,00	0,00	10,55	0,00	0,00
28a	1,67	14,99	1,67	1,67	0,00	0,00	0,00	0,00	0,00	9,99	0,00	0,00
27	0,00	14,99	5,00	0,00	0,00	0,00	0,00	0,00	0,00	9,99	0,00	0,00
26d	0,00	14,99	2,50	2,50	0,00	0,00	0,00	0,00	0,00	9,99	0,00	0,00
26c	0,73	0,73	1,10	0,73	0,00	1,10	0,00	0,00	0,00	1,10	0,00	0,00
26a	0,79	0,79	1,18	1,18	1,18	0,79	0,00	0,00	0,00	1,18	0,00	0,00
25	0,44	5,29	0,44	0,00	0,00	0,00	0,44	0,00	0,00	0,00	0,00	0,00
24	0,00	16,88	1,88	0,00	0,00	1,88	0,00	0,00	0,00	1,88	0,00	0,00
23b	8,88	13,32	2,22	0,00	0,00	2,22	0,00	0,00	0,00	0,00	0,00	0,00
23a	3,30	0,00	0,00	0,28	0,00	0,28	0,28	0,00	0,00	0,00	0,00	0,00
22d	3,30	0,18	0,18	0,18	0,18	0,18	0,18	0,00	0,00	0,00	0,00	0,00
21c	1,97	0,00	0,00	0,00	0,00	0,00	5,91	0,00	0,00	0,00	0,00	0,00
21b	12,45	0,00	0,83	0,00	0,00	0,83	0,83	0,00	0,83	0,00	0,00	0,00
21a	2,89	0,00	0,96	0,00	0,00	0,00	0,00	0,00	0,00	0,00	0,00	0,00
20d	2,91	0,00	0,48	0,48	0,00	0,00	0,00	0,00	0,00	0,00	0,00	0,00
20c	7,47	0,00	0,50	0,50	0,00	0,50	0,00	0,50	0,50	0,00	4,98	0,00
20b	11,83	0,00	1,31	1,31	0,00	0,00	0,00	0,00	0,00	0,00	0,00	0,00
20a	3,74	0,00	0,62	0,00	0,00	2,49	0,00	0,00	0,00	0,00	0,00	0,00
19i	14,99	0,00	1,67	0,00	0,00	1,67	9,99	0,00	1,67	0,00	0,00	0,00
19h	0,00	0,00	0,00	0,00	0,00	0,00	0,00	0,00	0,00	0,00	0,00	0,00
19f	0,00	0,00	0,00	0,00	0,00	0,92	0,00	0,00	0,00	0,00	0,00	0,00
19c	0,00	0,00	0,00	0,00	0,00	0,00	0,00	0,98	0,00	0,00	0,00	0,00
19b	1,66	1,66	1,66	0,00	0,00	0,00	0,00	0,00	0,00	0,00	0,00	0,00
19a	2,49	2,49	0,00	0,00	0,00	0,00	0,00	0,00	0,00	0,00	0,00	0,00
18b	5,26	7,89	0,66	0,66	0,00	0,66	0,66	0,00	0,00	0,00	0,00	0,00
17b	10,63	2,36	0,00	7,08	0,00	2,36	7,08	0,00	10,63	0,00	0,00	0,00
17a	22,48	1,50	0,00	0,00	0,00	1,50	0,00	0,00	1,50	0,00	0,00	1,50
16e	3,65	0,00	0,00	0,00	1,22	0,00	10,95	1,22	1,22	0,00	0,00	3,65
16d	0,00	0,28	0,28	0,28	0,00	0,28	0,00	0,00	0,00	0,00	0,00	3,30
16b	5,53	8,30	0,69	0,00	0,00	0,69	0,69	0,00	0,00	0,00	0,69	0,00
16c	0,66	2,63	0,66	0,00	0,00	0,66	0,00	0,66	0,00	0,00	7,89	2,63
16a	7,50	22,50	7,50	0,00	2,50	0,00	0,00	2,50	0,00	0,00	2,50	0,00
15	23,76	35,64	11,88	0,00	0,00	0,00	0,00	0,00	0,00	0,00	0,00	0,00
13b	6,24	9,36	1,04	0,00	0,00	0,00	0,00	1,04	0,00	0,00	1,04	0,00
12b	1,25	7,47	4,98	0,00	1,25	0,00	0,00	0,00	0,00	0,00	0,00	0,00
12a	15,83	23,75	2,64	0,00	0,00	2,64	0,00	2,64	0,00	0,00	0,00	0,00
11b	1,31	7,89	5,26	0,00	1,31	0,00	0,00	0,00	0,00	0,00	0,00	0,00
10	6,00	27,00	6,00	0,00	6,00	0,00	0,00	0,00	0,00	0,00	0,00	0,00
9b	0,00	0,00	0,00	0,00	52,50	0,00	0,00	0,00	0,00	0,00	0,00	0,00
8b	0,00	0,00	0,00	2,33	7,00	0,00	0,00	0,00	0,00	4,67	0,00	0,00
7	0,00	24,00	0,00	0,00	16,00	0,00	0,00	0,00	0,00	0,00	0,00	0,00
6a	0,00	0,00	0,00	3,33	6,67	0,00	0,00	0,00	0,00	10,00	0,00	0,00
5	0,00	33,75	3,75	0,00	0,00	0,00	0,00	0,00	0,00	3,75	3,75	0,00
4b	0,00	2,71	2,71	0,00	10,83	0,00	0,00	0,00	0,00	16,25	0,00	0,00
4a	0,00	2,16	2,16	0,00	12,99	0,00	0,00	0,00	0,00	2,16	2,16	0,00
3	0,00	0,98	0,16	0,00	0,00	0,00	0,16	0,16	0,00	0,00	0,00	1,47
2	1,46	1,46	11,67	1,46	17,50	0,00	0,00	0,00	0,00	0,00	1,46	0,00
1b	3,32	0,00	3,32	2,21	2,21	0,44	0,44	0,44	0,00	0,00	0,44	0,00
1a	0,48	0,00	5,81	0,00	0,48	3,87	0,48	0,00	0,00	0,00	0,00	0,00
Ma2												
24	0,00	0,00	0,00	0,00	0,00	0,00	0,00	0,00	0,00	100,00	0,00	0,00
23	0,00	0,00	0,00	0,00	0,00	0,00	0,00	0,00	0,00	100,00	0,00	0,00
21	0,00	25,00	2,78	2,78	2,78	0,00	0,00	0,00	0,00	16,67	0,00	0,00
20	4,17	37,50	4,17	0,00	0,00	0,00	0,00	0,00	0,00	4,17	0,00	0,00
19	4,69	56,25	4,69	0,00	4,69	0,00	0,00	0,00	0,00	4,69	0,00	0,00
18	2,21	3,32	3,32	2,21	0,00	3,32	0,00	0,00	0,00	2,21	0,00	0,00
17	14,70	4,90	4,90	0,00	2,45	2,45	0,00	0,00	0,00	0,00	0,00	0,00
16	3,05	3,05	2,03	0,51	0,51	0,51	0,00	0,00	0,00	2,03	0,00	0,00
15	8,30	5,53	1,38	0,00	0,00	0,00	0,00	0,00	0,00	0,00	0,00	1,38
14	11,03	2,45	11,03	0,00	0,00	2,45	0,00	0,00	0,00	2,45	0,00	0,00
10	4,20	0,35	2,80	0,35	0,35	0,35	0,00	0,00	0,00	0,00	0,00	0,00

Table A4: Relative abundances of foraminifera in percent of skeletal components total

Sample	Lith ramos	Lith sp1	L/P sp1	L/P indet	Mes curt	Mes sancti	Mes sp1	Mes sp2	Mes indet	Melobes ind	Spong alb	Spong sp1	Lit inc	Lit dent
VO22	0,00	0,00	0,00	19,41	0,00	0,00	0,00	0,00	4,85	4,85	29,12	0,00	0,00	0,00
VO21b	11,25	0,00	3,75	11,25	0,00	0,00	0,00	0,00	3,75	0,00	33,75	0,00	0,00	0,00
VO21a	17,50	0,00	0,00	2,92	0,00	26,25	0,00	0,00	0,00	0,00	0,00	0,00	0,00	0,00
VO20c	0,00	0,00	0,00	0,00	0,00	25,00	0,00	0,00	8,33	0,00	8,33	0,00	0,00	0,00
Vo20b	33,32	0,00	0,00	0,00	0,00	0,00	0,00	0,00	22,21	0,00	5,55	0,00	0,00	0,00
Vo20a	2,34	0,00	0,00	0,00	0,00	0,00	0,00	0,00	0,00	28,13	2,34	0,00	0,00	2,34
Vo17	23,32	0,00	0,00	0,00	0,00	0,00	0,00	0,00	23,32	0,00	0,00	0,00	0,00	0,00
V016	0,00	0,00	0,00	5,94	0,00	0,00	0,00	23,75	0,00	0,00	35,63	0,00	0,00	0,00
V015	0,00	0,00	0,00	0,00	0,00	13,13	0,00	0,00	0,00	0,00	0,00	0,00	0,00	0,00
Vo14a	0,00	0,00	0,00	0,00	0,00	12,66	0,00	0,00	0,00	0,00	12,66	0,00	0,00	0,00
Vo13	0,00	0,00	0,00	0,00	0,00	0,00	4,17	16,67	0,00	0,00	25,00	0,00	0,00	0,00
Vo12	0,00	0,00	0,00	0,00	0,00	0,00	0,00	0,00	0,00	0,00	19,69	0,00	3,28	0,00
Vo11	0,00	0,00	0,00	0,00	0,00	0,00	0,00	9,33	0,00	0,00	13,99	0,00	13,99	0,00
Vo10	0,00	0,00	0,00	0,00	33,75	0,00	0,00	0,00	0,00	5,63	22,50	0,00	0,00	0,00
Vo9	0,00	0,00	0,00	0,00	0,00	0,00	0,00	0,00	0,00	10,00	0,00	0,00	0,00	10,00
V08f	11,67	0,00	0,00	0,97	0,00	0,00	0,00	0,00	0,97	0,97	17,50	0,97	0,97	0,00
Vo8e	20,00	0,00	0,00	0,00	0,00	0,00	0,00	0,00	13,33	0,00	0,00	0,00	3,33	0,00
Vo8d	42,19	0,00	0,00	0,00	0,00	0,00	0,00	0,00	0,00	0,00	7,03	0,00	0,00	0,00
Vo8c	12,50	0,00	0,00	0,00	0,00	0,00	0,00	0,00	0,00	0,00	0,00	0,00	8,33	0,00
Vo8b	0,00	0,00	11,25	0,00	0,00	0,00	0,00	0,00	11,25	0,00	0,00	0,00	3,75	0,00
Vo8a	0,00	0,00	0,00	24,99	0,00	0,00	0,00	0,00	0,00	0,00	0,00	0,00	8,33	0,00
V07b	0,00	0,00	6,64	0,00	0,00	0,00	0,00	0,00	0,00	0,00	0,00	0,00	0,00	0,00
V07a	25,00	0,00	0,00	0,00	0,00	0,00	0,00	0,00	0,00	0,00	0,00	0,00	0,00	0,00
V05b	0,00	0,00	2,80	2,80	0,00	0,00	0,00	0,00	7,00	7,00	2,80	7,00	2,80	2,80
Vo5a	0,00	0,00	0,00	0,00	0,00	2,63	0,00	0,00	0,00	7,89	2,63	0,00	1,31	1,31
Vo3	10,00	10,00	30,00	0,00	0,00	0,00	0,00	0,00	0,00	0,00	0,00	0,00	10,00	0,00
Vo1	5,00	0,00	22,50	5,00	0,00	0,00	0,00	0,00	0,00	5,00	0,00	0,00	3,75	3,75
KL														
30	0,00	0,00	0,00	0,00	0,00	0,00	0,00	0,00	0,00	26,25	17,50	0,00	0,00	0,00
29b	0,00	0,00	0,00	5,63	0,00	0,00	0,00	0,00	22,50	0,00	33,75	0,00	0,00	0,00
29a	10,00	0,00	0,00	0,00	0,00	0,00	0,00	0,00	6,67	0,00	1,67	0,00	0,00	0,00
28	26,25	0,00	0,00	0,00	0,00	0,00	0,00	0,00	0,00	4,38	17,50	0,00	0,00	0,00
27	0,00	0,00	0,00	0,00	0,00	0,00	0,00	0,00	5,25	0,00	31,50	5,25	0,00	0,00
26b	0,00	0,00	0,00	0,00	0,00	0,00	0,00	0,00	25,50	0,00	38,25	0,00	0,00	0,00
26a	0,00	0,00	0,00	0,00	0,00	0,00	22,50	0,00	2,50	0,00	15,00	2,50	0,00	0,00
25	0,00	0,00	0,00	0,00	0,00	0,00	25,00	0,00	4,17	4,17	0,00	37,50	0,00	0,00
24	0,00	5,28	0,00	5,28	0,00	0,00	11,88	11,88	5,28	0,00	0,00	0,00	0,00	3,96
22	0,00	0,00	0,00	0,00	0,00	0,00	7,50	0,00	0,00	7,50	7,50	0,00	0,00	0,00
21	0,00	0,00	0,00	0,00	0,00	0,00	53,44	0,00	0,00	0,00	0,00	0,00	8,91	0,00
20a	0,00	0,00	0,00	0,00	0,00	0,00	0,00	0,00	0,00	0,00	56,25	0,00	0,00	0,00
19	0,00	0,00	0,00	0,00	0,00	4,17	0,00	0,00	25,00	0,00	4,17	0,00	8,33	0,00
18	10,00	0,00	0,00	0,00	0,00	0,00	0,00	0,00	0,00	10,00	30,00	0,00	5,00	0,00
16	0,00	5,63	0,00	22,50	0,00	0,00	0,00	0,00	0,00	0,00	33,75	0,00	0,00	0,00
12b	0,00	0,00	0,00	0,00	0,00	0,00	0,00	0,00	2,50	10,00	15,00	0,00	0,00	0,00
12a	20,83	0,00	0,00	0,00	0,00	0,00	0,00	0,00	0,00	0,00	13,88	0,00	3,47	0,00
11	0,00	0,00	0,00	0,00	0,00	0,00	0,00	0,00	11,88	0,00	35,63	11,88	3,96	0,00
10	0,00	0,00	14,06	0,00	0,00	0,00	0,00	0,00	14,06	0,00	0,00	0,00	9,38	0,00
8b	0,00	0,00	0,00	29,16	0,00	0,00	0,00	0,00	19,44	0,00	0,00	0,00	0,00	0,00
8a	0,00	0,00	0,00	0,00	0,00	3,33	0,00	0,00	0,00	3,33	3,33	0,00	3,33	0,00
4	0,00	4,69	0,00	28,13	0,00	0,00	0,00	0,00	0,00	0,00	4,69	0,00	0,00	0,00
2	0,00	0,00	37,50	0,00	0,00	0,00	0,00	0,00	0,00	0,00	25,00	0,00	12,50	0,00
1b	0,00	0,00	0,00	0,00	0,00	0,00	0,00	0,00	0,42	0,00	0,42	0,00	4,98	0,00
MS1														
22	0,00	0,00	0,00	0,00	0,00	0,00	0,00	0,00	0,00	0,00	8,96	0,00	5,98	0,00
21	0,00	0,00	0,00	0,00	0,00	5,00	0,00	0,00	0,00	0,00	0,00	0,00	0,00	0,00
20	0,00	0,00	0,00	0,00	0,00	0,00	35,00	0,00	0,00	0,00	0,00	0,00	0,00	0,00
19	0,00	0,00	0,00	0,00	0,00	0,00	0,00	0,00	0,00	10,82	32,46	0,00	10,82	0,00
14	0,00	0,00	0,00	0,00	0,00	0,00	0,00	0,00	8,30	0,00	0,00	0,00	0,00	0,00
13	6,08	0,00	0,00	18,24	0,00	0,00	0,00	0,00	0,00	0,00	0,00	0,00	6,08	0,00
10	0,00	0,00	25,90	0,00	0,00	0,00	0,00	38,85	0,00	0,00	0,00	0,00	12,95	0,00
9	0,00	0,00	0,00	0,00	0,00	0,00	0,00	0,00	0,00	0,00	18,75	0,00	0,00	0,00
8	0,00	0,00	45,00	0,00	0,00	0,00	0,00	0,00	0,00	0,00	0,00	0,00	0,00	0,00
7	0,00	0,00	0,00	0,00	0,00	0,00	83,30	0,00	0,00	0,00	0,00	0,00	0,00	0,00
5	0,00	0,00	26,25	0,00	0,00	0,00	0,00	0,00	0,00	0,00	0,00	0,00	17,50	0,00
3	0,00	0,00	27,00	0,00	0,00	0,00	0,00	0,00	40,50	0,00	0,00	0,00	0,00	0,00
2	0,00	0,00	0,00	0,00	0,00	0,00	0,00	0,00	0,00	0,00	0,00	0,00	0,00	0,00
1	0,00	0,00	45,00	0,00	0,00	0,00	0,00	0,00	0,00	0,00	0,00	0,00	30,00	0,00
MO1														
29	0,00	0,00	0,00	0,00	0,00	0,00	50,00	0,00	0,00	0,00	0,00	0,00	0,00	0,00
28a	0,00	0,00	0,00	6,66	0,00	0,00	0,00	0,00	9,99	0,00	0,00	0,00	0,00	0,00
27	0,00	30,00	0,00	0,00	0,00	0,00	0,00	0,00	0,00	0,00	0,00	0,00	0,00	0,00
26d	0,00	0,00	0,00	0,00	0,00	0,00	0,00	0,00	16,67	0,00	25,00	0,00	0,00	0,00
26c	0,00	36,00	0,00	0,00	0,00	0,00	0,00	0,00	24,00	0,00	0,00	0,00	0,00	0,00
26a	0,00	5,00	0,00	30,00	0,00	0,00	0,00	0,00	10,00	0,00	10,00	0,00	0,00	0,00
25	0,00	56,25	0,00	0,00	0,00	0,00	0,00	0,00	0,00	0,00	0,00	0,00	0,00	0,00
24	1,46	0,00	0,00	0,00	0,00	8,75	0,00	0,00	5,83	0,00	0,00	0,00	1,46	0,00
23b	0,00	0,00	0,00	0,00	0,00	0,00	0,00	0,00	0,00	0,00	26,25	0,00	0,00	0,00
23a	0,00	3,33	0,00	10,00	0,00	15,00	0,00	0,00	0,00	0,00	15,00	0,00	3,33	0,00
22d	0,00	0,00	0,00	0,00	0,00	0,00	0,00	0,00	1,67	0,00	14,99	0,00	0,00	1,67
20e	0,00	0,00	0,00	0,00	0,00	10,50	0,00	0,00	10,50	0,00	31,50	0,00	0,00	0,00
20d	0,00	0,00	0,00	0,00	0,00	0,00	0,00	0,00	0,00	0,00	39,38	0,00	0,00	0,00
20c	0,00	0,00	0,00	0,00	0,00	0,00	0,00	0,00	4,38	0,00	26,25	0,00	4,38	0,00
20b	0,00	0,00	0,00	0,00	0,00	0,00	0,00	0,00	0,00	0,00	50,63	0,00	8,44	0,00
20a	0,00	0,00	0,00	0,00	0,00	0,00	0,00	0,00	37,50	0,00	25,00	0,00	0,00	0,00
19i	0,00	0,00	0,00	0,00	0,00	0,00	0,00	0,00	0,00	0,00	25,00	0,00	0,00	0,00
19b	0,00	0,00	0,00	0,00	0,00	24,00	0,00	0,00	16,00	0,00	0,00	0,00	0,00	0,00
19a	0,00	0,00	0,00	0,00	0,00	18,00	0,00	0,00	0,00	0,00	27,00	0,00	0,00	0,00
18b	5,00	0,00	0,00	0,00	0,00	0,00	5,00	0,00	0,00	0,00	45,00	5,00	0,00	0,00
17b	0,00	0,00	0,00	0,00	0,00	0,00	0,00	0,00	0,00	33,30	0,00	0,00	0,00	0,00
17a	0,00	0,00	0,00	0,00	0,00	0,00	0,00	0,00	0,00	0,00	33,75	0,00	0,00	0,00
16e	0,00	0,00	0,00	0,00	0,00	0,00	0,00	0,00	0,00	0,00	26,64	0,00	0,00	0,00
16d	0,00	0,00	0,00	0,00	0,00	0,00	24,99	0,00	0,00	0,00	4,17	37,49	4,17	0,00
16c	37,50	0,00	0,00	25,00	0,00	0,00	0,00	0,00	0,00	0,00	0,00	0,00	12,50	0,00
16b2	0,00	0,00	0,00	0,00	0,00	0,00	75,00	0,00	0,00	0,00	0,00	0,00	0,00	0,00
16b1	0,00	0,00	0,00	24,00	0,00	0,00	36,00	0,00	0,00	0,00	0,00	0,00	0,00	0,00
16a	6,64	0,00	0,00	0,00	0,00	4,43	0,00	0,00	0,00	0,00	0,00	0,00	0,00	0,00
13b	0,00	0,00	0,00	0,00	0,00	0,00	0,00	0,00	0,00	0,00	79,20	0,00	0,00	0,00
12b	0,00	0,00	0,00	2,64	0,00	23,75	0,00	0,00	0,00	0,00	15,83	0,00	2,64	0,00
11b	0,00	0,00	0,00	0,00	0,00	0,00	8,80	0,00	0,00	0,00	0,00	0,00	0,00	0,00
9b	0,00	5,53	0,00	0,00	0,00	0,00	0,00	0,00	0,00	0,00	1,38	0,00	8,30	0,00
8c	0,00	0,00	0,00	8,25	0,00	0,00	0,00	0,00	0,00	0,00	0,00	0,00	0,00	0,00
8b	0,00	0,00	0,00	0,00	0,00	0,00	15,00	0,00	0,00	0,00	0,00	0,00	0,00	0,00
5	0,00	0,00	0,00	0,00	0,00	0,00	0,00	0,00	13,28	0,00	0,00	0,00	0,00	0,00
3	0,00	0,00	34,99	0,00	0,00	0,00	11,66	0,00	0,00	0,00	0,00	11,66	0,00	0,00
2	0,00	0,00	0,00	6,64	0,00	0,00	0,00	0,00	9,96	0,00	0,00	0,00	0,00	0,00
1b	0,00	0,00	0,00	5,63	33,75	0,00	11,25	0,00	0,00	0,00	11,25	0,00	5,63	0,00
1a	0,00	0,00	0,00	0,00	0,00	0,00	0,00	0,00	0,00	0,00	40,50	0,00	27,00	0,00

Table A5: Relative abundances of non-geniculate coralline red algae in volume percent of skeletal components total